RECOVERY OF POSITIVE ELECTRODE ACTIVE MATERIAL FROM SPENT LITHIUM-ION BATTERY

Samuel D. Widijatmoko

Thesis submitted to the University of Nottingham for the degree of Doctor of Philosophy

June 2020

Abstract

This thesis aims to design and develop environmentally friendly process by using mineral processing technique in liberating and concentration positive electrode active material. The original contribution to the body of knowledge is related to the unique insights into the selective liberation of lithium-ion battery (LIB) by applying cutting mill and attrition scrubbing aim at concentrating $LiCoO_2$ particles.

The current research practice often involves the use of organic solvent such as n-methyl-pyrrolidone (NMP) to dissolve the polyvinylidene fluoride (PVDF) to obtain $LiCoO_2$ concentrate. However, the use of mechanical treatment to effectively liberate $LiCoO_2$ is still under examined.

This study is carried out by employing mineral processing techniques. The initial liberation by using only cutting mill produce selective liberation with optimum cut point of 850 μm. However, 56.3 wt% of $LiCoO_2$ active materials are still held together by the PVDF binder and laminating the surface of the current collector in the size fraction of > 850 μm. This result suggests that the selective liberation by only using cutting mill is sub-optimum.

The lack of liberation prompted the use of attrition scrubbing as a secondary stage of mechanical treatment. Attrition induces abrasion and it is shown to effectively liberate the $LiCoO_2$ particles. The proof of concept shows 80.0 wt% $LiCoO_2$ particles can be recovered in the size region of < 38 μm with 7.0 wt% aluminium and 6.1 wt% copper recovery, making attrition scrubbing a suitable second stage mechanical treatment for the recovery of $LiCoO_2$ particles. The relative breakage rate between $LiCoO_2$, copper and aluminium during attrition have

also been studied. To further the discussion, parameters affecting attrition scrubbing liberation have been studied and presented.

The proof of concept to further separate the attrition product have also been reported. The separation techniques involve electrostatic separation to separate copper and aluminium in the larger size fraction (> 38 µm) and froth flotation to separate the graphite from the finer size region (< 38 µm).

Dedication

I dedicated this entire work to the memory of my father, Widijatmoko Ngadijoto, you used to tease me that I need to do a PhD. You are gone but I believe this work make you proud.

This page is intentionally left blank.

Acknowledgement

This page intentionally left blank.

Affirmation

I certify that the work presented in this thesis is, to the best of my knowledge and belief, original and my own work except as acknowledged in the thesis. I hereby declare that I have not submitted this material, either in whole or part, for a degree at this or any other institution.

This page is intentionally left blank.

List of Publications

GU, F., GUO, J., YAO, X., SUMMERS, P. A., WIDIJATMOKO, S. D. & HALL, P. 2017. An investigation of the current status of recycling spent lithium-ion batteries from consumer electronics in China. Journal of Cleaner Production, 161, 765-780. https://doi.org/10.1016/j.jclepro.2017.05.181

WIDIJATMOKO, S. D., GU, F., WANG, Z. & HALL, P. 2020. Selective liberation in dry milled spent lithium-ion batteries. Sustainable Materials and Technologies, 23, e00134. https://doi.org/10.1016/j.susmat.2019.e00134

WIDIJATMOKO, S. D., FU, G., WANG, Z. & HALL, P. 2020. Recovering lithium cobalt oxide, aluminium, and copper from spent lithium-ion battery via attrition scrubbing. Journal of Cleaner Production, 260, 120869. https://doi.org/10.1016/j.jclepro.2020.120869

The evidence supporting refereed status of publications are available in Appendix I.

This page is intentionally left blank.

X

Table of Contents

List of Figures

List of Tables

This page is intentionally left blank.

Chapter 1 Introduction

1.1 Rechargeable batteries

Energy is the basis of our modern lifestyle. The majority of our global energy needs are met from burning fossil fuels. Wind and solar energy are present throughout the world and can be converted locally into electrical energy. The electrical energy derived from such sources requires a degree of concentration prior harvesting, and its sporadic nature has challenged its on-demand availability therefore storage solutions are required.

Nature stores energy in many sophisticated forms and this stored energy has benefited the entire human population. With fossil fuels, nature's energy is stored as chemical energy. Fossil fuel marks the storage of solar energy over hundreds of millions of years. Fossil fuel is converted into energy using combustion producing greenhouse gases and other pollutants which have a significant environmental effect. In a shorter time-frame, nature stores energy in the form of biomass and hydropower which can be used to produce electricity. Solar and wind provide a potentially abundant source of energy. The currently challenge is to convert solar and wind energy into on-demand energy sources that are available at all times. To overcome the sporadic nature of renewable energy, electrochemical energy storage has been gaining importance.

The use of electrochemical energy storage has become an everyday requirement in our daily life in the form of batteries which are needed to power everything from mobile phones to cars. Such electrochemical technologies have offered the interconversion of electrical and chemical energy on a minute

by minute time-frame. A battery cell consists of two electronically conductive electrodes. The positive and negative electrode are separated from each other by an electrolyte. There are two types of batteries that can be found on the market; based on whether it can be recharged or not. Small, low power consumption electronics such as a TV remote may use the non-rechargeable battery as its power source. However, for more complex electronic equipment that requires higher power consumption such as mobile phones and electric vehicles, rechargeable batteries are used as it produces less waste and is more cost-effective in the long run.

The invention of rechargeable batteries have allowed us to have a mobile and reliable access to electricity. Rechargeable batteries can only be used for a certain number of cycles of charging and discharging before they begin to fail and require replacing with new batteries. This irreversible process is ageing, and is a time-progressive decline in the capability and functionality of a battery. The second law of thermodynamics states that the natural tendency of things is to increase in disorder, also known as entropy. The second law of thermodynamics also holds a deep and profound implication; that is, time always flows in the direction of increasing entropy. This by implication means that ageing is irreversible as well and batteries have finite life.

The demand for rechargeable batteries is increasing every year with no evidence on how to combat the ageing process. This has led to a large increase in the number of rechargeable batteries requiring disposal or recycling.

Rechargeable batteries are available on the market in many different types; the most common types include lead-acid battery, nickel cadmium (Ni-Cd) batteries, nickel-metal hydride

(NiMH) batteries, and lithium-ion (Li-ion) batteries. From the different types of rechargeable batteries in the market, the lithium-ion battery (LIB) is still the main choice for most consumer electronics.
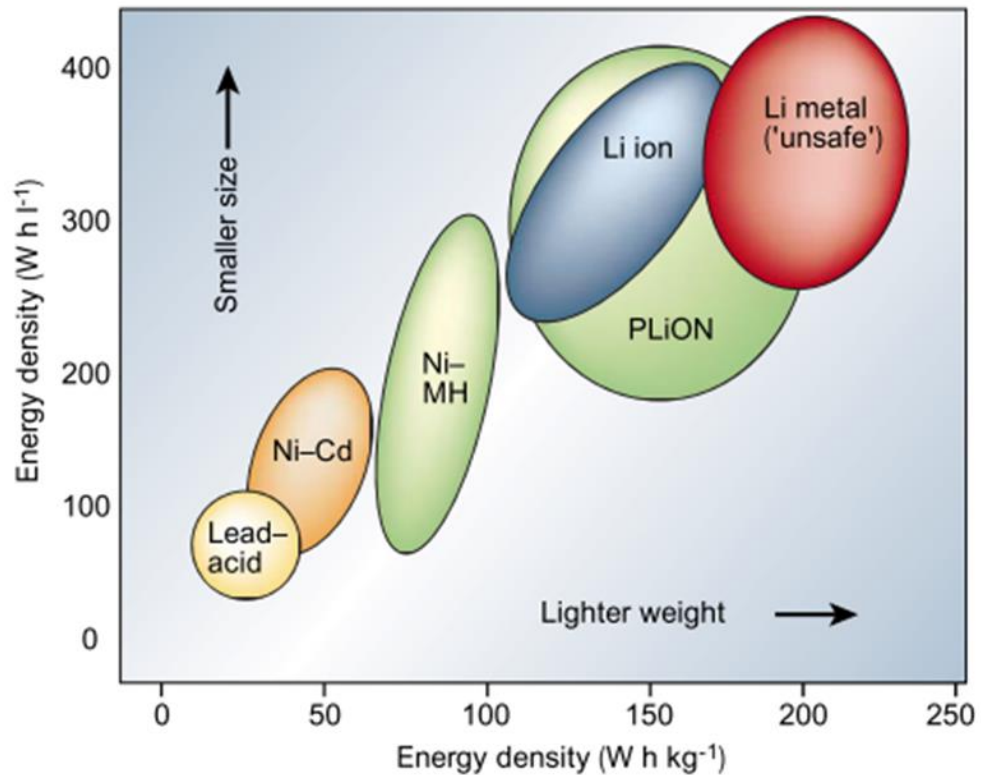
Figure 1-1 – Comparison of the different batteries technologies in terms of volumetric and gravimetric energy density (Tarascon and Armand, 2001).

Figure 1-1 shows that lithium-based batteries can be manufactured smaller and lighter while having equal amount of stored energy compared to other rechargeable batteries. This has allowed the domination of LIB in all type of consumer electronics. Today most portable electronic devices and electric vehicles are being extensively powered with LIB's (Crawford et al., 2018). Furthermore, presently LIBs meets most of the requirements dictated by the large volume of the applications linked to renewable energy (Winslow et al., 2018, Crawford et al., 2018). With the ever-growing need for LIBs, a large amount

of LIBs consequently enter the waste stream ([Huang et al., 2018](#)). Moreover, the LIBs contain highly critical metal resources and are defined as hazardous waste. They require special treatment and especially recycling to minimise the risk to the environment and the depletion of critical metals ([Olivetti et al., 2017](#)).

1.2 The Lithium-ion battery
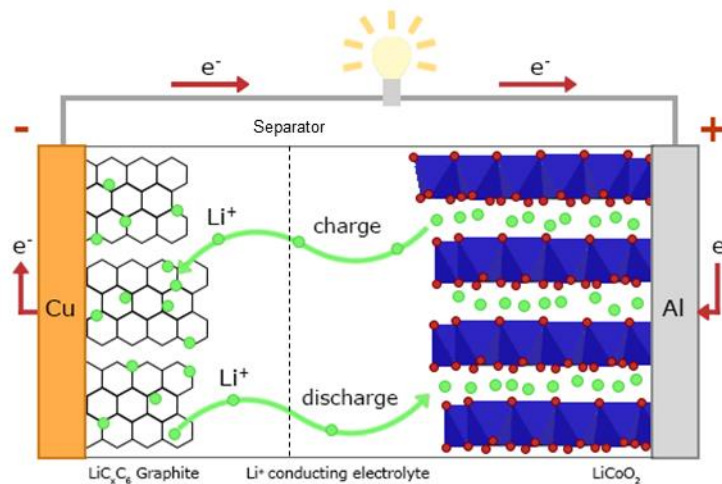
Figure 1-2 - Main components of a LiCoO$_2$/ graphite battery cell (current direction for discharging mode only; re-drawn from ([Gallo et al., 2016](#))).

A battery may consist of one or several cells that may be connected in series or parallel. In its conventional form, the main component of LIBs cell comprises of a graphite negative electrode (e.g. mesocarbon microbeads, MCMB) with a copper foil current collector, a positive electrode formed by a lithium-transition metal-oxide (Li-M-O$_2$, e.g. LiCoO$_2$) with an aluminium current collector, a liquid electrolyte consisting of lithium salts (e.g. LiPF$_6$) in a mixed organic solvent (e.g. ethylene carbonate-dimethyl carbonate, EC-DMC), all imbedded in a separator layer (e.g. polypropylene/ polyethylene, PP/PE). The active materials for positive and negative electrode are in the form of powder, cast onto the current collector and held by a

binder, commonly polyvinylidene fluoride (PVDF) (Zeng et al., 2014, Moradi and Botte, 2016). During discharging, Li^+ ions move from the negative electrode to the positive electrode, through the non-aqueous electrolyte and separator diaphragm while the reverse process occurs during charging (Figure 1-2). The Li^+ ions are nested in the porous electrode active materials in a process known as intercalation (Su et al., 2012).

Although LIBs represent a great success in modern electrochemistry, they are still susceptible to ageing, causing capacity loss and cell impedance and need to be replaced. During the first charge, a solid interface on the electrolyte/graphite electrode in naturally created, termed the Solid Electrolyte Interphase (SEI) (Arora and White, 1998). The SEI plays an important role in protecting the negative electrode from corrosion and electrolytes from reduction (Gallo et al., 2016, Peled and Menkin, 2017). However, the SEI is unstable as it works outside the design voltage. Lithium plating can also occur as a side reaction, where lithium ions are reduced to metallic lithium instead of intercalating into the negative electrode active material (Ecker et al., 2017). The plated lithium is highly reactive and reacts directly with the electrolyte creating the SEI (Leng et al., 2017). This causes the SEI to develop over time, which induces the continuous loss of lithium ions and electrolyte decomposition. Further cycling of LIBs also results in exfoliation of the graphite electrode and a structural change in the positive electrode active materials (Leng et al., 2017, Song and Jeong, 2018). Intensive research is still required in developing an optimum SEI and better positive electrode active materials to prolong the LIB lifespan (Blomgren, 2017, Peled and Menkin, 2017).

As the demand for LIBs has increased, this has led to a large amount of waste being generated. Spent LIBs are considered to be hazardous waste and should not be released into the environment (Winslow et al., 2018). However, the collection and recycling rates of LIBs are low (Gu et al., 2017). In the past decade, LIBs contained within consumer electronics were relatively small in size and were generally stored by the consumer or disposed of improperly through landfill at the end-of-life. There is the need to tackle the LIB waste stream now as it will promote the circular economy and mitigate resource scarcity (Prieto-Sandoval et al., 2017, Swain, 2017). This has led to extensive research into the processing for the recovery of valuable metals found in spent LIBs.

LIBs are made from several different components as previously described. The positive electrode active materials being the most targeted component for recycling, which is where the incentive of LIBs recycling originated (Richa et al., 2017). To date, $LiCoO_2$ is the most common positive electrode active material found in small devices due to its high tap density and maturity in its production (Zhou et al., 2017). Electric vehicles are more likely to use nickel-rich, $LiNi_xCo_yMn_zO_2$ (x>0.6, NMC), active materials with the current day generation employing $LiNi_{0.5}Co_{0.2}Mn_{0.3}O_2$ (NCM523) due to its higher energy density (Schipper et al., 2017). For this reason, modern high energy density LIBs tend to contain imbedded cobalt, which have the highest commodity value when compared to other battery components (Table 1-1).

Table 1-1 - Price comparison of metals found in spent LIBs (LME, 2019, SMM, 2019).

Metal	Price (US$ tonne^{-1})
Cobalt[a]	31,500.00
Nickel[a]	15,755.00
Lithium[b*]	13,000.00
Copper[a]	5,675.00
Aluminium[a]	1,746.00
Manganese[a]	1,592.00
Iron[a]	294.00

[a]London Metal Exchange (23rd August 2019)

[*]Price of Lithium Hydroxide (LiOH)

[b]Shanghai Metal Market (23rd August 2019)

Next-generation nickel rich active materials are in development. Probabilistic estimates, up to 2030, show an improvement in battery chemistry and manufacturing are possible, leading to cost reduction and performance improvement. However, these estimates are not inevitable (Few et al., 2018). This uncertainty plays an important role in the recovery of positive electrode active materials.

1.3 Research landscape of lithium-ion battery recycling

Current strategies to recover positive electrode active materials from LIBs may be classified into four major categories: (1) Physical process, (2) Chemical process, (3) Bioleaching, and (4) Resynthesizing.

1.3.1 Physical processes

Physical processes are pre-treatment steps to liberate and concentrate positive electrode active materials from other components such as current collectors and binders to facilitate

the downstream processes. Physical processes exploit the different physical characteristics of different components contained within LIBs. The difference in the physical property of LIBs components such as density, magnetic properties, conductivity, solubility, and hydrophilicity are the foundation of physical separation.

The mechanical separation processes aim to concentrate positive electrode active materials by means of crushing (Diekmann et al., 2017, Wang et al., 2016c, da Costa et al., 2015, Zhang et al., 2014a), sieving (Wang et al., 2016c, Zhang et al., 2014a, Zhu et al., 2011), flotation (He et al., 2017b, Yu et al., 2017, Yu et al., 2018, Zhang et al., 2014b, Zhan et al., 2018), gravity separation (Diekmann et al., 2017, da Costa et al., 2015, Zhu et al., 2011, Marinos and Mishra, 2015, Bertuol et al., 2015), and magnetic separation (Gratz et al., 2014).

Liberation

The liberation is carried out via size-reduction or comminution techniques that expose the desired material as well as giving size range adjustment. Prior to liberation, LIBs require discharging to minimise the fire hazards associated with potential runaway reactions during mechanical liberation processes (Diekmann et al., 2017). Other precautions can also be carried out such as using an inert atmosphere as well as low-temperatures (Diekmann et al., 2017, Dorella and Mansur, 2007).

Size-based separation (sieving)

Sieving is a preliminary physical process following liberation. The aim of sieving is to separate different materials based on size. Several researchers suggest that the materials contained within the LIBs are reduced to different size ranges (Zhang et

al., 2013, Yu et al., 2018, Silveira et al., 2017). For instance, the electrode active materials are concentrated in the finer size region (< 1 mm) while the polymeric materials, current collector, and chassis are concentrated in the coarser size fraction (> 1 mm) (Wang et al., 2016c). The combination of liberation and sieving allows the various components to be separated into a controllable range of particle size. The benefit of liberation and sieving also suggested being useful for the downstream process, such as leaching (Shin et al., 2005).

Flotation

Flotation is a physicochemical process that exploits the difference in the surface wettability of different component. The particles that is hydrophobic or made hydrophobic is floated and collected as lauder. Whereas the hydrophilic particles are collected as sink. Positive electrode active materials are hydrophilic and graphite negative electrode active materials are hydrophobic (Zhan et al., 2018). However, it requires the prior removal of PVDF binder that is hydrophobic (Zhang et al., 2014b). Thus, surface modification is carried out before flotation (Yu et al., 2017, He et al., 2017b).

Density separation

The gravity separation allows the separation of different components based on their difference in density. The difference in density would result in a different relative movement when subject to a flowing media such as air (Diekmann et al., 2017, Bertuol et al., 2015). Other components which contain ferrous metals can be separated using magnetic separation (Shin et al., 2005, Xu et al., 2008).

9

1.3.2 Chemical processes

Chemical processes include a process that inherently alters either the atomic, molecular composition or the structure of a component involved. Chemical process can be broken down into thermal treatment, mechanochemical, leaching, purification (i.e. precipitation and extraction) which recover cobalt and lithium in the form of a compound.

Thermal treatment

Thermal treatment includes the heating of materials at an elevated temperature to remove certain component such as polymeric material, binder, and electrolytes from spent LIBs to liberate active materials from the current collector (Zheng et al., 2016, Lee and Rhee, 2002, Zhang et al., 2016, Sun and Qiu, 2011, Lu et al., 2013). Other than being the removal of the certain component inside LIBs, a form of thermal treatment called pyrolysis is able to produce compound or pristine electrode active materials (Hu et al., 2017, Li et al., 2016, Xiao et al., 2017b, Xiao et al., 2017a).

Thermal treatment often requires demanding gas emission standard and high energy requirement. The simplicity of thermal treatment has been outweighing by the potential pollution it can be generated. In practice, thermal treatment often used as a pre-treatment process prior to any other processes.

Mechanochemical

Mechanochemical process refers to the chemical process that is driven by mechanical energy, which often supplied by high energy milling (Ou et al., 2015, Baláž et al., 2013). Other than size reduction, the mechanochemical process inherently differs from a mechanical process in which the crystal structures of the

active materials in LIBs have been altered. Mechanochemical often used as a pre-treatment process to facilitate leaching by forming a readily dissolve compound by means of chelating agent or surface active grinding media (Zhang et al., 2000, Guan et al., 2016, Wang et al., 2016b, Saeki et al., 2004, Wang et al., 2017).

Leaching

Leaching is the transfer of metals from active materials into solution. This is done by employing acidic or alkaline lixiviant to dissolve cobalt and lithium. The selectivity towards the metals being used can also be adjusted such as in the case of nickel and cobalt, in which it forms a stable ammonia complex (Ku et al., 2016, Zheng et al., 2017b). In the same way as thermal treatment and mechanochemical treatment, leaching is considered to be a pre-treatment process. The leaching efficiencies would set the trajectory of the following purification and hence the overall recovery of metals.

Researchers have extensively studied the use of acid leaching to achieve high leaching efficiencies of both cobalt and lithium by means of HCl (Li et al., 2009b, Barik et al., 2017, Wang et al., 2009, Li et al., 2009a, Takacova et al., 2016, Zhang et al., 1998, Liu and Zhang, 2016), H_2SO_4 (Nan et al., 2005, Shin et al., 2005, Zheng et al., 2016, Meshram et al., 2015b, Li et al., 2017a, Zhu et al., 2012, Swain et al., 2007, Kim et al., 2014, Ferreira et al., 2009, Jha et al., 2013b, Mantuano et al., 2006, He et al., 2017a), HNO_3 (Lee and Rhee, 2002, Kim et al., 2014, Castillo et al., 2002), and H_3PO_4 (Chen et al., 2017, Pinna et al., 2017, Meng et al., 2017). To achieve high efficiency, leaching with the presence of reductant such as H_2O_2, $Na_2S_2O_3$ or glucose are often employed to manipulate the metal oxidation states (i.e. Co^{3+} converted to a more soluble Co^{2+})

(Meshram et al., 2015b, Meng et al., 2017, Granata et al., 2012a, Meshram et al., 2015a, Tanong et al., 2017, Joulié et al., 2017, Pagnanelli et al., 2014, Wang et al., 2012b). However, leaching with a strong acid such as HCl, HNO$_3$, and H$_2$SO$_4$ may potentially cause secondary pollution problems (toxic gas and water emission) being the downside of this method. To eliminate the pollution problems that have been encountered by the mineral acids, the use of organic acid has been gaining popularity in the recent years (Li et al., 2018b, Zeng et al., 2015, Chen et al., 2015b, Chen et al., 2016c, Nayaka et al., 2016c, He et al., 2016, Li et al., 2015b, Gao et al., 2017, Nayaka et al., 2016b, Li et al., 2010b, Li et al., 2010a, Sun and Qiu, 2012, Li et al., 2013a, Nayaka et al., 2015, Nayaka et al., 2016a, Golmohammadzadeh et al., 2017).

Leaching has been explored to an extent that the mechanisms have been well understood. There are four leaching mechanism models which have been investigated for kinetic studies; the shrinking core (Zheng et al., 2017b, Jha et al., 2013b, Zeng et al., 2015, He et al., 2016, Gao et al., 2017), the empirical (Meshram et al., 2015b, Chen et al., 2017, Meshram et al., 2015a), Avrami (Zhang et al., 2015), and the revised cubic rate law (He et al., 2017a). From the four leaching models, the shrinking core models achieve the most agreement within the literature. The shrinking core models explain that the particles undergo loosening-breaking-shrinking change during the acid leaching process. In accordance with the shrinking core model, the leaching reactions are subject to liquid film mass transfer, surface chemical reactions, and residue layer diffusion.

Chemical precipitation

The metals dissolved during leaching can be made into a separable solid substance from the solution. This is done by

changing the composition of the solvent to change the solubility and precipitate the metal of interest. For example, the cobalt and lithium from leach liquor can be recovered through precipitation, in which insoluble compound is from via precipitants such as sodium hydroxide, oxalic acid, ammonium oxalate, and sodium carbonate. The precipitated compound that have been reported include cobalt hydroxide (Contestabile et al., 2001, Pegoretti et al., 2017), cobalt oxalate (Nan et al., 2005, Li et al., 2017a, Chen et al., 2015b, Nayaka et al., 2016b, Sun and Qiu, 2012, Nayaka et al., 2015, Wang et al., 2016a, Chen et al., 2011), lithium phosphate (Yang et al., 2017b, Pinna et al., 2017, Chen et al., 2015b, Guo et al., 2017), and lithium carbonate (Nan et al., 2005, Zhu et al., 2012, Granata et al., 2012a, Gao et al., 2017).

Other than to recover the precious elements contained within spent LIBs, precipitation has been proposed to remove trace amount of impurities such as iron, copper, or aluminium (Granata et al., 2012a, Chen et al., 2011, Zheng et al., 2017a, Joo et al., 2016b). However, the removal of impurities have not been adopted by many and still relies on manual dismantling and aluminium dissolution using NaOH followed by calcination to remove binder (Senćanski et al., 2017, Ziemann et al., 2018) or dissolution of binder by using N-Methyl Pyrrolidone (NMP) to obtain a high grade positive electrode active materials concentrate prior leaching (He et al., 2015, Xin et al., 2016, Nayaka et al., 2016c).

Also, the chemical precipitation separation process requires careful control of parameters related to different solubility for a different compound such as pH and temperatures.

Solvent extraction

Solvent extraction is a process in which a two-phase system exists, which contains an organic and an aqueous phase. The separation is achieved by the concentration gradient in different phases and carried out after leaching. High selectivity extractant has been reported, such as bis-(2,4,4-tri-methyl-pentyl) phosphinic acid (Cyanex 272)(Granata et al., 2012b, Jha et al., 2013a, Kang et al., 2010, Nan et al., 2006, Pagnanelli et al., 2016, Pranolo et al., 2010, Swain et al., 2008), phosphonic acid mono-2-ethylexyl ester (PC-88A) (Suzuki et al., 2012, Joo et al., 2015, Wang et al., 2012a), triocetylamine (TOA) (Suzuki et al., 2012, Virolainen et al., 2017), and di-(2-etylhexyl) phosphoric acid (D2EHPA) (Granata et al., 2012b, Pagnanelli et al., 2016, Chen et al., 2015a, Joo et al., 2016a), and able to separate specific transition metals while leaving lithium ion in the aqueous solution.

Solvent extraction only requires ambient temperature with a relatively short amount of time to produce high purity metal products. The downside of this process lies in its complexity and the high cost of solvent.

Apart from the chemical processes described above, other processes such as recrystallization and electrodeposition have also been extensively studied (Ferreira et al., 2009, Barbieri et al., 2014a, Barbieri et al., 2014b, Freitas et al., 2010, Lupi et al., 2005).

1.3.3 Bioleaching

Bioleaching combines chemistry, biology, and metallurgy, which requires further attention to understand its potential. Recently, bioleaching of spent LIBs has gained attention from researchers (Li et al., 2013b, Bahaloo-Horeh and Mousavi,

2017, Cerruti et al., 1998, Horeh et al., 2016, Mishra et al., 2008, Xin et al., 2009). Bioleaching is carried out by employing chemolithotropic and acidophilic bacteria to produce metabolites such as sulphuric acid and ferric ions to facilitate leaching with elemental sulphur and ferrous ions as substrate (Li et al., 2013b, Mishra et al., 2008, Xin et al., 2009). Other than bacteria, fungi have also been reported to produce organic acid that facilitates dissolution (Bahaloo-Horeh and Mousavi, 2017, Horeh et al., 2016).

1.3.4 Re-synthesis of positive electrode active material

To have a closed loop recycling process that relies on hydrometallurgy, it is then important to be able to re-synthesis the solutions obtained from acid leaching. The new positive electrode active materials can be re-synthesis via thermal treatments (Nie et al., 2015, Zhang et al., 2016, Chen et al., 2016a, Chen et al., 2016b, Kim and Shin, 2013, Zhang et al., 2014c, Song et al., 2017), co-precipitation (Gratz et al., 2014, Zheng et al., 2017a, Zou et al., 2013, Sa et al., 2015b, Weng et al., 2013, Sa et al., 2015a), and sol-gel methods (Li et al., 2017b, Yao et al., 2015, Yao et al., 2016a, Li et al., 2018a). Re-lithiation is another type of resynthesizing in which positive electrode active materials were treated by adding lithium via electrochemical or thermal treatment into the positive electrode active material crystal without going through leaching (Ganter et al., 2014, Kim et al., 2004).

1.4 Pyrometallurgical treatment

Pyrometallurgical or thermal treatment involves the smelting of battery components at elevated temperatures. This process only allows metallic elements to be recovered. Components such as polymeric materials and graphite were burned off or serve as a reductant for some of the metals (Dunn et al., 2014, Gaines et al., 2011, Moradi and Botte, 2016).
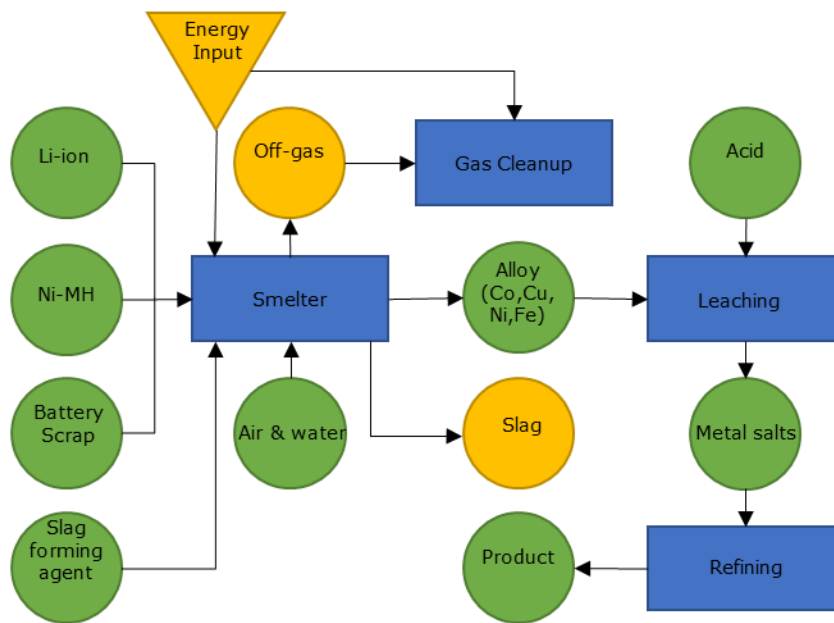
Figure 1-3 – Schematic diagram of Umicore pyrometallurgical battery recycling process, re-drawn from (Sonoc et al., 2015).

Umicore, Belgium, has developed the VAL'EASTM process for recycling batteries, including LIBs (Figure 1-3). The process is based on pyrometallurgical methods. The spent LIBs are introduced to a high temperature (1400°C) smelter with no pre-treatment processes (Moradi and Botte, 2016). The organics materials such as plastics, electrolytes, and solvent are burnt. On the other hand, graphite present acts as a reducing agent. The alloy product is then treated via leaching to recover the cobalt and nickel as a precursor. Whereas, the lithium, aluminium, and manganese is loss as slag.

To date, pyrometallurgical treatment is not considered a suitable choice for LIBs recycling. Pyrometallurgical treatment is neither economically feasible nor environmentally friendly. While most metals are recovered as elements by this process, lithium and aluminium are end up in the recycling slag and not economically feasible to be recovered (Gaines et al., 2011). Umicore claims that the use of recycled cobalt would reduce the energy required to produce $LiCoO_2$ active materials by 70 % (Gaines et al., 2011). However, this process has not taken into account the potential cobalt reduction in the manufacturing of LIBs in the near future. Cobalt has been the most expensive elements in a battery component. A reduction in the amount of cobalt found in LIBs would be made the Umicore's processes uneconomical.

1.5 Hydrometallurgical treatment
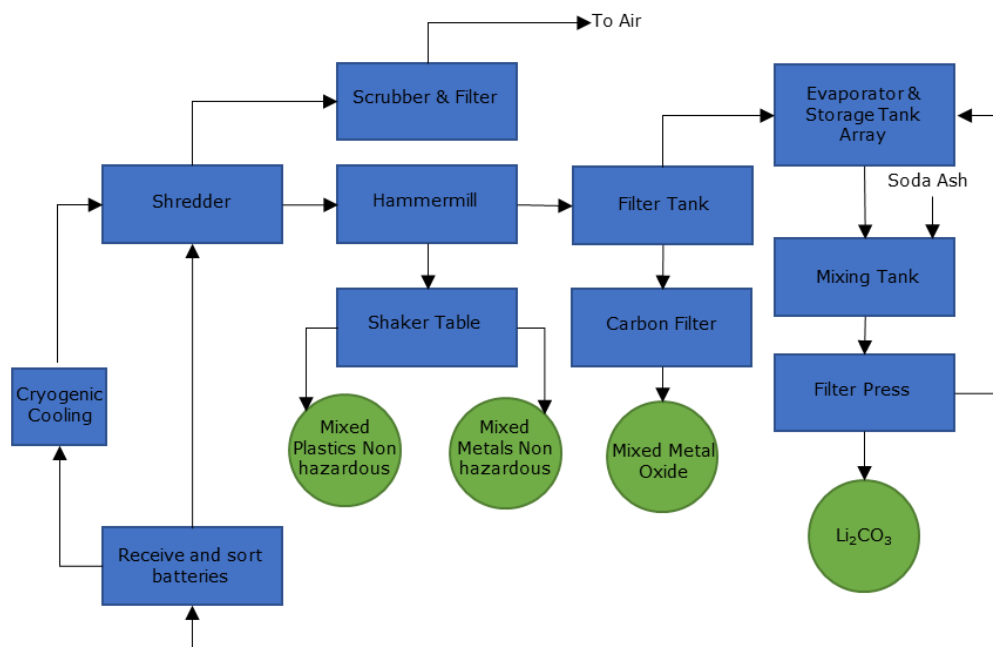
Figure 1-4 – Schematic diagram of Toxco recycling process, re-drawn from (Gaines et al., 2011).

Hydrometallurgical processes involve the use of acid or base to leach the components inside the LIBs and are followed by

17

purification processes such as chemical precipitation, filtration, solvent extraction, and electrochemical winning. This method allows the total recovery of metal components in LIBs. Negative electrode active materials may also potentially be recovered in this process.

Most of the developed commercial recycling processes for LIBs are the hydrometallurgical processes. Toxco Incorporated, has developed a series of low temperature mechanical and chemical processes to recover key components in spent LIBs (Figure 1-4). Lithium dissolution is carried out during milling using hammer mill (Saloojee and Lloyd, 2015). There are three streams of materials from the Toxco process. The first stream contains mainly plastics. The second stream is rich in cobalt, copper, nickel, and aluminium. The third stream contains cobalt and other metal oxide. It is not clear in open literature whether cobalt is separated from other metals and this is achieved (Kellner and Goosey, 2019). Lithium carbonate is separated from the resulting solution by using soda ash.

AEA Technology Batteries, United Kingdom, have designed and developed a sequence of mechanical treatment, solvent extraction, and electrochemical processes for the recovery of LIBs (Lain, 2001). The electrolyte is recovered through extraction. The active materials are detached from the current collector by dissolving the binder followed by filtration. The separated positive and negative electrode active materials are free from current collectors, plastics, and steel. Eventually, the lithium and cobalt are separated using an electro-reduction process that reclaims lithium and cobalt in its elemental form.

1.6 Direct physical treatment

The direct physical process is designed for the recovery of key components in its original form as it is found in spent LIBs. The process involves a series of mechanical processes with low temperature and energy required to separate the battery components. This process can recover all active materials and metals, except for the separator. In order to turn the recovered materials into battery grade materials, an extra step of purification or activation is required (Moradi and Botte, 2016). However, such a process is still in development and not commercialised yet (Dunn et al., 2014).
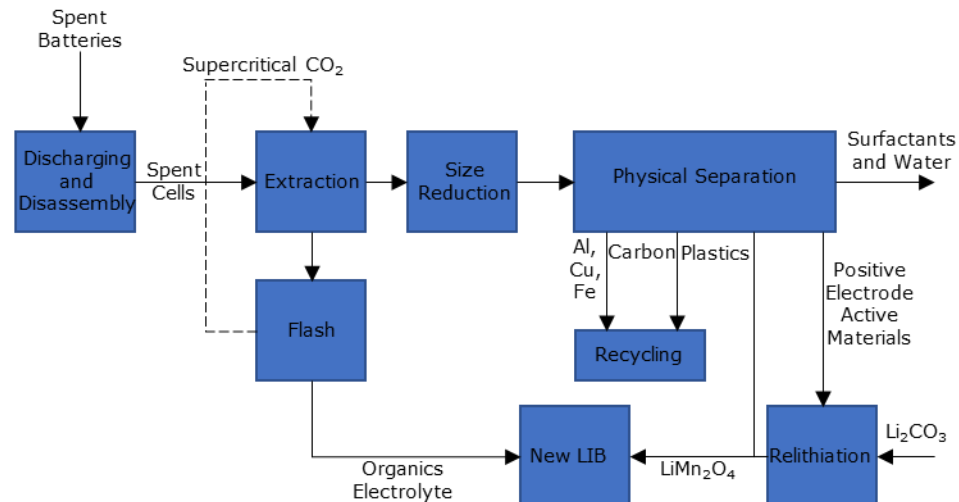
Figure 1-5 – Schematic of Eco-Bat direct physical recycling process for spent LIBs with LiMn$_2$O$_4$ positive electrode active material (Dunn et al., 2014).

Eco-Bat Technologies, mainly focussed on closed loop recycling of lead-acid batteries (the materials recovered can be re-used to fabricate fully functioning lead-acid battery), have developed a bench-scale LIB recycling process (Moradi and Botte, 2016). The components are recovered as high-quality battery grade materials. The process is shown in Figure 1-5, and it is noted that there is minimum energy consumption in separating and concentrating the key components of LIBs. The battery

19

undergoes minimal disassembly. To extract the electrolytes, supercritical carbon dioxide extraction is used. Afterwards, the battery undergoes size reduction. A series of separation processes based on the difference in electrical conductivity and density such as capacitor plates, a cyclonic fluidised bed, and solution dispersion followed by decantation and filtration are also used. Using this method, components such as the electrode active materials, chassis, and current collector are recovered without taking them back to elemental form. From this entire process, only the separator is not recycled.

1.7 The consequence of battery chemistry for the recycling of LIBs
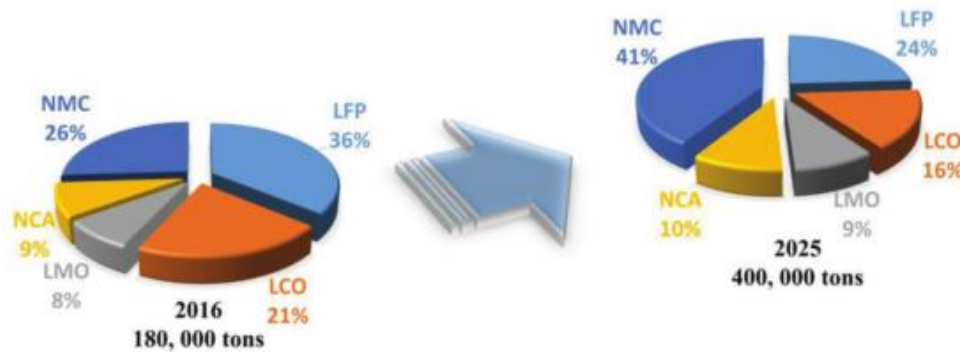
Figure 1-6 – Mass per cent of all LIBs shares of the leading materials in 2016 forecasted to 2025 (Li et al., 2018c).

The positive electrode active materials are the main cost when manufacturing of LIBs (PILLOT, 2013). The recovery of cobalt has been the main objective of LIB recycling due to its high value (Gaines, 2018). However, as the cobalt content decreases, due to the shift of preference of active materials from lithium cobalt oxide (LCO) to other types of active material those are relatively cheaper with higher energy density (Figure 1-6). From Figure 1-6, the biggest increase is expected to come from the lithium nickel manganese cobalt oxide (NMC) battery chemistry. The reported composition of different LIBs with

different positive electrode active materials are summarised in Table 1-2. It can also be seen from Table 1-2 that the cobalt content in NMC battery is eight times lower than that of LCO.

Table 1-2 - Different composition of LIBs with different positive electrode active material (Richa et al., 2014, Wang et al., 2014).

Materials	LCO wt%	LFP wt%	LMO wt%	NMC wt%
Aluminum	5.2	6.5	1.1	8.5
Cobalt	17.3	0.0	0.0	2.0
Copper	7.3	8.2	1.1	16.3
Lithium	2.0	1.2	1.5	2.4
Manganese	0.0	0.0	20.4	7.5
Nickel	1.2	0.0	0.0	8.0
Steel/ Iron	16.5	43.2	16.5	0.0
Phosphorus	0.0	5.4	1.1	0.0
Graphite	23.1	13.0	33.6	20.6
Carbon black	6.0	2.3	0.0	2.0
$LiPF_6$	3.7	1.2	0.0	14.7
EC/ Other	10.3	13.7	0.3	10.4
Binders (PVDF)	2.4	0.9	0.0	2.8
Plastics	4.8	4.4	20.1	4.9
Total (wt %)	100.0	100.0	100.0	100.0

Table 1-3 – Difference in recycling revenue for different active materials.

Active Material	Revenue* (US$)/ tonne
$LiCoO_2$ (LCO)	7,503.31
$LiFePO_4$ (LFP)	1,473.74
$LiMnO_2$ (LMO)	1,730.82
$LiNi_{1/3}Co_{1/3}Mn_{1/3}O_2$ (NMC)	4,530.46

*Does not include production cost.

The difference in revenue for different active materials is summarised in Table 1-3. The calculation assumes that the components in the LIB are recovered as metals, graphite is recovered, and organic materials are not being recovered. From Table 1-3, LCO batteries have the highest revenue as compared to other types of LIBs. The NMC revenue contains less cobalt, this is compensated by the higher concentration of lithium, nickel, manganese, and aluminium. Despite the over eight-time reduction of cobalt content in NMC batteries, the potential revenue of NMC batteries is only decreased by 39.6% when compared to LCO batteries. However, much of the developed methods have been designed for LCO batteries. The pyrometallurgical process developed by Umicore may not be economically feasible for NMC batteries (Moradi and Botte, 2016). Both hydrometallurgical treatments developed by Toxco Incorporated and AEA Technology Batteries would also be economically questionable for batteries apart from LCO (Gaines, 2018). The direct physical recycling process is still in development and not commercialised yet.

From the three major processes reported for LIBs recycling, although they have not yet been commercialised, the direct physical recycling process is the most favoured route. Especially when the materials contained within a battery are recovered in its physical and chemical form. Moreover, the revenue for recycling would also increase as the positive electrode active materials are more valuable as a compound than that of the constituent elements.
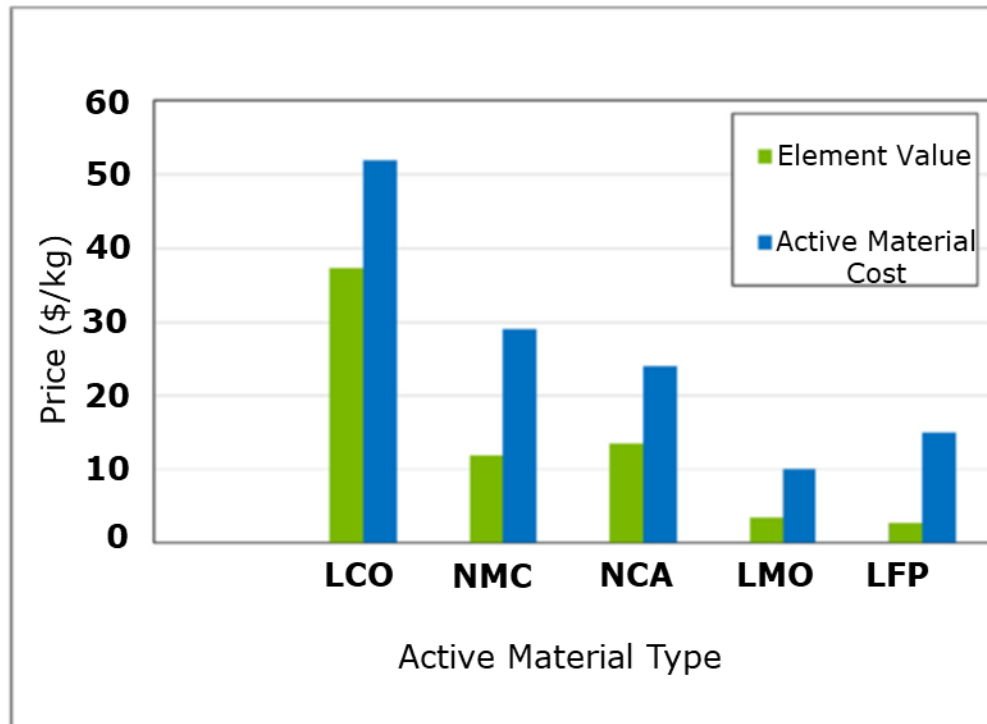
Figure 1-7 – Comparison of positive electrode active material cost to constituent element cost, re-drawn from (Gaines, 2018).

The positive side of breaking down the structure of positive electrode active materials into a component is that the generic products allow versatility of use. Meaning, the products are not specified to a particular positive electrode active materials structure and therefore can be used as an input to produce a wide range of material while the product of direct physical recycling process has a well-defined positive electrode active material structure. Although the retention of active material structure can be seen as an advantage (Figure 1-7), the input of this process requires prior segregation of batteries based of the same type of positive electrode active materials or the resulting product mixture would be of significantly reduced value (Gaines, 2018).

1.8 Bridging the research-industry divide

There is the need to recycle the spent LIBs generated as it contains valuable metals that is finite to minimise the supply disruption risk. The recycling of spent LIBs has been extensively studied, and different processes have been proposed. The processes can be classified into modular characteristics of physical, pyrometallurgical, and hydrometallurgical treatment. The combination of such a process is often employed to achieve an acceptable separation and purity of precursor compounds.

It is projected that the future positive electrode active materials would have a reduced content of cobalt. This then challenges the economic feasibility of the recycling process that has been implemented at the industrial scale (Ciez and Whitacre, 2019). Pyrometallurgical treatment would be obsolete due to several reasons such as; energy intensity, demanding gas emission standards, and loss of lithium and aluminium as slag. Therefore, the reported research mainly deals with low temperature processes.

As far as the recycling LIBs are concerned, research surrounding the recovery of positive electrode active materials have extensively revolved around the hydrometallurgical recovery. This can be understood as the products of hydrometallurgical treatments are of versatile precursor products. Due to the uncertainty regarding the type of positive electrode active materials in the future, hydrometallurgical treatment appears to be a pragmatic option.

The progress that has been made towards hydrometallurgical recycling of positive electrode active materials is apparent. The positive electrode active material solution obtained from

leaching can be turned into a new fully functioning active materials while also providing the versatility as to what type of positive materials is desired. However, there is a key issue that requires further attention. The hydrometallurgical processes that have been reported often rely on manual dismantling. NMP then used to obtain positive electrode active material powder that has minimum copper and aluminium contamination by dissolving the PVDF binder (Peng et al., 2018, Gao et al., 2019, Sun et al., 2018), this is not viable on an industrial scale. The inherent toxicity of NMP to human's reproductive system and its challenging reusability means that this method may not be sustainable.

The used sodium hydroxide to dissolve the aluminium current collector, followed by calcination has been proposed to obtain high-grade positive electrode active materials (Senćanski et al., 2017, Ziemann et al., 2018). However, the recovery of positive electrode active materials is only second to aluminium. High-grade aluminium contained within spent LIBs is the largest contributor to cell material production energy and greenhouse gasses (Dunn et al., 2014). Thus, this process is not environmentally friendly.

The proposed hydrometallurgical processes has been hindered by the use of impractical methods to obtain high-grade positive electrode active materials. Mechanical treatment that is able to produce high-grade positive electrode active materials has also been reported to have a low yield. There is an apparent unbalanced landscape between the hydrometallurgical and physical processes. The mechanical liberation and separation of positive electrode active materials requires further improvement to be able to be retrofitted prior hydrometallurgical processes.

1.9 Aims and objective

Therefore, the aim of this research is to design and develop an environmentally friendly process by using mineral processing techniques in liberating and concentrating positive electrode active materials.

The above aim will be accomplished by fulfilling the following research objective:

1. Review the literature concerning selective liberation in mineral processing and its elucidation in the field of LIBs recycling. Moreover, the literature related to the physical separation and concentration of positive electrode active materials also needs to be explored.

2. Investigate the selective liberation of positive electrode active materials in a dry milled environment.

3. Investigate the selective liberation of positive electrode active materials by using attrition scrubbing as a second stage wet liberation method.

4. Investigate the separation method to recover other battery components, mainly copper and aluminium.

1.10 Thesis outline

This thesis consists of 7 chapters. The following gives a brief description of each chapter contained.

The current chapter, <u>Chapter 1</u> gives a general background context and motivation against which this study was carried out. Introduction regarding the Lithium-ion battery as well as the current strategy to recover positive electrode active materials was briefly discussed in this chapter. Finally, the aims and objective of this work and the outline structure of the thesis are presented.

<u>Chapter 2</u> is a literature review concerning the required knowledge of two topics, namely the physical properties of components that are assembled to make Lithium-ion battery and the physical treatment to liberate and concentrate positive electrode active material.

<u>Chapter 3</u> details the experimental methodology in which the sample preparations and the analysis technique being employed are explained in this section.

<u>Chapter 4</u> covers the selective liberation of positive electrode active materials by using a cutting mill. The comparison between spent and pristine LIBs are made and discussed.

<u>Chapter 5</u> focuses on the further liberating positive electrode active materials by using an attrition scrubber with silica sand as attrition media. Parameters affecting attrition scrubbing in

accordance with the ability to selectively concentrate positive electrode active materials in the finer size region are conveyed.

Chapter 6 concerns the proof of concept to separate copper and aluminium from the attrition media in the coarser size region by using electrostatic separator. Moreover, the collector-less flotation of graphite particles in the finer size region is demonstrated.

Chapter 7 draws together the conclusion of this thesis and discusses the implication of the present findings for research and practice. Possible future work to advance the present research is suggested and discussed.

Chapter 2 Literature Review

2.1 Introduction

The current research landscape in lithium-ion batteries (LIBs) recycling has been laden with physical and hydrometallurgical processes. The ever-decreasing price of LIB and combined with the uncertainty regarding the future of positive electrode active materials type, has challenged the currently available pyrometallurgical treatment in recovering valuable materials from spent LIBs (Diouf and Pode, 2015, Few et al., 2018, Gaines, 2014). The combination of physical and chemical treatment has been perceived by researchers to be an environmentally friendlier and economically more feasible as compared to pyrometallurgical treatment (Vieceli et al., 2018, Winslow et al., 2018, Meng et al., 2018, Diekmann et al., 2017, Yao et al., 2016b). One of the main reasons being the loss of lithium and aluminium as slag (Meshram et al., 2014). Furthermore, the use of high energy treatment would not be economically feasible to keep up with the decreasing price of LIBs (Diekmann et al., 2017).

Physical treatment in the case of LIBs recycling involves the liberation and separation of different components contained within spent LIBs. The liberation of LIBs aims at exposing the different component of LIBs as well as giving size range adjustment for further separation (Zhang et al., 2013, Yu et al., 2018, Silveira et al., 2017). The separation process following liberation may come in the form of magnetic separation, size-based separation (sieving), density separation, and separation based on the difference on surface properties (Wang et al.,

2017, Wang et al., 2016c, da Costa et al., 2015, Zhan et al., 2018). The different types of physical processes can be integrated to form a single line process that allows initial removal of easy to separate material and producing positive electrode active materials concentrate. A positive electrode active material concentrates with a low amount of leachable contamination (i.e. iron, copper and aluminium) may undergo chemical processes and re-synthesized to make positive electrode active materials (Pagnanelli et al., 2017, Li et al., 2018a, Senćanski et al., 2017, Meng et al., 2018, Yang et al., 2017a, Yao et al., 2016b). The combination of physical and chemical processes allows the efficient recovery of different components inside LIBs. The components that do not need to undergo chemical treatment may be minimised in the physical separation stage (Liu et al., 2019a).

From the Scopus database, by January 2020, there are 80 papers that discuss physical processes as compared to 215 papers that discuss chemical processes. It is apparent that more research articles are dedicated for chemical processes than physical processes. There is an imbalance research landscape when physical treatment is compared to chemical treatment. Efficient physical treatment that can produce a positive electrode active material concentrate with minimum contamination of leachable contaminations (i.e. copper and aluminium). This would reduce the cost incurred for subsequent chemical processes. It has been reported that the positive electrode active materials are concentrated in the finer size region (Zhang et al., 2013, Yu et al., 2018, Silveira et al., 2017). This phenomenon is the main advantages of physical treatment in LIBs recycling and is of a unique phenomenon. Nonetheless,

there is a minimum effort from the research community to exploit this selective liberation phenomenon.

The fine size fraction from selective liberation comprises of hydrophilic positive electrode active materials and hydrophobic negative electrode active materials that can be further separated based on the surface difference. However, the positive electrode active materials are still laminated by the PVDF binder that render the particles to be hydrophobic. Mechanical treatment via the ball milling of active materials concentrate has also been reported to be able to partially delaminate PVDF binder that coats positive electrode active materials. The positive and negative electrode active materials can then be separated via froth flotation (Yu et al., 2018).

The progress made in the field of the physical processing of spent LIBs has been minimal as compared to the chemical processing counterpart. Therefore, it is worthy of attention to study and develop mechanical processes that can be used either as a direct physical treatment or meet the requirement for the subsequent hydrometallurgical processes.

This literature review will firstly detail the components inside LIBs and followed by a discussion of the pre-treatment and liberation of spent LIBs components to obtain positive electrode active materials concentrate. The physical processes related to the separation and concentration of positive electrode active materials will then be discussed. Finally, the effect of impurities on the re-synthesis of positive electrode active materials is reviewed.

2.2 The Lithium-ion battery

LIBs employ lithium storage compounds as the positive and negative electrode active materials (Blomgren, 2017). During

charging and discharging cycle, lithium ions (Li^+) are exchanged between the positive and negative electrodes. The positive electrode active material is typically a metal oxide with a layered structure, as in lithium cobalt oxide ($LiCoO_2$), or a material with a tunnelled structure, as in lithium manganese oxide ($LiMn_2O_4$), on an aluminium current collector ([Reddy, 2011](#)). The negative electrode active material is typically a graphitic carbon, also a layered structure, on a copper current collector ([Reddy, 2011](#)).

The electrochemically active electrode materials are lithium metal oxide or lithium metal phosphate for the positive electrode and a lithiated graphite for the negative electrode ([Aurbach et al., 1999](#), [Ellis et al., 2010](#)). The materials are adhering on to the surface of the current collector with a binder. To date, the binder for the positive electrode is still polyvinylidene fluoride (PVDF) ([Grissa et al., 2019](#)). The positive electrode active materials binder requires a more rigorous quality than that of the negative electrode due to the unstable oxidation atmosphere ([Yoshio et al., 2010](#)). In contrast, the negative electrode can employ either PVDF or a styrene-butadiene rubber – carboxy methylated cellulose (SBR-CMC) binder ([Yen et al., 2012](#)).

In the positive electrode fabrication process, the active materials are coated onto the metal foils and calendered. The positive electrode consists of active materials such as $LiCoO_2$, $Li(Ni_xCo_yMn_z)_{x+y+z=1}O_2$, or other types of lithium transition metal oxide or phosphate; a carbon-conductive agent such as acetylene black, ketjenblack, and graphite; and PVDF binder ([Tagawa and Brodd, 2009](#)). The powder solids are initially dry mixed and further mixed with a prepared solution of PVDF dissolved in N-methyl pyrrolidone (NMP).

The fabrication of the negative electrode has the same steps than that of the positive electrode but with different materials. Carbon or graphite is used for the negative electrode active material. PVDF or SBR-CMC are used for the binder. Depending on the binder, the solvent can be NMP for PVDF or water for SBR-CMC.

The coating operation can use a slot die, reverse roll coating, or doctor blade coating equipment. Close control of coating thickness is essential to ensure that all the parts fit into the chassis during final assembly. Usually, a second coating is applied onto the opposite side to produce a double-sided electrode foil. The coating may be interrupted at regular intervals that correspond to the length of the electrode for winding into the cell core in preparation for winding the cell. Following coating, the dried electrode is compressed with roller press machine (calendered) to provide accurate control of electrode thickness and to increase the density of the electrode mass. After calendering, the master roll is slit to the width specified for cell construction and wound onto a roll for the winding operation.

The positive and negative electrodes are then immersed in a non-aqueous lithium electrolyte. The liquid electrolytes are solutions of a lithium salt in one or more organic solvents, typically carbonates (Zhang, 2006). The electrolyte is almost completely absorbed into the electrode and separator materials. Most LIB electrolytes use LiPF$_6$ as the salt because it offers high ionic conductivity and high lithium-ion transference number. The salt is dissolved in one or more mixture of organic solvent that can contain ethylene carbonate (EC), dimethyl carbonate, ethyl methyl carbonate (EMC), and diethyl carbonate (DEC); as well as some propylene carbonate (PC).

Inside LIB cell, the positive and negative electrode are separated to each other by a porous separator (Zhang, 2007). The separator prevents the contact of positive and negative electrode while allowing the lithium ions to travel. The separator is made of polyolefins such as polypropylene (PP), polyethylene (PE) or a multilayer of both PP and PE (Geiger et al., 1994). A three layer material of PP-PE-PP has also been patented and commercialised (Yu and Hux, 1999). The combination of PP and PE allows the cell to shut down and prevent explosion. The PP layer, melting point of 165°C, is designed to maintain the integrity of the film while the lower melting point of PE (135°C) is intended to shut down the cell if an overtemperature condition is reached, causing porosity to be lost, and shut down the cell.

2.2.1 Cell identification
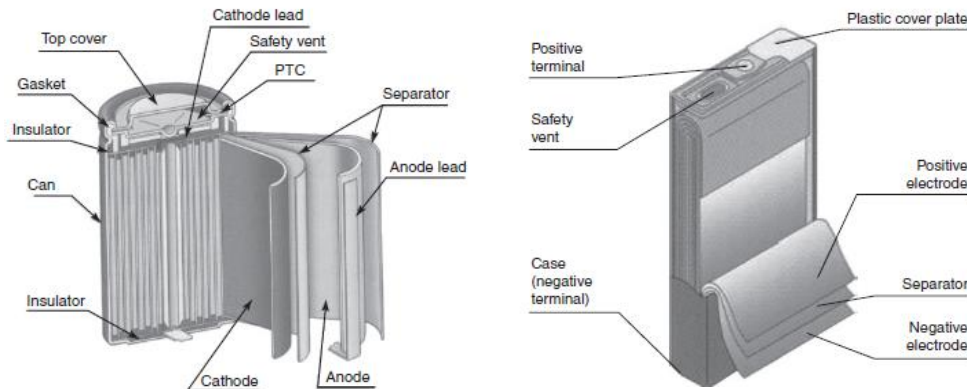
Figure 2-1 Example of cylindrical (left) and prismatic (right) Lithium-ion battery assembly (Reddy, 2011).

The LIB can be manufactured in the form of cylindrical or prismatic as illustrated in Figure 2-1. Once the cell assembly process in complete, the final step in the overall production process that follow are the formation and charging of the cells. The LIB cells are assembled in the discharged condition and must be activated by charging. The first charge is called "formation", which activates active material in the cells and

establishes the ability to function. The battery then tested according to BS EN 61960-3:2017 for quality control and assurance.

To identify the type of active materials present inside a cell, the International Electrochemical Commission (IEC) has developed standards for designation, marking, electrical testing and safety testing of LIB and other types of battery (IEC 61960-3:2017/ BS EN 61960-3:2017) (British Standard Institution, 2017). The IEC designation and marking system for LIB cell utilises five numbers for cylindrical cell and six numbers for prismatic battery. For cylindrical cells, the first two digit designate the diameter in millimetres and the next three digit designates the length in tenth of millimetres. For example, 18650 cell is 18 mm in diameter and 65.0 mm in length. For prismatic cells, the first two digit designate the thickness in tenth of millimetres, the next two designate the width in millimetres, and the last two designates the length of the cell in millimetre. For example, a P564656 is 5.6mm thick x 46 mm wide x 56 mm long.

Reddy (2011) have gave some example of marking found in commercialised LIBs; E-One Moli Energy lists an IMR26650 cell, which has an intercalation chemistry (I), a manganese-based positive electrode (M) and is round (R) or cylindrical. In addition, Samsung has marketed the ICR18650-30A, which is a 3.0 Ah cell having cobalt base positive electrode active materials.

Lithium-ion battery (LIB) technology has become the dominant energy storage for many consumer electronics and electric grids (Blomgren, 2017). Despite the advancement of battery technology, present LIBs meet most of the requirements dictated by the large volume of the application linked to renewable energy and electric transportation field (Winslow et

al., 2018). The spent LIBs from electric vehicles will emerge as the future waste problem with at least 25 billion units and 500 thousand tonnes of spent LIBs would be generated by 2020 (Richa et al., 2014, Zeng et al., 2014). Therefore, there is the need to develop an efficient material recovery method for the materials found in spent LIBs. Mechanical treatments that include liberation and separation would be discussed further in the following sub-sections.

2.3 Liberation in LIBs recycling

2.3.1 Pre-treatment prior liberation

Prior liberation, discharging is often carried out to minimise the hazard associated with runaway reactions. During liberation, short circuiting can produces a spark, combined with flammable electrolytes and the presence of oxygen leading to a fire or explosion (Ojanen et al., 2018). There are several ways in which the battery voltage can be minimised and have been employed by researchers;

1. Discharging using resistor until the voltage is near 0V (Krüger et al., 2014).
2. Immersion of spent LIBs for 24h in 5 wt% of NaCl solution (He et al., 2015, Zhang et al., 2013, Zhang et al., 2014a, Lu et al., 2013, Shaw-Stewart et al., 2019).
3. The LIB can be immersed in liquid nitrogen, causing inactivation of galvanic elements, and also the temperature of all flammable materials are reduced below the flash point. Therefore, an ignition is prevented during mechanical liberation (Hanisch et al., 2015, Wang et al., 2016c, Li et al., 2010b).

The lack of standardisation related to LIB assembly causes problems for effective and efficient discharging (i.e. prismatic

for mobile phone and cylindrical for electric vehicle). The different geometry leads to different position of the positive and negative poles. Cylindrical batteries would have positive and negative pole that are opposite to each other. Whereas, the prismatic battery would have positive and negative pole that is next to each other. Thus, it requires manual handling to connect the positive and negative poles to the resistor on an industrial scale.

To ensure that the discharging step is viable on an industrial scale, the method used should be able to discharge batteries in bulk and of different geometry. One of the ways is to immerse LIB into a large volume of brine solution. By this way, the battery discharged through the combined effect of short-circuiting and electrolysis of salt solution (Lu et al., 2013). Discharging LIB in brine solution often assume that the battery is discharged by electrolysis of water in which oxygen and hydrogen are produced and the half-reaction is described in Equation 2-1 and Equation 2-2 (Ojanen et al., 2018).

Positive Electrode: $2H_2O \rightarrow O_2 + 4e^- + 4H^+$ **Equation 2-1** (E^o=1.23V)

Negative Electrode: $2H^+ + 2e^- \rightarrow H_2$ **Equation 2-2** (E^o=0.00V)
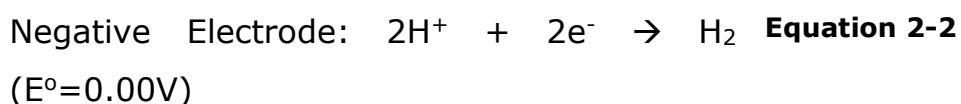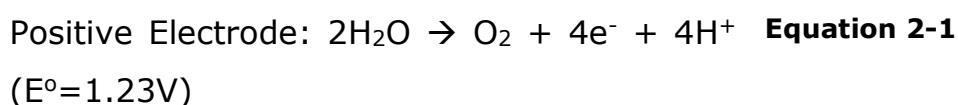
From Equation 2-1 and Equation 2-2 it can be seen that by applying voltage above 1.23V will cause water electrolysis. However, the above equation does not fully describe the full reaction and over–simplifies the system. When NaCl solution is used, there is also the danger of chlorine formation in the negative electrode. Even though the electrochemical potential in Equation 2-3 is higher than that of Equation 2-1, the reaction

described in Equation 2-1 has higher overpotential, which is the difference between the theoretical and the actual cell voltage that is necessary to cause electrolysis. This then cause the reaction described in Equation 2-3 cannot be negated (Ojanen et al., 2018).

Positive Electrode: $2Cl^- \rightarrow Cl_2 + 2e^-$ **Equation 2-3** ($E^o = 1.36V$)

Other than the production of chlorine gas, discharging via the use of brine solution may cause corrosion of the battery connection poles which may lead to incomplete discharge or even internal leakage (Lu et al., 2013, Ojanen et al., 2018). Given the above it may be challenging to carry out this type of discharging on an industrial scale. Especially as the corrosion would eventually lead to unwanted water contamination (Shaw-Stewart et al., 2019).

Other than for the safe liberation of LIBs, minimising the voltage also promote safety during storage and transportation of LIBs. Improper handling of LIBs may be regarded as a fire hazard during the keeping and transporting of LIBs (Wang et al., 2012c). Collecting and storing batteries in an unorganised manner may cause unwanted contact between batteries, which results in short-circuiting. Such occurrence may be minimised by discharging prior keeping.

From the discharging methods that have been reported, the discharging of spent LIBs by using resistor until the voltage is near zero being the least favoured options although it is arguably the safest discharging technique. The use of liquid nitrogen as to inactivate the galvanic element of the battery by using liquid nitrogen has also been suggested. However, due to

its expense may not be practical for an industrial scale. The convenience of battery discharging by using brine solution has outweighed the safety aspect of discharging. The importance of discharging often overlooked, although it is arguably a necessity to provide safe handling for both mechanical liberation and keeping of the batteries. Once the LIB has been discharged, it can then undergo comminution processes to liberate the materials contained within it.

2.3.2 Selective liberation in mineral processing research

Comminution, size reduction, or grinding are synonymous. It represents the breaking of material through an applied force in a confined compartment. In the case of LIBs recycling, comminution processes are employed to achieve a suitable degree of liberation for the different components that are contained within spent LIBs prior to further separation processes (Diekmann et al., 2017, Wang et al., 2016c, da Costa et al., 2015, Zhang et al., 2014a).

Different comminution processes may result in different size distributions due to the predominant force acting during comminution as well as the milling conditions being employed (Hesse et al., 2017, Leißner et al., 2014a). Selective liberation occurs when the breakage of a component is dependent on material and mechanical properties (King and Schneider, 1998, Gaudin, 1939, Mariano et al., 2016). Thus, the different predominant load being applied to a mineral would also result in different selectivity in the product.

The selective liberation in minerals processing has been reported to occur such as in the case of eudialyte bearing ore (Leißner et al., 2016), magnetite-bearing ore (Reichert et al., 2015), scheelite bearing ore (Sousa et al., 2018), and lead-zinc

ore (Hesse et al., 2017). The occurrence of selective liberation will vary from ore and ore and often does not result in generalizable understanding, due to different studies have used inherently different ore sample and comminution process (Little et al., 2016).

The main approach which has been used to quantify the selective liberation is via the measurement of phase-specific interfacial area before and after comminution (Fandrich et al., 1997, Garcia et al., 2009, Xu et al., 2013). This analysis can be carried out from the re-constructed three dimensional image from X-ray microtomography (XMT) (Xu et al., 2013) or the two-dimensional data from Scanning Electron Microscopy – Energy Dispersive X-Ray (SEM-EDX) (Leißner et al., 2016). A reduction in the phase-specific interfacial area would indicate the existence of phase boundary fracture and indicates the selective liberation of a specific mineral (Little et al., 2016).

One option for characterising a selective comminution effect and the selectivity of different material is the ore separation degree (η_{ore}) Equation 2-4 (Schulz, 1970, Hesse et al., 2017).

$$\eta_{ore} = R_V - R_W$$ **Equation 2-4**

η_{ore} indicates the difference between the percentage weight recovery of valuable R_V and the waste materials R_W. R_V is the mass recovery of the valuable component below the cut point t_d relative to the valuable component. R_W is the recovery of waste material in the same size fraction. If the concentration of the valuable component is dependent on the particle size, the η_{ore} would then depends on the separation cut t_d (Figure 2-2).
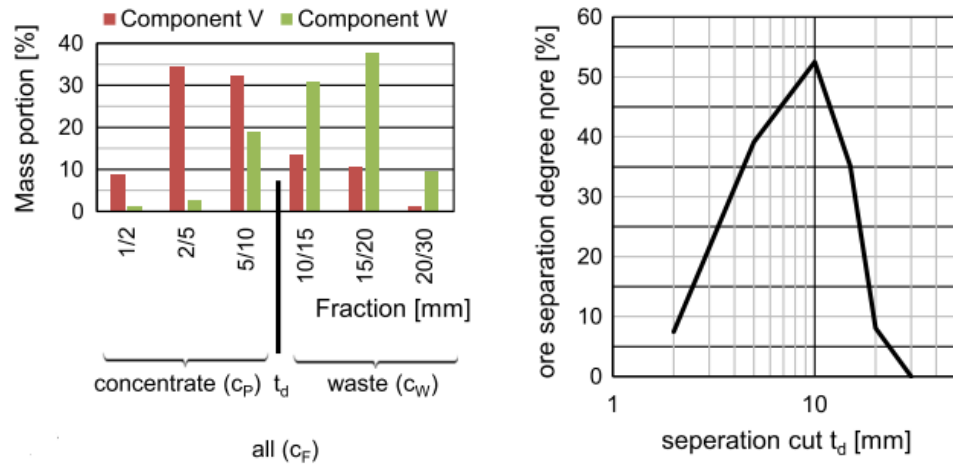
Figure 2-2 – (Left) Example for distribution of the mass proportion for the component V and W; (Right) graph of the corresponding ore separation degree η_ore (Hesse et al., 2017).

If just the concentration of the valuable component in the feed (F), the product (P) and the waste (W) are known, the η_ore can also be determined by Equation 2-5.
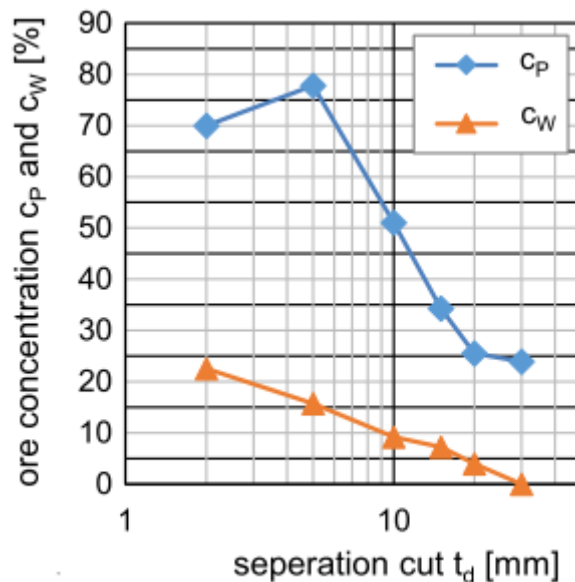
Figure 2-3 – Distribution of the ore concentration (from Figure 2-2).

$$\eta_{ore} = \frac{[(C_F - C_W) \times (C_P - C_F) \times 100\%]}{[C_F \times (100\% - C_F) \times (C_P - C_W)]} \times 100\%$$

Equation 2-5

The parameters are C_F – the concentration in the feed material, C_P – concentration in the product, and C_W – concentration in the waste material, respectively as the weight percentage of

41

the valuable component. The values of C_P and C_W is dependent on separation (Figure 2-3) cut t_d, and therefore, the maximum value for ore separation degree ($\eta_{ore,\ max}$) can be determined (Figure 2-2).

Equation 2-5 can also be used to determine the selectivity of the feed material, which is the classification of materials without undergoing the comminution process. By this way, the size fraction that has the desired degree of liberation can be firstly recovered. The size fraction that has not met the desired degree of liberation may undergo further comminution if it is proven to be beneficial. The difference between the η_{ore} before and after comminution can be used to evaluate the degree of selective liberation.
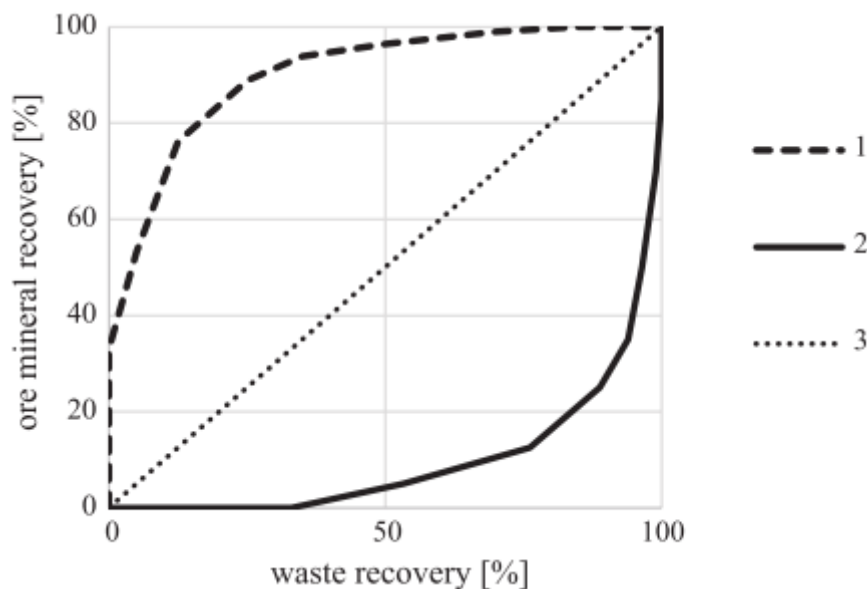
Figure 2-4 Recovery plot as Fuerstenau upgrading curve as percentage finer (Hesse et al., 2017).

A further method to evaluate selective liberation is to use the Fuerstenau upgrading curves in a recovery plot on the classified comminution product (Reichert et al., 2015, Leißner et al., 2014b). By this way, the selective comminution product is

always separated into two fractions of a fine and coarse fraction by the cut point t_d as shown in Figure 2-4.

From Figure 2-4, the recovery of valuable and the waste material can be plotted in the diagram with various cut point t_d for either percentage finer or coarser. The case shown in Figure 2-4 is recovery plot for percentage finer. A linear diagonal line (Line 3) indicates that there is no selective liberation. An enrichment of valuable component in the fine fraction (Line 1) would be graphically represented as a recovery curve above the diagonal line. A recovery curve below the diagonal line (Line 2) would indicate the enrichment of valuable component in the coarse size fraction.

The main difference of ore separation degree (η_{ore}) and Fuerstenau recovery curve lies in its graphical representation. In which the optimum cut point that can compensate the recovery of desired and un-desired materials can be found ($\eta_{ore,max}$). On the other hand, the Fuerstenau diagram gives graphical representation of whether or not the intended materials is being liberated in the finer or coarser size fraction. When the materials is being studied undergoes further comminution, the difference in area enclosed by different curves in Fuerstenau diagram is defined as the separation efficiency (Leißner et al., 2014a).
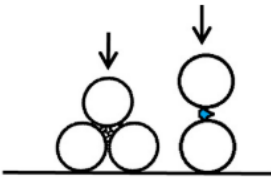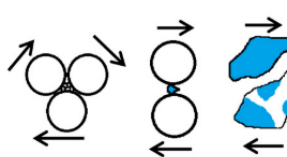
The occurrence of selective liberation is exclusive for the specific ore and the comminution technique being used (Little et al., 2016). Hesse et al. (2017) gives an explanation of selective liberation that occurs in the comminution of lead-zinc ore with different comminution technique. The large hardness difference between the intended minerals of galena and sphalerite towards the gangue of calcite would produce a selective liberation. Different comminution technique would

result in different predominant force acting on the particles. It was found that the different comminution technique would result in different size distribution. Moreover, the predominant load acting during comminution is also an important consideration that determine the occurrence of selective liberation.

The study conducted by Hesse et al. (2017) suggests that to be able to exploit selective comminution, it requires the knowledge of the desired minerals and the appropriate comminution technique. Where the difference in material and mechanical properties needs an appropriate comminution technique to exhibit selective liberation. The different breakage mechanism related to the load being applied is summarised in Table 2-1.

Table 2-1 Definition of breakage mechanism; circles represent grinding media, shaded and not-shaded represent different mineral phases (Little et al., 2016).

Grinding Action	Grinding Outcome	
Compression		Inter-granular fracture. Phase-boundary fracture. Grain-boundary fracture.
Impact		Preferential fracture. Selective breakage (one phase break at a faster rate than the other).
Shear/ Abrasion		Massive fracture. Random fracture.
		Abrasion. Attrition. Chipping.

Fragmentation mechanisms have attracted attention from researchers in the field of minerals processing. The nature of the comminution process relies on the intensity and the rate of application of stresses. The three main rupture mechanism have been identified (Varinot et al., 1997, Gao and Forssberg, 1995):

1. **Abrasion** which results from the local low-intensity surface stresses. This then leads to a bimodal particle size distribution comprising of fine particles taken from the surface of mothering particles and particles of size close to that of the mother particles. One characteristic is that, there is no immediate size particle. (size reduction by shear)

2. **Cleavage** results from the slow application of relatively intense stress or compression from. This produces fragments of slightly smaller than the initial particles.

3. **Fracture** results from the rapid application of intense stresses. This leads to a fragment which is relatively small with respect to initial particle size and having a relatively wide particle size distribution. (Size reduction by an impact)
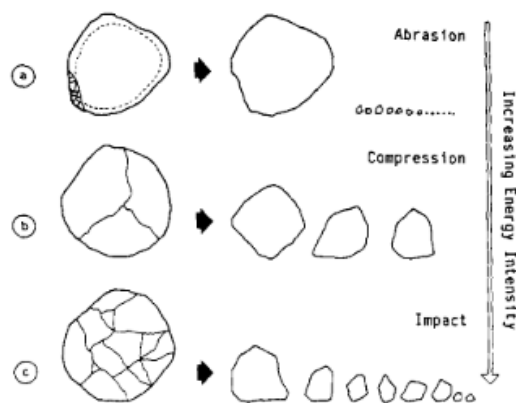
Figure 2-5 Representation of the mechanisms of particle fracture and its relative energy intensity (Gao and Forssberg, 1995).

When comparing energy consumption, the liberation by abrasion requires the least amount of energy intensity and impact liberation would be the most energy intensive (Figure 2-5) ([Gao and Forssberg, 1995](#)). Other than the energy intensity requirements, the different types of load would also result in different particle size distributions (Figure 2-6).
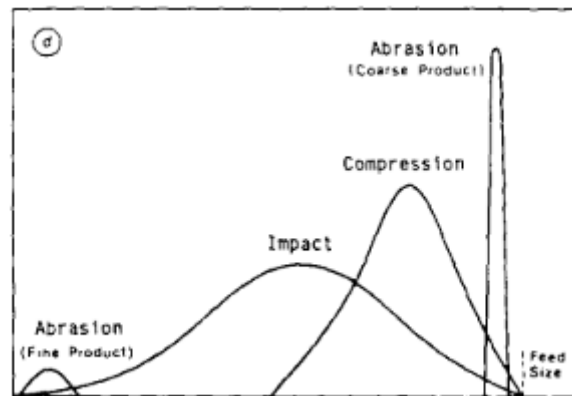
Figure 2-6 The dependence of particle fracture mechanisms and the resulting size distribution([Gao and Forssberg, 1995](#)). (It is believed that compression would be the predominant force in crushers, the impact would be predominant force in tumbling mills, and abrasion would be the predominant force for the ultra-fine grinding machines).

From Figure 2-6, it can be seen that abrasion gave the narrowest size distribution, followed by compression that has intermediate size distribution, and finally, the impact that produces the widest size distribution range. Having discussed the forces involved in comminution, it is important to realise that the forces acting in a comminution process do not occur in isolation but with one normally dominating.

It is therefore, prior knowledge of materials and mechanical properties of the minerals in conjunction with the appropriate liberation technique is important to effectively exploit selective liberation.

2.3.3 Selective liberation in spent LIBs

Currently the integration of different materials in the form of manufactured composites has reached a very high level. Such integration in the electrical and electronic equipment is to achieve a compact and flexible form for the consumer products. For example, a printed circuit board contains almost every element found in the periodic table. Similarly, LIB is also a composite of materials and manufactured in different geometries for different application purposes (Figure 2-7).
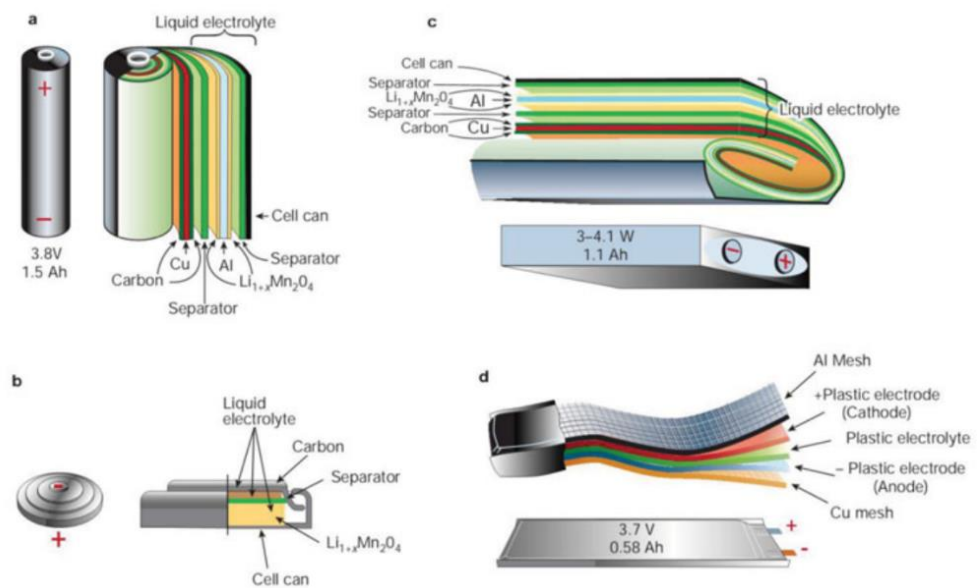
Figure 2-7 Batteries with different geometry; a) cylindrical b) coin c) prismatic d) pouch (Tarascon and Armand, 2001).

The positive and negative electrode in LIB is essentially made of copper and aluminium coated with its respective active materials. The graphite would be attached to the copper current collector and held together by the PVDF binder making a negative electrode. Similarly, lithium-transition metal-oxide would be cast onto the surface of the aluminium current collector and held together by the PVDF binder making a positive electrode. Inside the chassis, the positive and negative electrode are separated by a porous separator and immersed

47

in lithium-ion conducting electrolytes. The electrolytes have cyclic conductive lithium ions that are supplied by the dissolved lithium salts such as $LiPF_6$.

Comparing the assembly of naturally occurring ores and the assembly of LIBs, it is apparent that the arrangement of LIBs assembly is simpler.
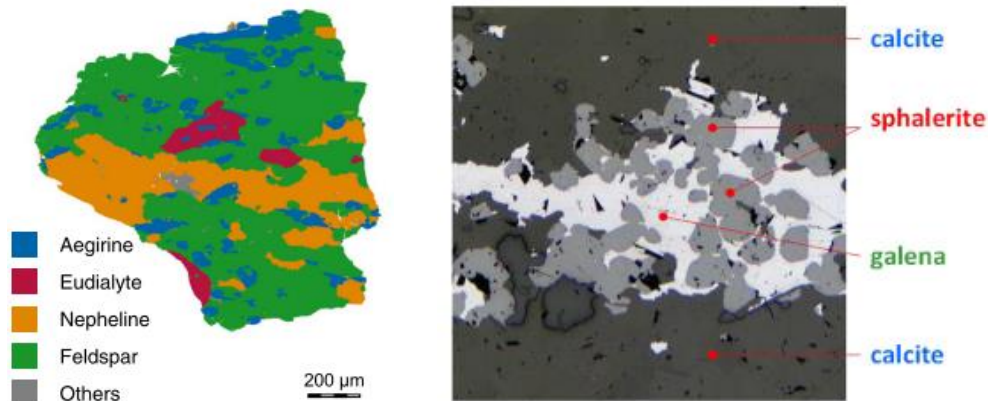
Figure 2-8 Example of naturally occurring ores under mineral liberation analysis by using SEM-EDX (Leißner et al., 2016, Hesse et al., 2017).

Naturally occurring ore consist of islands of valuable minerals that are interlocking with the gangue, as shown in Figure 2-8.
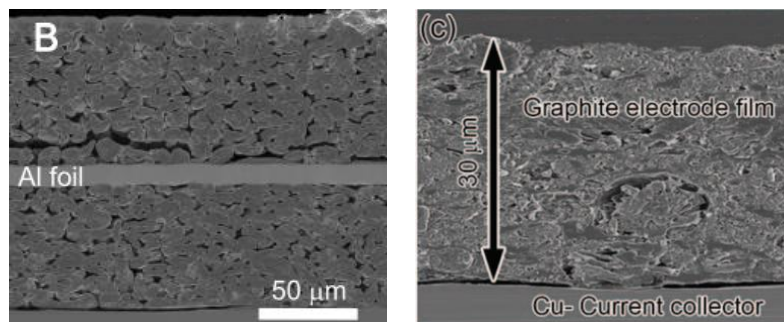
Figure 2-9 Cross-sectional picture of positive (B) and negative (C) electrode taken by using SEM-EDX (Kim et al., 2017, Chen et al., 2013).

The gangue often takes the majority of the ore portion, and the desired minerals exist only in small fractions. From Figure 2-9, much simpler geometry can be seen in the case of LIBs. The active materials are cast onto the current collector and held

together by the binder for both positive and negative electrode. The bonds between the active materials to the current collector are geometrically simple, whereas the interface of locked minerals is of a fractal arrangement. Therefore, liberation of active materials in LIB assembly can be achieved in a simpler way when compared to the naturally occurring ore.

In a LIB assembly, Polyvinylidene Fluoride (PVDF) is the common binding agent for both positive and negative electrode active materials onto the current collector (Liu et al., 2019b, An et al., 2019). PVDF binder is used due to its amorphous properties that allows lithium ions to pass through a thin layer of swollen PVDF (Yoshio et al., 2010). From a mineral liberation perspective, knowing the mechanical properties of different components in the LIBs is important as it would set the trajectory of whether or not selective liberation would be exhibited. From the morphology of positive and negative electrode in Figure 2-9 it is hypothesized that the liberation of positive and negative electrode active materials can be achieved through liberation via detachment. However, such understanding has never been reported or explored. Hence, comminution based on abrasion would be beneficial where scouring can induce detachment of active materials.

The comminution of LIBs has been reported to be of a selective phenomenon (Zhang et al., 2013, da Costa et al., 2015, Zhang et al., 2014a, Zhang et al., 2014b, Wang et al., 2016c). The positive and negative electrode active materials can be concentrated without over crushing of other battery components (i.e. copper and aluminium) (Zhang et al., 2013). The positive and negative electrode active materials are being enriched in the finer size region (ca. <1 mm), while the coarser size fraction contains the chassis, the separator, aluminium foil

and copper foil (ca. >1 mm) ([da Costa et al., 2015](#), [Zhang et al., 2013](#), [Wang et al., 2016c](#)). However, the efficiency of selective liberation is not often explicitly discussed. Much of the conclusions imply that the different size fractions would concentrate different components of batteries such that the chassis would be in the biggest size fraction, a current collector in the intermediate size fraction, and the positive and negative electrode active materials in the finer size fraction.

[Zhang et al. (2014a)](#) have reported the elemental composition of spent $LiCoO_2$ LIBs. Their findings reveal that the elements in the spent LIBs are mainly carbon, oxygen, copper, cobalt, aluminium, fluorine. A small amount of manganese was found with a concentration of less than 5 wt%. Other elements such as silicon, phosphorus, iron, calcium, tin, titanium, sulphur, lead, nickel, magnesium, chlorine, bromine, and zinc are found as traces (i.e. <1wt%). Moreover, from the X-Ray Diffraction (XRD, Bruker D8 advance, Germany) analysis, it was also found that there are no structural changes on the positive electrode active material crystals before and after shredding ([Zhang et al., 2014a](#)).

From the findings reported by [Zhang et al. (2014a)](#); it is understood that the main metallic components found in spent $LiCoO_2$ LIBs are aluminium, copper, and cobalt. Moreover, the mechanical liberation does not induce structural changes on to the positive electrode active materials. The positive electrode active material is $LiCoO_2$. Hence, the recovery of positive electrode active materials can be determined by one of the elements from its compound in this case Cobalt. Also, the recovery positive and negative electrode foil can be calculated based on the detection of aluminium and copper respectively.

Wang et al. (2016c) reported the combination of selective liberation of positive electrode active materials with size-based separation to concentrate $LiCoO_2$ from spent cylindrical LIBs. A commercial granulator with 7 mm grid was used (cutting mill, EconoGrind 180/180). From the findings, the size-recovery hierarchy for the pre-recycling process was proposed (Figure 2-10).
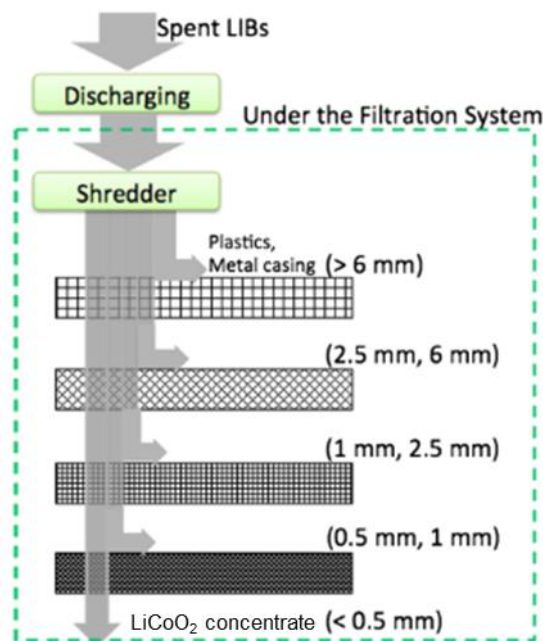
Figure 2-10 Flow sheet of end-of-life LIB pre-recycling process (Wang et al., 2016c).

Referring to the published data from Wang et al. (2016c), the elements were analysed for the different size fractions. However, the cobalt, copper and aluminium with concentration of less than 5 wt% were not reported. This is attributed by the experimental design flaw that utilize a handheld X-Ray Fluorescence (XRF) with limited detection limit.

Comminution of non-brittle material, inside a cutting chamber, the size reduction occurs through shearing and cutting stress (Schubert and Bernotat, 2004). The cutting action applies a localised force that induces failure of the materials right next to

the knife edge as a result of shear and tensile stresses. It is expected that material with larger shear and tensile strength requires more energy to undergo size reduction. For metallic components (i.e. current collector and steel chassis), the tensile strength is directly proportional the shear strength (Dahle et al., 2003). The tensile strength of the different component inside LIB is summarised in Table 2-2.

Table 2-2 The difference in tensile strength and for the different LIB components.

LIB Component	Tensile Strength (Mpa)
Separator (Chen et al., 2014)	175.2
Steel chassis (MatWeb, 2019)	505.0
Aluminium (Butt et al., 2016)	105.0-145.0
Copper (Butt et al., 2016)	220.0

Moreover, the LIB also consists of flexible plastics such as separator and polymeric chassis for pouch battery. Take for an example of Celgard 2325 with PP-PE-PP arrangement that has been reported to have a tensile strength of 175.2 Mpa and 155.9% elongation before breaking (Chen et al., 2014). Despite the lower tensile strength of the separator, it is tougher than the metallic counterparts and able to prevent breakage during milling. Due to this, the polymeric materials can be expected to be concentrated in the larger size region.

From Table 2-2, in the case of cylindrical battery, the steel chassis should be concentrated in the larger size region similar to that of the polymeric materials. Whereas, the copper and aluminium should be concentrated in the smaller size region relative to the chassis and the separator. Moreover, when comparing the tensile strength of copper to aluminium, assumption is taken such that there is no interaction between

the active materials assembly with the respective current collector. It is expected that the aluminium would be concentrated in the finer size region relative to copper.

However, such assumption may not be applicable considering the difference in adhesive strength for positive and negative electrode. The adhesive strength of PVDF on to copper (2856. kPa) current collector is lower than the aluminium (841.2 kPa) counterparts in a new LIB cell (Dai et al., 2019). Moreover, the adhesive strength of PVDF degrades as the battery going through multiple charge and discharge cycle. Dai et al. (2019) reported that the adhesive strength of PVDF onto copper and aluminium current collector decreases into 55.5 kPa and 132.8 kPa respectively. Other that the weaker adhesive strength of PVDF onto current collector, the copper and aluminium also undergoes degradation in terms of its mechanical properties. The copper current collector undergoes reduction in elastic modulus (ca. 78.06% - 80.01% reduction) (Dai et al., 2019). The aluminium current collector also undergoes localised corrosion and produces perforation that also potentially weaken the mechanical properties of the aluminium current collector (Braithwaite et al., 1999).

The selective liberation of spent LIBs allows the chassis and separator to be concentrated in the larger size region (Zhang et al., 2013, da Costa et al., 2015, Zhang et al., 2014a, Zhang et al., 2014b, Wang et al., 2016c). Whereas the current collectors and the active materials are found in the smaller size regions. This occurrence can also be expected when looking into the mechanical properties of the LIB components. However, there is minimum discussion related to the selective liberation between copper and aluminium components. It became difficult to predict whether the copper or aluminium would be the main

contamination in the finer size region. Moreover, when the interaction between the PVDF binders onto the current collectors is considered, the stronger adhesiveness of PVDF onto the aluminium than that of the copper may cause the aluminium to break slower than the copper counterpart. Other than the breakage of copper and aluminium, the weaker bonds between PVDF towards the copper current collector as compared to the aluminium collector also suggest that the selective liberation of positive electrode active materials would be followed by a degree of liberation of the negative electrode active materials.

2.4 Separation and concentration in LIBs recycling

Following liberation, subsequent mechanical separations are often favourable as to concentrate positive electrode active materials. Mechanical separation and concentration are done by exploiting the difference in physical and mechanical properties of different components contained within LIBs. The difference in the physical property of LIBs components such as density, magnetic property, conductivity, and hydrophilicity are the foundations of physical separation. Moreover, the selective liberation that resulted due to the difference in mechanical properties can be exploited via size-based separation.

2.4.1 Magnetic separation

Magnetic separators exploit the difference in magnetic properties between different materials (Veit et al., 2005, Wilson et al., 1994). All materials are affected in some way when placed in a magnetic field and can be classified into two broad groups of diamagnetic and paramagnetic (Wills and Finch, 2016d). A wide variety of material exhibit linear magnetisation,

which is the internal magnetisation M depends on the field H as shown in Equation 2-6.

$$M = X_m H$$ **Equation 2-6**

Where X_m is the magnetic susceptibility.
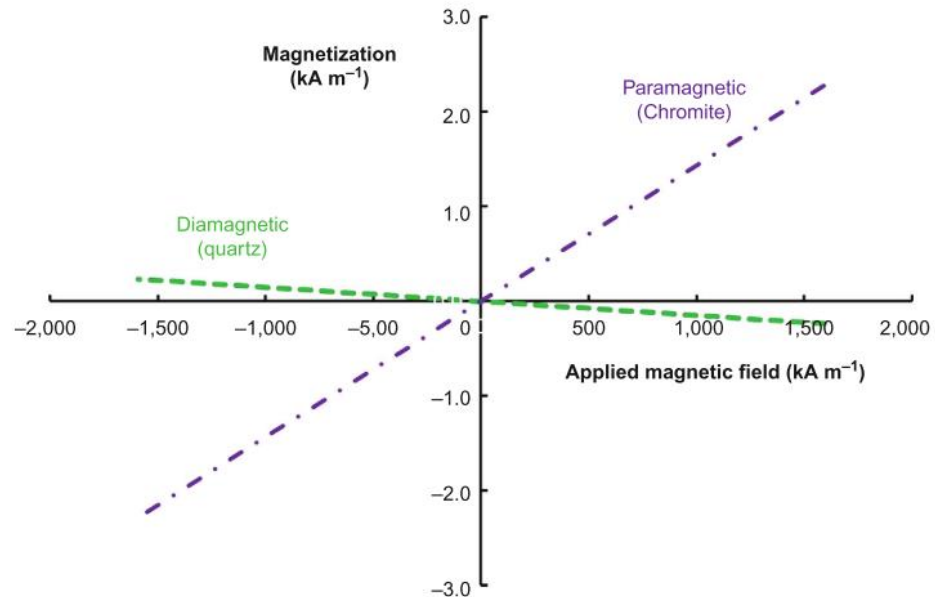
Figure 2-11 Magnetization versus applied magnetic field strength for idealized paramagnetic and diamagnetic minerals (Wills and Finch, 2016d).

If X_m is less than zero, the magnetic field is decreased by the materials and correspond to diamagnetic materials. If X_m is greater than zero, the magnetic field is increased by the material and correspond to paramagnetic material. Figure 2-11 shows the comparison of paramagnetic materials of chromite with positive X_m and diamagnetic material of quartz with negative X_m.
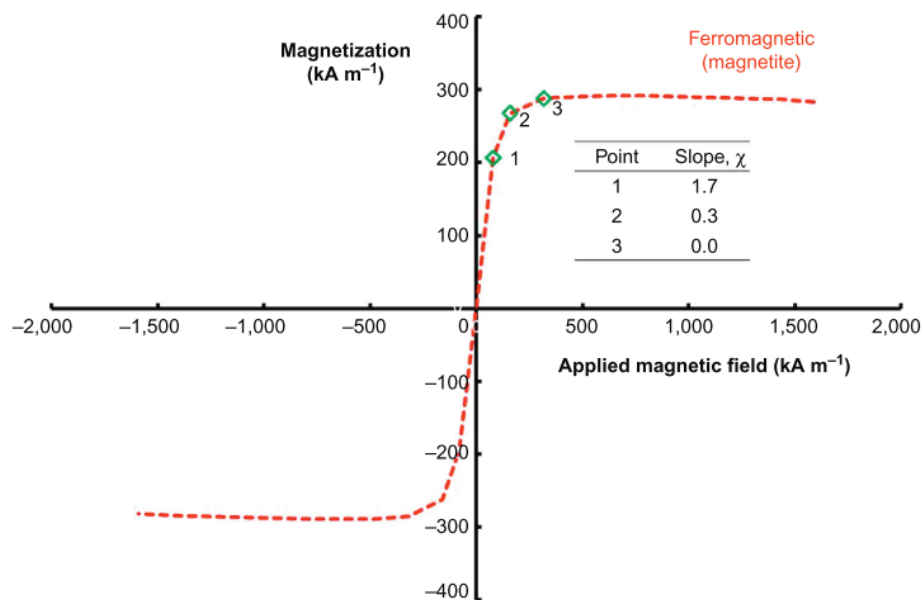
Figure 2-12 Magnetization versus applied magnetic field strength for a ferromagnetic mineral (Wills and Finch, 2016d).

Ferromagnetism can be regarded as a special case of paramagnetism in which the key features is that it is non-linear. The M and H from Equation 2-6 does not have a simple linear relation between one another. Magnetic dipoles of the material undergoes exchange coupling so that they can rapidly align themselves with an applied magnetic field (Wills and Finch, 2016d). From Figure 2-12, due to the exchange coupling, ferromagnetic material will have a very high initial susceptibility to magnetic force until all the exchange coupled magnetic moments have aligned with the applied magnetics force. This then results in a rapidly decreasing values of susceptibility with increasing applied magnetic field (Figure 2-12, points 1-3).

Ferromagnetism is a special case of paramagnetism. The key main difference lies in the alignment of many atomic scale moments. In the case of paramagnetic material, the moments are randomly arranged until an external field comes along and aligns them. Whereas in the case of ferromagnetic material, the moments of many atoms or molecules tend to be aligned in

small regions. Enough atomic scale moments that aligned together forming domain of magnetisation. Each domain is fairly small and randomly oriented with respect to its neighbour. Furthermore, it is important to point out that the magnetic field is intense in a domain, but the domain is randomly arranged. Thus, the material as a whole has no net magnetisation. This is also why a random piece of iron is often not magnetised. The randomly domains can be realigned when the material is placed into a strong enough external magnetic field. However, when the external magnetic field is removed, ferromagnetic materials is energetically favourable to remained aligned and this does not occur in the paramagnetic materials. Hence, the domain is aligned and pointing in a fixed direction and therefore ferromagnetic material can become a permanent magnet.

Due to the above described phenomenon, the strong response of ferromagnetic material to magnetic field as compare to the paramagnetic material with implication. The separation of ferromagnetic materials in turn requires weaker magnetic field due to its high initial magnetic susceptibility. Compared to paramagnetic materials, which requires high-intensity (high magnetic field) magnetic separators to report to the magnetic product, ferromagnetic materials are recovered in low-intensity magnetic separators.

Removal of tramp iron and strongly magnetic impurities or the concentration of a strongly magnetic valuable component is the main application of dry magnetic separators for the recovery of metals from consumer waste (Svoboda and Fujita, 2003, Wilson et al., 1994). The dry magnetic separation in LIBs recycling is often used for the recovery of ferromagnetic materials such as the steel chassis (Shin et al., 2005, Gratz et al., 2014, Al-Thyabat et al., 2013).

Table 2-3 Reported Magnetic Susceptibility (Ellis and Montenegro, 2016).

Active Materials	$X_m \ 10^5$ (m^3/kg)
$LiFePO_4$	482
$LiMn_2O_4$	352
$LiNiCoMnO_2$	226
$LiNi_{0.833}Co_{0.17}O_2$	134
$LiCoO_2$	8.91
Graphite	Diamagnetic

Other than ferromagnetic materials, a wet magnetic process to separate a mix positive electrode active materials concentrate has also been patented by Ellis and Montenegro (2016). Ellis and Montenegro (2016) have investigated the wet magnetic separation of active electrode materials, including graphite from spent LIBs. By exploiting the difference in magnetic susceptibility of different electrode active materials, it is possible to recover valuable materials with high gradient wet magnetic separation. The magnetic susceptibility summarized in Table 2-3 shows the different magnetic susceptibility of different active materials, while graphite collected as non-magnetic product. However, this patent has not yet been implemented on an industrial scale.

The use of low intensity magnetic separation can also be used to recover the cobalt contained within spent LIBs. Li et al. (2016) have shown that the cobalt is required to be taken back to its metallic form that is ferromagnetic. This is achieved via oxygen-free roasting (1000°C) with graphite as the reductant. While, the lithium then recovered as Li_2CO_3. This process may

be beneficial for $LiCoO_2$ active material but its application towards other types of active materials is potentially limited.

The use of high gradient magnetic separator to separate different type of positive electrode active materials have been proposed. However, this has not yet been proven and assumes that the feed contains only the positive and negative electrode active materials. To further the discussion, the low yield of selective liberation previously discussed would affect the proposed method. Whereas, the use of low intensity magnetic separator to recover the positive electrode active materials can only recover cobalt metal. The use of high temperature being the major drawback of this method. Hence, the use of magnetic separation to recover the positive electrode active materials either between different type of materials or from liberated spent LIBs require further exploration.

However, the use of magnetic separation in spent LIBs is still useful to separate the initial easy to remove contamination in the first line of processing of spent LIBs recycling. Following liberation, low intensity magnet can be effectively used to screen for ferromagnetic material such as the steel chassis from cylindrical battery. The iron contamination can be initially recovered and does not have the need to be involved in the subsequent mechanical processes.

2.4.2 Sieving

Sieving or size-based separation can be seen as a part of the screening process. The industrial screening in mineral processing is often carried out to give size range adjustment for scalping, grading, dewatering, de-dusting, grinding media recovery, or trash removal (Wills and Finch, 2016c). In the case of LIBs recycling, selective liberation produces positive

electrode active materials in the finer size region. Therefore, the occurrence of selective liberation is often reported in conjunction with size-based separation ([Wang et al., 2016c](#), [Zhang et al., 2014a](#), [Zhang et al., 2014b](#)).

For size testing purposes there are different scale in which the sieves aperture are designed. The scale of the aperture may follow the $\sqrt[2]{2} \approx 1.4142$ sequences. The $\sqrt[2]{2}$ sequences have the characteristics of the aperture area that is doubled with the aperture width at every other sieve in the series. There is another sequence of $\sqrt[4]{2} \approx 1.1892$. When the size analysis requires a closer sizing, the combination of difference sequences can be used such that the $\sqrt[4]{2}$ sequence will fills the size between the $\sqrt[2]{2}$ sequences and therefore narrower size range can be achieved.

The overall screening efficiency is markedly reduced by the proportion of near-mesh particles (blinding) ([Liu, 2009](#), [Wilson et al., 1994](#)). The effect of near mesh particles would be compounded as these particles tend to plug and progressively reduce the screening efficiency. Moreover, the shape of the particle is important as spherical particles pass with equal probability in any orientation. However, most of the particles in spent LIBs are of irregular shapes and must orient in an attitude that permits them to pass. As liberation of spent LIBs exhibit selective crushing that is dependent on size, it is imperative to have the sieve that is not easily blocked with the near-size particles and therefore biased the results reported.

In LIBs recycling, the sieving efficiency is not commonly discussed. This may be due to the fact that the sieving analytical procedures have basic concept and the equipment is deceptively simple and probably the most abused method of

particle size analysis and separation of particulate materials. Four to eight sets of sieves with the range of 6000 μm to 45 μm were employed to characterise particle size distribution of milled spent LIBs (Wang et al., 2016c, Zhang et al., 2014a).

The choice of sieve size often relies on the judgement of the experimenter. In the case of LIBs recycling, selective liberation followed by sieving has been proposed and used to concentrate positive electrode active materials before further separation. The cut point proposed to concentrate positive electrode active materials varies from 0.212 mm to 1 mm (Shin et al., 2005, Diekmann et al., 2017, He et al., 2017b, Silveira et al., 2017, Wang et al., 2016c, Zhang et al., 2013, da Costa et al., 2015). However, this cut point size range is substantially larger when compared to the positive electrode active materials powder found in LIBs (ca. 1.50 μm – 7.80 μm) (Pavoni et al., 2018). Smaller cut point such as 0.25 mm has been reported to give high purity of positive electrode active material, but it only recovers 56.38% positive electrode active material (He et al., 2017b). This indicate that the liberation technique proposed is of sub-optimum.

Having known that the selective liberation of spent LIBs is sub-optimum, there is minimum effort to improve its yield. The reported case often correlates the selective liberation of positive electrode active materials to the cut point being used. There is lack of understanding to what causes the low degree of positive electrode active materials liberation. Moreover, the larger cut point proposed as compared to the actual size of active materials found in LIBs indicates that it is liberated in the form of aggregates. However, it has not yet been confirmed.

2.4.3 Gravity separation

In mineral processing, gravity concentration is the separation of minerals based upon the difference in density. Techniques of gravity concentration has been around for centuries. To give an example, the spanning of gold and quartz by using water as carrier liquid has been known for centuries. This method separate components of different specific gravity by their relative movement in response to gravity or more other force, the latter being the resistance to motion offered by a viscous fluid, such as water or air.

The use of Wilfley table (wet density separation) with water as the separation media has been reported to be useful in separating copper in the size fraction of greater than 1 mm with the resulting grade of 66.38 wt% (da Costa et al., 2015). While, the size fraction below 1 mm initially removed and concentrates the $LiCoO_2$ particles.

The use of dry density separation with air as the separation media has also been reported to be useful in the separation of different components of spent LIBs. The use of spouted bed elutriation that utilize the principle of fluidization enables the entrainment of different particles depending on the air velocity being used (Bertuol et al., 2015). The optimum condition allows the grade of 17.2 wt% of Cu and Al, 15.8 wt% of chassis, 42.7wt% of $LiCoO_2$/graphite, and 6.1 wt% of polymers to be obtained(Bertuol et al., 2015). Furthermore, Diekmann et al. (2017) demonstrated that dry density separation by using air classifier is also able to separate different liberated components in spent LIBs. Similarly, to the spouted bed elutriation, the separation depends on the air velocity being used to entrain the fine particles. Moreover, two stage milling is used to further improve the liberation of positive electrode active materials.

The optimum condition that combined two stage milling with optimum air velocity resulted in 75 wt% recovery rate of positive electrode active materials with minimum (< 2.5 wt%) contamination of copper, aluminium, and iron.

The use of density separation in separating spent LIBs component have been shown to be able to separate various different components. The main challenges in using gravity separation to concentrate positive electrode active materials lies in the characteristics of the selective liberation of spent LIBs. Most of the positive electrode active materials are being liberated or concentrated in the finer fraction as discussed previously. The smaller particle size, in turn increases the complexity in designing density separation.

Dry density separation gives the advantage of negating the needs of dewatering, while the wet density separation gives the advantage of fewer materials lost by less dusting. The use of either wet or dry density separations allows the concentration copper and aluminium components from spent LIBs. A more recent progress indicates that the use of air classifier can concentrate fine particles of positive electrode active materials with overall recovery rate of 75 wt% (Diekmann et al., 2017). However, the two-stage milling proposed for the air classifier has been indicated to be sub-optimum. Therefore, a better liberation technique is required to improve the recovery rate of positive electrode active materials via density separation.

The engineering approach for gravity separation is to quantify the concentration criterion $\Delta\rho$ (Wills and Finch, 2016b):

$$\Delta\rho = \frac{(\rho_h - \rho_f)}{(\rho_l - \rho_f)}$$

Equation 2-7

Where ρ_h is the density of heavier component, ρ_l is the density of lighter component, and ρ_f is the density of the fluid medium.

Taking the separation of gold and quartz with water as the carrier fluid, where the density of gold is 19300 kgm^{-3}, quartz is 2650 kgm^{-3}, and water is 998 kgm^{-3}. The resulting concentration criterion is 11.1, which is why it is relatively easy to separate gold from quartz through density separation.

Moreover, the motion of particles in a fluid is not only dependent on its specific gravity, but also its size. The particles required to carry out density separation needs to be coarse enough that their movement is not affected by surface friction and therefore follows the Newton's law. Hence the difficulties in implementing gravity concentration increases as the particle size decreases. The qualitative judgement related to the concentration and the particle size is summarised in Table 2-4.

Table 2-4 Dependence of Concentration Criterion (Wills and Finch, 2016b)

Concentration Criterion	Separation Difficulties	Useful Size Range (µm)
2.5	Relatively Easy	+75
1.75 – 2.5	Possible	+150
1.5 – 1.75	Difficult	+1700
1.25 – 1.5	Very Difficult	-
<1.25	Not Possible	-

Table 2-5 Density of Lithium-ion Battery Components

Component	Density (kg/m^3)
LiCoO$_2$[*a] ([Villars and Cenzual, 2012b](#))	5020
LiNi$_{0.33}$Mn$_{0.33}$Co$_{0.33}$O$_2$	a>x>c
LiNi$_{0.8}$Co$_{0.15}$Al$_{0.05}$O$_2$	a>x>b
LiNiO$_2$[*b] ([Villars and Cenzual, 2012e](#))	4800
LiMn$_2$O$_4$[*c] ([Villars and Cenzual, 2012d](#))	4520
LiFePO$_4$[*] ([Villars and Cenzual, 2012c](#))	3600
Graphite[*] ([Villars and Cenzual, 2012a](#))	2260
Acetylene Black ([Aesar, 2012a](#))	1800 - 2100
Aluminium ([Aesar, 2012b](#))	2700
Copper ([Aesar, 2012c](#))	8940
Polypropylene ([Hindle, 2017](#))	905
Polyethylene ([Aesar, 2012d](#))	910 – 980
PVDF ([Kynar, 2017](#))	1770

* Theoretical density

The concentration criterion is the calculated for the different components that are found in spent LIBs based on the density summarised in Table 2-5. It is assumed that the separation media is either water or air with the density of 993 kgm^{-3} and 1.27 kgm^{-3}. The separations of different positive electrode active materials (i.e. mixed positive electrode active material) have generally the concentration criterion of less than 2. Also, knowing the size that the positive electrode active materials being used in LIBs is less than 75 μm. Hence the gravity separation would be difficult to carry out to separate mixed stream of positive electrode active materials.

Moreover, the separation of negative electrode active materials from various positive electrode active materials have been calculated. Based on the concentration criterion, the separation of graphite from various positive electrode active materials can

be easily achieved by using water than air as medium. The separation of graphite from LCO, NMC, NCA, and LMO gives the concentration criterion of greater than 2.5 in water medium. However, some positive electrode active materials such as LTI and LFP has density criterion that is less than 2.5 and therefore challenging to be separated via density separation. Nonetheless, LTI and LFP have expected lower recycling needs than that of other type of positive electrode active materials as it has lower market share.

The occurrence of selective liberation has allowed the concentration of positive electrode active materials in the finer size region. Whereas, the copper and aluminium current collector is concentrated in the larger size fraction above 1 mm. Therefore, the concentration criterion of 1.5 is taken as the minimum to use the density separation to separate the copper and aluminium. It takes the assumption that the active materials are fully liberate from the surface of copper and aluminium current collector. From the calculated concentration criterion, it is observed that the density separation allows the separation of copper and aluminium from the various active materials. Moreover, the separation between copper and aluminium can be achieved via density separation.

Other component such as the separator that can be made from either polypropylene or polyethylene or the combination of both can be separated by either using water or air as the separation medium.

Having shown the qualitative assessment regarding the plausibility to use density separation to separate and concentrate different components of liberated spent LIBs. The separation based on wet and dry density separations that have been reported often target the easiest recovered materials such

as copper that is attributed by the large density difference and the active materials fine powder whereby the drag force of the flowing media.

2.4.4 Electrostatic separation
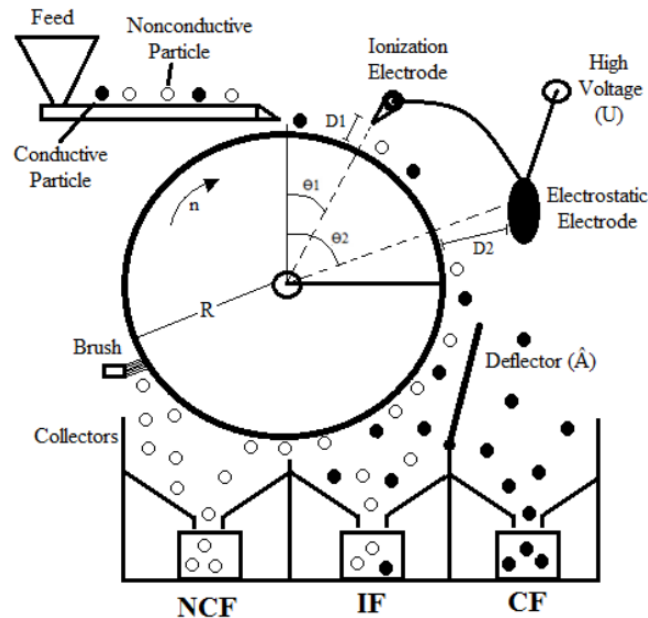
Figure 2-13 Schematic illustration of the roll-type electrostatic separator (Silveira et al., 2017). NCF: Non-conductive fraction; IF: Intermediate fraction; CF: Conductive fraction.

The electrostatic separator allows the separation of materials based on the difference in surface conductivity (electrodynamic or high tension mode) or by the preferential charging and attraction materials to an electric field of opposing charge potential (static mode) (Kelly and Spottiswood, 1989). The electrodynamic mode uses the combination of ionizing and static electrode (Figure 2-13). In the electrodynamic mode, the feed would be bombarded with ions by the ionizing electrode. The conducting particles loses charge on to the grounded rotor and thrown from the rotor and the conductive materials further attracted away from the rotor by the static electrode. Whereas, the non-conducting particles remain held to the rotor until their charge slowly dissipate. In the static mode, the separations

only employ a static electrode and does not have the ionizing electrode to attract more conductive particles away from the rotor. In its application, the use of electrodynamic and static mode can be employed to achieve the desired degree of separation.

LIB comprises of conductive and non-conductive materials. The conductive materials from spent LIBs include the copper current collector, aluminium current collector, graphite, and steel chassis. Whereas, the non-conductive include the polymeric materials and the positive electrode active materials.

Electrostatic separations has also found it ways to be useful in the case of LIB recycling in separating the conductive from the non-conductive components. Silveira et al. (2017) demonstrate that the combination of size-based separation to concentrate $LiCoO_2$ in the finer size region and electrostatic separations to separate the coarser size fraction. The separation then results in four different product class of active materials powder, polymers, mixture (polymers and metal), and the metallic fractions. However, there is no means of quantifying the recovery rate of such separation (i.e. the amount of $LiCoO_2$ in the conductive materials). Rather, it is reported as the amount of conductive fraction that is recovered. When considering the recovery rate from selective liberation that has been previously discussed, it is expected that the conductive fraction would be contaminated with substantial amount of $LiCoO_2$ particles.

2.4.5 Froth Flotation
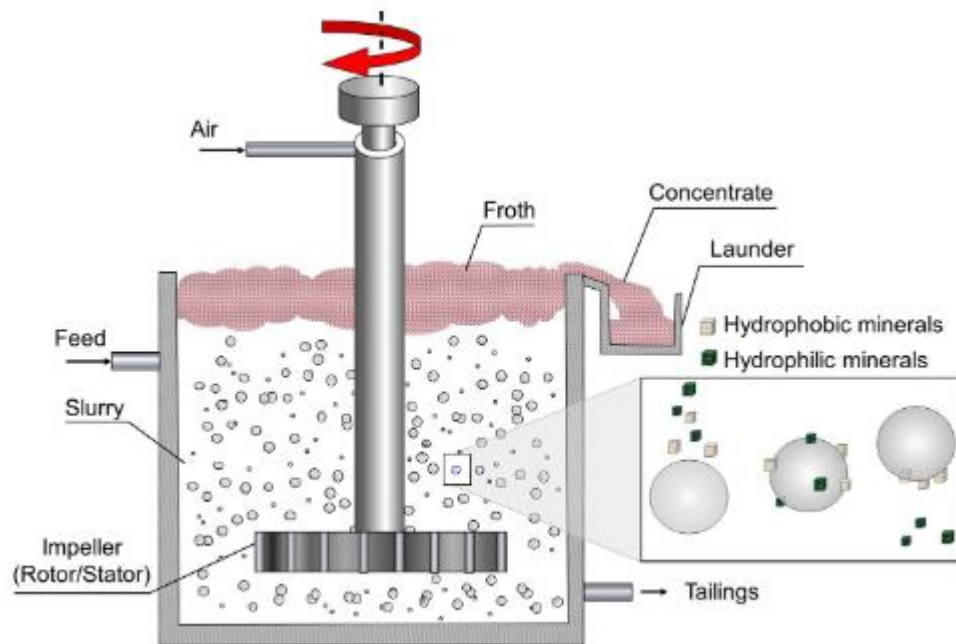
Figure 2-14 Schematic diagram of the principle of flotation (Wills and Finch, 2016a).

Flotation is a separation process that exploits natural or induced differences in hydrophobicity of the fine particles. The flotation principle is shown in Figure 2-14, the hydrophobic minerals floats and concentrated in the froth while leaving the hydrophilic minerals in the tailing. Initially, flotation has been developed to treat the sulphide minerals of copper, lead, and zinc. The use of flotation then expanded to separate nickel, platinum, and gold-hosting sulphide such as hematite and cassiterite and non-metallic minerals such as fluorite, talc, phosphates, potash, and coal (Wills and Finch, 2016a). Other than in the mining industry, flotation has also find application in dealing with environmental issue such as deinking recycled paper pulp (Hardie et al., 1999) and removal of oil refinery effluents (Rawlins, 2009).

According to the surface characteristics, all minerals can be classified in to polar and nonpolar types. The surface of nonpolar minerals does not readily attach to the water dipole, and as a result, inherently hydrophobic. Mineral of this type such as graphite, sulphur, diamond, coal, and talc thus have high natural floatability (hydrophobic). Minerals with strong covalent or ionic surface bonding are known as polar type and react strongly with water molecules; these minerals are naturally hydrophilic. The example of interaction of a surface with water is illustrated in Figure 2-15. Freshly broken quartz has an unsatisfied Si and O bonds, and hydrolyse to form SiOH(silanol) groups, which in turn hydrogen bond with the water dipoles (Wills and Finch, 2016a).
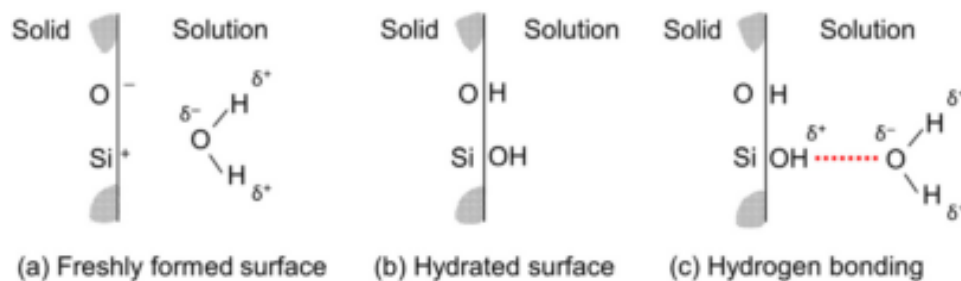
Figure 2-15 Stages in exposure of quartz to water (Wills and Finch, 2016a).

Hydrophobicity has to be imparted to most minerals in order to float them. To achieve this, surfactants known as collector are added and time allowed for adsorption during agitation is known as conditioning period. Collectors are organic compound which render the selected minerals to be water repellent by adsorbing on to the mineral surface to such a level that attachment of the particles to the bubble can be made. Collector may be non-ionizing compounds, which are practically insoluble and strongly hydrophobic. Flotation of naturally hydrophobic minerals such as coal and molybdenum that uses

kerosene to boost the floatability, sometimes referred to as oil-assisted flotation.
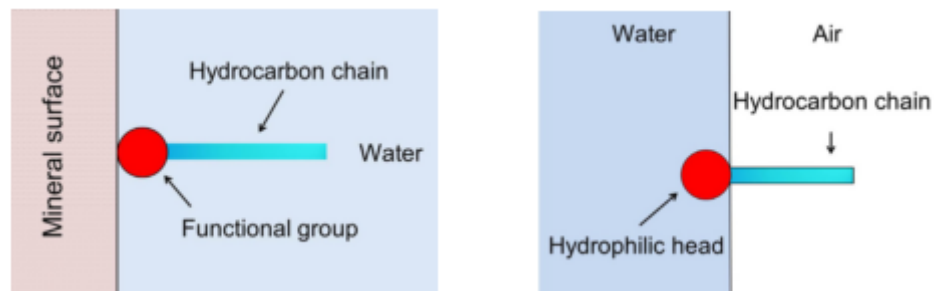
Figure 2-16 Comparison of collector and frother based on the acting interface (Wills and Finch, 2016a).

Another surfactant that is use in froth flotation is called frothers. Frothers differs from collector in several ways. From Figure 2-16, frothers act between the water and air interface, whereas collectors act on the mineral and water interface. Although, both frother and collector are surfactants, the selection of frother is ruled by in which it does not interacting with the minerals. Moreover, there are three main functions of frother in froth flotation which are; aid formation and preservation of small bubbles, reduce the bubble rise velocity, and aid formation of froth.

Reduction in bubble size increases the number and total surface area of bubble, which in turn increases the collision rate and flotation kinetics. Reducing the bubble rise velocity increases the residence time of bubbles and hence also increase the collision rate and flotation kinetics. Furthermore, the formation of froth means that the bubble does not burst when it reaches the top of the pulp and hence allowing the collectors particles to overflow as the float product. An example of common alcohol base frother is methyl isobutyl carbinol (MIBC) (Farrokhpay, 2011).
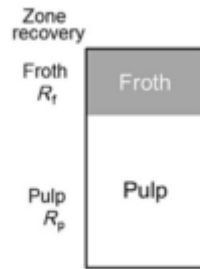
Figure 2-17 Simplified diagram between froth (zone recovery) and pulp (Wills and Finch, 2016a).

Froth structure and stability plays important role in determining mineral grade and recovery in flotation and is the main determining parameter in overall industrial flotation (Tsatouhas et al., 2006). Figure 2-17 shows the difference of froth and pulp, where the recovery zone is the froth layer. A too stable froth is not desirable, on the other hand, unstable forth is also not desired. Therefore, a froth with correct stability is the outmost important (Subrahmanyam and Forssbeg, 1988). While a stable froth will recover a greater amount of valuable particles, it also entrains more gangue (Farrokhpay, 2011). Therefore, from a viewpoint of increasing recovery and concentrate grade, there is an optimum froth stability and operating condition. These include chemical condition (frother, collector, and pH), number of hydrophobic particles in the feed, particle size distribution of the feed, aeration rate, and density of the slurry. Generally, for a given froth flotation, increasing forth depth increases the concentrate grade with the decrease in mass rate (Neethling and Cilliers, 2008).

In LIB recycling, the use of froth flotation is proven to be useful. The positive electrode active materials are concentrated in the finer size region that is also contaminated by the graphite. Graphite is naturally hydrophobic, while all positive electrode active materials are hydrophilic. The main issue with the use of

selective liberation and froth floatation not only came from the poor liberation of positive electrode active materials. Also, the presence of PVDF that is not removed after crushing and enclose the active materials making both the graphite and positive electrode active materials hydrophobic (Zhang et al., 2014b). Thus, surface modification by removal of PVDF encloses the active materials is the most pragmatic way, which may be done via thermal treatment to decompose the PVDF at 500^oC – 700^oC for 1h – 5h or chemical treatment to dissolve the PVDF by using NMP or DMF (Li et al., 2010a, Guo et al., 2016, Chen et al., 2015b, Song et al., 2013).
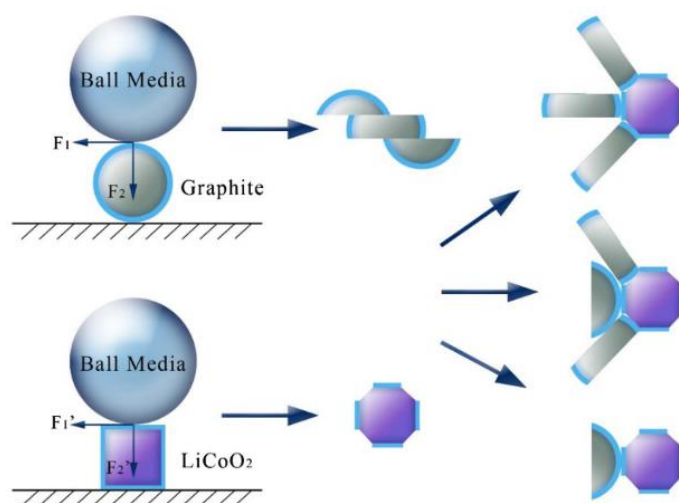
Figure 2-18 Dry modification mechanism by impact abrasion during fine grinding (Yu et al., 2018).

Other than thermal treatment and chemical dissolution, mechanical treatment has also been reported to help remove the PVDF binder. The batteries can be initially liberated and sieved to obtain $LiCoO_2$ and graphite concentrates. The $LiCoO_2$ concentrates then subjected to fine grinding in a planetary ball mill and have been reported to helps regain the hydrophobicity of the $LiCoO_2$ particles with the mechanism shown in Figure 2-18 (Yu et al., 2018). It was reported that the recovery and grade of $LiCoO_2$ particles depends on the grinding time. The

optimum grade of flotation concentrates can be achieved with 5 minutes grinding time ([Yu et al., 2018](#)). The proposed method enables 97.19 wt% grade of $LiCoO_2$ with recovery rate of 43.92 wt%.

Other novel flotation method, recovery of cathode active materials and graphite by Fenton reagent-assisted flotation, in which oxygen radicals being produced ([He et al., 2017b](#)). The Fenton's reagent (oxygen radicals) able to decompose the PVDF layer into small molecules and new chemical state such as – CF_2CH_3 detected after Fenton's reagent treatment with optimum condition of Fe^{2+}/H_2O_2 ratio of 1:120 in 30 minutes, the particles then subjected to froth flotation with the parameters of particle size, pulp density, impeller speed, pH, and aeration are -0.25mm, 40g/L, 1800rpm, 9, and 0.8 L/min respectively, with Methyl isobutyl carbinol (MIBC) and n-dodecane as frother and collector with the dosage of 150 g/t and 300 g/t respectively. Although the Fenton's reagent seems promising, the recovery rate of $LiCoO_2$ and graphite concentrates were only 39.6wt% and 16.8wt% respectively. The low recovery was caused by the poor liberation during preliminary treatment.

The use of froth flotation in the separation of $LiCoO_2$ and graphite mixture has been proven to be an effective method. However, it can be deduced that the poor initial liberation to obtain the $LiCoO_2$-graphite concentrates have made the overall recovery rate to be lower than expected.

2.5 The effect of impurities on positive electrode active materials resynthesizing

The positive electrode active materials concentrate obtained via mechanical treatment may be re-synthesized with or without undergoing hydrometallurgical steps. The latter can be done when the positive electrode active materials can be recovered as it is found in spent LIBs and undergo re-lithiation. The selective liberation of positive electrode active materials often entailed with liberations of other components such as copper and aluminium.

2.5.1 Re-synthesis via chemical treatment

In conventional hydrometallurgy-dominant process, the key steps are of leaching, precipitation, and solvent extraction. Leaching of LIBs, is the dissolution of targeted elements by lixiviant that may include mineral acids, organic acids, and alkaline solutions (Liu et al., 2019a).

The leaching mechanism by HCl (Wang et al., 2009, Zhang et al., 1998), HNO_3 (Myoung et al., 2002, Li et al., 2011), and H_2SO_4 (Ferreira et al., 2009, Nan et al., 2005) in dissolving $LiCoO_2$ are described in the Equation 2-8, Equation 2-9, and Equation 2-10.

$3HCl+LiCoO_2=LiCl+CoCl_2+1.5H_2O+0.25O_2$	**Equation 2-8**
$3HNO_3+LiCoO_2=LiNO_3+Co(NO_3)+1.5H_2O+0.25O_2$	**Equation 2-9**
$3H_2SO_4+2LiCoO_2+H_2O_2=Li_2SO_4+2CoSO_4+5H_2O+1.5O_2$	**Equation 2-10**
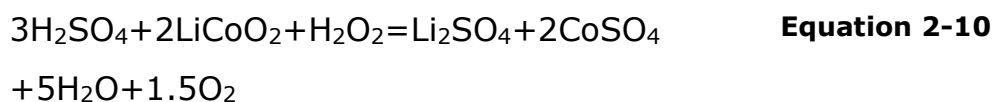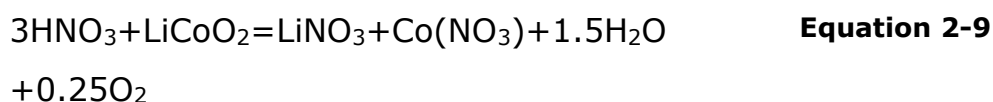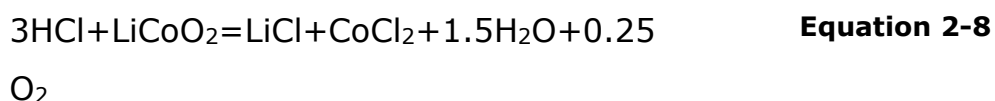
Organic acid such as citric acid (Li et al., 2013a), formic acid (Gao et al., 2017), malic acid (Li et al., 2013a), aspartic acid (Li et al., 2013a), ascorbic acid (Nayaka et al., 2016b), oxalic acid (Zeng et al., 2015), and glycine(Nayaka et al., 2016c) can also be used to effectively leach the positive electrode active materials. The leaching reaction, such as in the use of citric acid as lixiviant (Chen et al., 2016c), can be described as Equation 2-11. Other organic acids also presents similar mechanism (Liu et al., 2019a).

$$18H_3Cit+18LiNi_{1/3}Co_{1/3}Mn_{1/3}O_2+C_6H_{12}O_6=$$
$$6Li_3Cit+2Ni_3(Cit)_2+2Co_3(Cit)_2+2Mn_3(Cit)_2+$$
$$33H_2O+6CO_2$$

Equation 2-11
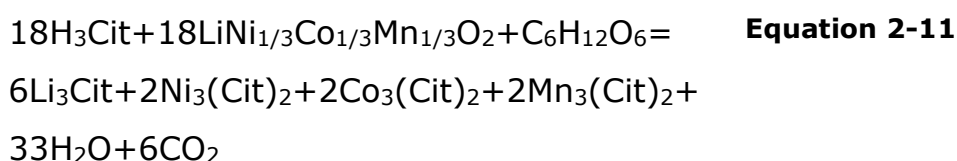
Furthermore, the use of alkaline system has also been explored to selectively dissolve nickel, cobalt, copper, and lithium from ore and waste materials (Meng and Han, 1996, Sun et al., 2015), while manganese is seldom dissolved (Ku et al., 2016, Zheng et al., 2017b). The formation of nickel and cobalt containing amine complexes under proper pH can be described in Equation 2-12 and Equation 2-13 (Liu et al., 2019a).

$$Ni^{2+}+nNH_3=Ni(NH_3)n^{2+}$$

Equation 2-12

$$Co^{2+}+nNH_3=Co(NH_3)n^{2+}$$

Equation 2-13

The significant of ammoniacal leaching lies in its selectivity towards nickel, cobalt and copper. While, other metal such as iron, magnesium, manganese, and calcium are less readily to form ligand with the ammonia.

Solvent extraction can be used to obtain the desired components in the form of pure metal or pure metal compound by exploiting the advantage of different relative solubility of the same compound in different immiscible liquid. The extraction mechanism of D2EHPA and Cyanex 272 can be described by Equation 2-14 and Equation 2-15 (Granata et al., 2012b, Swain et al., 2008).

$$M^{2+}+A^-+2(HA)_{2org}=MA_2.3HA_{org}+H^+ \qquad \textbf{Equation 2-14}$$

$$MOH^++2(HA)_{2org}=M(OH)A.3HA_{org}+H^+ \qquad \textbf{Equation 2-15}$$

Where $A^-_{org}+2(HA)_{2org}$ indicates the extractant saponified by the Equation 2-16.

$$2Na^++(HA)_{2org}=2NaA_{org}+2H^+ \qquad \textbf{Equation 2-16}$$
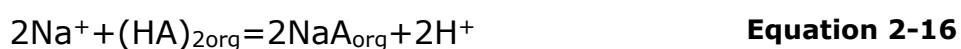
Extractant often have selectivity for different metal ions and it is dependent on the equilibrium pH. For example, D2EHPA can selectively extract Cu and Mn ions, whereas its extraction selectivity is poor for Co at pH 2.2-3.0 (Wang et al., 2016a).

Other than the solvent-solvent extraction, precipitation has also been widely used to extract metal or metal compound from liquid system. It has been reported that dimethylglyoxime reagent (DMG, $C_4H_8N_2O_2$) and ammonium oxalate is capable of selectively precipitate Ni^{2+} and Co^{2+} from the mixed solutions (Chen et al., 2015c). The precipitation mechanisms are shown by Equation 2-17 and Equation 2-18.

$$Ni^{2+}+2C_4H_8N_2O_2=Ni(C_4H_7N_2O_2)_2+2H^+ \qquad \textbf{Equation 2-17}$$

$$Co^{2+}+(NH_4)_2C_2O_4+2OH^- \qquad \textbf{Equation 2-18}$$
$$=CoC_2O_4.2H_2O+2NH_3$$
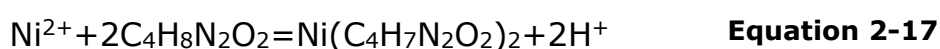
After removing Ni^{2+} and Co^{2+}, the Li^{1+} can be separated by adding Na_2CO_3 or H_3PO_4, as described in Equation 2-19 and Equation 2-20 (Chen et al., 2015c, Pant and Dolker, 2017).

$$2Li^{+}+CO_3^{2-}=Li_2CO_3 \qquad \textbf{Equation 2-19}$$

$$3Li^{+}+PO_4^{3-}=Li_3PO_4 \qquad \textbf{Equation 2-20}$$

Other than to recover the precious elements contained within spent LIBs, precipitation has been proposed to remove trace amount of impurities such as iron, copper, or aluminium (Granata et al., 2012a, Chen et al., 2011, Zheng et al., 2017a, Joo et al., 2016b).

Table 2-6 Reported case of impurities towards the performance of re-synthesized positive electrode active materials.

Reference	Method/ Impurities	Capacity Performance
(Weng et al., 2013)	Co-precipitation/ Magnesium <360mg/L	94%
(Zou et al., 2013)	Co-precipitation/ Iron <N/A	N/A
(Gratz et al., 2014)	Co-precipitation/ Iron and copper 0.6 wt%	N/A
(Sa et al., 2015b)	Co-precipitation/ Copper < 5wt%	100%
(Chen et al., 2016b)	Thermal treatment/ Al< 0.4wt% and Cu<0.6wt%	100%

The hydrometallugical process of LIBs recycling is a complex process in nature. Most researcher obtain the high-grade positive electrode active materials via manual dismantling that is often not practical in industrial scale. In a mechanical treatment of spent LIBs leachable contamination such as iron,

copper, and aluminium are often expected. Several notable researches have been dedicated in understanding the effect of such impurities in re-synthesis of positive electrode active materials with the co-existence of such impurities. The performance of positive electrode active materials together with the amount of impurities is summarised in Table 2-6.

From Table 2-6, it can be understood that a tolerable amount of impurities does exist and there is the need to minimise such impurities to be able to re-synthesis the dissolved targeted metals into fully functioning positive electrode active materials. It is also important to point out that the iron impurities can be efficiently removed by adjusting the pH. Moreover, the aluminium impurities can be removed by selectively dissolving it in NaOH. The main concern of LIBs recycling is the contamination from copper. The 5 wt% of copper contamination has been reported to be tolerable as a precursor. The battery produces acceptable capacity retention rate (Sa et al., 2015b).

2.5.2 Re-lithiation

Re-lithiation is the process in which the active materials does not need to undergo hydrometallurgical processes. Instead, the active materials is resynthesized in a single step treatment. Kim et al. (2004) proposed a simultaneous separation and regeneration of $LiCoO_2$ with the use of hydrothermal method at 200^oC in a concentrated LiOH solution. The reported impurities is Al/Co of 0.03. Ganter et al. (2014) demonstrated that it is possible to do lithiation to spent $LiFePO_4$ via the electrochemical and chemical lithiation.

2.6 Conclusion and research gap

The liberation of spent LIBs potentially cause explosion due to the combination of short circuit (from the leftover voltage) and flammable electrolytes with the presence of oxygen. One of the three components that can cause explosion may be minimised in several ways.

Discharging to minimise the voltage to near zero can be used to prevent spark and minimise heat from the short circuit. The discharging can be carried out with different method such as via the immersion of battery into brine solution or using resistor. The latter being safer, as it does not produce chlorine gas as well as unwanted water contamination. Due to the different geometries in which LIBs are produce, the use of resistor to discharge spent LIBs being the least favourite option. Moreover, it may require strenuous amount of labour work to connect the positive and negative pole to the resistor.

Furthermore, the spent LIBs can be immersed in liquid nitrogen. The use of low temperature causes the inactivation of the galvanic element inside LIB (i.e. battery capacity last shorter during winter) and reduces the flammability of the electrolytes as the temperature is below its flash point. However, due to its expense it may not be practical in an industrial scale.

Other precautionary step such as the liberation in an inert atmosphere can be carried out to prevent explosion. The oxygen concentration is minimised and hence the explosion is prevented.

Safe liberation of spent LIBs requires pre-treatment of spent LIBs in which it eliminates one of the three main components that is required to cause explosion. Discharging can be regarded as the simplest and the most favourite option as it

removes the ignition source. The immersion of spent LIBs in a brine solution expected to discharge the battery via the electrolysis of water. However, there is a design flaw in this step as it does not take account the possibility of chlorine gas formation. Overpotential is the difference in the theoretical and the real voltage that is required to carry out electrolysis. In the case of discharging LIBs in a brine solution, the higher overpotential of oxygen in the negative electrode as compared to chlorine causes problem. In practice, chlorine gas would be formed instead of oxygen. Moreover, other techniques to minimise the explosion hazard is still unpractical on an industrial scale. Therefore, there is the need for innovation in discharging spent LIBs.

In minerals engineering research, the difference in mechanical and physical properties of different components causes different components to break into different sizes during the comminution process. Moreover, a suitable comminution technique (i.e. suitable load) is required to exploit the difference in mechanical and physical properties that allows the valuable component to be selectively liberated. The analysis related to the selective liberation of mineral can be done by measuring the phase-specific interfacial area. The measurement can be done in two dimensional by using SEM-EDX or three dimensional such as XMT. The latter being less bias, for the two-dimensional observation would depends on which side and depth of the rock being chosen for observation. A reduction in the phase-specific interfacial area would indicate the existence of selective liberation.

The occurrence of selective liberation in the comminution of spent LIBs is based on the dependence of recovery of different components related to different particle size range. Chassis

material such as steel or polymer are concentrated in the coarser size fraction. Followed by the copper and aluminium current collector in the mid-range size fraction. Finally, the positive and negative electrode active materials are concentrated in the finer size region. The LIBs assembly is much simpler when compared to the assembly of naturally occurring minerals. The positive and negative electrodes inside LIBs are made of aluminium and copper foils that are coated with active materials on either one or both sides and held together by the binder. Makin a planar assembly that can be effectively observed and interpreted in two dimensional as compared to the naturally occurring mineral ore that may be bias with the same technique. Despite the known phenomenon of selective liberations in the comminution of spent LIBs, there is minimum effort to study and understand the mechanism.

Following comminution, the steel can be efficiently separated by using dry magnetic separator. The liberated spent LIBs that has minimum contamination from iron can be further separated to take the advantage of the selective liberation phenomenon. The positive electrode active materials that is concentrated in the finer size region can be concentrated by using size-based separation or gravity separation such as by using air classifier. Both methods produce fine positive electrode active materials concentrates. The reported recovery rate of size-based separation and gravity separation are 56.4 wt% and 75.0 wt% respectively. The low recovery rate may be due to the sub-optimum liberation method being employed. However, morphological analysis related to the classified comminution product have not been reported to confirm this phenomenon.

The exploitation of selective liberations produces two streams of different size fractions that have different predominant

component in coarser and finer size fraction. For the coarser size fraction, gravity and electrostatic separation can be used to separate the copper and aluminium foil from the polymeric materials from the separator and the chassis. However, the reported results do not report the problems related to the sub-optimum selective liberation. The problems related to the sub-optimum selective liberation is more apparent in the recovery of positive electrode active materials in the finer size region.

The use of froth flotation is useful to separate the fine fractions after size. Due to the weaker PVDF-Graphite than the PVDF-$LiCoO_2$ towards the current collectors, the liberation of $LiCoO_2$ particles would also follow by at least the same amount of liberation of graphite particles. However, the comminution of spent LIBs does not remove the PVDF binder that makes both $LiCoO_2$ and graphite particles hydrophobic. Thus, to restore the hydrophilicity of $LiCoO_2$ particles, the removal of PVDF is necessary. The use of thermal treatment or organic chemicals allows the decomposition or dissolution of PVDF binder. More recently, the use of planetary ball mill after size-based separation can induce the removal of PVDF that coats the $LiCoO_2$ particles that is caused by the impact abrasion of the grinding media. Despite the applicability of ball milling in restoring the hydrophilicity of $LiCoO_2$ particles, the recovery rate is only 43.92 wt% that is mainly caused by the sub-optimum selective liberation.

The uncertainty related to the type of positive electrode active materials for the future in LIBs production have made hydrometallurgical process to be a pragmatic option. The hydrometallurgical process involves the transfer of desired metals into the solution via leaching and recovered as precursor materials to be re-synthesised as new positive electrode active

materials. The extraction of desired component also followed by the extraction of unwanted metals and need to be minimised. The liberation of positive electrode active materials would also result in the breakage of unwanted metals that cannot be removed via magnetic separation such as copper, aluminium, and iron (i.e. from the milling machine). The iron impurities can be efficiently removed by adjusting the pH. Moreover, the aluminium impurities can be removed by selectively dissolving it by NaOH. The main concern of LIBs recycling is the contamination from copper. The 5 wt% of copper contamination has been reported to be tolerable as a concentrate that can be further processed.

Other than hydrometallurgical processes, the positive electrode active materials concentrate that have minimum to no metal contamination can be re-lithiated to be used in the production of new LIBs. However, the concept of re-lithiation requires the prior segregation of different types of battery as well as higher purity than that of hydrometallurgical processes. Moreover, it is also expected that the future LIBs would use another type of positive electrode active material as to have higher energy density as the current generation.

In conclusion, physical or mechanical processes has always been perceived by researchers as a pre-treatment steps to liberate and concentrate positive electrode active materials from spent LIBs recycling. In this literature review, some research gaps have been notes. The use of brine solution as to discharge the leftover energy in spent LIBs have an obvious problem in practice. Moreover, the occurrence of the selective liberation has not been given much attention. The sub-optimum selective liberation causes low recovery rate of positive electrode active materials in the subsequent physical processes.

Moreover, the use of physical treatments also produces copper, aluminium, and iron contaminations that may affect the subsequent hydrometallurgical processes. The contamination of iron and aluminium can be efficiently and selectively removed via hydrometallurgical processes. The challenges came from the copper contamination and hence the development of suitable mechanical process needs to focus in minimising such contamination that is at least lower than 5 wt%.

This page is intentionally left blank.

Chapter 3 Experimental Methodology

3.1 Introduction

The work presented in this section covers the preparation of the samples used in this research as well as the analysis carried out. To ensure continuity, the attrition scrubber, electrostatic separator, and froth flotation will be explained in the introduction of the chapter where it covers. Therefore, this methodology presented covers the sample preparation and analysis carried out for the entire thesis.

This chapter would firstly describe the overview of the experimental design that is intended to be carried out in this project. Following the experimental design, details regarding samples selected for this study and subsequent treatment to obtain representative sample which captures the physical and chemical characteristics of the bulk sample is discussed. The qualitative and quantitative analytical techniques were used in understanding the liberation and concentration of $LiCoO_2$ particles is discussed.

3.2 Experimental design
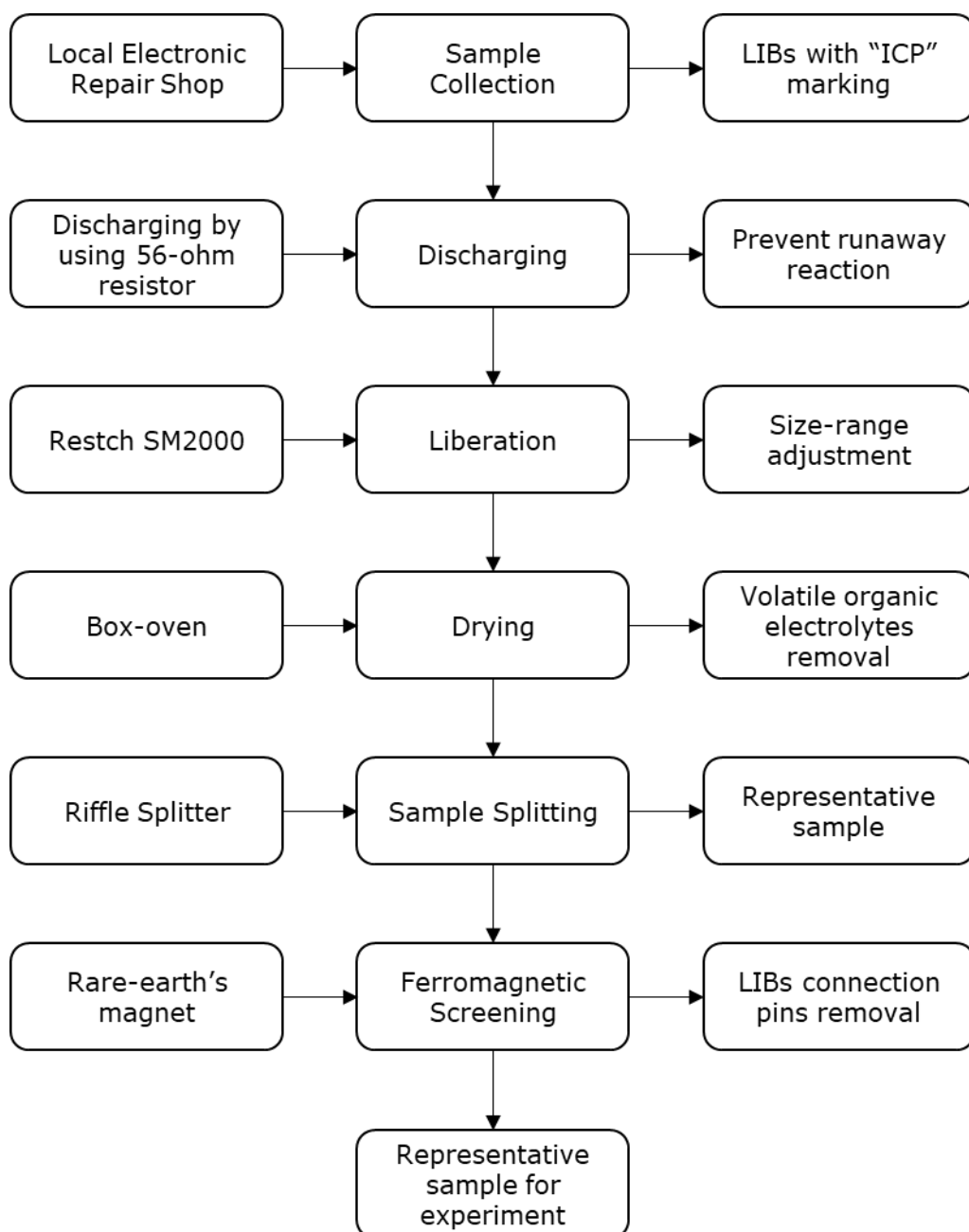
Figure 3-1 Flow diagram for the sample preparation for this thesis.

Figure 3-1 presents the process flow diagram to produce samples for this experimental study. The collected prismatic spent LIBs were initially discharged and then liberated using a cutting mill. The bulk liberated sample was then dried in a box oven to remove volatile organic electrolytes. The dried sample was then split into aliquots, producing representative samples.

The reduced size sample was then screened for ferromagnetic materials that mainly came from the positive and negative connection pins. The reduced size dried sample with minimum iron contamination is then characterised and also used for subsequent experimental study.

Characterisation is carried out to understand whether the cutting mill induces an acceptable degree of liberation. The sample is sieved to different size fractions and analysed for the crystallinity by using XRD, morphology by using SEM-EDX, and elemental analysis via acid-microwave assisted digestion and detected by using ICP-MS. The characterisation aims at identifying the type of materials contained within spent LIBs as well as the selective liberation induced by the cutting mill.

The representative samples was sieved into different size fractions. The fine size fraction of < 38 μm is tested for crystal structure by using an XRD to confirm the type of active materials that are $LiCoO_2$ and graphite.

The different size fractions were subjected to morphology observation by using SEM-EDX. For the larger size fraction > 850 μm the copper foil, aluminium foil, and separator were removed manually. Whereas, the finer size fraction < 850 μm is directly mounted on to the carbon adhesive tape. Furthermore, other than the morphological observation, the EDX also helps in identify the type of the binder being used as well confirming the type of positive electrode active materials via the absence of other transition metals (i.e. Mn, Ni).

```
                    ┌─────────────────┐
                    │  Representative  │
                    │   sample for    │
                    │   experiment    │
                    └─────────────────┘
                             │
                             ▼
┌──────────────┐    ┌─────────────────┐    ┌──────────────────┐
│ Sieve & sieve│───▶│     Sieving     │───▶│  Particle size   │
│    shaker    │    │                 │    │  distribution    │
└──────────────┘    └─────────────────┘    └──────────────────┘
                             │
                             ▼
┌──────────────┐    ┌─────────────────┐    ┌──────────────────┐
│Size fraction │    │                 │    │  Confirm the     │
│of < 38 µm    │───▶│Crystal structure│───▶│  types of active │
│tested with   │    │                 │    │  materials       │
│XRD           │    └─────────────────┘    └──────────────────┘
└──────────────┘             │
                             ▼
┌──────────────┐    ┌─────────────────┐    ┌──────────────────┐
│Different size│    │   Morphology    │    │    Particle      │
│range tested  │───▶│  observation    │───▶│ morphology for   │
│using SEM-EDX │    │                 │    │ different sizes  │
└──────────────┘    └─────────────────┘    └──────────────────┘
                             │
                             ▼
┌──────────────┐    ┌─────────────────┐    ┌──────────────────┐
│Different size│    │   Elemental     │    │   Size-based     │
│range tested  │───▶│   analysis      │───▶│ recovery rate of │
│using ICP-MS  │    │                 │    │ Co, Cu, and Al   │
└──────────────┘    └─────────────────┘    └──────────────────┘
                             │
                             ▼
                    ┌─────────────────┐
                    │  Data analysis  │
                    └─────────────────┘
```

Figure 3-2 Flow diagram for the sample characterisation.

The characterisation step is summarised in Figure 3-2. To assess the occurrence of selective liberation, elemental analysis of the different size fractions concerning aluminium, cobalt and copper is carry out. The copper and aluminium reflect the recovery rate of the negative and positive electrode. Whereas, the cobalt reflects the recovery rate of the positive electrode active materials (i.e. $LiCoO_2$). The results can then be assessed by using Fuerstenau upgrading curve and ore separation degree curve to assess the occurrence of selective liberation as well as the optimum cut point to concentrate the $LiCoO_2$ particles.

Furthermore, it is not the intention of this study to selectively liberate graphite and hence the selective liberation of graphite is not considered in the experimental design stage. When considering the weaker attachment of graphite laminate on to the copper current collector than the $LiCoO_2$ laminate on to the aluminium current collector. The degree of graphite liberation can be assumed to be equal than that of the $LiCoO_2$ counterparts. One point to be noted from this assumption is that; it may underestimate the degree of graphite liberation.

As single stage liberation using cutting mill is expected to have low recovery rate that concentrate $LiCoO_2$ particles (Yu et al., 2018), the use of an attrition scrubber is proposed as a secondary liberation step.

The attrition scrubbing is carried out with the use of silica sand as the abrasive media. Wet sieving is carried out with 212 µm test sieve to prevent damage to the 38 µm sieve. The products then dried in a box oven until constant weight with the parameters previously stated. The dried sample then dry sieved into various size fractions and would be described further in Chapter 5. The size fractions from the dry sieving that have the same size fraction than that of the wet sieving is re mixed. Each different size fraction then analysed for metallic elements aluminium, cobalt, and copper. The size-based recovery rate is then calculated and the improvement in selective liberation in $LiCoO_2$ particles can then be compared for the samples before and after attrition.

```
                    ┌─────────────────┐
                    │ Representative  │
                    │   sample for    │
                    │   experiment    │
                    └─────────────────┘
                            │
                            ▼
┌──────────────┐    ┌─────────────────┐    ┌─────────────────┐
│Attrition with│    │                 │    │   Selective     │
│ silica sand  │──► │   Attrition     │──► │ liberation of   │
│    media     │    │   Scrubbing     │    │ LiCoO₂ particles│
└──────────────┘    └─────────────────┘    │   and PVDF      │
                            │               │  delamination   │
                            ▼               └─────────────────┘
┌──────────────┐    ┌─────────────────┐    ┌─────────────────┐
│212 µm & 38 µm│    │                 │    │ Fine(< 38 µm) & │
│    sieves    │──► │  Wet Sieving    │──► │ coarse(> 38 µm) │
└──────────────┘    └─────────────────┘    │   products      │
                            │               └─────────────────┘
                            ▼
┌──────────────┐    ┌─────────────────┐    ┌─────────────────┐
│              │    │                 │    │  Dried fine &   │
│   Box-oven   │──► │    Drying       │──► │ coarse products │
└──────────────┘    └─────────────────┘    └─────────────────┘
                            │
                            ▼
┌──────────────┐    ┌─────────────────┐    ┌─────────────────┐
│Sieving of    │    │                 │    │ Different size  │
│coarse size   │──► │  Dry Sieving    │──► │   fractions     │
│fraction      │    └─────────────────┘    │ (fines are mixed)│
└──────────────┘            │               └─────────────────┘
                            ▼
┌──────────────┐    ┌─────────────────┐    ┌─────────────────┐
│Different size │    │                 │    │   Particle      │
│range tested   │──► │  Morphology     │──► │ morphology for  │
│using SEM-EDX  │    │  observation    │    │ different sizes │
└──────────────┘    └─────────────────┘    └─────────────────┘
                            │
                            ▼
┌──────────────┐    ┌─────────────────┐    ┌─────────────────┐
│Different size │    │                 │    │  Size-based     │
│range tested   │──► │  Elemental      │──► │ recovery rate of│
│using ICP-MS   │    │  analysis       │    │ Co, Cu, and Al  │
└──────────────┘    └─────────────────┘    └─────────────────┘
                            │
                            ▼
                    ┌─────────────────┐
                    │  Data analysis  │
                    └─────────────────┘
```

Figure 3-3 Flow diagram for the attrition scrubbing experiment.

The flow diagram for the attrition scrubbing experiment is presented in Figure 3-3.

The coarse and fines attrition product can be further separated based on the difference surface conductivity and surface

hydrophobicity. Electrostatic separation is to separate the coarse product based on specific gravity and surface conductivity.
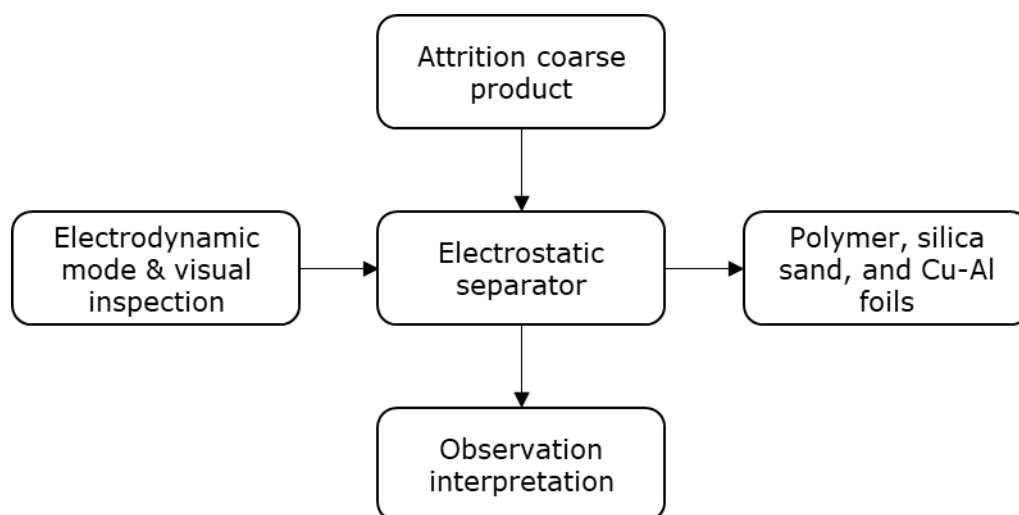
Figure 3-4 The use of electrostatic separator in separation of attrition coarse product.

Figure 3-4 shows the intended use of electrostatic separator in this study. The electrodynamic mode, the combination of ionising and lifting electrode, is used to separate the coarse product. The resulting product is expected to concentrate three main components of polymeric materials, silica sand media, and the copper and aluminium foils. The experiment would be carried out based on the trial and error method and checked via visual inspection.

Furthermore, the use of fine grinding such as ball mill has been shown to be able to restore the hydrophilicity of $LiCoO_2$ particles that can be separated via the use of froth flotation. Thus, in this thesis, flotation test is carried out to also study whether attrition scrubbing allows the removal of PVDF coating that render both $LiCoO_2$ and graphite hydrophobic.
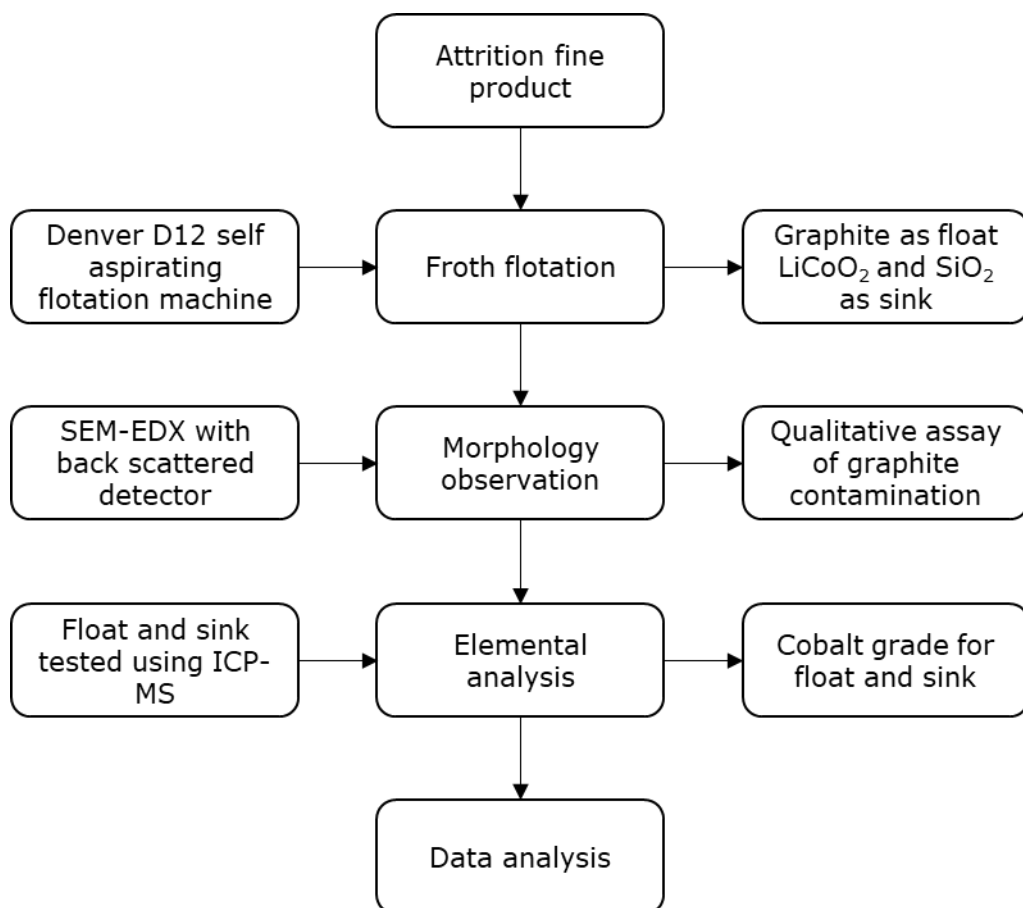
Figure 3-5 The intended use of froth flotation in separation of attrition fine product.

From Figure 3-5 the flotation product is assessed by using SEM-EDX and elemental analysis that involve acid-microwave digestion and detected by using an ICP-MS. The SEM-EDX observation is carried out by using back scattered detector to qualitatively differentiate the graphite from other component based on the perceived contrast. Elemental analysis is then carried out to determine the cobalt grade for the float and sink. A substantial difference in cobalt grade in the float and sink indicates that attrition scrubber does induce delamination of PVDF binder.

3.3 Sample preparation for experiment

3.3.1 Sample selection and pre-treatment

The spent LIBs used in this study were collected from local electronic repair shops within Ningbo China. The batteries were previously used in smartphones and came from a range manufacturer. Only prismatic LIBs with predominantly cobalt as positive electrode active materials were used. The type of active materials within a LIB can be identified by the marking that follows *BS EN 61960-3:2017* (British Standard Institution, 2017).

Figure 3-6 Photograph of new ICP-LIBs and spent ICP-LIBs (left); and an example of battery discharging (right).

This is identified by the "ICP" marking (Figure 3-6); the letter "I" designates the carbon negative electrode basis; the letter "C" designates the cobalt positive electrode basis; the letter "P" designates the prismatic shape of the cell. From Figure 3-6 1ICP4/49/120, the number one means use as one cell, followed by carbon and cobalt as the main component enclosed in prismatic form factor, and the subsequent numbering of 4/49/120 means it has a dimension of 4 mm thickness, 49 mm

width, and 120 mm in length. Other designations for other types of positive and negative electrode basis as well as the shape of the cell can be found in *BS EN 61960-3:2017*.

The spent LIBs protective cap and connector were firstly open and detached to expose the positive and negative poles. The LIBs then discharged by using crocodile clips connected to a load of 56-ohm resistor (Figure 3-6) until the voltage is near zero (0.2 V – 0.5 V). Depending on the initial voltage of the battery, the discharging time can take from one to several days. Prior liberation, the voltage of the battery is checked by using a digital multi meter to ensure safe voltage for liberation.

3.3.2 Sample preparation and size reduction

Discharged LIBs were shredded by using a cutting mill (Restch SM 2000) with an 8 mm grid until no more particles passing through the grid. To remove the volatile electrolytes, the shredded LIBs are dried in a box oven at 80°C (Yin Jing Machine (Shanghai) Co., LTD). The equipment for size reduction and drying are shown in Figure 3-7.

According to *BS 812-109: 1990*, The determination of dry mass of a material from water requires the drying of materials between 105°C to 110°C until constant weight is achieved (British Standard Institution, 1990).

Figure 3-7 – Photograph of cutting mill (left) and the box oven (right).

In the field of LIBs recycling, drying temperature from room temperature up to 90°C is commonly employed (Li et al., 2010b, Mantuano et al., 2006, Nayaka et al., 2015, Diekmann et al., 2017, Wang et al., 2016c). The use of this temperature range is used to prevent the production HF gas from the decomposition of the electrolyte ($LiPF_6$) at temperature greater than 85°C under atmospheric pressure (Yang et al., 2006). Due to safety aspects, in this study the temperature of 80°C is used for the entire dry mass determination. The samples were dried to constant weight, when the mass change is < 0.1 wt% it is then taken as the dry mass. The use of 80°C in determination of water moisture content have been reported to not substantially affect the accuracy of the results as compared to 110°C (O'Kelly and Sivakumar, 2014). Therefore, *BS 812-109:1990* was modified to take the safety issue into account with confidence that accuracy has not been compromised.

3.3.3 Representative sample

Representative samples were prepared using a riffle splitter with each chute size of 31 mm x 160 mm with 16 alternating chutes (Figure 3-8). The general principle is that the bulk

sample is divided by parallel chutes leading to two separate receptacles.

Figure 3-8 – Photograph of the riffle splitter.

Petersen et al. (2004) showed the appropriate design and use of riffle splitter. For this device to work properly, it needs to have an even number of chutes of which every second leads to the two alternate receptacles. All the chute needs to have the same the same size and form. Moreover, the width of the chutes also to have a certain minimum with at least two times the maximum particle size plus 5 mm. In this project, the sampling method is adapted from BS 3406-1: 1986 (British Standard Institution, 1986). The division method employed is of with the reduction ratio of $1/2^n$, with n the reduction stage. It is important to point out that it is not possible to ascertain whether a particular sample is representative or not (Petersen et al., 2005). The acceptable coefficient of variation of sub sample masses by using riffle splitter is 5.9 wt% to 9.0 wt% *BS 3406-1: 1986* (British Standard Institution, 1986). To obtain the coefficient of variation of < 9.0 wt%, the deviation of the sub sample mass from the parenting bulk is minimised by allowing maximum of 5 wt% from the ideal half parenting bulk mass. When the

deviation is more than 5 wt % form the ideal split of $1/2^n$, the sample is re-mixed and re-split until de deviation from the ideal mass is less than 5 wt%.

The representative sample is then subject to magnetic separation to remove ferrous materials by using a rare earth magnet enclosed in a PVC pipe. Producing representative LIB samples that have minimum ferrous material.

3.4 Analysis techniques

3.4.1 Particle size distribution by sieving

Figure 3-9 Photograph of the certified test sieve (left) and stacked sieves on a sieve shaker (right).

To obtain the particle size distribution, sieving is used. The assessment of the particle size distribution are carried out by using certified test sieve (Endecotts, *ISO 13310-2* and *ISO 13310-1*) and a fixed amplitude shaker (Capco Inclino Sieve Shaker 3) shown in Figure 3-9 (British Standard Institution, 2013, British Standard Institution, 2016). The sieving test carried out is in accordance with the *BS EN 933-1: 2012* (British Standard Institution, 2012). The sieving is carried out until the change in mass is < 1 wt% in one minute.

The results of sieving should always be plotted graphically to assess their full significance, the most common being that plotting either cumulative undersize or oversize against particle size (Wills and Finch, 2016e). The plot of cumulative undersize is a mirror image of cumulative oversize, and therefore, it is not necessary to plot both curves. The plot is carried out using a semi-logarithmic coordinate to avoid finer aperture sizes become congested. In this thesis, the cumulative undersize is used as a means to interpret the particle size distribution.

3.4.2 X-Ray Diffraction (XRD)

X-Ray Powder Diffraction (XRD) is a rapid analytical technique to identify phase of a crystalline materials. The XRD technique in laboratories has its beginning from X-ray crystallography, where it can determine the atomic and molecular structure of crystals. The crystalline atom will cause the incoming X-rays to diffract into many specific directions. The angles and energy of the diffracted X-rays can be interpreted into three-dimensional structure of the electron density within the crystal. Moreover, the positions of the atom in the crystal can then be determined along with the bond.

Figure 3-10 Photograph of the X-ray powder diffraction machine.

In its conventional form, incident beam of X-rays is directed upon the sample crystal, the X-ray will diffract according to the atom spacing in the crystalline lattice. The majority of the incident X-ray is transmitted through the sample, while a small portion is diffracted onto the photographic plate. The X-ray is able to undergo scattering as their wavelengths are similar to that of the spacing between the planes in the crystals. The diffracted X-rays emanate out from the sample crystal in cone patterns according to the relationships between the crystal lattice spacing (d) and θ of Equation 3-1.

$$n.\lambda = 2d.\sin(\theta)$$ **Equation 3-1**

where d is the atomic spacing within the crystal, n is an integer, and theta (θ) is the angle between the sample and the detector.

In this thesis, XRD with Cu-Kα source made by Bruker with AXS D8 Advance model is used to identify the type of positive electrode active materials inside LIBs (Figure 3-10). Instead of vertical or horizontal XRD (θ-2θ geometry), the vertical θ-θ Bragg-Brentano setup has become more popular (Figure 3-11). The sample is mounted in on a goniometer and gradually rotated while being bombarded by X-rays, producing a diffraction pattern on regularly spaced spots known as reflection. The two-dimensional images taken at different rotations are converted into a three-dimensional model of the density of the electrons by using a mathematical model of Fourier transform.
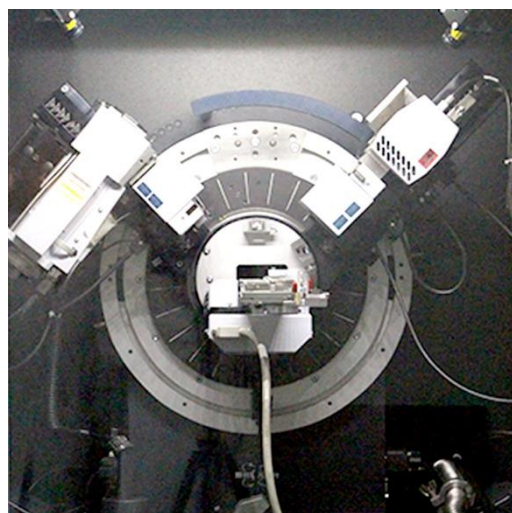
Figure 3-11 Photograph of the Goniometer known as the vertical θ-θ Bragg-Brentani setup.

The XRD spectra that are generated by most software processing are not in the form of diffraction patterns. The data obtained is in the form of an x-axis and y-axis scale. The x-axis is multiple of the diffraction angle 2θ and the y-axis is the intensity in arbitrary unit. In this thesis, the XRD parameters adapted from Li et al. (2010a). The XRD parameters include, scanning angle, step size, and count time of 10°-100°, 0.5^o, and 1s respectively are used.

3.4.3 Scanning Electron Microscopy – Energy Dispersive X-Ray (SEM-EDX)

Field emission scanning electron microscopy (FESEM) is achieved through the use of field emission gun (FEG) instead of conventional scanning electron microscopy (SEM) that uses tungsten hairpin or lanthanum hexaboride (LaB_6). FESEM provides higher resolution in the whole range of accelerating voltage in which may be able to take better image at higher magnification. While the energy dispersive spectrometry (EDS) system detects X-rays emitted from the sample as a result of high-energy electron beam penetrating into the sample and collected by EDX detector, yielding the elemental analysis of

the sample. The combination of FESEM and EDX called FESEM-EDX.

For the purpose of this research, SEM-EDX from Zeiss with Oxford/ Sigma VP EDX detector is used. In this SEM, there are several detectors used for image capture, the detectors used in this project are back scattered detector (BSD) and secondary electron detector (SE). The difference between BSD and SE are the depth of penetration in which SE penetrated shallower depth than BSD and BSD able to differentiate different elements according to the contrast of the image being captured, where lighter elements are darker than the heavier elements.

Figure 3-12 Photograph of the Field Emission Scanning Electron Microscopy (FESEM) and equipped with an Energy Dispersive X-Ray (EDX) (left); and the gold sputtering machine (right).

Moreover, to improve the imaging of the sample, the surface was made conductive by applying 4 nm of gold coating by using a gold sputtering maching as shown on Figure 3-12 (LEICA EM SCD 500) with a coating thickness controller (LEICA EM QSG 100). The gold coating on the sample inhibits charging that may otherwise results in un-observable morphology.

3.4.4 Acid-microwaves assisted digestion

Elemental analysis is carried out to quantify the elemental composition of a sample. In this study, the elemental analysis is carried out by using Inductively Coupled Plasma – Mass Spectrometer (ICP-MS). However, a liquid sample is required to carry out this analysis. Thus, acid-microwaves assisted digestion is carried out to dissolve the element of interest into aqueous solution.
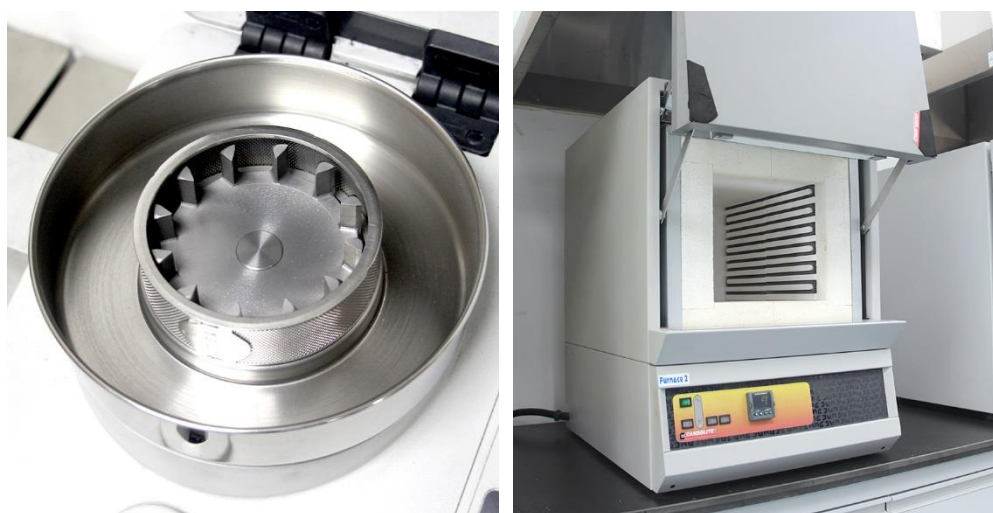
Figure 3-13 Photograph of centrifugal mill (left) and muffle furnace (right).

The digestions were adapted from *BS EN 62321-5:2014* (British Standard Institution, 2014*)*. Samples were first transferred to porcelain lidded crucibles and calcined in a muffle furnace (Carbolite, CWF 2000, Figure 3-13) to remove difficult to mill materials (e.g. polymer materials). The calcination was performed in multiple stages to prevent a sudden release of gas. The temperature was increased at a rate of 10^oC min^{-1} up to 350^oC with 2h holding time. Followed an increase in temperature at the same rate to 500^oC with 3h holding time. The sample was then allowed to cool to room temperature. The samples were then milled using a centrifugal mill (Retsch ZM 200, Figure 3-13) with a 0.25 mm grid. Samples from inside

and outside the grid were collected and sieved using 212 μm nominal aperture size, and the size fraction >212 μm was re-milled until the recovery rate < 212 μm was >95 wt%. The samples that initially had particle sizes of < 212 μm were excluded from the above steps.

Figure 3-14 Photograph of the MILI-Q machine.

The 68 wt% HNO_3, 30 wt% HCl, and 30 wt% H_2O_2 used are purchased from Jingrui with UP-S grade. Moreover, only MILI-Q water that comply Grade 1 *BS EN ISO 3696:1995* is used (Figure 3-14) is used for the entire digestion and dilution (British_Standard_Institution, 1995).
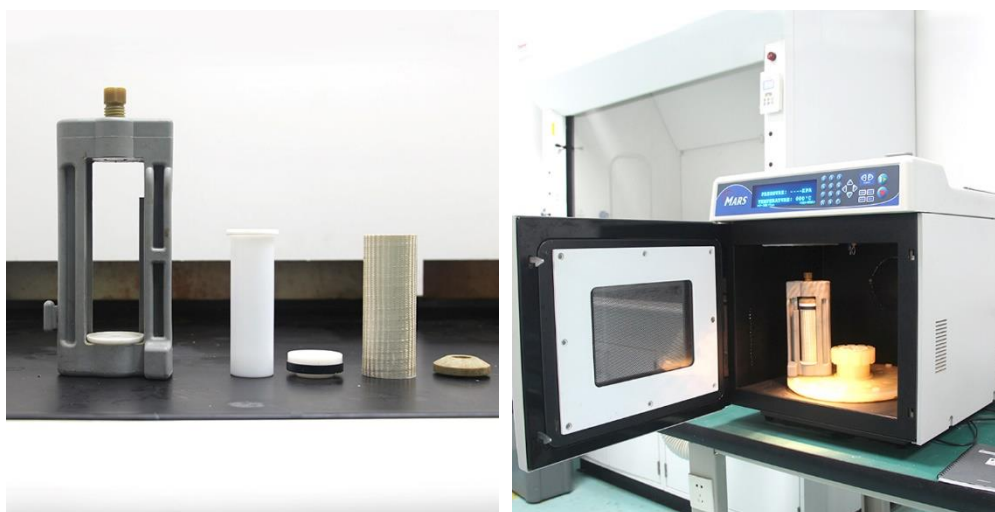
Figure 3-15 Photograph of the digestion vessels (Left) and the microwave digester (Right).

Approximately 0.2 g of sample was weighed to four decimal places using an analytical balance. Microwave digester (CEM MARS 5, Figure 3-15) equipped with temperature control was used to digest the samples and dissolve the materials present to enable analysis. The digestion is carried out in multiple stages, and the details are summarised in Table 3-1.

Table 3-1 – Microwave digester operating parameter

Stage	Number of Vessels	Power Level (W)	Ramp Time (min)	Temperature (°C)	Hold Time (Min)	Description
1	8	800	8	80	2	~ 0.2g of solid with
2	8	800	4	120	5	1ml H_2O+4 ml UP-S Grade 68 wt% HNO_3 + 1ml H_2O_2.
3	8	800	8	80	2	The solution then
4	8	800	4	120	5	allowed to cool down below 30°C then 4ml of UP-S Grade 30 wt% HCl was added.

The digested samples are then diluted with 3 wt% HNO_3 to prevent precipitation. Following dilution, the sample then analysed using Inductively Coupled Plasma – Mass Spectrometry (ICP-MS, Nexion 300x). Multi-elements external standard calibration curves were made by diluting and mixing different single element standard reference stock solutions from Sigma-Aldrich (see Appendix II).

3.4.5 Inductively Coupled Plasma – Mass Spectrometer (ICP-MS)
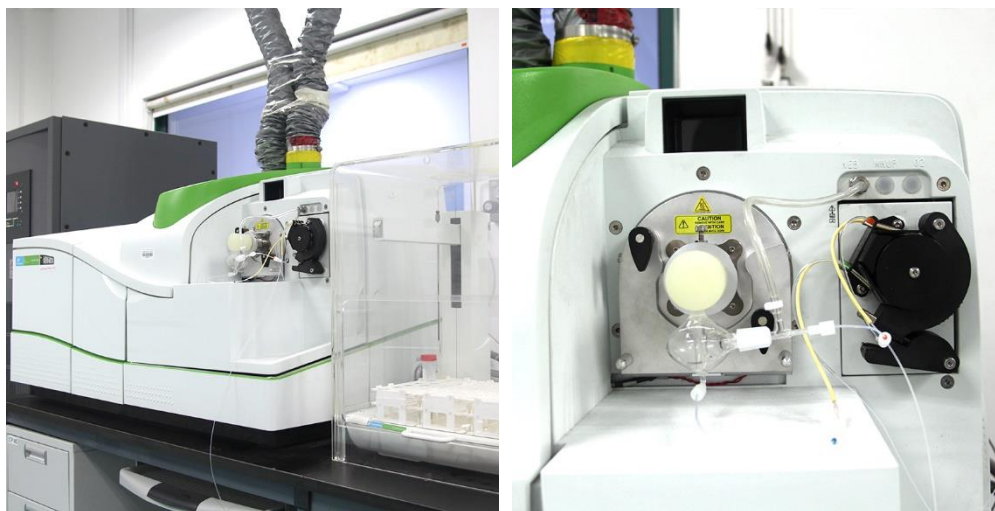
Figure 3-16 Photograph of the Inductively Coupled Plasmas – Mass spectrometer (ICP-MS) whole equipment setup (left) and the sample introduction chamber (right).

Inductively coupled plasma source with the addition of a mass spectrometer as the detector. This type of instrument is called Inductively Coupled Plasma-Mass Spectrometer (ICP-MS). In this instrument, the plasma torch to ionize the elements allowing their gas-phase separation and measurement using mass analysers. The mass spectrometer measures the ionized elements. Thus, the mass-to-charge ratio (m/z) measured is usually the atomic mass of the elements. In this thesis, the ICP-MS from PerkinElmer, NexION® 300x, is used (Figure 3-16). The sample is introduced using a peristaltic pump to move the sample solution into the nebulizer and producing small droplets, followed by spray chamber. The argon plasma torch then ionize the sample.
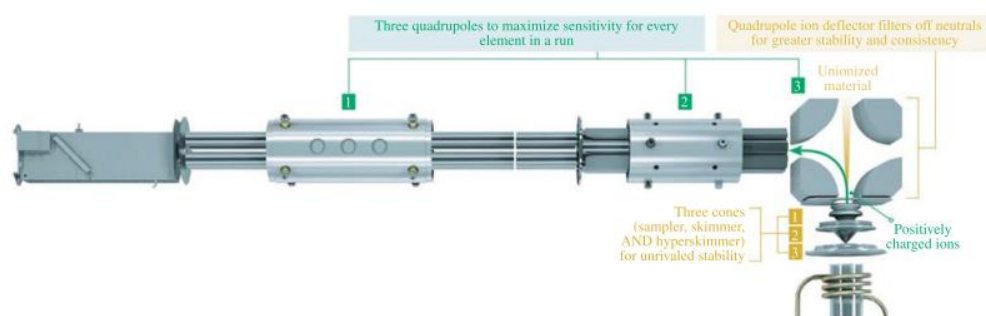
Figure 3-17 Inner working of ICP-MS, NexION® 350.

The interface is the introduction area of the instrument from the plasma torch into the lower pressure inside of the ICP-MS. The interface in Figure 3-17 is the triple cone interface where the ions produced from plasma torch at atmospheric pressure enter the instruments where the environment is under vacuum pumped down by vacuum pumps. Keeping the system under vacuum reduces interferences from ambient gasses and helps keeping the system dry. The vacuum is controlled by two pumps, a mechanical rough pump and a turbomolecular pump. The ions produced in the torch and neutral enter the instrument into the quadrupole ion defector (QID). The QID functions to remove the interferences and allow ions to continue on into the interior of the instrument. From Figure 3-17, the QID is a quadrupole that has been set at a right angle to the incoming ion beam. This alignment will bend the ion beam at a 90° angle. The neutrals and solvent will continue on their straight path and does not enter the equipment.

Spectroscopic interferences are one of the largest interferences in ICP-MS and are caused by atomic or molecular ions that have the same mass-to-charge ratio as analytes of interest. The ICP-MS instrumental software supplied is able to correct for all known "isobaric" interferences that are caused by overlapping isotopes of different elements. However, the ICP-MS

instrumental software does not remove the polyatomic interferences that are formed from precursors such as the sample matrix, reagent used for preparation, plasma gasses, and entrained atmospheric gasses.

Table 3-2 Table of polyatomic interferences in ICP-MS (May and Wiedmeyer, 1998)

Isotope	Abundance wt%	Interference
^{27}Al	100.0	$^{12}C^{15}N^+$, $^{13}C^{14}N^+$, $^{1}H^{12}C^{14}N^+$
^{59}Co	100.0	$^{43}Ca^{16}O^+$, $^{42}Ca^{16}O^{1}H^+$, $^{24}Mg^{35}Cl^+$, $^{36}Ar^{23}Na^+$, $^{40}Ar^{18}O^{1}H^+$, $^{40}Ar^{19}F^+$
^{63}Cu	69.1	$^{31}P^{16}O_2^+$, $^{40}Ar^{23}Na^+$, $^{47}Ti^{16}O^+$, $^{23}Na^{40}Ca^+$, $^{46}Ca^{16}O^{1}H^+$, $^{36}Ar^{12}C^{14}N^{1}H^+$, $^{14}N^{12}C^{37}Cl^+$, $^{16}O^{12}C^{35}Cl^+$
^{65}Cu	30.9	$^{49}Ti^{16}O^+$, $^{32}S^{16}O_2^{1}H^+$, $^{40}Ar^{25}Mg^+$, $^{40}Ca^{16}O^{1}H^+$, $^{36}Ar^{14}N_2^{1}H^+$, $^{32}S^{33}S^+$, $^{32}S^{16}O^{17}O^+$, $^{12}C^{16}O^{37}Cl^+$, $^{12}C^{16}O^{37}Cl^+$, $^{12}C^{18}O^{35}Cl^+$, $^{31}P^{16}O^{18}O^+$
^{54}Fe	5.8	$^{37}Cl^{16}O^{1}H^+$, $^{40}Ar^{14}N$, $^{38}Ar^{15}N^{1}H^+$, $^{36}Ar^{18}O^+$, $^{38}Ar^{16}O^+$, $^{36}Ar^{17}O^{1}H^+$, $^{36}S^{18}O^+$, $^{35}Cl^{18}O^{1}H^+$, $^{37}Cl^{17}O$
^{56}Fe	91.7	$^{40}Ar^{16}O^+$, $^{40}Ca^{16}O^+$, $^{40}Ar^{15}N^{1}H^+$, $^{38}Ar^{18}O^+$, $^{38}Ar^{17}O^{1}H^+$, $^{37}Cl^{18}O^{1}H^+$
^{57}Fe	2.2	$^{40}Ar^{16}O^{1}H^+$, $^{40}Ca^{16}O^{1}H^+$, $^{40}Ar^{17}O^+$, $^{38}Ar^{19}F^+$
^{58}Fe	0.3	$^{40}Ar^{18}O^+$, $^{40}Ar^{17}O^{1}H^+$

A prior knowledge of the polyatomic interferences is necessary as it would guide the experimenter for what type of reagent is used to minimise the source of interferences. The list of

polyatomic interferences that is relevant to this project is summarised in Table 3-2. From Table 3-2, it can be seen that the two elements of aluminium and cobalt does not have any isotope, selective detection of isotope is not applicable from these two elements. Moreover, aluminium cannot be completely digested with a single acid (i.e. HNO_3 alone) and thus the use of second stage digestion with HCl is necessary. Moreover, modification from that of *BS EN 62321-5:2014* is made to minimise the interference of fluorine atom to cobalt detection by the exemption of HBF_4. The dilution is carried out with 3 wt% HNO_3. It is important to point out that nitrogen can possibly interference with the aluminium detection, however it requires organic solvent matrix and therefore it can be assumed that the HNO_3 would not form any polyatomic interference with carbon. Thus, no interference with aluminium. The same judgement also made for the choice of ^{63}Cu and calibrated against the same isotope by using ICP-MS.

The detection of iron would use the highest relative abundance as the proportion of different isotopes is highly disproportionate, such that the relative abundance of ^{56}Fe is 91.7 wt% as compared to 0.3 wt% of ^{58}Fe. The selection of isotope other than ^{56}Fe would increase the error as the intensity of measured elements would be significantly of reduced value and would reduce the sensitivity of the measurement. However, the iron is not detected as it may come from different sources such as contamination from the milling machine. Thus, making the conclusion derived from such quantification unreliable.

3.5 Conclusion

In this chapter, the intended use of attrition scrubber, electrostatic separator, and froth flotation in this project is presented and described. The qualitative and quantitative analysis that is going to be carried out to assess the outcome of the technique proposed have been explained.

Moreover, the representative samples used in this thesis has been dried and screened for ferromagnetic materials. It is important to point out the hazard of $LiPF_6$ from the battery electrolyte as it produces HF above 85^oC. Therefore, slight modification from *BS 812-109: 1990* is taken by reducing the recommended temperature from $105^oC - 110^oC$ to 80^oC. The use of this temperature is still within the range of the previously reported studies of recycling LIBs and also has been reported to have negligible difference than the recommended temperature. The drying is carried out in an open system box oven and until constant weight is achieved. The dried bulk samples then undergo sample splitting and ferromagnetic materials screening by using rare earth magnet.

As this project aims at the selective liberation of positive electrode active materials from spent LIBs, the analysis would involve the dependence of difference elements distribution on size that is analysed by size based separation by using certified test sieve and elemental analysis by using ICP-MS. Attempt to minimise the interference that potentially overestimate or underestimate the ICP-MS measurement by slight modification of *BS EN 62321-5:2014*. The HBF_4 is not used and the matrix used for dilution is 3 wt% HNO_3 rather than 5 wt% HCl. Furthermore, the total dissolution of intended elements is confirmed by using SEM-EDX. Other than the confirmation of total metal dissolution, SEM-EDX is also used to study the

morphology and breakage mechanism of LIBs after mechanical treatment. Along with the SEM-EDX, XRD is used to confirm the type of positive electrode active materials being studied.

Chapter 4 Particle Characteristics of Dry Milled LIBs

4.1 Introduction

The occurrence of selective liberation of positive electrode active materials have been observed and reported. The positive electrode active materials being concentrated in the finer size region. Results reported show a cut point of less than 1 mm is an appropriate cut point which is independent of the type of the milling machine and the LIB's geometry ([Zhang et al., 2013](#), [Yu et al., 2018](#), [Silveira et al., 2017](#), [Wang et al., 2016c](#), [da Costa et al., 2015](#)). The cut point of 1 mm is substantially larger than that of the active materials size found inside spent LIBs that ranges from 7.8 μm to 1.5 μm ([Pavoni et al., 2018](#)), indicating the sub-optimum selective liberation.

The occurrence of selective liberation depends on the difference between the mechanical properties (i.e. hardness) between minerals. In the case of LIBs, as the battery is being cycled, the copper and aluminium component shows disproportionate rate of mechanical degradation. The copper current collector is deteriorating at a faster rate than the aluminium current collector ([Dai et al., 2019](#)). The copper current collector eventually becomes weaker than that of the aluminium current collector. Furthermore, the PVDF binders' adhesiveness is stronger towards the aluminium than the copper current collector. From these reasons, it is hypothesized that there would be observable difference in the selective liberation performance the spent and new LIBs.

113

This chapter aims at understanding the selective liberation of LiCoO$_2$ in dry milled spent LIBs. The Fuerstenau and ore separation degree curves are used to assess the LiCoO$_2$ selective liberation. Morphological observation is carried out for the different classified size fraction. The combination of elemental and morphological analysis is used to understand the selective liberation of LIBs and the liberation mechanism. Furthermore, selective liberation of new and spent LIBs are compared to understand the effect of mechanical properties degradation as the battery used in multiple charging and discharging cycle towards the efficiency of selective liberation.

4.2 Experimental details

The selective liberation is assessed based on different components on classified sizes. The main components of spent LIBs can be broken down into two clusters of leachable and non-leachable components. The leachable components include the copper and aluminium current collectors as well as the LiCoO$_2$ positive electrode active materials. Whereas, the non-leachable component includes polymeric materials and graphite. The cobalt is taken as the desired (valuable) component and copper and aluminium are taken as the undesired (waste) component.

The sample preparation and analysis techniques has been described in <u>Chapter 3</u>. Three representative samples were used with average mass of 69.8 g (see Appendix III). The samples were analysed for particle size distribution using certified test sieve (Endecotts) and a fix amplitude shaker (Capco Inclino Sieve Shaker 3). As the battery has been milled by using cutting mill with 8 mm grid, the particle size analysis via sieving should be able to include the biggest possible size that can be expected. However, as the LIBs comprise of non-

brittle (flexible) components which allow larger particles to pass through the grid. The sieves with aperture size of 13200 μm and 38 μm are taken as the maximum and the minimum size for the particle analysis. This sieve size has taken into consideration, the cutting mill grid and the size of the active materials found in LIBs. The sieves used to assess the d_{95} had a nominal aperture of 13200 μm, 9500 μm, 6700 μm, and 4750 μm. The sieving was performed separately, and the sieves were brushed after use to collect fine particles that may be trapped between the joint of adjacent apertures. The size fraction of < 4750 μm then sieved with nominal aperture size of 2360 μm, 850 μm, 212 μm, and 38 μm. All the sieves for size fraction less than 4750 μm were put together to assess the particle size distribution. Each different size fraction then subject to morphological and elemental analysis. All the sieving test were carried out at 20 min.

New LIBs of the same type as that of the spent LIBs were used and subject to the same treatment as the spent LIBs. 94.8 g of dried milled new LIBs were used in this study.

The morphology study of the milled LIB particles was carried out using an SEM-EDX. The EDX helps in identifying the material being studied. The samples were mounted onto aluminium stage using conductive carbon tape. The surface of the sample was then made conductive by applying a 4 nm gold layer using a gold sputtering machine. The combination of size related recovery as well as the morphological analysis can then be used to draw the general understanding of the particles morphology in its relative size fraction and relative recovery rate when the given size fraction is isolated.

The initial EDX results also show that the positive electrode active material is $LiCoO_2$ due to the absence of other elements

such as Ni and Mn that may otherwise suggest other battery chemistry. To further confirm the EDX result, the size fraction of < 38 μm were analysed by using XRD. The peaks were compared with the data library and was found to be a mixture of $LiCoO_2$ and graphite. The results are also compared with standard XRD powder of $LiCoO_2$ and graphite purchased from Sigma-Aldrich and shown in Figure 4-1.
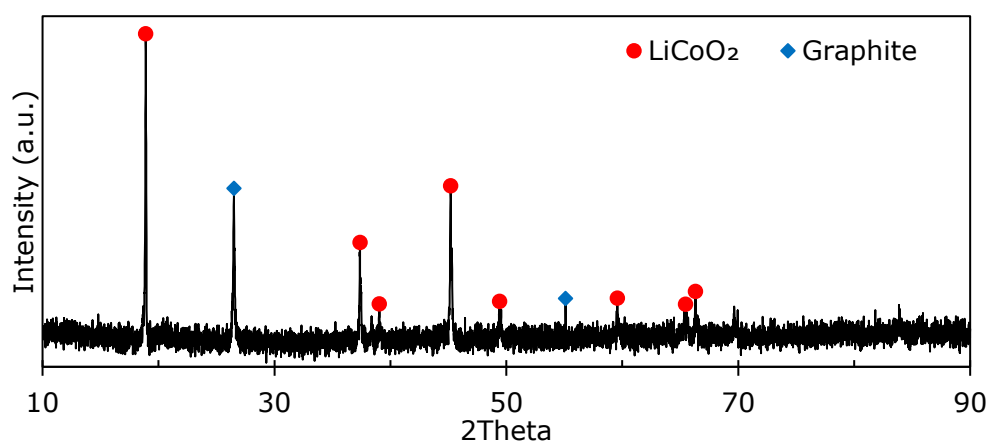
Figure 4-1 XRD spectra of classified milled LIBs in the size range of <38μm.

As the type of positive electrode active materials are known, this then simplifies elemental analysis. Mechanical liberation does not induce crystal changes to the positive electrode active materials. Therefore, the wt% recovery of Co can be assumed to the wt% recovery of the $LiCoO_2$. Additionally, in this study, all the detected copper and aluminium are assumed as the recovery of negative and positive electrode current collectors respectively.

4.3 Results and discussions

4.3.1 Size-based hierarchy

Milling spent LIBs by using a cutting mill with 8 mm grid produced a wide range of particle size distribution, from 13200 µm to less than 38 µm (Figure 4-2). By linear interpolation, the average particle size (d_{50}) was found to be 1552 µm.
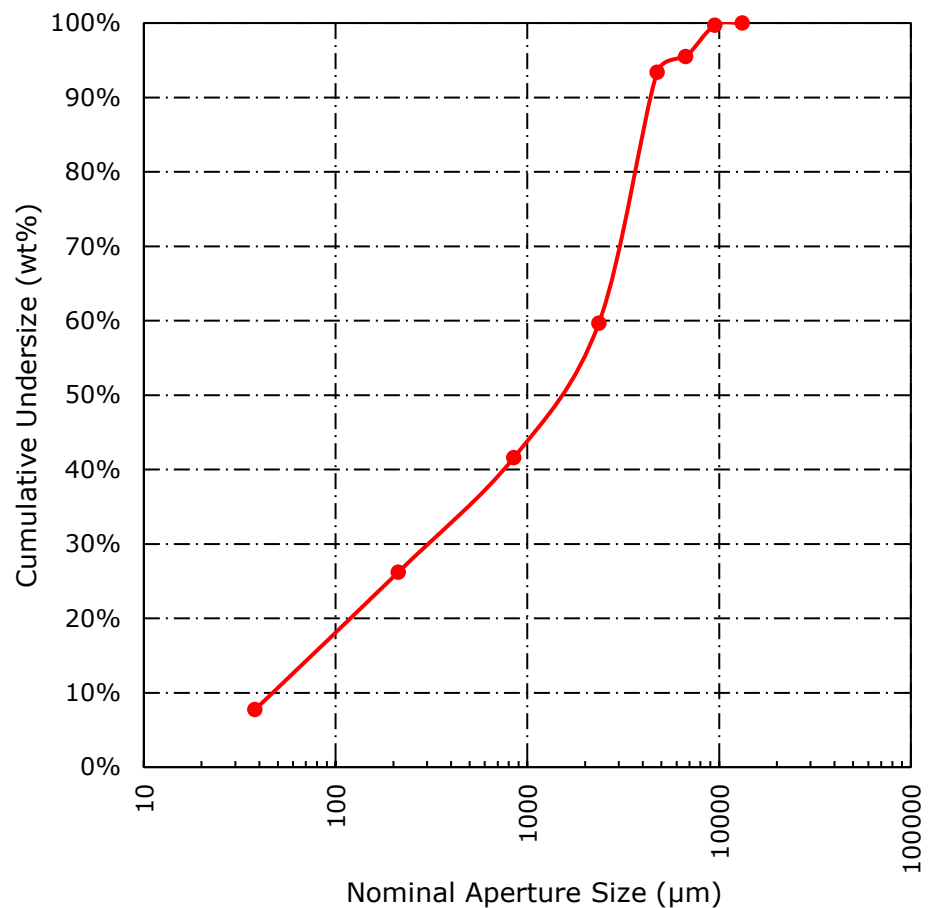
Figure 4-2 Particle size distribution of milled spent LIBs.

From Figure 4-3, visual inspection reveals that the battery separator and the polymeric chassis are mainly found in the size fraction of > 850 µm. Moreover, it is noted that the cutting mill produce 7.7 wt% (Figure 4-2) of particles in the size range less than 38 µm (Figure 4-3 H).
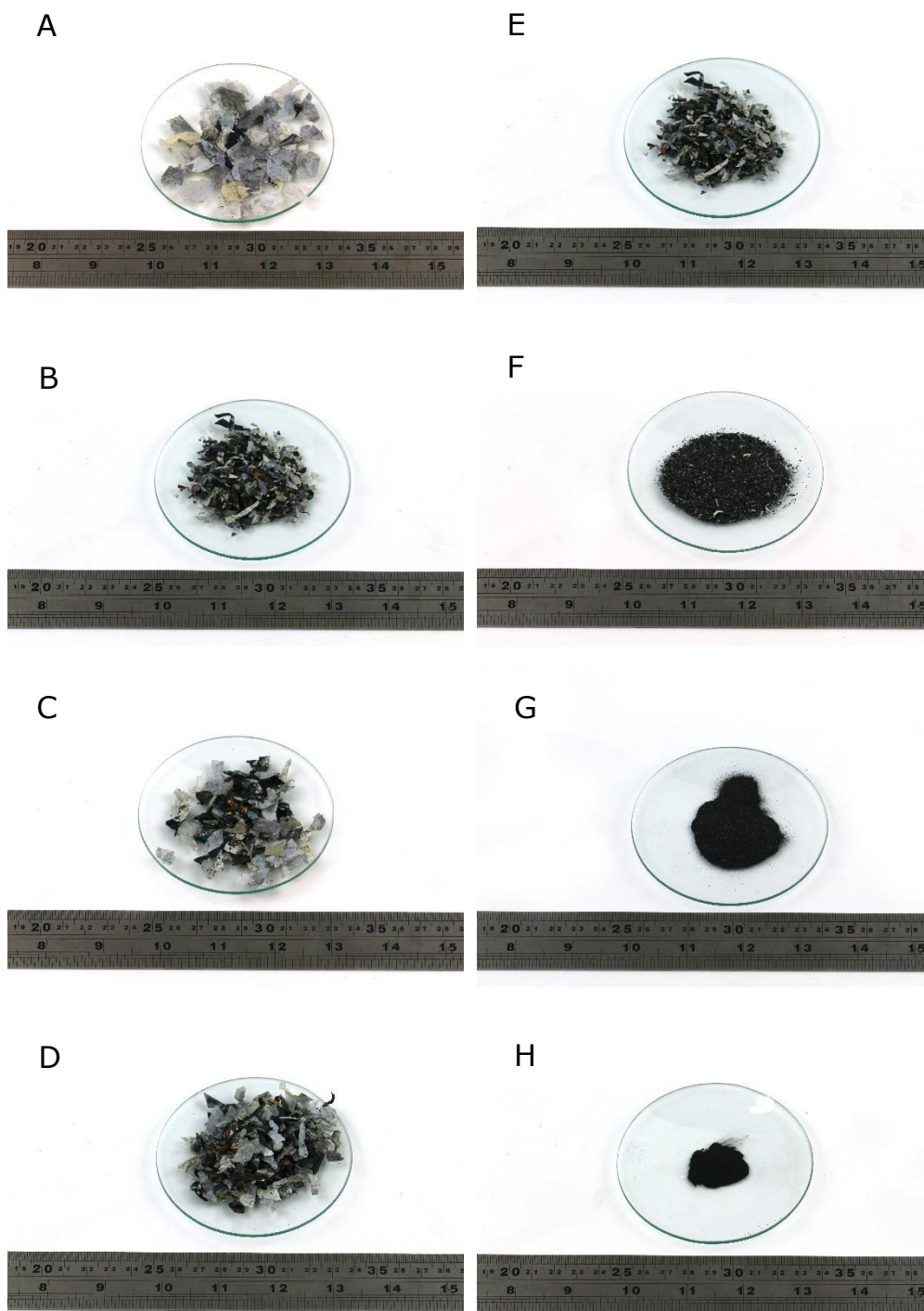
Figure 4-3 Photograph of the classified milled LIBs; A)13200μm-9500μm, B)9500μm-6700μm, C) 6700μm-4750μm, D)4750μm-2360μm, E)2360μm-850μm, F)850μm-212μm, G)212μm-38μm, H) <38μm.
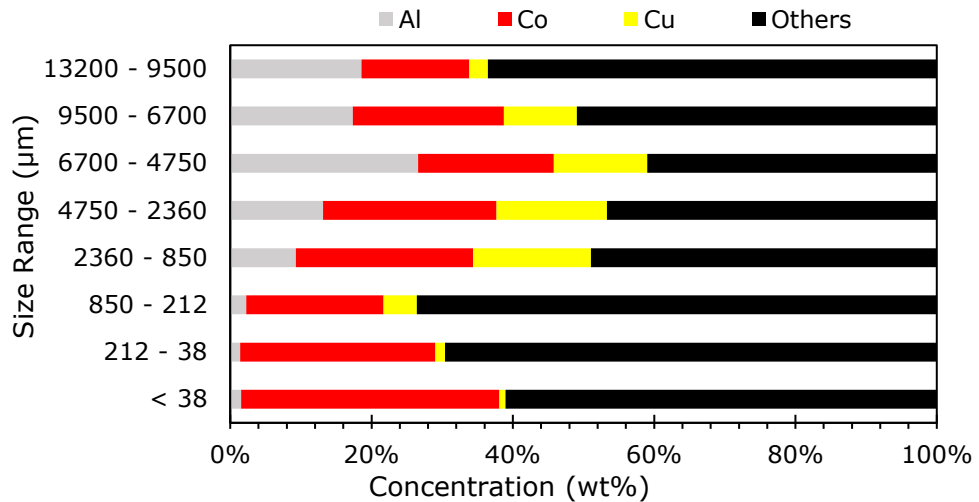
Figure 4-4 Concentration of key elements for a given size range of classified milled spent LIBs.

From Figure 4-4, it is shown that aluminium, cobalt, and copper are found in all size regions. The finer size region < 850 μm concentrated the $LiCoO_2$ particles. Comparing the cobalt grade of different size fractions, it was found that the size fraction of < 38 μm has the highest grade of 36.5 wt% cobalt. The size fraction of < 38 μm also has the lowest contamination from aluminium and copper which are 1.6 wt% and 0.8 wt% respectively. This size fraction only recovers 11.4 wt% $LiCoO_2$ from the feed.
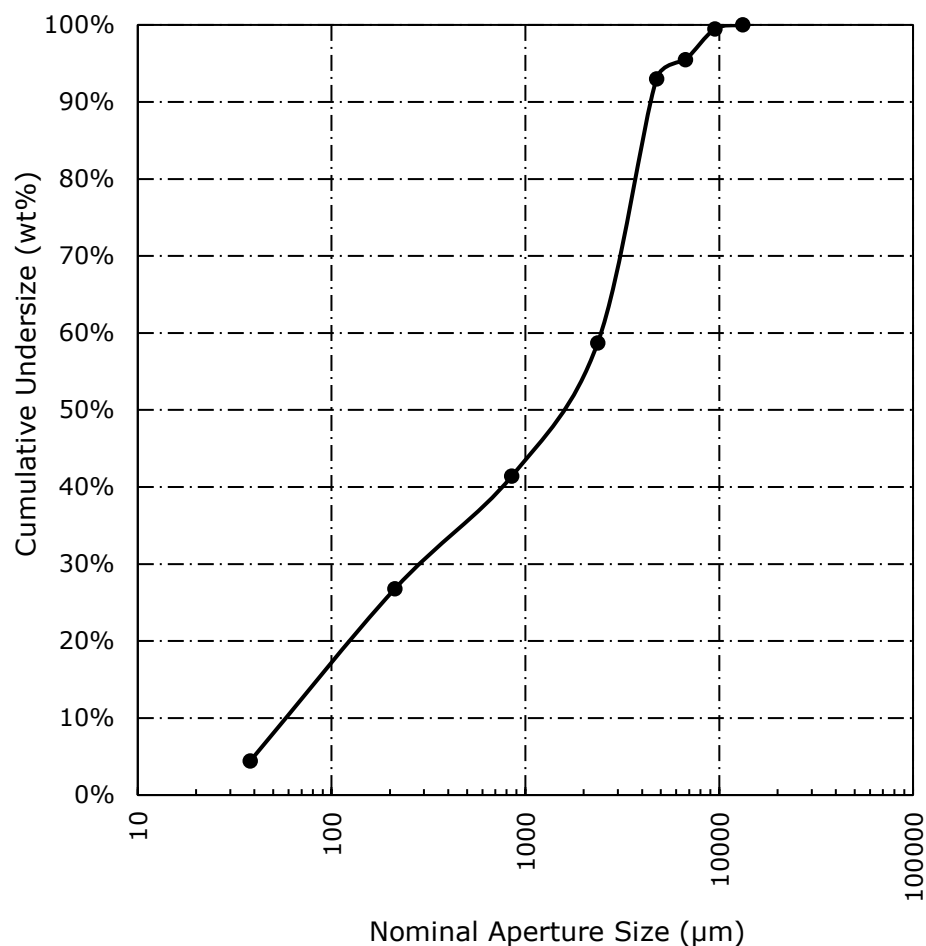
Figure 4-5 Particle size distribution of milled new LIBs.

The same assessment has also been carried out for the new LIBs. From Figure 4-5 it can be seen that milling new LIBs also produces a wide particle size distribution and the average particle size is 1600 µm.

The particle size distribution of milled new and spent LIBs does not differ significantly when comparing the average particle size. However, the amount of size fraction < 38 µm produced is lower in the milled new LIBs (4.4 wt%) compared to the milled spent LIBs (7.7 wt%).
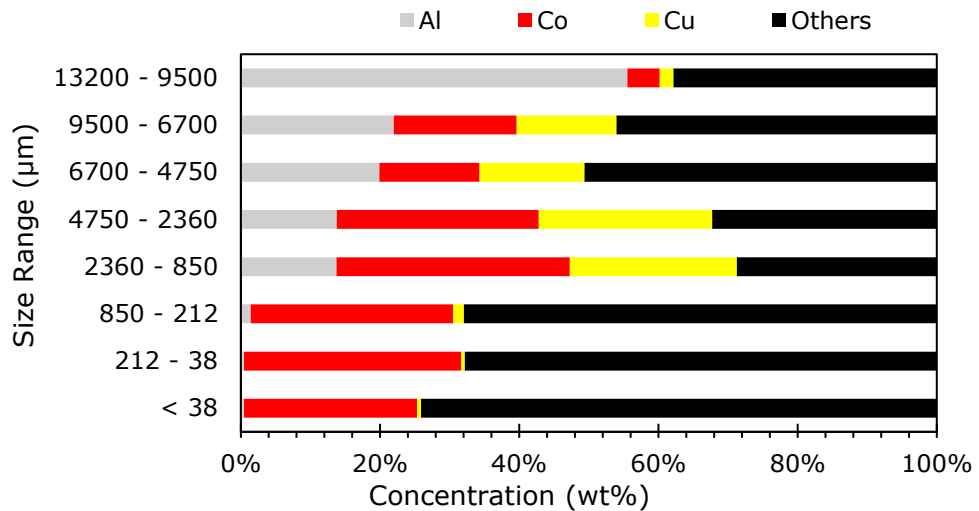
Figure 4-6 Concentration of key materials for a given size range of classified milled new LIBs.

The milled new LIBs also then assessed for the concentration of aluminium, copper and cobalt with respect to size and this is shown in Figure 4-6. From Figure 4-6, it can be seen that $LiCoO_2$ particles are concentrated in the finer size region. However, the main difference of new and spent LIBs lies in the size fraction that concentrate the highest amount of cobalt. From milling spent LIBs it was found that the size fraction of < 38 µm have the highest concentration of cobalt. Compared to that of the new LIBs (Table 2), the < 38 µm size fraction contains lower grade of 24.9 wt% cobalt with lower aluminium and copper contamination of 0.5 wt% and 0.6 wt% respectively. In new LIBs, the size fraction of 212 µm – 38 µm contains the highest grade of 31.2 wt% cobalt with minimum contamination from aluminium (0.4 wt%) and copper (0.5 wt%).

Therefore, to make an objective judgement to whether milling LIBs does induce selective liberation of $LiCoO_2$ particles, a Fuerstenau upgrading diagram, and η_{ore} was plotted. By this , the selective liberations of $LiCoO_2$ and the current collectors (Cu and Al) can then be identified. Moreover, a comparison between the new and spent LIBs can also be made to understand the

effect the different mechanical properties have on selective liberation.
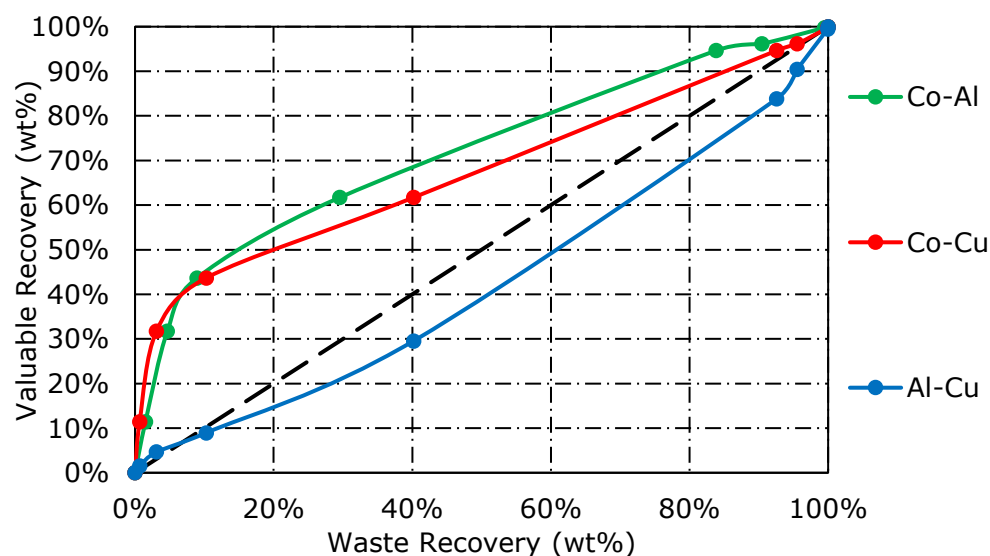
Figure 4-7 Fuerstenau recovery curve of milled spent LIBs.

Figure 4-7 shows Fuerstenau recovery curve for cobalt-aluminium (Co-Al) and cobalt-copper (Co-Cu) above the diagonal line. This finding confirm that milling spent LIBs does induce selective liberation of $LiCoO_2$ particles in the finer size region. The recovery of cobalt is greater than the recovery of copper and aluminium in the finer size region. In Figure 4-7, the Fuerstenau upgrading diagram can be broken down into two distinct regions. These are the recovering region and the re-mixing region. In the recovering region, the cobalt recovery increases by increasing the cut point size. It is also accompanied by a minimum increase in copper and aluminium recovery. A further increase in cut point yields higher wt% recovery of cobalt but the increase is outweighed by the increase in copper and aluminium recovery and called the re-mixing region. When there is a point of inflection, the recovering line changes into re-mixing line; it marks the optimum cut point that balances the recovery between valuable

material and waste material. For both Co-Al and Co-Cu, the transition can be seen at point 850 µm.

A better graphical representation to determine the optimum cut point is by plotting the ore separation degree curve (η_{ore}). As selective liberation dependent on size, the optimum cut point corresponds to the highest ore separation degree ($\eta_{ore,max}$) can be found and summarised in Figure 4-8.
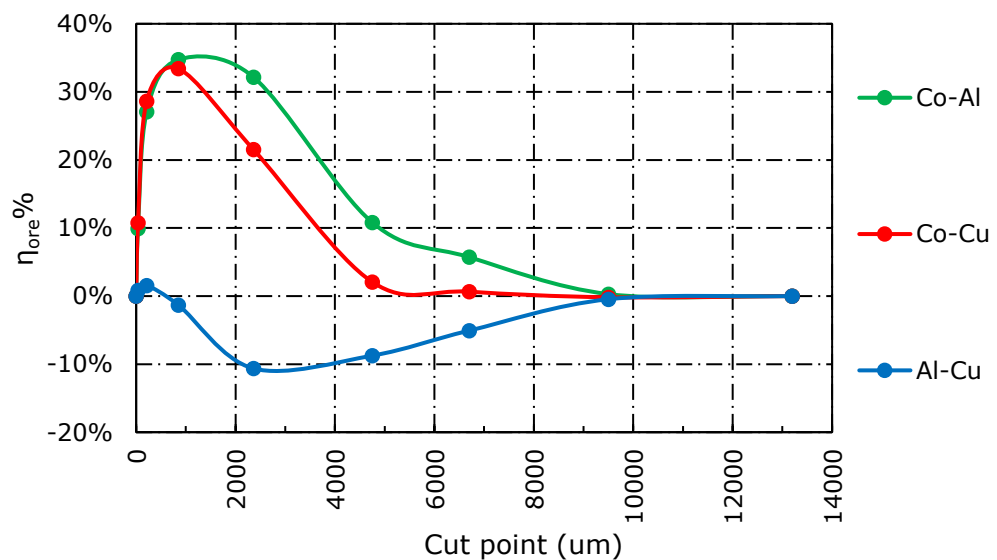
Figure 4-8 The ore separation degree (η_{ore}) of classified milled LIBs.

From Figure 4-8, the cut point 850 µm shows the highest efficiency to recover cobalt while minimising the contamination of aluminium and copper (Co-Al $\eta_{ore,max}$=37.8% and Co-Cu $\eta_{ore,max}$=33.4%). Moreover, a dramatic decrease in Co-Cu η_{ore} is observed when compared to Co-Al η_{ore} above cut point 850 µm. This indicates that above the cut point 850 µm, the copper contamination is more dominant than the aluminium contamination.

Inside the cutting chamber, size reduction occurs through shearing and cutting stress (Schubert and Bernotat, 2004). Cutting actions applies a localised force that induces failure of the material right next to the knife edge as a result of shear

and tensile stresses. With the assumption that there is no interaction between the active materials assembly and the electrode. The tensile strength of copper (220 MPa) has been reported to be higher than the tensile strength of aluminium (105 MPa – 145 MPa) ([Butt et al., 2016](#)). Moreover, copper (2.65 GPa) also has a higher ideal shear strength as compared to aluminium (1.85 GPa) shear strength ([Roundy et al., 1999](#)). In light of these facts, an inconsistency was found. By considering the shear and tensile strength of copper and aluminium, it is expected that the aluminium would be more readily liberated in the finer size region. However, the findings seem to contradict this fact. By comparing the plot of Co-Al and Co-Cu in the Fuerstenau recovery curve, there is a trend switch in the recovery and re-mixing region. Where, in the recovery region, increasing the cut point size leads to a higher increase in aluminium recovery rather than copper recovery. Additionally, in the re-mixing region, this trend does not hold true and switch towards more copper being recovered as the cut point become larger.

The interaction between aluminium and copper (Al-Cu) when plotted for a Fuerstenau recovery curve and η_{ore}, in which the aluminium is taken as the valuable component and shown in Figure 4-7 and Figure 4-8. As it can be seen from Figure 4-7, the Fuerstenau upgrading curve of Al-Cu also shows a switch in trend. Initially, the Fuerstenau upgrading diagram shows recovery of aluminium above the diagonal line prior to approaching cut point 212 µm. However, as the cut point size increased, the re-mixing line lies below the diagonal line. Similarly, for the η_{ore} curve, the efficiency is only positive in the region of < 212 µm and the η_{ore} become a negative value onwards. The η_{ore} negative value implies that the recovery rate

of waste material (Cu) is higher than that of the valuable material (Al) as the cut point size became larger. With the highest η_{ore} for Al-Cu is 1.6 % with cut point 212 µm. Moreover, the cut point 2360 µm gives the highest η_{ore} of copper towards aluminium.

From the findings described above, the interaction between the active materials assembly towards the current collector cannot be ignored. This also demonstrates that $LiCoO_2$-PVDF-Al is more resilient than that of C_6-PVDF-Cu. The mechanical strength of current collectors and the adhesive strength of the binder are dependent upon the number of discharging and charging cycle the battery has been through.

The repetitive cycle of charging and discharging the active materials undergoes repeated expansion and shrinkage due to the periodic intercalation and de-intercalation of lithium ions (Beaulieu et al., 2001, Obrovac et al., 2007, Li et al., 2015a). The repetitive deformation then induces mechanical ageing to the current collectors (Waldmann et al., 2014). Furthermore, degradation of PVDF adhesiveness on to the current collector has also been reported to weaken, causing contact loss of active material (Lee et al., 2016, Vetter et al., 2005). Therefore, a comparison to the new milled LIBs was made to observe the difference in selective liberation in new and spent LIBs.
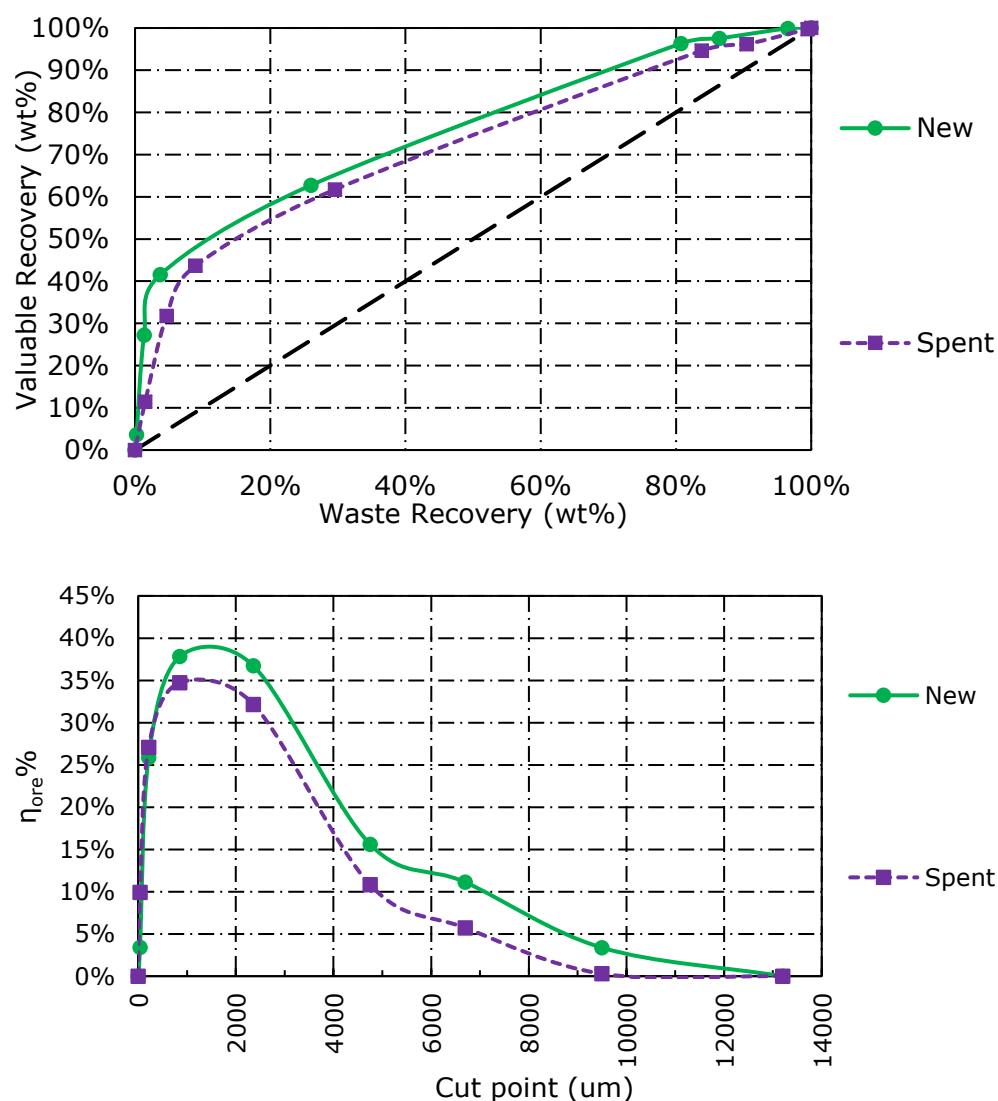
Figure 4-9 Co-Al Fuerstenau recovery curve and ore separation degree (η_{ore}) for new and spent milled LIBs.

From Figure 4-9 Fuerstenau recovery curve, it can be seen that the milling of both new and spent LIBs induce selective liberation of $LiCoO_2$ from the aluminium current collector. Furthermore, from Figure 4-9 it can be seen that better separation of $LiCoO_2$ from aluminium can be observed in the case of milling new LIBs than the spent LIBs. The cut point 850 μm ($\eta_{ore,max}$) in milling new LIBs is has higher separation efficiency than that of spent LIBs.
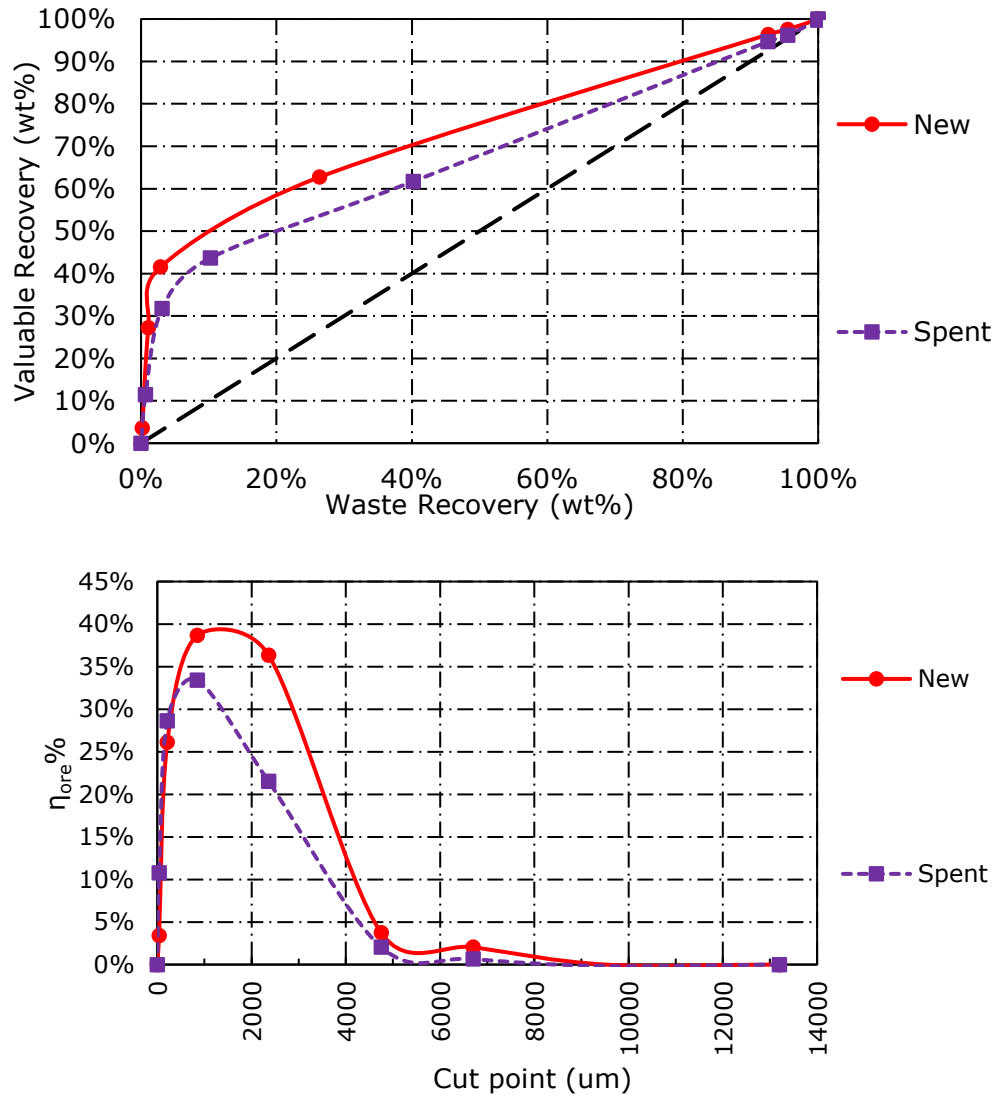
Figure 4-10 Co-Cu Fuerstenau recovery curve and ore separation degree (η_{ore}) for new and spent milled LIBs.

Similar observation also made in the case of selective liberation of $LiCoO_2$ from the copper current collector. From Figure 4-10 it can be seen that the selective liberation of $LiCoO_2$ from copper in milled new LIBs is better than that of milled spent LIBs. The cut point 850 µm ($\eta_{ore,max}$) in milling new LIBs has a higher separation efficiency than that of spent LIBs.

Comparing the new and spent LIBs, in Figure 4-9 and Figure 4-10, the Co-Al and Co-Cu curves indicate better separation efficiency for the new LIBs. Moreover, after Co-Al and Co-Cu curves approaches $\eta_{ore,max}$, the efficiency quickly decreases as

127

the cut point became larger for both LIBs. Furthermore, the decrease in efficiency is more apparent for the Co-Cu η_{ore} curve, compared to the Co-Al η_{ore} curve for spent LIBs. This is thought to occur due to the difference in adhesive strength of PVDF binder with the copper and aluminium current collector. The active materials on the copper current collector (graphite) and on the aluminium current collector ($LiCoO_2$) are held together by the PVDF binder to form a composite. The cushioning of copper and aluminium current collector by its respective active materials may help in prevent breakage during mechanical liberation. It has been reported that the adhesive strength of PVDF to copper (285.6 kPa) in a new LIB is lower than that of aluminium (841.2 kPa) (Dai et al., 2019). Therefore, in the case of new LIBs, the lower PVDF adhesive strength towards copper current collector as compared to the aluminium current collector counterpart, may help explain the higher rate of decrease in efficiency as the η_{ore} curve approaching $\eta_{ore,max}$ in the Co-Cu η_{ore} curve as compared to the Co-Al η_{ore} curve.

As the LIBs are used in multiple cycles, the adhesive strength of PVDF onto copper and aluminium current collectors decreases to 55.5kPa and 132.8 kPa respectively, after 200 cycles (Dai et al., 2019). Moreover, the elastic modulus of copper further decreases by 78.1%-80.0% as the battery cycled (Dai et al., 2019). For spent LIBs, the degradation of PVDF adhesive strength and the elastic modulus of the copper current collector may cause more copper to be liberated in the finer size region. The aluminium current collector counterpart also undergoes localised corrosion and produces perforation (Braithwaite et al., 1999). This corrosion induced perforation potentially weakens the mechanical properties of the aluminium foil in spent LIBs. Thus, in the case of spent LIBs,

the copper and aluminium current collectors are more contaminating in the finer size fraction (< 850 µm) and therefore translated as a lower overall $\eta_{ore,max}$ value.
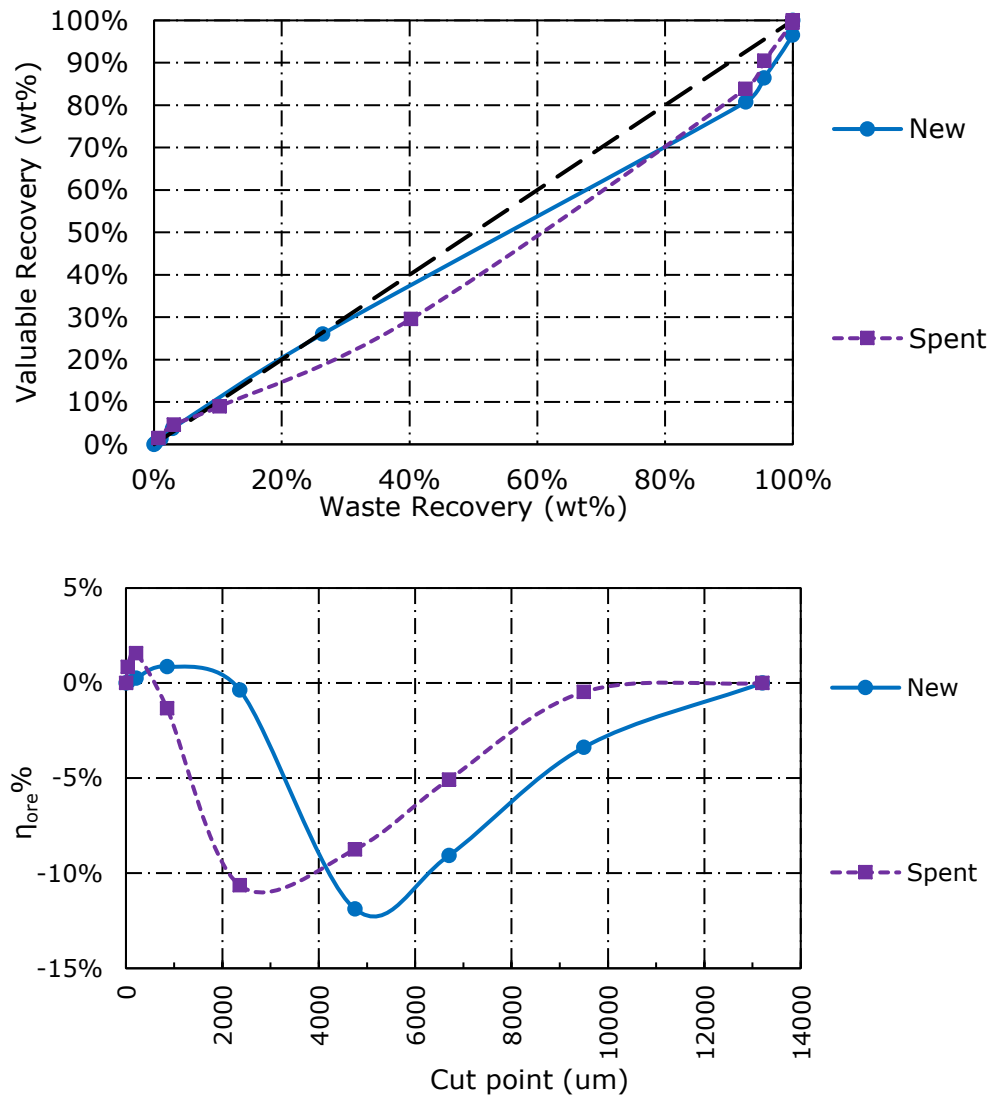
Figure 4-11 Al-Cu Fuerstenau recovery curve and ore separation degree (η_{ore}) for new and spent milled LIBs.

From Figure 4-11, the Fuerstenau upgrading diagram shows an Al-Cu curve of spent LIBs below the diagonal line in the size range of > 212 µm. Whereas, the new LIBs show a recovery curve below the diagonal line in the size range of > 2360 µm. Moreover, the η_{ore} curves reveal that the cut point required to exploit this selectivity increases from 2360 µm ($\eta_{ore,max}$= 10.6%) to 4750 µm ($\eta_{ore,max}$= 11.9%). It is also important to point out

that the Al-Cu η_{ore} curve predominant size is different for spent and new LIBs. The new LIBs have an Al-Cu η_{ore} curve that is more dominant towards the larger size region. Whereas, the η_{ore} curve of spent LIBs has shifted towards the finer size region. The change in predominant size towards the finer size region, indicates the copper and aluminium to favour further breakage into the smaller size region. Therefore, the better mechanical properties of positive and negative electrode in new LIBs synergistically translates to a larger cut point as compared to spent LIBs. While the increase in $\eta_{ore,max}$ is caused by the lower recovery of copper towards aluminium in size range of < 2360 µm.

4.3.2 SEM-EDX morphology study

Observation of different size fractions using SEM was made. This morphological analysis aims to understand the characteristics of active materials for different size fractions. Samples were mounted to aluminium stage with adhesive carbon tape. The size fraction of > 4750 µm was not analysed and based on visual inspection; it is assumed to be the same as the size fraction 4750 µm – 2360 µm. This is thought not to bias the results for the size fraction of > 4750 µm only holds less than 7wt%. The positive electrodes, negative electrodes, and separators were manually collected by using a tweezer for size fraction 4750 µm – 2360 µm and 2360 µm – 850 µm. Whereas, Size fraction 850 µm – 212 µm, 212 µm – 38 µm and <38 µm were directly mounted onto the adhesive carbon tape. The same preparation also carried out for the milled classified new LIBs. Gold sputtering was then carried out with a 4 nm thickness to make the surface conductive.
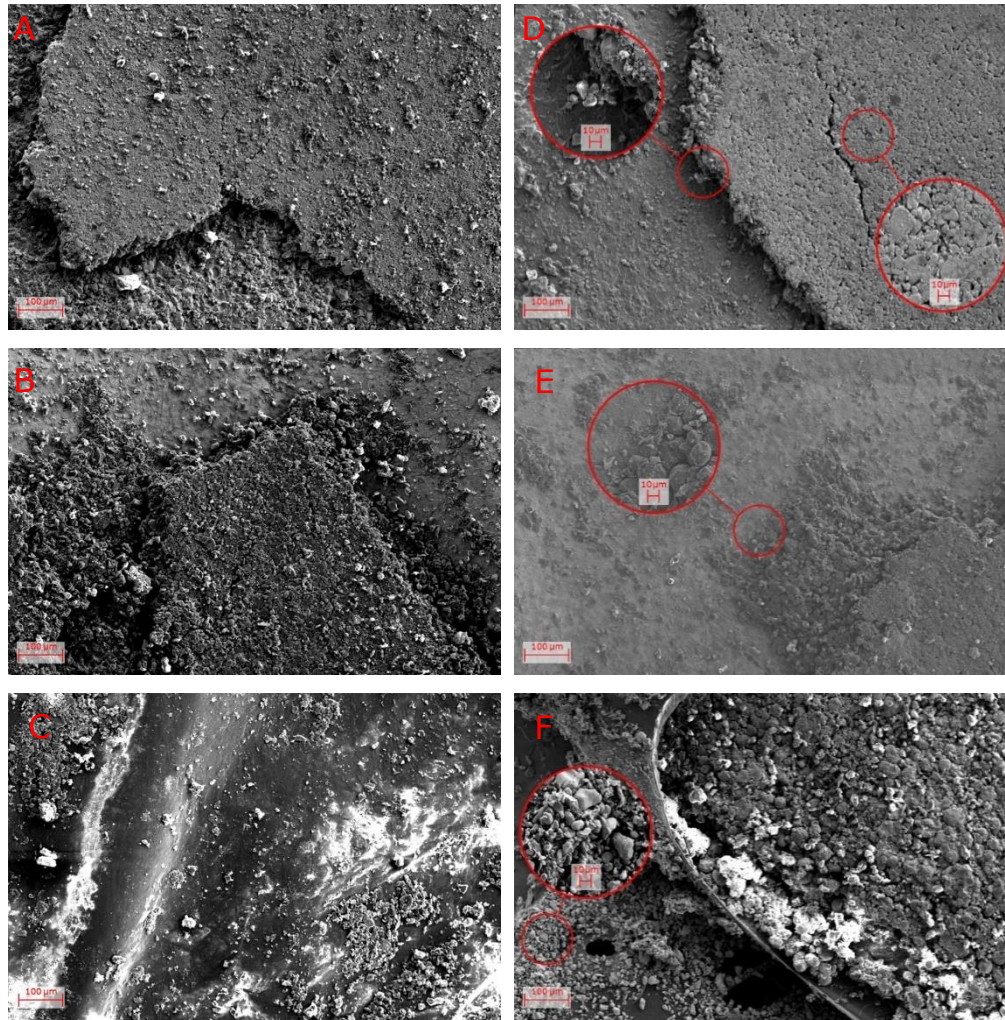
Figure 4-12 SEM image of size fraction 4750 µm – 2360 µm; New LIBs: A Positive electrode, B Negative electrode, C Separator; Spent LIBs: D Positive electrode, E Negative electrode, F Separator

From Figure 4-12, it was discovered that both positive and negative electrode active materials are contaminating the surface of the current collector. Figure 4-12 also demonstrates that there is no difference in terms of morphology for the new and spent LIBs. From Figure 4-12 A and D, there is a partial detachment of $LiCoO_2$ particles from the aluminium current collector. The $LiCoO_2$ that are still attached to the current collector is still firmly held by the binder. Moreover, the preliminary liberation induces the detachment of positive electrode active materials from its current collector in the form of a big package, indicated by the crack and the clear transition

between the side that has $LiCoO_2$ particles partially removed and intact (Figure 4-12 A and D). Moreover, the side that has already lost many of its active materials is still contaminated with a thin layer of $LiCoO_2$ laminate.

Similar observation also made with the negative electrode that still holds its graphite partially intact (Figure 4-12 B and E). However, there is a transition region between the side that has graphite particles that are partially removed and intact. This indicates that graphite-PVDF-graphite interaction is relatively weaker compared to $LiCoO_2$-PVDF-$LiCoO_2$ interaction.

The separators collected from the size fraction 4750 μm – 2360 μm are contaminated with both $LiCoO_2$ and graphite. This may have been due to the compression action in the cutting mill. However, the attachment of the active materials is weak. By manually folding the separator using a tweezer, the powders attached to the separator were transferred onto the carbon tape (Figure 4-12 C). This indicates that the attachment of positive and negative electrode active materials onto the separator is relatively weak but sieving alone does not help in detaching the active materials cast on the separator. The new LIBs also show the same characteristics (Figure 4-12 F).

For the size fraction >2360 μm, the particles in this region contain positive and negative electrodes that have undergone size reduction and accompanied by the partial liberation of active materials. The active materials are still firmly held by the binder and contaminating the surface of the electrodes. The analysis also shows that the graphite is more liberated compared to the $LiCoO_2$ particles. Some active materials are also found to be attached to the separator, and as a result, it may reduce the recovery of $LiCoO_2$ during size-based separation.
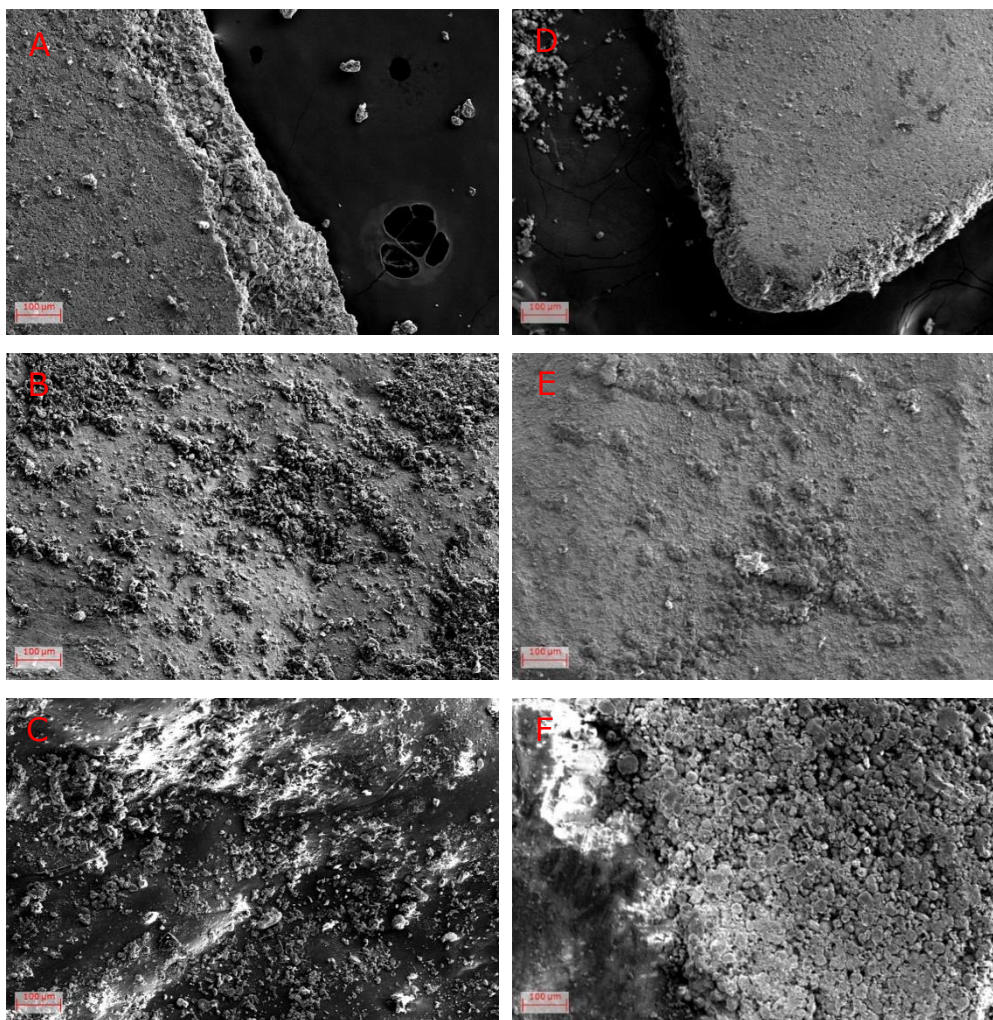
Figure 4-13 SEM image of size fraction 2360 μm – 850 μm; New LIBs: A Positive electrode, B Negative electrode, C Separator; Spent LIBs: D Positive electrode, E Negative electrode, F Separator.

Figure 4-13, which is the 2360 μm – 850 μm reveals that the positive and negative electrodes active material are still contaminating the surface of the current collector as well as the separator. Figure 4-13 also indicates no morphological difference between the new and spent LIBs. From Figure 4-13 A and D, $LiCoO_2$ particles in the size fraction of 2360 μm – 850 μm are firmly held by the binder and covers the aluminium current collector. This phenomenon indicates that the preliminary liberation also induces size reduction with the minimum liberation of $LiCoO_2$ particles from its aluminium current collector (i.e. the aluminium and active material breaks

in unity). From Figure 4-13 B and E, the copper current collector is still contaminated with graphite. However, it is cleaner when compared to the positive electrode. This also indicates that the graphite is readily liberated as compared to $LiCoO_2$ particles that remain fixed. From Figure 4-13 C and F, the separator is contaminated with $LiCoO_2$ and graphite particles. The attachment of $LiCoO_2$ and graphite particles to the current collector is relatively weak, as discussed in the size range 4750 µm − 2360 µm.

From the size fraction 2360 µm − 850 µm, it is shown that this region contains a positive electrode that has undergone a reduction in size with the minimum liberation of $LiCoO_2$ particles. However, the negative electrode is relatively clean from graphite. Similarly, with the finding from size range 4750 µm − 2360 µm, the graphite is more readily liberated than the $LiCoO_2$ particles from its current collector. Active materials also found to be contaminating the separator that also hinders size-based separation.
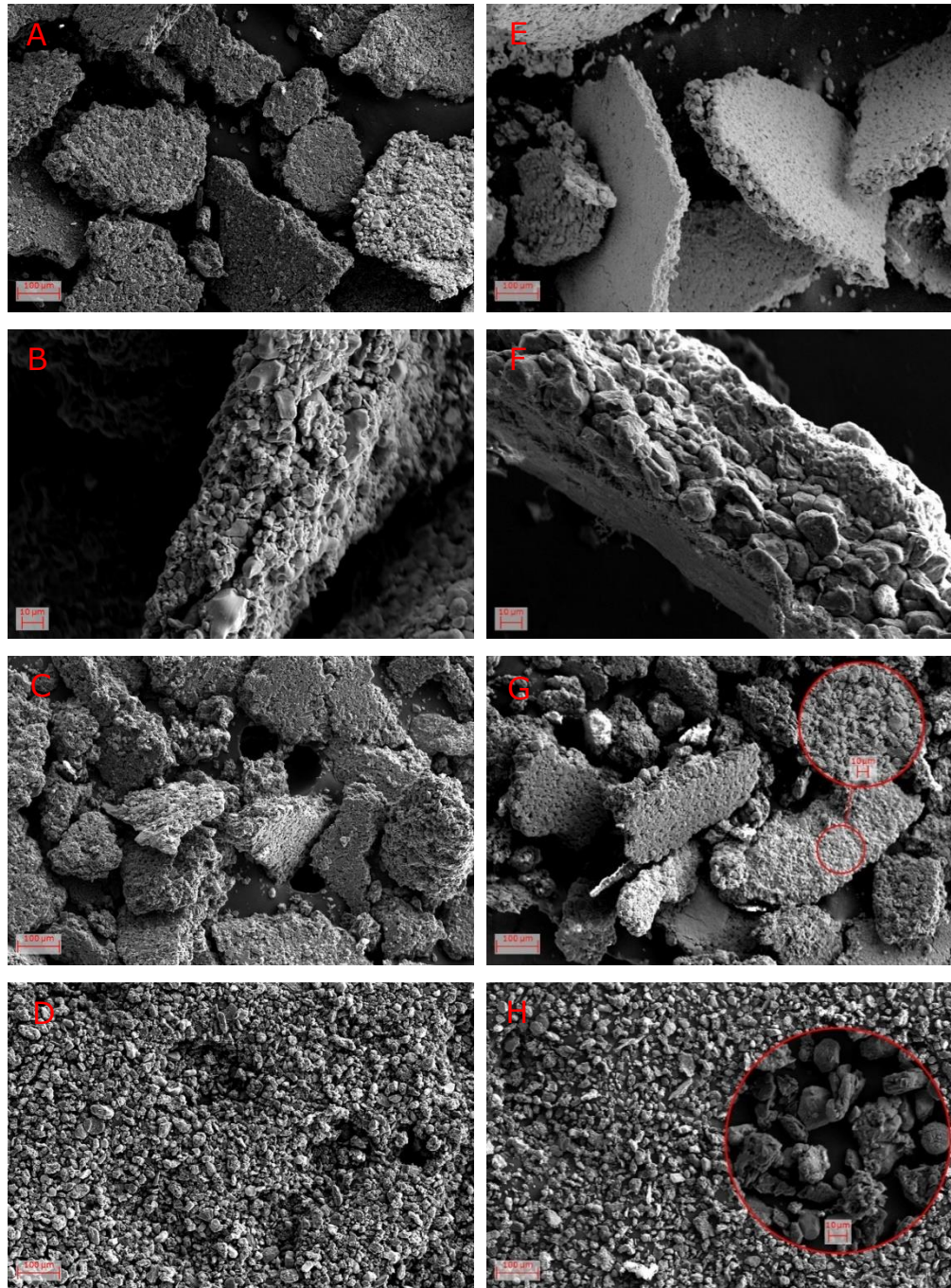
Figure 4-14 SEM image of size fraction < 850 μm ; New LIBs: A Powder from size fraction 850 μm – 212 μm, B Zoomed LiCoO$_2$-PVDF aggregate from size fraction 850 μm – 212 μm identified by EDX, C Powder from size fraction 212 μm – 38 μm, D Powder from size fraction < 38 μm; Spent LIBs: E Powder from size fraction 850 μm – 212 μm, F Zoomed LiCoO$_2$-PVDF aggregate from size fraction 850 μm – 212 μm identified by EDX, G Powder from size fraction 212 μm – 38 μm, H Powder from size fraction < 38 μm.

Figure 4-14 presents the morphology of new and spent LIBs in size range of < 850 μm, and it can be concluded that there is no significant difference between the two. From Figure 4-14 A and E, the size fraction 850 μm – 212 μm contains lumps of graphite and $LiCoO_2$ particles that have been detached from its current collector and only held together by the binder. Moreover, there are substantial $LiCoO_2$ fine particles aggregates (Figure 4-14 B and F) that are covered by the binder. Similar observation also made for the size range of 212 μm – 38 μm (Figure 4-14 C and G) as well as size range of < 38 μm (Figure 4-14 D and H). With the only difference being the size of the aggregates, where the size fraction < 38 μm shows the least aggregation between particles. Thus, the size fraction of < 850 μm may be classified as the size fraction that concentrates detached active materials but is still held together by the PVDF binder.

The surface morphology study allows the identification of the breakage mechanism of LIBs during mechanical liberation. The combination of size-based hierarchy and morphology study can be used to understand the impact of PVDF adhesiveness towards the current collector breakage in mechanical liberation by comparing the new and spent LIBs and further discussed.

4.3.3 The concurrence of morphology observation and size-based hierarchy

From the observation above, the new and spent LIBs does not exhibit a significant difference in terms of morphological characteristics. From the morphological analysis, a distinct property is observed above the cut point 850 μm. The copper foils are cleaner compared to the aluminium foils due to graphite particles are more readily liberated as compared to $LiCoO_2$ particles. The positive and negative electrode active

materials show similar morphology behaviour below the cut point of 850 µm. Moreover, the separator is also contaminated by positive and negative electrode active materials.

From the morphological study that has been carried out using SEM, the liberated LIBs can be classified into four major categories based on the attachment of active materials onto the current collector and the size of the active materials detached. The larger size fractions with active materials still attached on to it are categorised as Category 1 and Category 2. While the detached active materials that are still aggregated and held together by the binder are categorised as Category 3 and Category 4. The characterisation are described as follow;
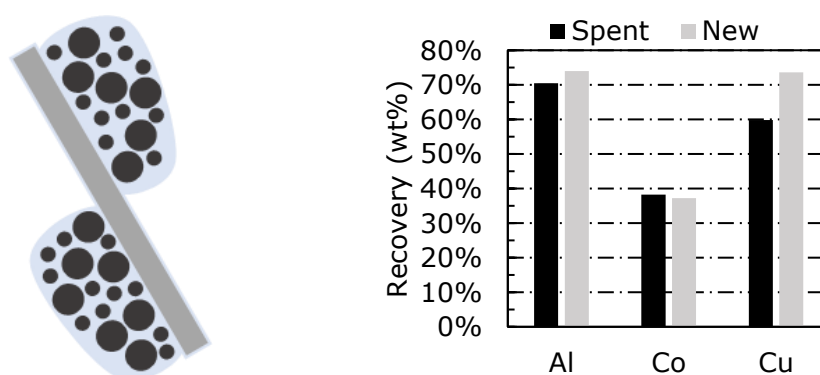
Figure 4-15 Schematic diagram of Category 1 particle and its respective size-based recovery rate

Category 1: Include the majority of particles that have experienced reduction in size, accompanied by some detachment of its active materials such as particles in the range of >2360 µm. The schematic diagram and the recovery rate of the size range > 2360 summarised in Figure 4-15.
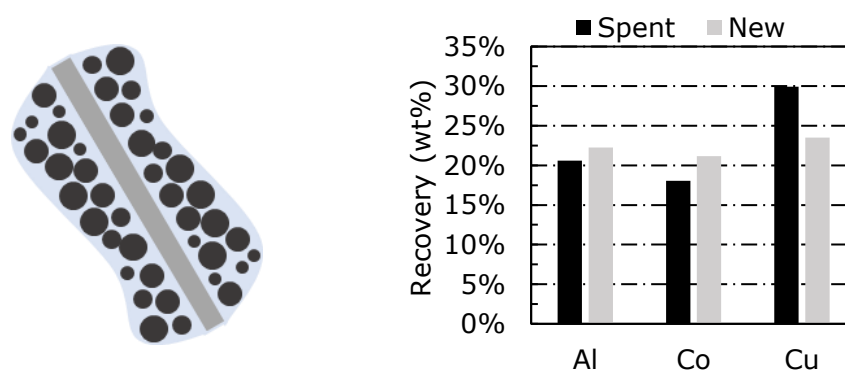
Figure 4-16 Schematic diagram of Category 2 particle and its respective size-based recovery rate

Category 2: Include particles that have a reduction in size with the active materials held by the binder and attached to its current collector, such as in the range of 2360 μm – 850 μm. The schematic diagram shows in Figure 4-16 is only true for positive electrode while the negative electrode is relatively cleaner.
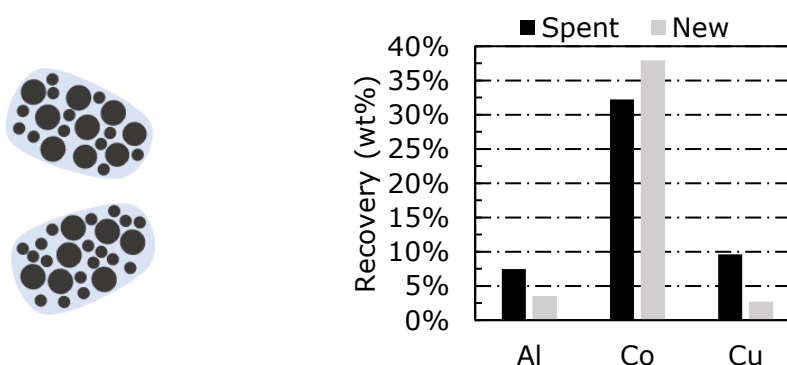
Figure 4-17 Schematic diagram of Category 3 particle and its respective size-based recovery rate

Category 3: Active materials that have been detached from its current collector and still held together by the binder. This type of particles appear as aggregates for the particle size of 850 μm – 38 μm. The schematic diagram and the recovery rate of the size range 850 μm - 38 μm summarised in Figure 4-17.
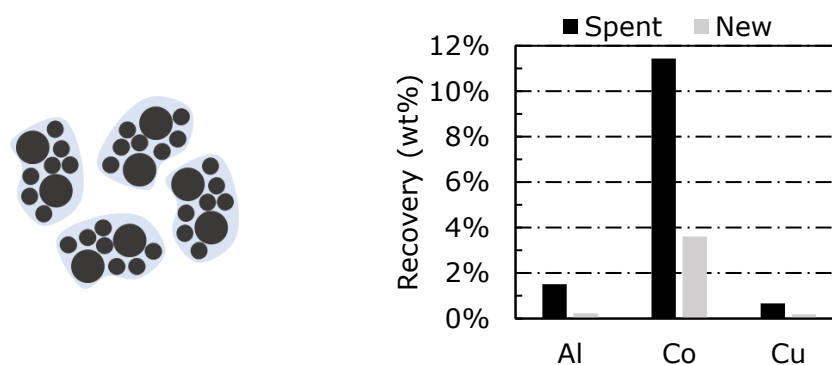
Figure 4-18 Schematic diagram of Category 4 particle and its respective size-based recovery rate

Category 4: Active materials that have been detached from current collector and accompanied with minimum aggregation for the particle size of < 38 μm. The schematic diagram and the recovery rate of the size range < 38 μm summarised in Figure 4-18.

In the case of spent LIBs, the stronger attachment of PVDF-LiCoO$_2$ onto the aluminium current collector compared to PVDF-graphite onto the copper current collector may help in explaining the change of trend in the re-mixing line of Fuerstenau upgrading diagram discussed in the previous section. The positive electrode found in the size region of 2360 μm – 850 μm were aluminium foils covered with LiCoO$_2$ particles and held together by the binder. The negative electrode counterpart has a minimum attachment of graphite particles. Therefore, the attachment of PVDF-LiCoO$_2$ particles onto the aluminium foil prevents it from breaking even further. While the the weaker attachement of PVDF-graphite onto the copper current collector have minimised this benefit and therefore concentrated at smaller size fraction. This can be seen from the size-based recovery rate presented in Figure 4-15 to Figure 4-18. The size-based recovery rate explains the recovery rate of a certain recoverable given it is isolated in a

given size range and the sum of recovery rate of a certain recoverable for the entire size range is unity.

From the characterisation of milled spent LIBs, when the size fraction above 2360 µm is isolated, the recovery rate of aluminium is higher than that of copper. Moreover, the recovery rate of copper is higher than aluminium in size range of 2360 µm to 212 µm and became aluminium dominant in the size fraction < 212 µm. Although copper has better ideal mechanical properties and the perforation that occurs on the aluminium current collector, the stronger attachment of PVDF-$LiCoO_2$ to aluminium current collector seems to improve its overall mechanical properties and preventing it from breaking during milling. Instead, the shear and tensile stresses induced by the cutting mill dislodged the $LiCoO_2$ laminates in the form of aggregates and forming Category 1 particles and the dislodged $LiCoO_2$ package concentrated in the size region of < 850 µm (Category 3 and 4). However, when the stress-strain induced by the cutting mill does not dislodge the materials on its surface. Instead, it reduces the particle size while maintaining the active materials intact, covering the whole surface area of the current collector resulting in Category 2 particles. Conversely, there may not be a tangible benefit towards the mechanical properties for copper current collector. This is due to the weak bonding between PVDF-graphite to the copper current collector. This is combined with the reduction in elastic modulus of copper current collector as the battery is cycled, causing the copper to be selectively liberated in the finer region when compared to aluminium.

As a baseline, comparison with milled new LIBs was carried out. From the size-based recovery hierarchy, it can be seen that the new LIBs have minimum contamination from copper and

aluminium in the size region of < 850 µm. The better mechanical properties of the current collector and attachment of PVDF binder translates to lower contamination of copper and aluminium in the finer size region. A dramatic difference can be observed when comparing the copper recovery in the size region of > 2360 µm (Category 1) for the new and spent LIBs. The milled new LIBs recover 73.6 wt% of copper, whereas the spent LIBs only recover 59.8 wt% of copper. The milled new LIBs produce more Category 1 copper particles that indicate the significance of the PVDF binder in preventing the breakage of the copper current collector. Moreover, the better mechanical properties of the copper current collector in the new LIBs inhibits the breakage of copper particles with minimum active materials attachment (2360 µm – 850 µm) into fine particles that contaminates the finer size region (< 850 µm).

Similar interpretation also made with the aluminium particles, in which in the case of new LIBs is less contaminating in the finer size region. Instead, an increase in the recovery of aluminium in the Category 1 and Category 2 particles are observed. The better mechanical properties of $LiCoO_2$-PVDF-$LiCoO_2$ also prevent the breakage of Category 3 particles into Category 4 particles during mechanical liberation.

4.4 Conclusion

This chapter presents a systematic experimental study aimed at understanding the selective liberation of positive electrode active material during milling. From the analysis that has been carried out, the liberation is indeed a selective phenomenon with the optimum cut point of 850 µm. In the size fraction <850 µm, the recovery for spent LIBs is 43.7 wt% of $LiCoO_2$ with a minimum recovery of aluminium and copper (8.8 wt% and 10.3 wt%) from the feed. However, more than 50 wt% of $LiCoO_2$ is

found in the size region of >850 μm, and it contains a substantial amount of aluminium and copper (91.2 wt% and 89.7 wt%) from the feed and are not suitable to be treated with leaching.

Milling spent LIBs induces selective liberation of $LiCoO_2$ particles. From the morphological analysis, $LiCoO_2$ particles have a stronger attachment to its current collector than the graphite counterparts. From the morphological analysis done, a significant difference between the positive and negative current collector's surface can be seen in the size fraction of 2360 μm – 850 μm where the negative electrodes are cleaner compared to the positive electrode. The contradiction between copper and aluminium recovery rate towards $LiCoO_2$ recovery rate in the re-mixing line of Fuerstenau upgrading curve may be explained by the stronger attachment of $LiCoO_2$-PVDF-Al compared to graphite-PVDF-Cu. Other than the positive and negative electrode, some of the $LiCoO_2$ particles adhere to the separator after liberation. This may be caused by the compression action of the cutting mill. It also reduces the recovery rate of liberated $LiCoO_2$ in smaller size fraction.

The comparison between new and spent LIBs was made with a distinct difference observed for the selective liberation of copper towards cobalt and aluminium. Better separation efficiency of $LiCoO_2$ particles is observed in the selective liberation of new LIBs. The better physical properties of current collectors and the adhesiveness of the binder in the new LIBs have made the finer size region to be contaminated by the copper and aluminium. The effect of PVDF binder in preventing the breakage of copper current collector can be observed by the more occurrence of copper related to the Category 1 particles in new LIBs than in spent LIBs. Whereas, the better

mechanical properties of new LIBs prevent the breakage of current collectors that contaminates the fine size region (< 850 µm).

The mechanism of the selective liberation of $LiCoO_2$ particles has been proposed. During milling, two possible outcomes may arise. Either $LiCoO_2$ particles are dislodged and released in the form of $LiCoO_2$-PVDF aggregates that are concentrated in the size fraction of < 850 µm or size reduction occurs while maintaining its attachment to the current collector. However, the size of the $LiCoO_2$-PVDF aggregates that are dislodged is still far from the actual size of $LiCoO_2$ particles as found in spent LIBs. Therefore, the optimum cut point proposed (850 µm) is greater than the actual size of $LiCoO_2$ particles found in spent LIBs (ca. 1.50 µm – 7.80 µm (Pavoni et al., 2018)).

This page is intentionally left blank.

Chapter 5 Selective Liberation of LiCoO₂ Particles

5.1 Introduction
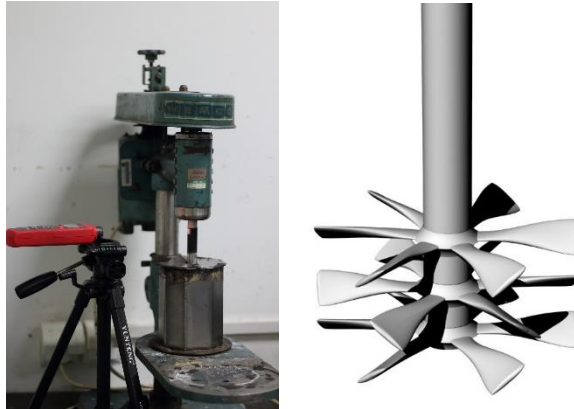
Figure 5-1 Photograph of the attrition scrubbing setup (left) and diagram of the reverse pitched impeller (right).

The attrition of particles are associated with impact-based stress that produce fine particles (Materic et al., 2014). Attrition scrubbers have been design to induce impact and shearing action between particles that promotes surface abrasion and produces fine particles (Kim et al., 2010, Bayley and Biggs, 2005, Du et al., 2019). Attrition scrubbing is conventionally used to upgrade minerals by removing surface impurities such as sand cleaning, delamination of kaolin and graphite and turning it into saleable products (Sandgren et al., 2016). A rotating impeller produces powerful attrition when particles rub against each other in a thick-high density pulp. The two distinct properties of attrition scrubbing are the opposing pitched blades that reverse the flow of the pulp and an octagonal tank that induces turbulent mixing (Figure 5-1). WEMCO 1L attrition cell was used to conduct the experiments as shown in Figure 5-1.

Looking at the morphology of particles after preliminary liberation, LiCoO₂ particles are still held by the PVDF binder. From Chapter 4, it was observed that the milled spent LIBs comprise of active materials that are still attached on to the current collectors in the size region of > 850 μm. The active materials that have been detached from the current collectors are concentrated in the size region of < 850 μm. Thus, by considering the morphology, the use of attrition scrubbing may be suited for the facilitate liberation of LiCoO₂ particles.

As the components found in LIBs comprises of inherently malleable materials and unable to abrade each other. Hence, the use of attrition media is deemed to be appropriate. Silica sand as the attrition media is used with the size range of 2360 μm – 850 μm. It was expected that the copper and aluminium current collectors that are still contaminated by the LiCoO₂ and graphite particles (> 850 μm) would be scrubbed during attrition. While the active materials aggregates (< 850 μm) would be disaggregated by the impact liberation during attrition. A schematic diagram of the potential liberation mechanism is presented in Figure 5-2.

Figure 5-2 The hypothesis of silica sand media on different particle morphology of dry milled LIBs in attrition scrubber; size fraction of > 850 μm (left) and size fraction of < 850 μm (right) with the silica sand media represented by the circles.

5.2 Experimental details
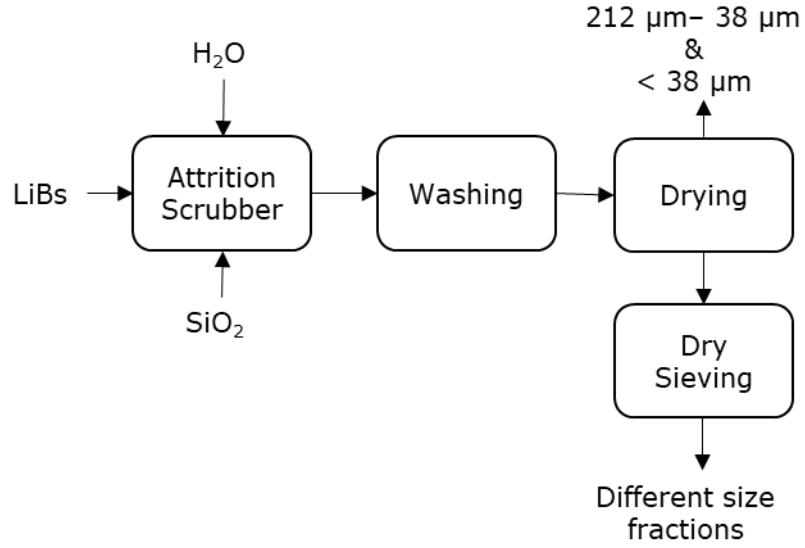
Figure 5-3 Flow diagram of the experimental design.

Attrition scrubbing were conducted in a WEMCO 1L standalone attrition cell. In this study, the impeller speed is set to be constant at 1000 rpm. Clean low iron silica sand in size range of 2360 μm – 850 μm was used. The flow diagram of the experiment is summarised in Figure 5-3. The calculation of LIBs to silica sand ratio and pulp density (wt%) are shown as Equation 5-1 and Equation 5-2.

$$LiBs \ to \ Silica \ sand \ ratio \ (wt\%) = \frac{m_{LIBs}}{m_{Sand}}$$ **Equation 5-1**

$$Pulp \ density \ (wt\%) = \frac{m_{LIBs} + m_{Sand}}{m_{LiB_s} + m_{Sand} + m_{water}}$$ **Equation 5-2**

Where, m_{LIBs} is the dry mass of spent LIB, m_{Sand} is the dry mass of the silica sand media, and m_{water} is the mass of the added water.

A certain amount of water, silica sand and shredded LIBs were added into the attrition cell. Once the attrition scrubbing experiment has finished, the product is wet sieved with 5L

147

water by using 38 μm nominal aperture size and a 212 μm sieve to prevent damage. The wet sieving produces size fraction of 212 μm – 38 μm and < 38 μm. The products then dried in an oven at temperature of 80°C, to prevent HF formation as explained in Chapter 3, until constant weight was achieved. Furthermore, the size fraction of > 212 μm is further sieved to assess the breakage mechanism. The particles are further sieved into the size fractions of > 4350 μm, 4350 μm – 2360 μm, 2360 μm – 850 μm, and 850 μm – 212 μm. The particle size of 212 μm – 38 μm and < 38 μm is mixed with the particle from the wet sieving and weighted together. Each different size fraction then analysed for morphological analysis by using SEM-EDS to confirm the breakage mechanism. The different size fractions also subject to elemental analysis using ICP-MS as described in Chapter 3 to assess the liberation rate of LiCoO₂ particles as compared to the breakage rate of the copper and aluminium component.

The representative samples used for this entire chapter can be found in Appendix III.

5.3 Results and discussions

5.3.1 Suitability of attrition scrubber for the selective liberation of LiCoO₂ particles
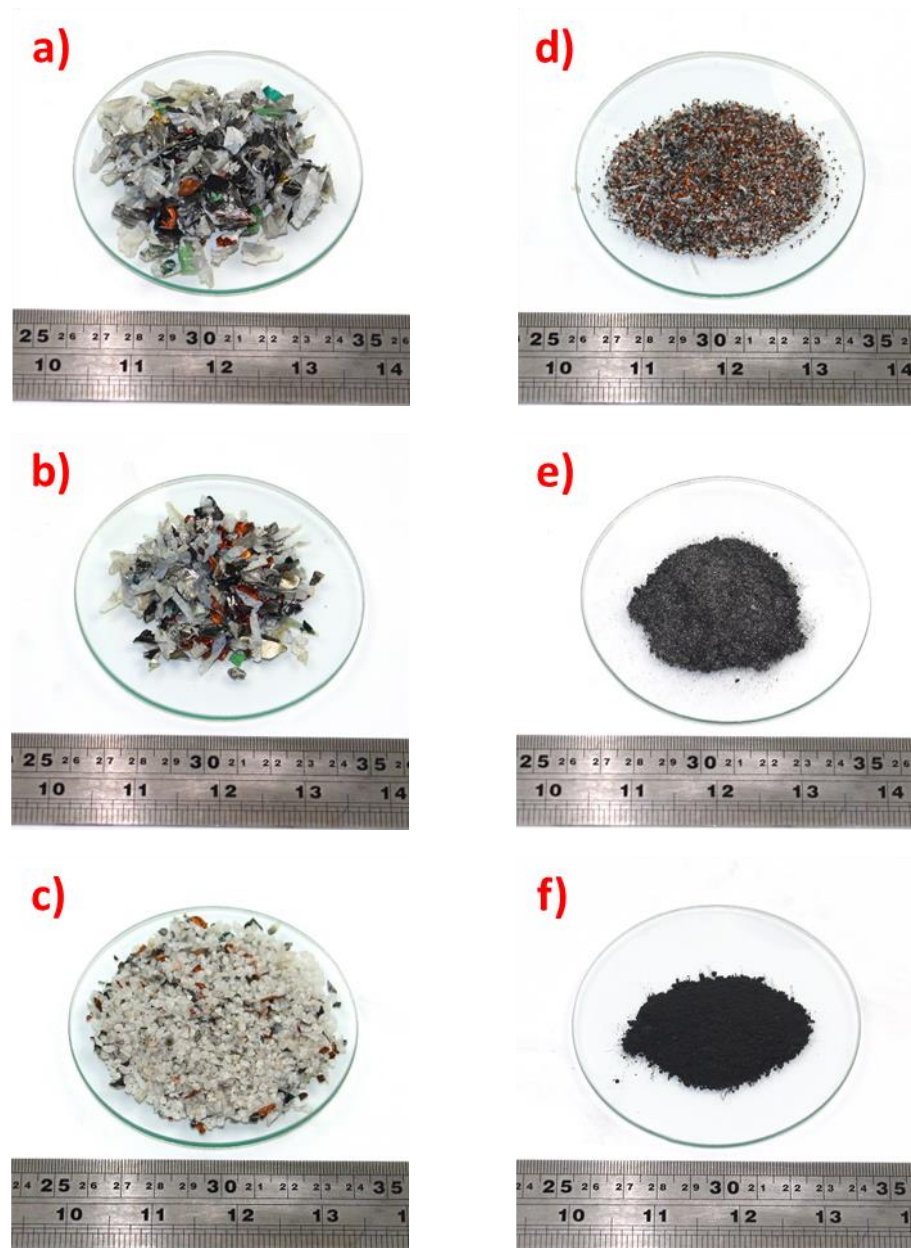
Figure 5-4 Photograph of 2.5 min attrition time products: a) > 4750 μm, b) 4750 μm – 2360 μm, c) 2360 μm – 850 μm, d) 850 μm – 212 μm, e) 212 μm – 38 μm, f) < 38 μm.

The ability of attrition scrubber to selectively liberate LiCoO₂ is initially measured by assessing 2.5 min attrition time with 70 wt% pulp density and 10 wt% of LIBs to silica sand ratio. The

experiment is carried out in triplicate. The photograph of the classified products is presented in Figure 5-4. Visual inspection reveals that the battery separator is predominantly found in the larger size fraction (> 850 µm) and minimum in the smaller size region (< 850 µm), indicating that the flexible separator undergoes minimum breakup during attrition scrubbing.
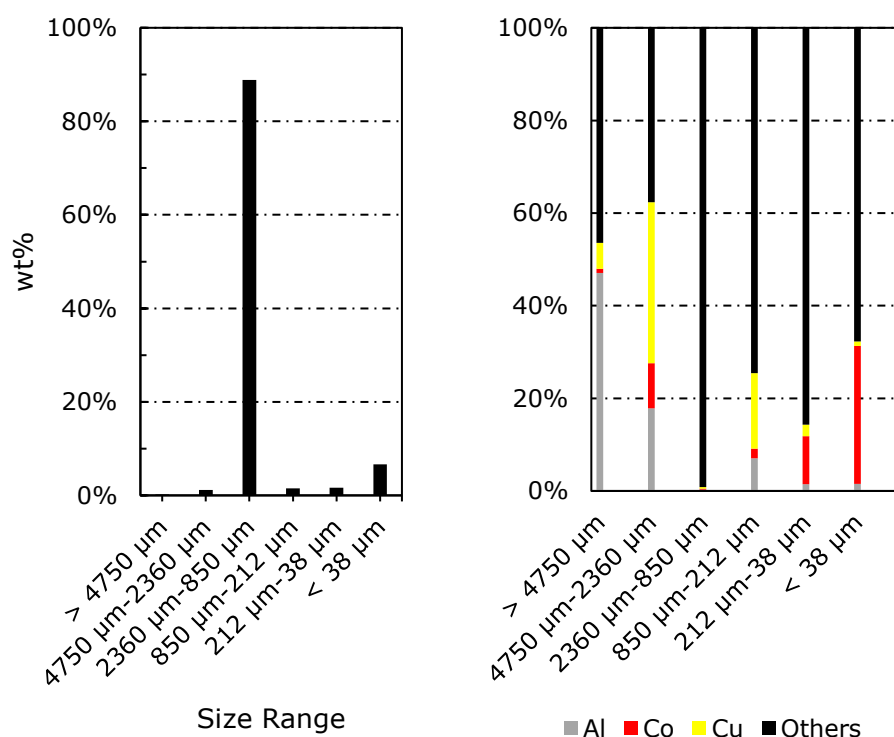
Figure 5-5 Size distribution (left) of classified 2.5 min attrition product and key elements distribution (right).

From Figure 5-5 it can be seen that the classified attrition products in the size range of 2360 µm – 850 µm and < 38 µm have the largest wt%. The 2360 µm – 850 µm, which is the size range of the attrition media being used is expected to have the highest mass proportion (88.9 wt%) that indicates minimum breakage of the silica sand media. The second highest mass proportion was found from the size range of < 38 µm (6.7 wt%). The production of fine particles is the expected outcome from the attrition scrubbing. The size range of < 38 µm also has the highest concentration of cobalt 29.8 wt%. This

translates to 49.5 wt% $LiCoO_2$ and a recovery rate of 78.9 wt%. Moreover, the size fraction of < 38 μm contains minimum amount of copper and aluminium. From analysis, the concentration of aluminium and copper in the size region of < 38 μm are 1.5 wt% and 0.9 wt% respectively. The copper and aluminium concentration translates to an overalls recovery rate of 13.2 wt% and 5.8 wt%. Thus, it can be shown the attrition scrubber does induce selective liberation of $LiCoO_2$ particles in the finer size region.

Table 5-1 Comparison of the Fuerstenau recovery curve of the shredded LIBs (1ˢᵗ stage) and attrited shredded LIBs (2ⁿᵈ stage).
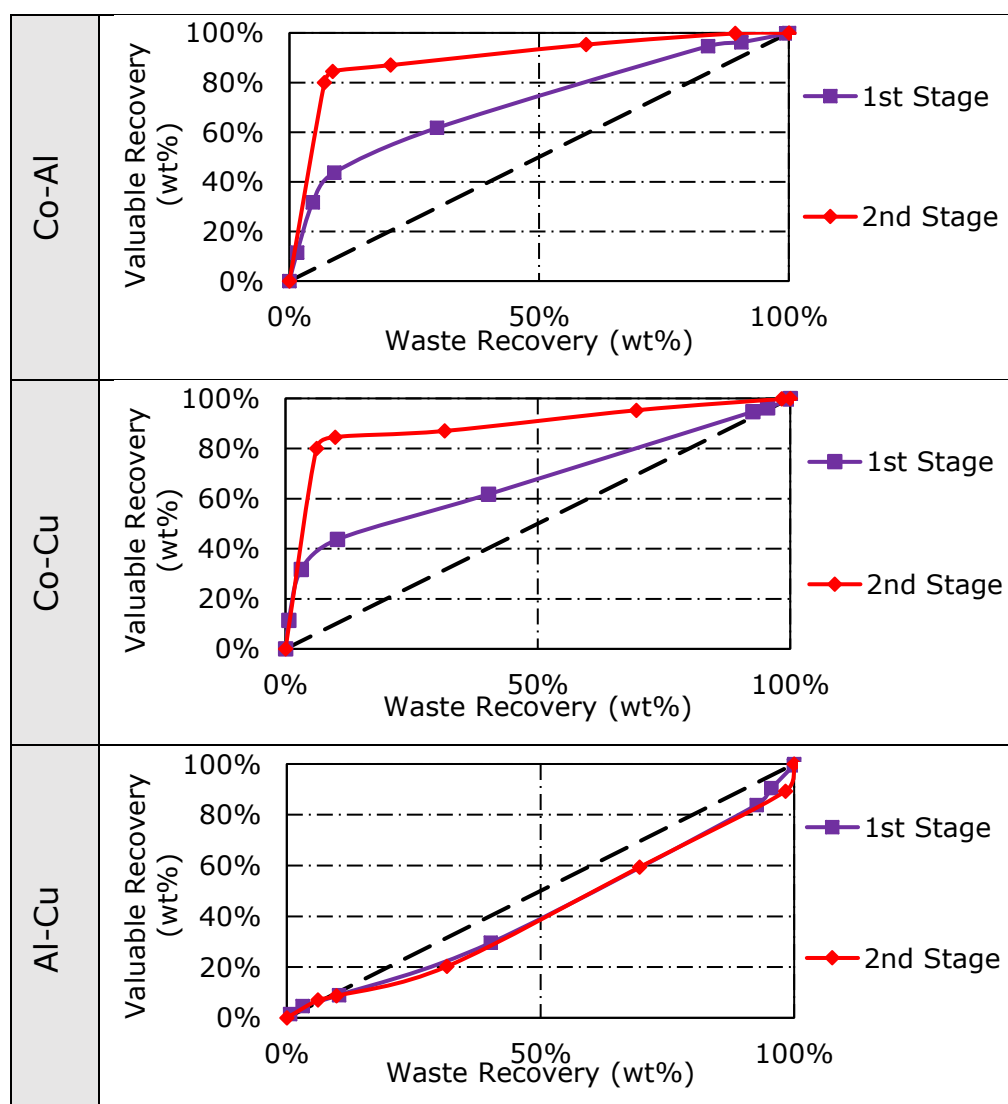
To have a better understanding, the Fuerstenau recovery curve of before and after attrition is then compared and summarised in Table 5-1 for the different interactions between cobalt, copper, and aluminium. From Table 5-1 the Co-Al and Co-Cu recovery lines are further apart above the diagonal line from the 1st stage initial liberation compared to the 2nd stage when applying attrition scrubbing. However, the Al-Cu Fuerstenau recovery curve shows minimum selective liberation in 1st and 2nd stage of liberation.

The improvement of the selective liberation can be measured by integrating the Fuerstenau recovery curve. It is important to point out that the area of 0.5 arbitrary unit (a.u) is the highest possible area bound by the recovery line and the diagonal line. In this study, the integration is done by employing trapezium method of integration and the results are presented in Table 5-2.

Table 5-2 Area bound by the recovery line and the diagonal line.

Recovery Line	Area (arbitrary unit)					
	1st Stage		2nd Stage		Change	
	a.u.	%	a.u.	%	a.u.	%
Co-Al	0.21	42.7	0.40	79.3	0.18	36.6
Co-Cu	0.17	34.4	0.38	77.0	0.21	42.6
Al-Cu	0.07	14.3	0.08	16.5	0.01	2.2

From the results presented in Table 5-2, the initial liberation using only a cutting mill does induce a degree of selective liberation of cobalt towards aluminium and copper by 42.7 % and 34.4 %respectively. Attrition scrubbing as the second stage of liberation improves the selective liberation of cobalt towards aluminium and copper by 36.6 % and 42.6 % respectively.

There is only a slight increase in the selective liberation efficiency between aluminium and copper by 2.2 %. Thus, the separation of aluminium and copper based on size for attrition scrubbing product is still unlikely.

Furthermore, the optimum cut point that concentrates LiCoO$_2$ particles with minimum contamination from aluminium and copper can then be assessed based on the ore separation degree (η_{ore}) plot. The $\eta_{ore,max}$ is compared for the first and second stage liberation and shown in Table 5-3.

Table 5-3 Comparison of ore separation degree of the shredded LIBs (1st stage) and attrited shredded LIBs (2nd stage).
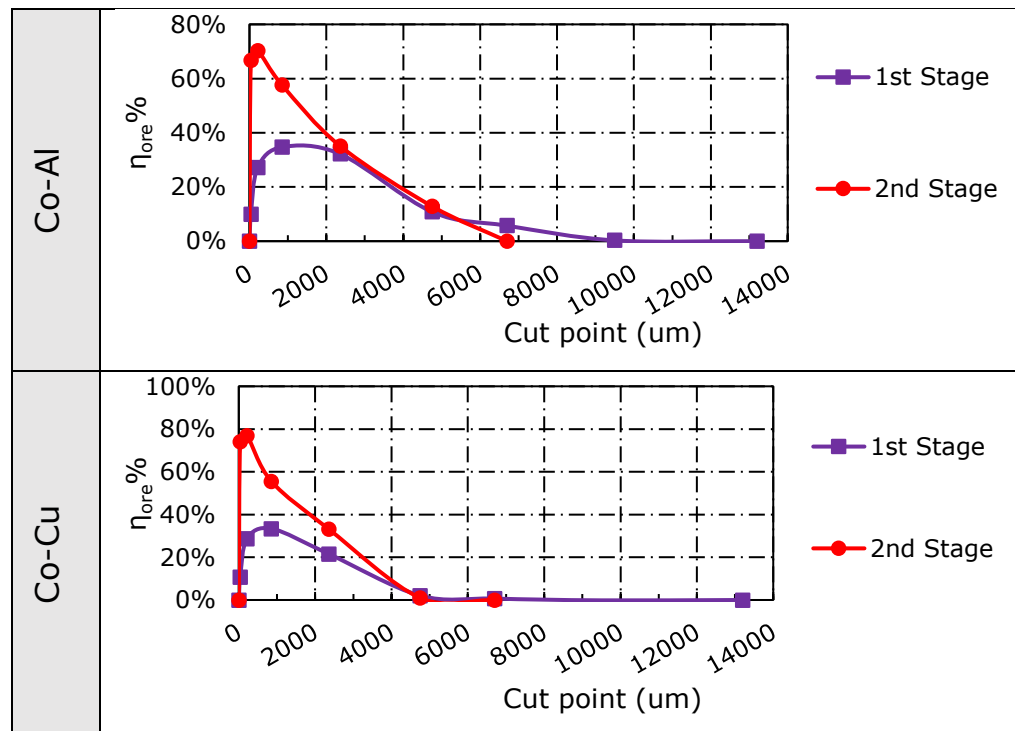
From Table 5-3, comparing the ore separation degree from the first and second liberation stage, it can be observed that the second stage is able to selectively liberate LiCoO$_2$ particles closer to the particle size that is found inside spent LIBs. The $\eta_{ore,max}$ improves when applying attrition scrubbing as a second stage liberation process and was found to be 70.2% and 77.0% for Co-Al and Co-Cu respectively with the cut point of 212 μm.

However, it is suspected that the cut point of 212 µm still contains LiCoO$_2$ particles that are not well liberated and still held together on the PVDF binder. Moreover, the smaller cut point of 38 µm produce a lower separation efficiency of 66.7 % and 74.0% for Co-Al and Co-Cu respectively.

Morphology analysis by using SEM-EDX with back scattered detector was then carried out for the different size fractions to understand the liberation achieved by attrition scrubbing. The morphological observations for the different size range is presented in Figure 5-6.
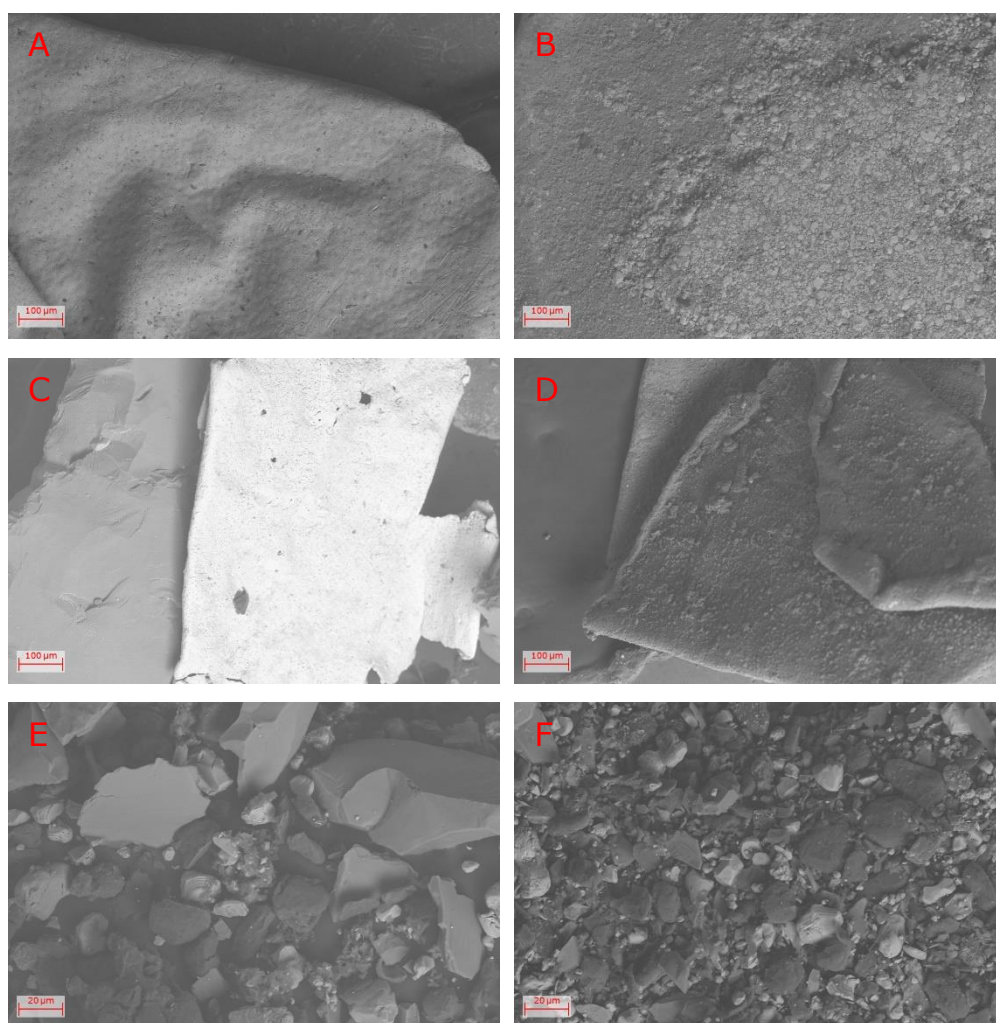
Figure 5-6 SEM image from 2.5 min attrition product; A 2360 µm – 850 µm copper foil, B 2360 µm – 850 µm aluminium, C 850 µm – 212 µm copper, D 850 µm – 212 µm aluminium, E 212 µm – 38 µm powder, F < 38 µm powder.

From Figure 5-6 A and B, it can be seen that the copper and aluminium in the size fraction of 2360 μm – 850 μm foils are relatively clean from the active materials laminates as compared to the particles, previously discussed in Chapter 4, prior attrition scrubbing. The copper current collector is relatively cleaner than that of the aluminium counterpart. This phenomenon can be explained by the weaker attachment of graphite on the copper current collector as compared to the aluminium counterparts. Therefore, it is expected that the liberation of LiCoO₂ is also accompanied by the liberation of graphite.

Figure 5-6 C and Figure 5-6 D shows clean copper and aluminium in the size fraction of 850 μm – 212 μm. Prior attrition, this size fraction concentrates LiCoO₂ and graphite aggregates and shows the least amount of copper and aluminium components. The observation suggest that the copper and aluminium found in this size region is attributed from the breakage of copper and aluminium from the size fraction > 850 μm after 2.5 min attrition time. Furthermore, the initially aggregated LiCoO₂ particles can no longer be found in this size fraction. Instead, the particles have been disaggregated into the size fraction of < 212 μm as observed in Figure 5-6 E and Figure 5-6 F.

From Figure 5-6 E and F, it can be seen that the both size fractions of 212 μm – 38 μm and < 38 μm concentrates the LiCoO₂ and graphite particles. However, it is important to point out that the LiCoO₂ particles in the size range of 212 μm – 38 μm are still held together by the PVDF binder. Whereas, the LiCoO₂ particles in the size range of < 38 μm have been disaggregated. However, the copper and aluminium components were not observed in Figure 5-6 F and suspected

to break into fine particles and contaminated the surface of the larger particles.
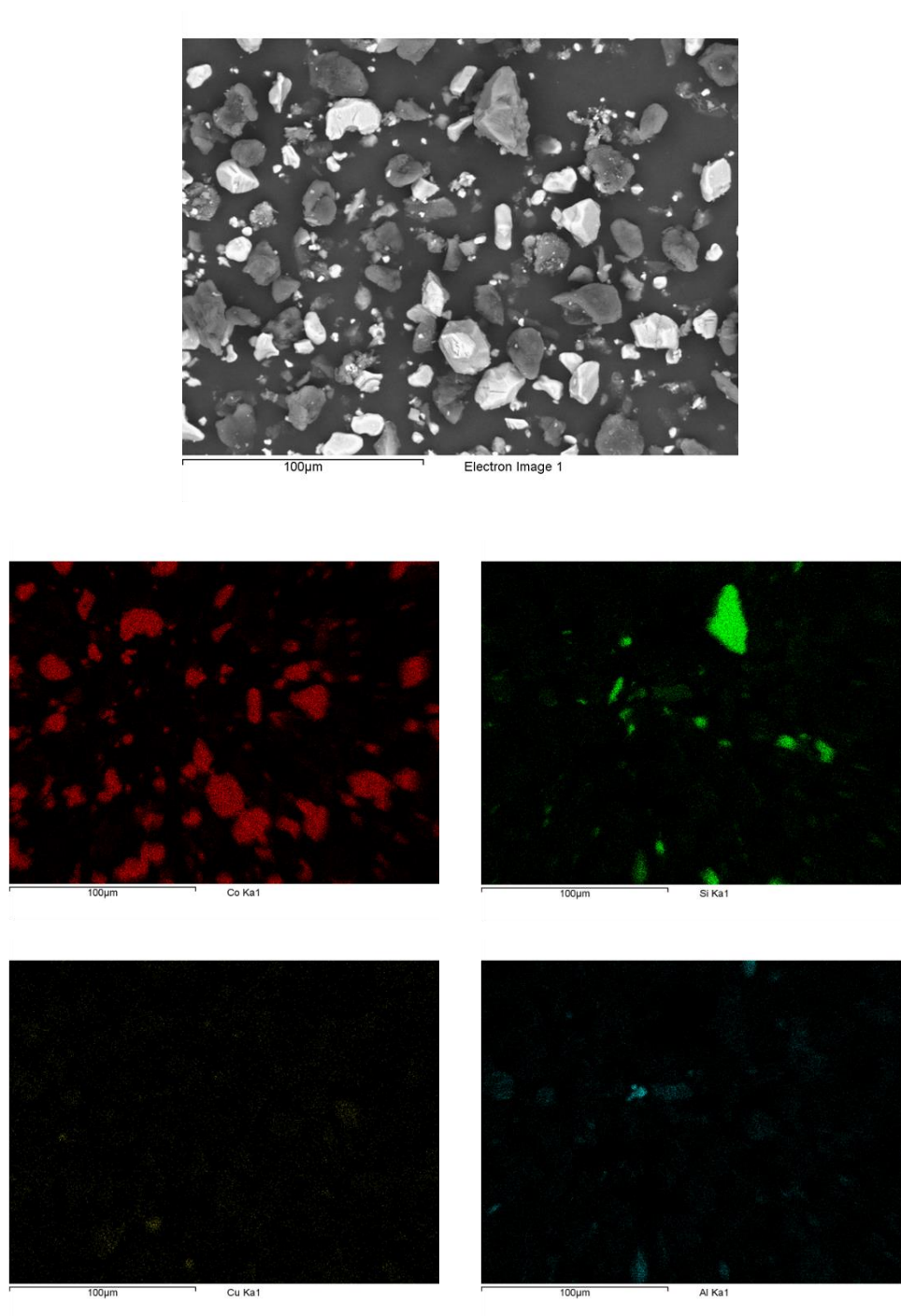
Figure 5-7 EDX Elemental mapping of 2.5 min < 38 μm attrition product.

To confirm that the copper and aluminium contaminating the surface of the larger particles, elemental mapping by using EDX was carried out for the attrition product of < 38 μm. The EDX-

elemental mapping was set to detect the cobalt, silica, copper and aluminium elements and the results of the elemental mapping is presented in Figure 5-7. From the observation, it was found that some of the graphite, LiCoO$_2$ and SiO$_2$ particles are contaminated by copper and aluminium fine particles. From the elemental mapping results, it is understood that further mechanical separation of copper and aluminium from this powder may be challenging.

Comparing the particle morphology of before and after attrition, the impact and shearing load appears to liberate the active materials that laminate the positive and negative electrodes. The impact load causes the disaggregation of LiCoO$_2$ and graphite and is concentrated in the size fraction < 38 μm and scours the particles from the aluminium and copper current collectors. The size fraction of 850 μm - 212 μm does not initially have clean copper and aluminium. However, after attrition, clean copper and aluminium can be found in this region. Thus, the liberation of LiCoO$_2$ and graphite particles also followed by the breakage of copper and aluminium. The breakage of copper and aluminium current collector is deduced to be slower than that of the active materials. To confirm this, the study related to the breakage kinetics of LiCoO$_2$ laminate as compared to the copper and aluminium current collector was carried out.

5.3.2 The breakage kinetics and its implication

To understand the liberation mechanism induced by attrition scrubber, the attrition time from the previous sub section is then extended. The pulp density and the LIBs to silica sand ratio was kept constant at 70 wt% and 10 wt% respectively. Each attrition time is carried out in triplicate. Samples from the size fractions 4750 μm – 2360 μm, 2360 μm – 850 μm, 850

µm – 212 µm, 212 µm – 38 µm, and < 38 µm with different attrition time is varied and assessed for key elements analysis of aluminium, cobalt, and copper.

The comparison between the breakage kinetics of the different components inside spent LIBs. Breakage kinetics of wet and dry grinding has been reported to be a first order ([Sadler III et al., 1975](#)). The rate of disappearance, by breakage, from a given narrow size, is given by Equation 5-3.

$$\frac{dw}{dt} = -kw$$

Equation 5-3

Where w is the weight of material in the given size fraction, t is time, and k is milling rate constant for the given size fraction. k is, in general, different for each size fraction present and is dependent on the operating parameters.

Equation 5-3 may be integrated to give Equation 5-4.

$$w = w_o e^{-kt}$$

Equation 5-4

Where w_o is the initial amount of material present in the specific size range. Equation 5-4 suggest that a plot of ln w versus t should be a straight line with ordinate intercept ln w_o and slope equal to −k.

Two cut points of 2360 µm and 38 µm are assessed for the breakage kinetics. The cut point 2360 µm assess the delamination of LiCoO₂. Whereas, the cut point 38 µm assess the disaggregation of the LiCoO₂ laminates.

The fines generated in the size fraction of < 38 µm is firstly discussed. The cobalt is plotted in different figure than that of copper and aluminium component to prevent the copper and aluminium plot became constricted.

(5-8 a) 2360 μm

y = -0.0152x + 4.4215
R² = 0.9918

y = -0.0335x + 4.3148
R² = 0.9972

(5-8 b) 2360 μm

y = -0.0694x + 2.7102
R² = 0.9805

(5-8 c) 38 μm

y = -0.0013x + 4.5369
R² = 0.9793

y = -0.0015x + 4.5167
R² = 0.9477

(5-8 d) 38 μm

y = -0.0399x + 3.0602
R² = 0.8988
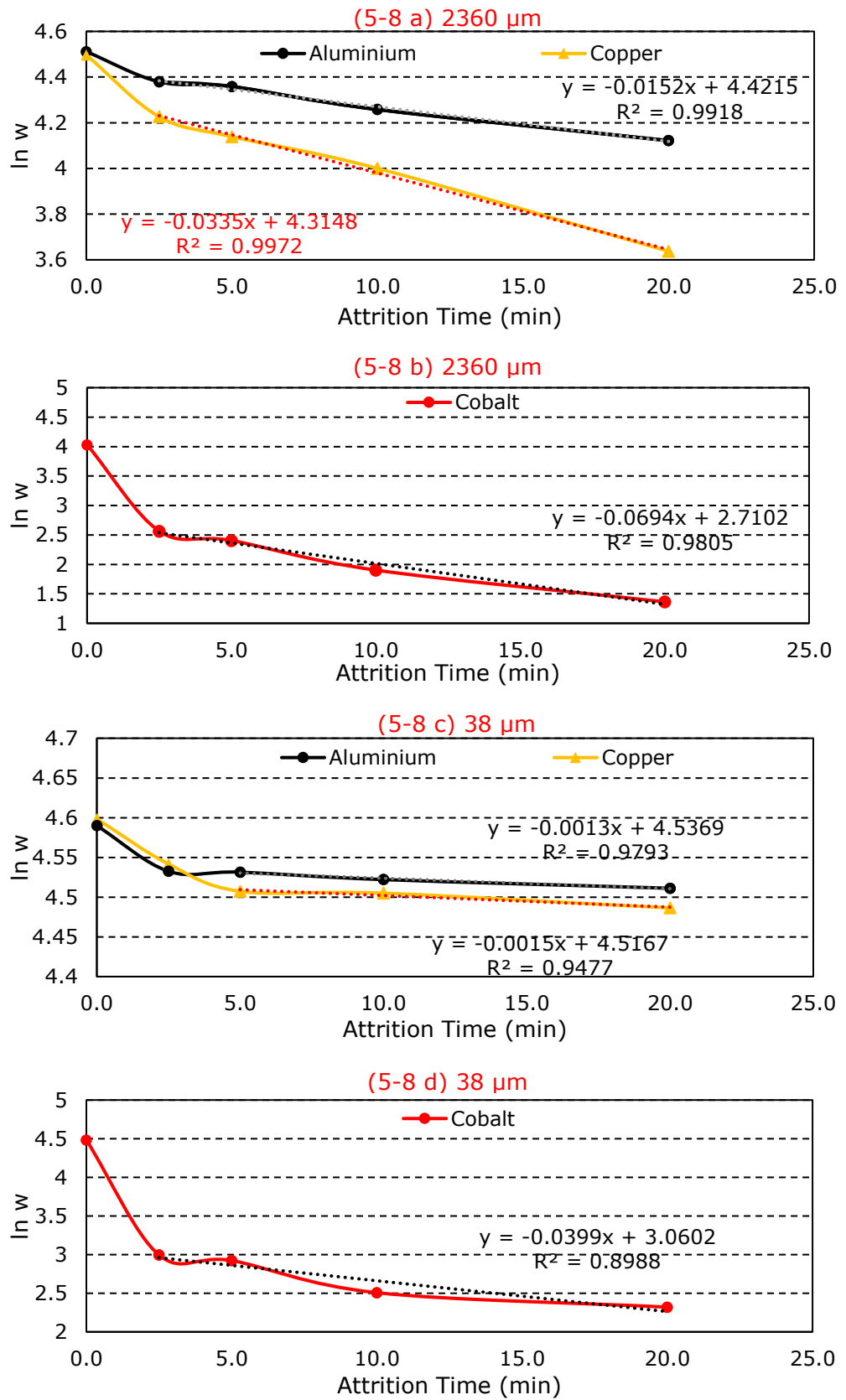
Figure 5-8 The breakage kinetics of aluminium, copper, and LiCoO₂ laminate (cobalt) for less than 2360 μm and 38 μm.

From Figure 5-8, in the initial phase, the breakage kinetics of aluminium, copper, and cobalt does not initially follow the first-order breakage kinetics for both the 2360 μm and 38 μm cut point. This is ignored when calculating the breakage kinetics. The breakage rate comparison of aluminium, copper and cobalt is calculated using the linear region. Therefore, in this study, the breakage kinetics were calculated using the points after initial breakage.

From Figure 5-8 a, by comparing the aluminium and copper breakage gradient, it can be seen that the aluminium component experiences a slower breakage rate than that of the copper component. This can be explained via the copper foil mechanical degradation after the battery is being cycled that makes copper mechanically weaker than aluminium. The weaker attachment of graphite laminate on to copper than that of LiCoO$_2$ laminate on to aluminium may also help to explain this phenomenon. The copper became more susceptible to breakage by the attrition media as compared to the aluminium foil that is more protected by the LiCoO$_2$ laminate.

Figure 5-8 b shows the breakage kinetics of the LiCoO$_2$ particles via the detection of cobalt through the cut point 2360 μm. Comparing the gradient of LiCoO$_2$ laminate breakage kinetic to that of aluminium and copper, it can be seen that the LiCoO$_2$ laminate breaks at a faster rate than that of copper and aluminium. This also implies that the liberation of LiCoO$_2$ particles is required prior to the breaking of the aluminium. Hence, this also confirms that the LiCoO$_2$ laminate prevents the breakage of the aluminium component.

The breakage kinetics of aluminium and copper passing through the cut point of 38 μm is presented in Figure 5-8 c.

Similarly, to the phenomenon described for Figure 5-8 a, the aluminium breaks slower than that of copper.

From Figure 5-8 d, it can be seen that the LiCoO$_2$ laminate breakage rate towards the cut point of 38 µm is faster than that of copper and aluminium. The gradient of the cobalt breakage kinetics is much higher than that of copper and cobalt. The substantially faster breakage of LiCoO$_2$ laminates towards the cut point of less than 38 µm is expected. The LiCoO$_2$ particle size range found in spent LIBs is between 1.50 µm – 7.80 µm (Pavoni et al., 2018). This indicates that the liberation of LiCoO$_2$ particles that are still held together by the binder is much faster than the fines produced by the breakage of aluminium and copper.

The comparison of the breakage kinetics of aluminium, copper and LiCoO$_2$ laminate shows that the LiCoO$_2$ laminate breaks faster than that of copper and aluminium. The faster rate of LiCoO$_2$ laminate shows that it is selectively liberated during attrition. Moreover, the copper component breaks faster than the aluminium component. These may be caused by the following factors:

• The copper and aluminium foils in the larger size fraction are still coated by the active materials and thus resulting in the liberation of active material laminates prior to the breakage of the copper and aluminium component during attrition.

• The weaker attachment of graphite lamination on to copper current collector is than that of LiCoO$_2$ lamination on to aluminium. Moreover, as the battery is cycled, the mechanical properties of copper degrade more severely than the aluminium

counterparts. These helps explain the faster breakage rate of copper when compared to aluminium.

- The LiCoO₂ laminate is held together by PVDF binder that has weaker mechanical properties than that of copper and aluminium. The copper and aluminium foil has higher tensile strength than PVDF (Butt et al., 2016, Group, 2011).As a result, the LiCoO₂ particles are being disaggregated and thus resulting in faster liberation rate as compared to the copper and aluminium counterparts. This effect is more apparent for the breakage rate of cobalt in comparison with copper and aluminium into the size fraction of less than 38 µm.

Figure 5-9 Recovery rate of aluminium, LiCoO₂ (cobalt) and copper in the size fraction of less than 38 µm with varying attrition time.

Figure 5-9 presents the recovery rate of aluminium, cobalt and copper concentrated in the size fraction of less than 38 µm. From Figure 5-9, LiCoO₂ has the highest recovery rate compared to copper and aluminium. The increase recovery of LiCoO₂ particles also followed by the decrease in LiCoO₂ grade. With the assumption that the graphite is liberated with the same degree than that of LiCoO₂ particle and the ratio of LiCoO₂ to graphite is constant. The concentration of the graphite particles in the size fraction < 38 µm is calculated based on the ratio of cobalt to graphite in LiCoO₂ batteries from the published

data by (Wang et al., 2016c). By this way, the concentration of the silica sand in the < 38 μm attrition product can also be estimated and summarised in Table 5-4.

Table 5-4 Composition of attrition products following attrition against time.

Attrition Time (min)	Concentration (wt%)				
	Al	LiCoO$_2$	Cu	Graphite	Sand
0.0	1.6	60.7	0.8	36.9	0.0
2.5	0.8	48.7	1.0	39.1	10.4
5.0	0.8	45.6	1.3	36.7	15.6
10.0	0.9	44.6	1.3	35.9	17.4
20.0	0.9	40.9	1.3	32.9	23.9

From Table 5-4, despite the increase in recovery of LiCoO$_2$ particles as attrition time increases, the LiCoO$_2$ grade decreases as the attrition time increases. This is attributed to the contamination caused by the silica sand media as attrition time increases. This is caused following the breakage of silica particles. The contamination from the attrition media is expected, and low iron silica sand has been chosen for it is chemically resistance to the lixiviant which has been proposed by researchers to leach the LiCoO$_2$ particles. Therefore, the main leachable contamination of attrition products is copper and aluminium. From previously reported literature, a proportion of 5 wt% copper relative to LiCoO$_2$ is a tolerable contamination for leaching and resynthesizing (Sa et al., 2015b). Aluminium can initially be removed via dissolution by using NaOH. From Table 5-4, the 20 min attrition time results in only 3 wt% copper relative to LiCoO$_2$. Therefore, the attrition product can be concluded to be suitable for subsequent

hydrometallurgical processes. Remaining graphite can be separated from silica sand by using froth flotation due to the hydrophilicity difference (i.e. graphite is hydrophobic and silica sand is hydrophilic) (Lu and Forssberg, 2001).

5.3.3 Parameters affecting attrition liberation

From the results laid out in the previous sub sections, the LiCoO$_2$ and graphite particles that were contaminating the surface of the current collectors are able to be liberated and concentrated by the impact and shearing load induced by the attrition scrubbing. The parameters affecting attrition scrubbing efficiency include the energy input into the system (i.e. residence time and impeller speed), contamination type and concentration (i.e. adsorbed or chemically bonded), and the particle morphology (i.e. entrapped in pores or surface contamination) (Bayley and Biggs, 2005). This sub-section aims at understanding the parameters affecting the efficiency of attrition scrubber in liberate and concentrate LiCoO$_2$ particles while minimising the contamination from copper and aluminium.

The parameters considered in this study include the pulp density, the LIBs to the attrition media ratio, and the attrition time. Moreover, parameters such as temperature and impeller speed are not included in this study. Parameter such as temperature does not directly correlates with the abrasive profile, rather it is useful towards organic species that its physical properties is dependent upon the temperature (Bayley and Biggs, 2005). Furthermore, the power consumption of an attrition scrubber can be controlled in two ways, by the attrition time or increase in impeller speed with lower attrition time. This correlation of attrition time and impeller speed also holds true in a pilot scale (Pétavy et al., 2009). Therefore, this study does not include variable impeller speed and temperature.

New sets of representative samples were prepared. Due to the time limitation, the experiment for each different attrition parameter is not repeated. To ensure that the composition from each sample does not significantly varies, five representative samples were analysed for key elements content and summarised in Table 5-5.

Table 5-5 Representative sample assay (dry basis)

Al (wt%)	Co (wt%)	Cu (wt%)	Others[a] (wt%)
8.65 ± 0.84	25.26 ± 0.76	9.73 ± 0.20	56.36 ± 1.27

[a]Others include non-detected elements by ICP-MS

*Standard error calculated based on 95% degree of confidence.

From Table 5-5, the average cobalt concentration in the shredded dried LIBs was found to be 25.26 wt%. The copper and aluminium current collectors were found to be 9.73 wt% and 8.65 wt% respectively. Other component such as polymeric materials, graphite and lithium can be estimated. By considering the atomic proportions of LiCoO₂ that translates 25.26 wt% cobalt would bind with 2.98 wt% lithium and 13.72 wt% oxygen, making 41.96 wt% of LiCoO₂. Thus, the amount of polymeric materials and the graphite is estimated to be 39.66 wt%.

To study the effect of pulp density in attrition scrubbing liberation, the various pulp density was subject to 20 min attrition time with LIBs to media ratio of 20 wt%. The pulp density was varied from 50 wt% to 80 wt%. Once the attrition scrubbing has commenced, the product was classified using a 38 μm sieve to produce LiCoO₂ concentrate. The results are shown in Figure 5-10.
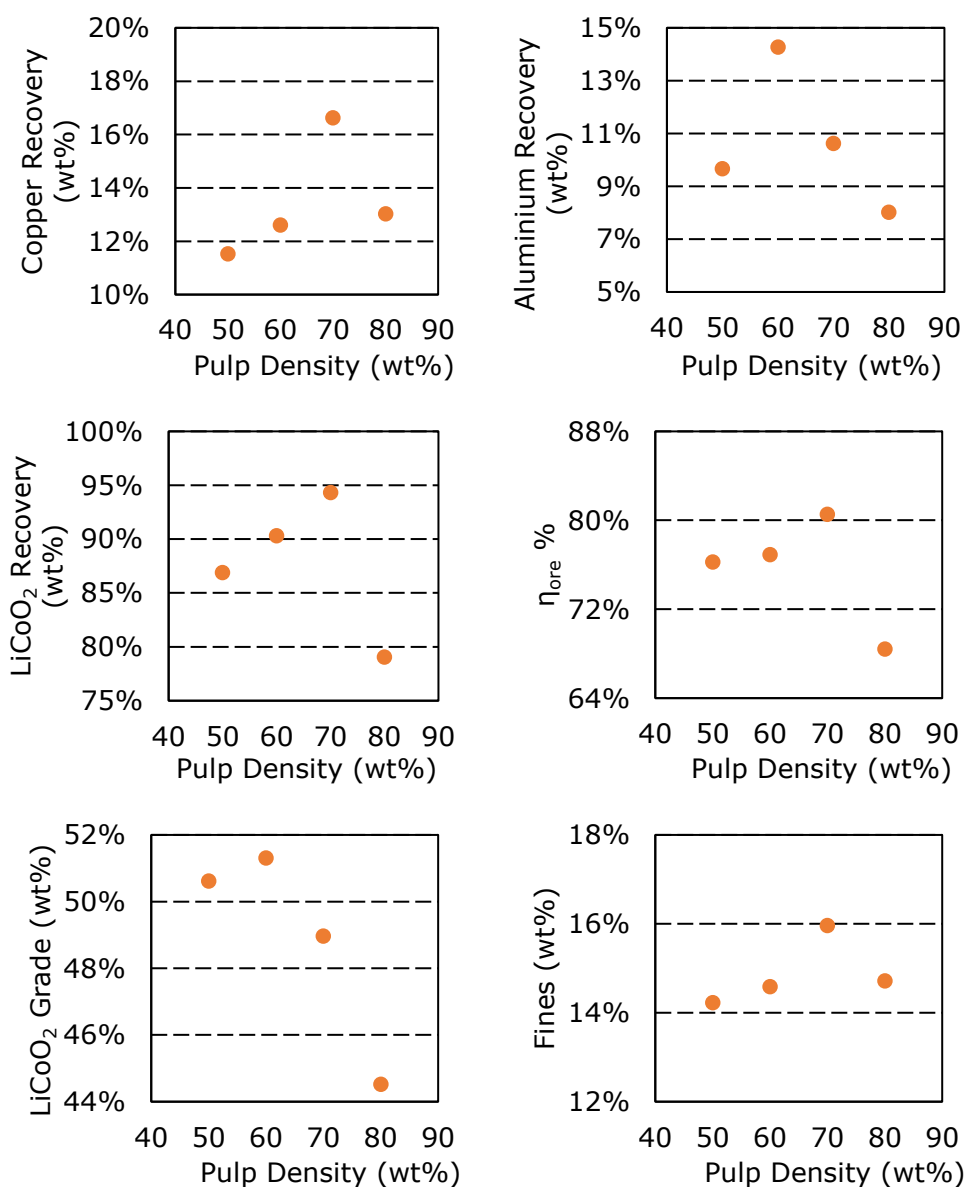
Figure 5-10 Trend in attrition product with varying pulp density.

Attrition scrubbers that are commonly used for soil remediation work with the pulp density of 70 wt%. The pulp density relates to the scrubbing efficiency directly as it directly affects the inter particle collision. From Figure 5-10, it was revealed that the fines generated are generally increase as the pulp density increase. This is caused by the increase in probability of particle colliding with each other by increasing the pulp density. Moreover, the recovery of LiCoO$_2$ increases as the pulp density increases. The increase in LiCoO$_2$ recovery also followed by an increase in copper and aluminium recovery. However, the fines

produced and the recovery of LiCoO$_2$, copper and aluminium quickly decrease as the pulp density approaching 80 wt%. This is due to the fact that a very thick pulp density causes the solids to rotate as one body with the impeller instead of bashing with each other and therefore decrease the scrubbing efficiency. The poor efficiency of 80 wt% pulp density also indicated by the sudden decrease of η_{ore} to 64.8% as well as the LiCoO$_2$ grade of 44.52 wt%.

The spent LIBs are made of malleable materials that are easily packed together. These malleable materials are easily packed inside the attrition chamber and deposited in the dead zones inside the cell. This phenomenon may cause problems in an industrial scale as attrition scrubber works in a continuous manner and the gradual growth of solids accumulation in the dead zone may potentially interlock with the impeller. One of the ways to reduce this occurrence is by employing a more dilute pulp density that would give freer path for the particles but not too dilute that it will reduce the attrition efficiency. Other than the accumulation of solids in the dead zones, a more dilute pulp density also reduces the collision between the media itself and therefore improve the grade of LiCoO$_2$ concentrate being produced. This can be seen from Figure 5-10, where the LiCoO$_2$ grades decreases as the pulp density increases due to the increase in SiO$_2$ in the concentrates. The pulp density of 60 wt% gave the best LiCoO$_2$ grade. The η_{ore} signifies the efficiency of LiCoO$_2$ recovered towards the copper and aluminium contamination with the chemically inert component of SiO$_2$ and graphite are not considered. From Figure 5-6, the maximum η_{ore} can be obtained by using 70 wt% pulp density, resulting in 80.53% efficiency. The optimum pulp density lies between 60 wt% to 70 wt%. The 60 wt% would give a better

grade of LiCoO$_2$ concentrates, whereas the 70 wt% would give a better efficiency of LiCoO$_2$ recovery towards the copper and aluminium. However, when the effect of dead zones is considered, the pulp density of 60 wt% would be a practical choice. It was also observed that 70 wt% causes particles to build up at the bottom of attrition cells that are difficult to collect.

The ratio of spent LIBs to the attrition media was varied while holding the attrition time and pulp density constant at 20 min and 60 wt% respectively. The spent LIBs to silica sand was varied from 10 wt% to 40 wt%. Once the attrition scrubbing has commenced, the product was classified using a 38 µm sieve to produce LiCoO$_2$ concentrate. The LiCoO$_2$ and graphite powder are cast on to the aluminium and copper current collector and held together by the binder. In the attrition scrubber, the silica sand induces scouring that liberate the LiCoO$_2$ and graphite powders. Once the LiCoO$_2$ and graphite particles has been liberated, the attrition media abrade the surface of copper and aluminium current collector and liberate copper and aluminium in the fine size region. The range selected for this study has been selected that which induce scrubbing action by the attrition media towards the LIBs particles and avoid LIBs particles deposits on the wall inside the attrition chamber due to low proportion of attrition media. The results are shown in Figure 5-11.
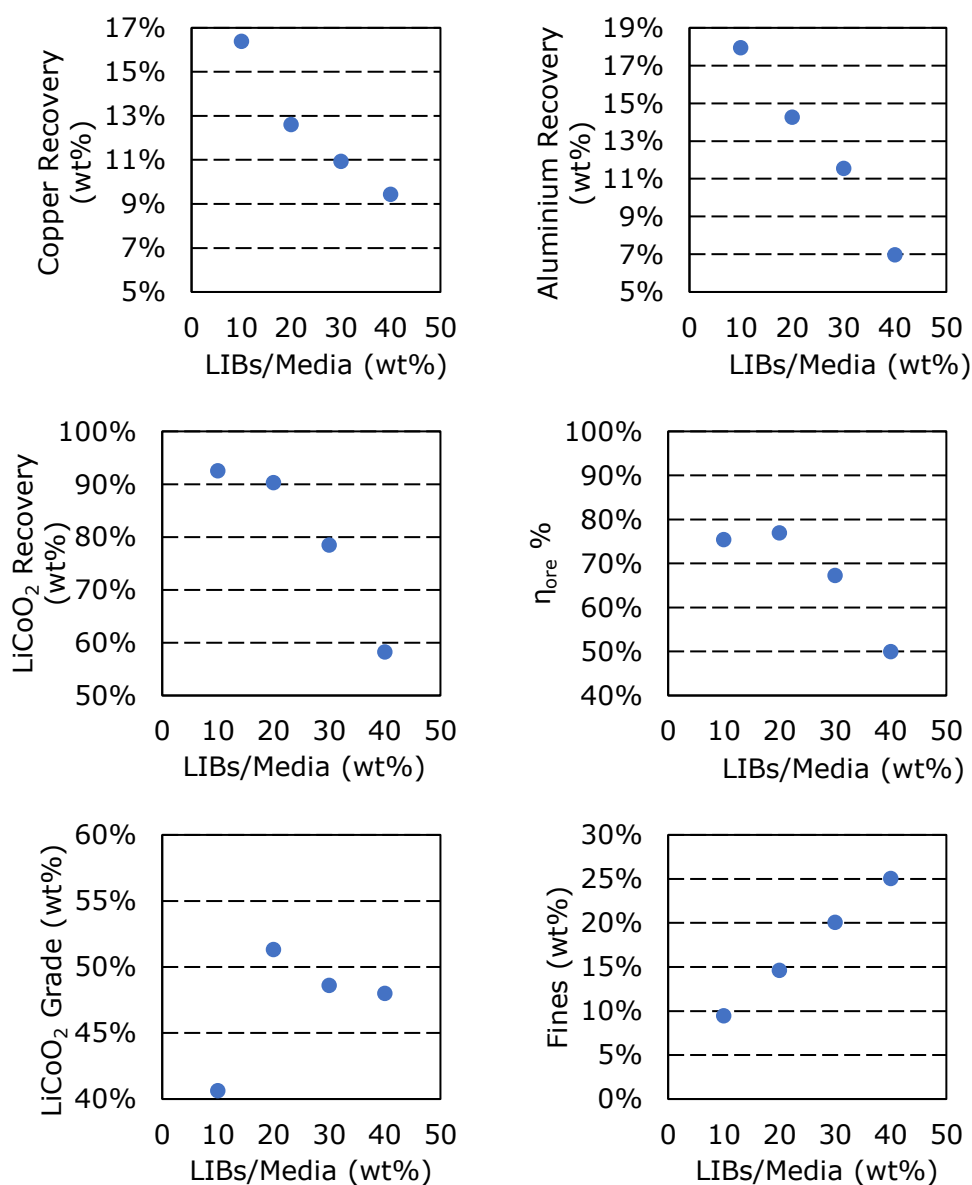
Figure 5-11 Trend in attrition product with varying LIBs to attrition media ratio

As the proportion of LIBs increases, the availability of $LiCoO_2$ and graphite powders ready to be liberated also increases. Figure 5-11 reveals that the fines < 38 μm generated as well as the $LiCoO_2$ increases as the ratio of LIBs to media increased. This indicates that attrition scrubbing is a useful technique in liberating the $LiCoO_2$ and graphite fine particles. From Figure 5-11 the $LiCoO_2$ recovery decreases substantially as the ratio of LIBs to attrition media increases. As the concentration of attrition media decreases, it also decreases the likelihood of

interaction between the attrition media. Therefore, it is expected that the mass generated due to the breakage of the attrition media is decreases as the LIBs to media ratio increases. Subsequently, the increase in fines generated together with the decrease in cobalt recovery and potentially reduction in fines generated due to the breakage of attrition media lead to the conclusion that the fines generated increase is attributed by the predominant liberation of graphite particles. This is further strengthened the argument when the decrease of LiCoO$_2$ recovery is followed by the decrease of copper and aluminium and copper recovery. This phenomenon is expected as the concentration of attrition media is decreased, it also decreases the chances of over crushing towards the aluminium and copper current collector. Moreover, it is noted that the decrease in aluminium recovery indicates that the LiCoO$_2$ are being held together by the binder and attached to the aluminium current collector. This in turn, preventing scouring of the aluminium current collector. The same reason also applies for the decrease in copper recovery. Therefore, it is imperative to consider the balance of spent LIBs and the attrition media that can give optimum throughput. From Figure 5-11, despite the decrease in copper and aluminium contamination, the η_{ore} decreases as the ratio of LIBs to the attrition media increased. This means that the decrease in LiCoO$_2$ recovery is more severe than the benefit of decrease in aluminium and copper contamination. It is favourable that a higher ratio of LIBs to attrition media is desirable as it increases the throughput of the process. Therefore, the 20 wt% of LIBs to media ratio gives a balance between the LiCoO$_2$ product grade and η_{ore} of the process.

The effect of scrubbing time was also investigated while holding the LIBs to silica sand ratio constant at 20 wt% and pulp density

of 60 wt%. Once the attrition scrubbing has commenced, the product was classified using a 38 μm sieve to produce LiCoO$_2$ concentrate. The power input to the system is directly related to the attrition time. In a real industrial situation, attrition scrubbers are connected in series to control the residence time. The results are shown in Figure 5-12.

The control for zero attrition time has been done; following screening by using sieve of nominal aperture diameter of 38 μm, it reveals that the fines produced is only 1.43 wt%. The zero-attrition time have low aluminium and copper recovery of 0.93 wt% and 3.11 wt% respectively with low LiCoO$_2$ recovery of 6.02 wt%. These recoveries then translate to η_{ore} of 3.94%. From Figure 5-12, the increase in attrition time predictably increase the fines generated and overall recovery of LiCoO$_2$ particles. The increase in recovery of LiCoO$_2$ combine with lower recovery rate of copper and aluminium over time most clearly provides the evidence that attrition scrubbing is able to selectively liberate and concentrate LiCoO$_2$ particles. It is observed that the η_{ore} increases as the attrition time increases. However, it is also observed that the slope of LiCoO$_2$ change from positive to negative at attrition time of 10 min. The change in LiCoO$_2$ grade curve indicates that the average grade of subsequent fine particles being produce contain lower LiCoO$_2$ concentration.
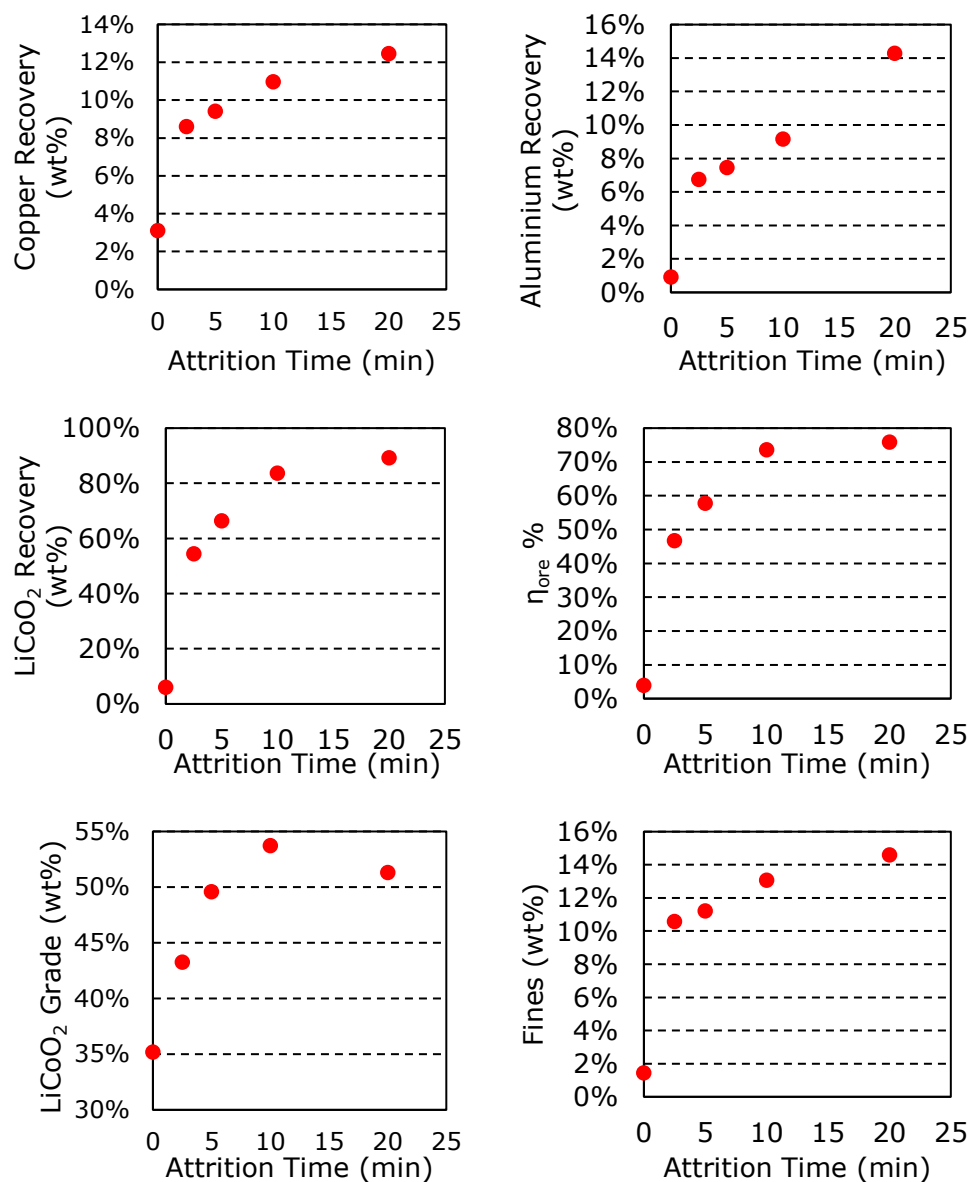
Figure 5-12 Trend in attrition product with varying attrition time

As more fine particles are liberated from the copper and aluminium current collector, the attrition media have higher probability of abrading the surface of the current collectors. From Figure 5-12, there is a substantial increase in aluminium recovery after 10 min attrition. However, such substantial increase was not observed for the copper current collector which may be attributed by the inherently stronger physical properties that cause aluminium current collector to be more readily liberated than the copper current collector. When looking at the initial stage of attrition, it can be observed that

the fines generated increases significantly from 1.43 wt% at 0 min attrition time to 10.57 wt% at 2.5 min attrition time. This indicates that the liberation of LiCoO₂ happens almost instantaneously. From Figure 5-12, the recovery of LiCoO₂ below the size of 38 µm has an increase of 48.44 wt% from time 0 min to 2.5 min. The significant increase of LiCoO₂ recovery also followed by a significant recovery of aluminium and copper recovery below the size of 38 µm by 5.83 wt% and 5.49 wt% respectively from 0 min to 2.5 min attrition time.

5.4 Conclusion

From the proof of concept with a 2.5 min attrition time, 70 wt% pulp density and 10 wt% of LIBs to silica sand shows that attrition scrubbing is a useful technique in selectively liberate and concentrate LiCoO₂ particles. The liberation of LiCoO₂ particles also followed by the liberation of graphite particles. The elemental analysis suggest that the optimum cut point that correspond to the $\eta_{ore,max}$ is 212 µm with 70.2% and 77.0% for Co-Al and Co-Cu respectively. However, the morphological observation shows that the size fraction of 212 µm – 38 µm concentrates LiCoO₂ particles that have not yet been well liberated and still held together by the binder. The size fraction of < 38 µm concentrates LiCoO₂ particles that shows no PVDF lamination. However, the use of 38 µm cut point corresponds to lower η_{ore} of 66.7 % and 74.0% for Co-Al and Co-Cu respectively. When further mechanical separation such as froth flotation is favoured, the use of 38 µm cut point may be beneficial as the graphite particles, which is hydrophobic, is the definite contamination from this liberation technique. Other contamination such as copper and aluminium are contamination the surface of the larger LiCoO₂, silica sand and graphite particles.

173

The breakage kinetics of LiCoO$_2$, copper, and aluminium has also been studied for two cut points of 2360 µm and 38 µm. The results show that the breakage rate follows the order of LiCoO$_2$>Cu>Al for both cut points. Furthermore, when comparing the two cut points, LiCoO$_2$ has substantially higher breakage kinetics than copper and aluminium towards the cut point 38 µm. This result indicates that the LiCoO$_2$ delamination and disaggregation is faster than the breakage of the copper and aluminium foil.

Parameters affecting attrition liberation have been carried out with the findings as follow:

- An extended period of scrubbing only marginally increases the recovery of LiCoO$_2$ particles. Despite the higher recover of LiCoO$_2$, the η_{ore} slowly decreases indicating that more copper and aluminium also recovered in the size region of < 38 µm.

- Pulp density also plays a crucial role in the efficiency of LiCoO$_2$ recovery. From the analysis, it reveals that a range between 60 wt% to 70 wt% is the optimum values. Beyond this range, poor attrition occurs and the recovery of LiCoO$_2$ decreases together with its efficiency.

- Additionally, the ratio between spent LIBs to the attrition media correlates with the recovery of LiCoO$_2$ particles. Increasing the proportion of spent LIBs to attrition media results in a decrease in copper and aluminium contamination. The decrease in copper and aluminium contamination also followed by a decrease of LiCoO$_2$ recovery. The ratio of 20 wt% spent LIBs to media was found to be the most optimum value that maximises the throughput of attrition liberation as well as the separation efficiency.

Chapter 6 Attrition Product Separation: A proof of concept

6.1 Introduction

In the previous chapter, attrition scrubbing allows the delamination and disaggregation of spent LIBs active materials. The well liberated active materials are concentrated in the size fraction of < 38 µm. Whereas, the size fraction of > 38 µm comprises of mainly silica sand and other components from spent LIBs (aluminium, copper, and polymer). This chapter aims at recovering copper and aluminium from the size fraction of > 38 µm and further concentration of $LiCoO_2$ in the size fraction of < 38 µm.

In the larger size fraction of > 38 µm, different surface properties exist particularly differences in conductivity. Components for instance copper and aluminium are more conductive compared to the polymeric materials as well as the silica sand attrition media. The use of electrostatic separator after shredding and size based separation to recover copper and aluminium has been shown by Silveira et al. (2017) to be a viable option. The $LiCoO_2$ and graphite particles are recovered in the fine size fraction < 212 µm. However, the recovery rate of $LiCoO_2$ and graphite was not discussed and is suspected to be low due to the sub optimum liberation (i.e $LiCoO_2$ lamination in the larger size fraction). Hence, the use of electrostatic separator can be better applied in this case as the copper and aluminium are clean from the active materials after attrition.

Also, for the well liberated LiCoO$_2$ particles in the size range of < 38 µm, a difference in surface properties exists in the form of hydrophobicity. Graphite particles are hydrophobic, whereas the other components such as silica sand, LiCoO$_2$, copper and aluminium are hydrophilic. Therefore, froth flotation could be used to float the graphite particles.

6.2 Experimental details

6.2.1 Electrostatic separation

A roll-type electrostatic separator shown in Figure 6-1 (Carpco, HT (15,25,36)) was used to separate the attrition products > 38 µm. The size of the static electrode is 71.5 cm X 12.5 cm X 5 cm (length x width x height), ionization electrode is a 0.010 mm wire of 10 cm in length, and roll radius of 12.7 cm. The electrostatic separator comprises of two main components which are the beam and static electrode. The ionizing electrode pinned nonconductive materials on to the roll and collected at the end of the roll by a static brush. For the particles that are heavier than the pinning force are collected as middlings. The static electrode attracts conductive materials while leaving the non-conductive to fall through the roll and collected. Considering the composition of the sample, both electrodes were used to separate the sample into three different fractions. Such that the polymeric separator and fine silica sand would be pinned on to the roll and collected on the left hand side receptacle, the voltage is adjusted so that the silica sand > 850 µm would not be pinned as strongly as the polymeric separator and collected as middling, and the conductive materials are thrown into the right side receptacle.

Figure 6-1 Photograph of Carpco-HT (15,25,36).

Silveira et al. (2017) demonstrated that the combination of size-based separation and electrostatic separations in electro-dynamic mode allows the separation of milled LIBs components into four different product class of active materials powder, polymers, mixture (polymers and metal), and the metallic fractions. The feeder was maintained at a constant value of 30% of its maximum vibration. The best-operating conditions for the roll-type electrostatic separation are reported to be a rotation speed of 20 rpm, electrode voltage of 25 kV, electrode distance of 6 cm, ionisation and electrostatic angle of 25° and 75° respectively (Silveira et al., 2017). The reported parameters were initially used as a starting point and adjusted accordingly based on the visual inspection of the separated products.

177

6.2.2 Froth flotation

Figure 6-2 Photograph of Denver D-12 self-aspirating flotation machine.

Self-aspirating Denver D-12 flotation machine with 5L cell is used to carry out the flotation test (Figure 6-2). The sample used was produced by combining the attrition products in the size range of < 38 µm from different parameters.

In the previously reported methodology, frother and collector are often used to float the graphite particles. The frother used was methyl-isobutyl-carbinol (MIBC). Whereas, the collector used can be either be n-dodecane or kerosene (Zhan et al., 2018, Zhang et al., 2019). However, before froth flotation is used in the waste LIBs research, the separation of graphite from hydrophilic minerals can be done without collector (Lu and Forssberg, 2001). Thus, the aim of the flotation test is to show that collector-less flotation technique is a useful technique in separating graphite from other components.

To carry out the flotation test, a relatively dilute pulp of < 1wt% (20 g of dry powder) is used in this flotation test. Prior adding

collector and frother, the pH is adjusted to 8. This is done to ensure suitable working condition for the MIBC frother that is between pH 8 to pH 10 (Cleanese, 2016). The required dosage of collector and frother is then added by using hypodermic syringe. The Denver-D12 machine used in this study is self-aspirating by adjusting the ball valve as shown in Figure 6-2. The valve opening has been marked from 0% to 100% opening with 25% intervals. By controlling the valve that translates to the air flowrate, it can then be used to control the froth height. The 5 L flotation cell has been calibrated for froth height as shown in Figure 6-2. The froth height is defined as the distance between the lip to the live volume of the liquid while the impeller is rotating. In this study, the froth height used is 4 cm (adapted from Zhan et al. (2018)). The froth is collected by using a poly propylene scraper and only the very fine top layer of the froth is collected. The flotation is carried out for 5 min and the froth is collected every 30 seconds.

Once the experiment has been carried out, the float and sink are dried in a box oven at constant temperature of 80°C. The products are dried until constant weight and elemental analysis and morphological analysis were carried out.

6.3 Results and discussion

6.3.1 The separation of attrition coarse size fraction by using electrostatic separation
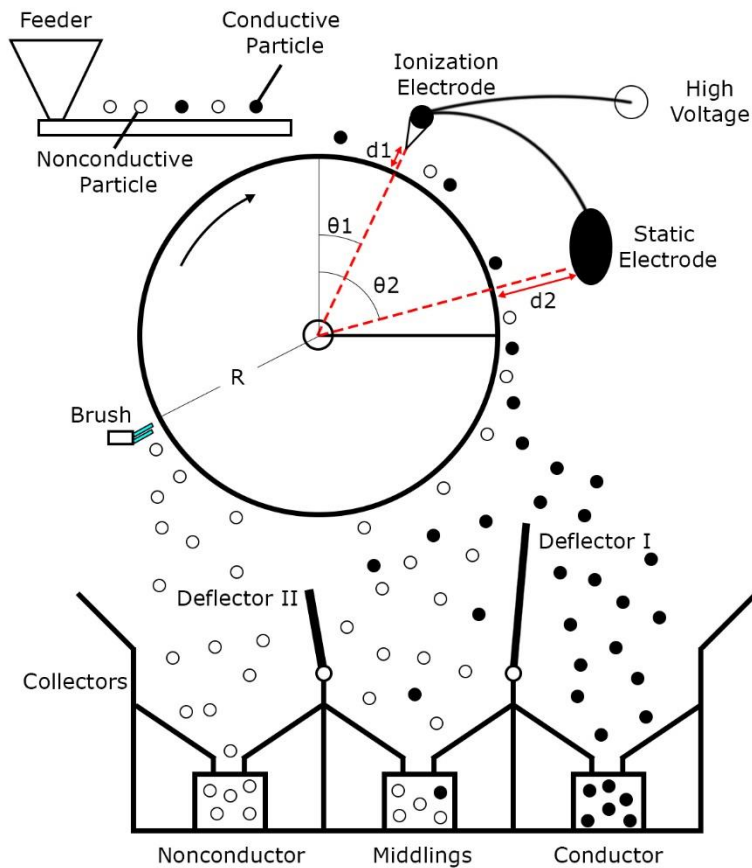
Figure 6-3 Schematic diagram of Carpco-HT (15,25,36).

The majority of the $LiCoO_2$ particles are concentrated in the size fraction of less than 38 µm. The size fraction > 38 then concentrates the copper and aluminium current collectors. The > 38 µm sample obtained then subject to the electrostatic separation to separate polymer, silica sand and the current collector. A roll-type electrostatic separator (Carpco, HT (15,25,36)) was used in this study. The schematic diagram of the Carpco-HT (15,25,36) is presented in Figure 6-3.

Table 6-1 Parameters set for the electrostatic separator

Parameters	(Silveira et al., 2017)	Adjusted Value
Roll Speed (RPM)	20	50
Electrode Voltage (kV)	25	20
d1-Ionization Electrode Distance (cm)	6	5
d2-Static Electrode Distance (cm)	6	8
Deflector I Angle (°)	0	50
Deflector II Angle (°)	N/A	35

The optimum conditions reported by Silveira et al. (2017) were initially used and need to be adjusted for a workable parameter. The particles were flowing unevenly and arching between the electrodes towards copper and aluminium foils was observed. Moreover, that the silica sand with particle size of > 850 μm was strongly pinned onto the roll and can be found in the non-conductor fraction. To overcome these issues, adjustment trial and error based on visual inspection was carried out to adjust the parameters and minimise these issues. The key parameters of the electrostatic separator are shown in Table 6-1.

The deflector angle I and II were kept constant at 50° and 35° respectively. The roll speed was initially 20 rpm and adjusted to 50 rpm to make the particle flows evenly. After adjusting the roll speed, the arching from the ionization electrodes to the copper and aluminium foils are still observed, the electrode voltage is then reduced from 25kV to 20kV. The decrease in electrode voltage also causes the larger silica sand > 850 μm to be less strongly pinned on to the roll and less lifting action for the copper and aluminium foils. This then result in LIB

separator found as middling and copper and aluminium foils were observed to falls together with the silica sand. The ionization electrode is then moved closer to the roll from 6 cm to 5 cm and cause more separator pinned onto the roll. However, visual inspection reveals that the copper and aluminium foil is visually flowing together with the silica sand. The distance between the ionisation electrode and the feeder (θ_1) was adjusted from 25° to 35°. This is done to extend the charging time for the particles to acquire charge. However, keeping the distance between the two electrodes constant seems to do not allow enough residence time for the copper and aluminium foils to undergoes charge reversal that is sufficient to lift the particles. The distance between the two electrodes was made narrower and adjusted from 50° to 40° (from θ_2=75° to θ_2=65°). After adjusting the ionizing and static electrode angle, the copper and aluminium is lifted and hitting the static electrode. Therefore, the static electrode (lifting electrode) is moved further from the roll to minimise the electrode getting hit by the copper and aluminium foils.

In a one-pass electrostatic separation, only copper and aluminium foils are registered as a conductive fraction. However, it was observed that the middling fraction still contains a substantial amount of conducting materials and therefore the middling fraction was re-introduced into the feeder. The middling was re-introduced to the feeder five times. To assess the grade of the resulting separation, manual picking was carried out. The resulting separated products are shown in Figure 6-4. The conductive fractions obtained (Figure 6-4 C) were of 97.65 wt% metal, the impurities came from the short-circuiting of the silica sand from the middling. The middling obtained (Figure 6-4 B) contain 99.01 wt% silica sand with

small impurities from the copper and aluminium current collector. The nonconductive (Figure 6-4 A) obtained contains 95 v% (14.87 wt%) battery separator, with the main contamination from the fine (< 850 μm) silica sand.

Figure 6-4 Photograph of the electrostatic separation products; A: non-conductor, B: middling, C: conductor.

Sieving with nominal aperture diameter of 850 μm was carried out for non-conducting materials and the middling fraction. It was found that the attrition media that has undergone size reduction < 850 μm is registered as non-conductive and collected with the polymeric media on the left-hand side. The middling fraction recovers the attrition media > 850 μm. This indicates that the electrostatic separation also allows material being differentiated based on size.

The results from this exploratory study suggest that the electrostatic separation is a useful technique in separating current collectors and polymeric material from the attrition media. Hence, the copper and aluminium can be further processes, while the attrition media can be re-used.

Difference in conductivity also exists in the fine size region of < 38 μm. Where, graphite is conductive and $LiCoO_2$ is not conductive. It is expected that the graphite would be thrown and collected as conductor, while the $LiCoO_2$ and silica sand particles would be pinned and collected as non-conductor. From the trial, the use of electrostatic separator for the separation of fine fractions cause severe dusting. For this reason, the experiment was then terminated for safety reason.

6.3.2 The separation of attrition product fine size fraction by using froth flotation

The flotation test was carried out as a single stage. An impeller speed of 1500 rpm is used to recover almost all the graphite particles. For the proof of concept, 20.0 g of < 38 µm sample with the combination of 20 µl of n-dodecane as collector, 40 µl MIBC as frother, and pH of 8 (adjusted by using 2M NaOH) are used for the single stage flotation. The froth height is maintained at 4 cm by adjusting the aeration valve and periodically adding top-up water. The flotation is carried out for 5 minutes and the froth is collected every 30 seconds by using a polypropylene scraper. The float and sink products then analysed for elemental content and the recovery is presented in Table 6-2.

Table 6-2 The recovery rate from the single stage flotation with collector.

Recovery Rate (wt%)				
Component	Mass	$LiCoO_2$	Cu	Al
Float	41.4	29.3	39.0	31.5
Sink	58.6	70.7	61.0	68.5

From Table 6-2, it is shown that the $LiCoO_2$ particles are predominantly found in the sink. The result indicates that froth flotation is a useful technique in recovering the graphite particles. Moreover, it is suspected that the entrainment in the float is caused by the short circuit of $LiCoO_2$, Cu, and Al fine particles.
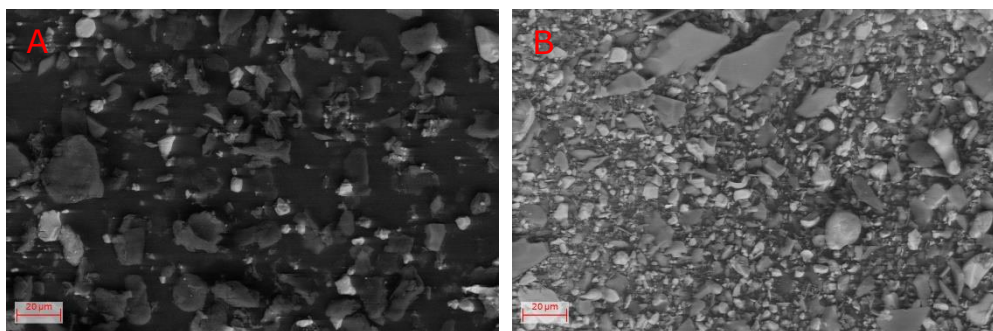
Figure 6-5 Morphology analysis of first stage froth flotation float and sink with collector; A-Float and B-Sink.

From Figure 6-5 B, the graphite particles are found to be minimum in the sink. Most of the graphite have been floated and concentrates in the float. However, the recovery of graphite as float also followed by the entrainment of fine $LiCoO_2$ particles (Figure 6-5 A).

It has been known that graphite is naturally hydrophobic. Whereas, other components such as $LiCoO_2$, silica sand, copper and aluminium are hydrophilic. It has been reported that the flotation of graphite from hydrophilic particles can be achieved by only using MIBC frother. Therefore, flotation test without collector with the same parameters was then carried out. In the case of flotation without collector, it was found that 100 µl of MIBC is needed to produce 4 cm of stable froth. The amount of MIBC needed in the flotation without collector is 2.5 times higher. This indicates that the presence of n-dodecane collector also contributes to the formation of froth. Moreover, the higher amount of MIBC collector may also results in higher water recovery in the froth during flotation and the entrainment of $LiCoO_2$ particles in the froth is still expected.

Table 6-3 The recovery rate from the single stage flotation without collector.

Recovery Rate (wt%)				
Component	Mass	$LiCoO_2$	Cu	Al
Float	42.6	33.2	37.1	33.2
Sink	57.4	66.8	62.9	66.8

From Table 6-3, it can be understood that the $LiCoO_2$ particles are predominantly found in the sink. Similarly, the froth flotation also entrains some of the copper and aluminium fine particles that are also collected as float. Morphology analysis then carried out to assess the graphite contamination in the sink.
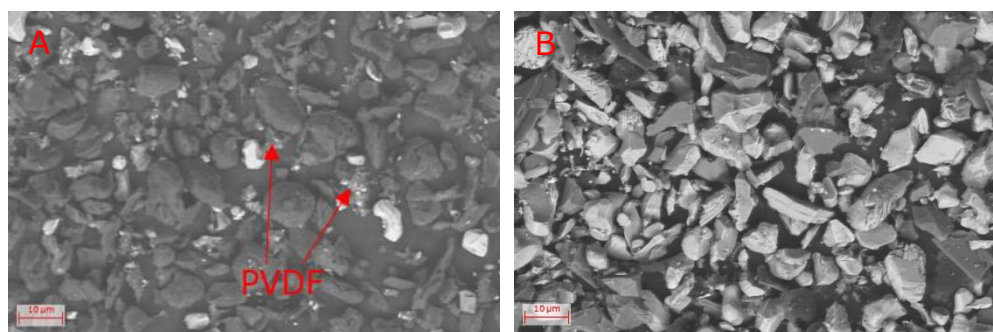
Figure 6-6 Morphology analysis of first stage froth flotation float and sink without collector; A-Float and B-Sink.

From Figure 6-6, similar observation from the 1st stage flotation with collector, it can be seen that there is minimum to no graphite in the sink. Other than the $LiCoO_2$ and graphite particles, the flotation with and without collector also concentrates PVDF binder in the float. However, flotation without collector entrains more $LiCoO_2$ particles onto the float. A 3.9 wt% higher recovery rate of cobalt in the float was observed.

The 2nd stage flotation is carried out with a lower impeller speed to re-float the float to recover more cobalt. The impeller speed was set to 1000 rpm. The rationale behind the lower impeller

speed is to float easily floatable materials. The flotation is carried out at pH 8 and froth height of 4 cm. It was found that an additional 80 µl MIBC is required to compensate the lower aeration rate (lower impeller speed). The results are presented in Table 6-4.

Table 6-4 The recovery rate from the second stage flotation without collector.

Recovery Rate (wt%)				
Component	Mass	$LiCoO_2$	Cu	Al
Float	82.4	72.8	78.2	84.0
Sink	17.6	27.2	21.8	16.0

Despite the reduction in impeller speed, the results presented in Table 6-4 shows that the majority of the particles are collected as float. The increase in the float mass recovery also followed by the increase in cobalt recovery as float. This phenomenon indicates that there is minimum selectivity for cobalt being concentrated in the sink.

6.4 Conclusion

The preliminary study presented in this chapter, electrostatic separator and froth flotation have been shown to be a useful technique in separating different components from the attrition products.

The use of electrostatic separator is beneficial for the coarser size fraction with the main target of recovering copper and aluminium current collector. The use of electrostatic separation technique in recovering graphite particles in the fine size region is promising in concept. In practice, due to the dusting problem, this technique is not recommended for the separation of fine particles product.

The use of froth flotation is more suitable to further process the attrition fine particles product. Initially, flotation test with n-dodecane collector and MIBC frother was carried out. From the single stage flotation test, it was found that almost all of the graphite particles were collected as float followed by entrainment of $LiCoO_2$ particles. Furthermore, the use of collector less flotation has also been shown to be able to take the advantage of the natural hydrophobicity of the graphite particles. However, from the single stage collector less flotation, more $LiCoO_2$ particles are entrained as float and results in 3.9 wt% higher cobalt recovery rate in the float. A second stage collector less flotation was then carried out to further concentrate the float from the first stage collector less flotation. The results from the second stage collector less flotation indicates minimum selectivity. The use of collector less flotation requires further attention and subject to the future works of this project.

188

Chapter 7 Conclusion and Future Work

7.1 Conclusion

The objective of this research was to investigate the selective liberation occurrence in the comminution of spent LIBs and the way to improve it. The approach of this study involves the application of mineral processing techniques in selectively concentrating $LiCoO_2$ particles. The following conclusion can be drawn from the investigation:

7.1.1 Selective liberation in cutting mill

- Characterisation of milled spent and new LIBs by using Fuerstenau recovery curve was carried out and found that the comminution of LIBs is of a selective phenomenon with optimum cut point of 850 µm.

- The comparison between new and spent LIBs was made with a distinct difference observed for the selective liberation of copper towards cobalt and aluminium. Better separation efficiency of $LiCoO_2$ particles is observed in the selective liberation of new LIBs. The better physical properties of current collectors and the adhesiveness of the binder in the new LIBs have made the finer size region to be less contaminated by the copper and aluminium. The stronger PVDF binder in new LIBs also helps in preventing the breakage of copper current collector. Whereas, the better mechanical properties of copper and aluminium in new LIBs helps prevent the breakage of current collectors that contaminates the fine size region (< 850 µm).

- Morphology analysis reveals that the initially liberated LIBs particles can be characterized into four different types:
  - Category 1: Particles that have experience reduction in size and accompanied by partial detachment of its active materials such as particles in the range of > 2360 μm.
  - Category 2: Include the particles that have a reduction in size with active materials lamination, such as in the range of 2360 μm – 850 μm. (Only true for positive electrode)
  - Category 3: Active materials laminate that have been detached from its current collector and still held together by the binder. This type of particles comes as aggregated for the particle size of 850 μm – 38 μm.
  - Category 4: Active materials laminate that have been detached from current collector and accompanied with minimum aggregation for the particle size of < 38 μm.
- During milling, two possible outcomes may arise. Either $LiCoO_2$ particles are dislodged and released in the form of $LiCoO_2$-PVDF aggregates that are concentrated in the size fraction of < 850 μm or size reduction occurs while maintaining its attachment to the current collector. However, the size of the $LiCoO_2$-PVDF aggregates that are dislodged is still far from the actual size of $LiCoO_2$ particles as found in spent LIBs. Therefore, the optimum cut point proposed (850 μm) is much greater than the actual size of $LiCoO_2$ particles found in spent LIBs (ca. 1.50 μm – 7.80 μm (Pavoni et al., 2018)).

- In the size fraction of <850 µm, the recovery rate for spent LIBs is 43.7 wt% of $LiCoO_2$ with a minimum recovery of aluminium and copper (8.8 wt% and 10.3 wt%) from the feed. However, more than 50 wt% of $LiCoO_2$ is found in the size region of >850 µm, and it contains a substantial amount of aluminium and copper (91.2 wt% and 89.7 wt%) from the feed and are not suitable to be treated with leaching. Thus, it is understood that the selective liberation by using only a cutting mill is sub-optimum.

7.1.2 Selective liberation by using attrition scrubbing

- Attrition scrubbing is then proposed as a second stage of liberation with low iron silica sand as the attrition media. The induced impact and shearing actions effectively liberates and concentrates $LiCoO_2$ in the finer size region.

- From the proof of concept, $LiCoO_2$ particles that were initially laminating the aluminium current collector or found as aggregates following initial size reduction have been liberated and disaggregated and concentrated in the size fraction < 38 µm.

- Two cut points of 2360 µm and 38 µm were selected. The cut points selected in order to study the different breakage rate for delamination (2360 µm) and disaggregation (38 µm) of $LiCoO_2$ particles. The breakage kinetics of $LiCoO_2$ particles for cut point 2360 µm is faster than that of cut point 38 µm. This indicates the delamination is faster than the disaggregation of $LiCoO_2$ particles. Moreover, the results show that the breakage rate follows the order of $LiCoO_2$>Cu>Al for both cut points. This result indicates that the $LiCoO_2$ delamination and disaggregation is faster than the breakage of the copper

and aluminium foil. This then results in 89.8 wt% $LiCoO_2$ recovery with minimum 9.0 wt% aluminium and 11.2 wt% copper recovery within 20 min attrition time.

- Parameters affecting attrition liberation have been carried out with the findings as follow:
  - o An extended period of scrubbing only marginally increases the recovery of $LiCoO_2$ particles. Despite the higher recover of $LiCoO_2$, the η_{ore} slowly decreases indicating that more copper and aluminium also recovered in the size region of < 38 µm.
  - o Pulp density also plays a crucial role in the efficiency of $LiCoO_2$ recovery. From the analysis, it reveals that a range between 60 wt% to 70 wt% is the optimum values. Beyond this range, poor attrition occurs and the recovery of $LiCoO_2$ decreases together with its efficiency.
  - o Additionally, the ratio between spent LIBs to the attrition media correlates with the recovery of $LiCoO_2$ particles. Increasing the proportion of spent LIBs to attrition media results in a decrease in copper and aluminium contamination. The decrease in copper and aluminium contamination also followed by a decrease of $LiCoO_2$ recovery. The ratio of 20 wt% spent LIBs to media was found to be the optimum value that maximises the throughput of attrition liberation as well as the separation efficiency.

7.1.3 The application of electrostatic separator and froth flotation

- The attrition product above 38 μm cut point can be separated by using electrostatic separation in electrodynamic mode. Three main products of conductors (copper and aluminium), middling (silica sand), and non-conductor (separator and fine silica sand) can be obtained. This demonstrate that the copper and aluminium can potentially be recycled, and the attrition media can be re-used.

- The attrition product below 38 μm cut point were subject to flotation test with n-dodecane collector and MIBC frother. Almost all the graphite particles were floated. However, the fine $LiCoO_2$ particles were also substantially entrained. Moreover, the silica sand particles do not seems to get entrained.

- The flotation test without using collector have also been carried out. Similar to the flotation with collector, almost all the graphite particles were floated with substantial entrainment of $LiCoO_2$ particles and minimum entrainment from silica sand.

- Considering the size of the size of $LiCoO_2$ particles that are less than 10 μm, it may be beneficial to carryout leaching prior flotation. Hence, clean graphite can be obtained and potentially recycled.

7.2 Contribution to knowledge

This thesis contributes to the knowledge in that:

- A comprehensive literature survey of mechanical liberation and separation for LIBs recycling and how minerals processing technique have been extensively adapted to this field.
- A further understanding towards the sub-optimum selective liberation of $LiCoO_2$ particles in a cutting mill that results in different particle morphologies.
- An insight into the difference in selective liberation performance for the milled new and spent LIBs has been given by plotting Fuerstenau recovery curve and ore separation degree curve.
- Attrition scrubbing have been identified to be a suitable technique in selectively liberate $LiCoO_2$ particles with minimum copper and aluminium breakage in the finer size region. The parameters affecting attrition scrubbing liberation were explored.
- The proof of concept for the recovery of copper and aluminium for the size fraction > 38 µm and the recovery of graphite from the size fraction < 38 µm have been proposed.

7.3 Further work

This section gives recommendation for future research in order to further advance the present research.

7.3.1 Different battery types

- The study only considers the prismatic battery. However, other batteries geometry such as cylindrical or coin may potentially result in different particle size distribution. One of the potential reasons being the different types of chassis where prismatic use polymer type while cylindrical and coin cells may use steel chassis that may impose different overall milling condition.

- Other than different battery geometry, this research only dealt with LIB with PVDF binder that is hydrophobic. The use of hydrophilic SBR-CMC binder for the graphite active materials are gaining popularities that may render the graphite hydrophilic when it is not removed. Thus, the ability of attrition scrubbing to remove SBR-CMC coating on the graphite particles may be considered for future studies.

7.3.2 Pilot scale trial

- This research only demonstrates the selective liberation of $LiCoO_2$ particles in a lab scale and have not yet been tested in a pilot scale. The scaling up of attrition scrubbing is important as the wall effect in lab scale is not the same as in the pilot scale.

7.3.3 Electrolytes recovery

- This research has not recovered the organic electrolytes such as ethylene carbonates, dimethyl carbonate, and

other electrolytes. Further works should include consideration to recover the evaporated electrolytes.

- The $LiPF_6$ salt that dissolve in the electrolytes may potentially cause harm in an industrial scale as there is the chance of HF formation. This research has been carried out in the safe temperature range to prevent such occurrence. However, it requires further attention to provide multiple layers of protections as to prevent the release of HF.

7.3.4 Separation of $LiCoO_2$ from SiO_2

- The separation of $LiCoO_2$ from SiO_2 have not been carried out in this project. One of the possible methods is by using sodium polytungstate (SPT) as the medium, with specific gravity of 2.8. This allow the SiO_2 to float while the $LiCoO_2$ to sink.

Bibliography

AESAR, A. 2012a. Safety Data Sheet. *Carbon black, acetylene, 100% compressed.* Thermo Fisher Scientific Chemical, Inc.

AESAR, A. 2012b. Safety Data Sheet. *Aluminum Foil.* Thermo Fisher Scientific Chemical, Inc.

AESAR, A. 2012c. Safety Data Sheet. *Copper Foil.* Thermo Fisher Scientific Chemical, Inc.

AESAR, A. 2012d. Safety Data Sheet. *Polyethylene Sheet.* Thermo Fisher Scientific Chemical, Inc.

AL-THYABAT, S., NAKAMURA, T., SHIBATA, E. & IIZUKA, A. 2013. Adaptation of minerals processing operations for lithium-ion (LiBs) and nickel metal hydride (NiMH) batteries recycling: Critical review. *Minerals Engineering,* 45**,** 4-17.

AN, S. J., LI, J., DANIEL, C. & WOOD, D. L. 2019. Effects of Ultraviolet Light Treatment in Ambient Air on Lithium-Ion Battery Graphite and PVDF Binder. *Journal of The Electrochemical Society,* 166**,** A1121-A1126.

ARORA, P. & WHITE, R. E. 1998. Capacity Fade Mechanisms and Side Reactions in Lithium-Ion Batteries. *Journal of The Electrochemical Society,* 145**,** 3647-3667.

AURBACH, D., MARKOVSKY, B., WEISSMAN, I., LEVI, E. & EIN-ELI, Y. 1999. On the correlation between surface chemistry and performance of graphite negative electrodes for Li ion batteries. *Electrochimica acta,* 45**,** 67-86.

BAHALOO-HOREH, N. & MOUSAVI, S. M. 2017. Enhanced recovery of valuable metals from spent lithium-ion batteries through optimization of organic acids produced by Aspergillus niger. *Waste Manag,* 60**,** 666-679.

BALÁŽ, P., ACHIMOVIČOVÁ, M., BALÁŽ, M., BILLIK, P., CHERKEZOVA-ZHELEVA, Z., CRIADO, J. M., DELOGU, F., DUTKOVÁ, E., GAFFET, E. & GOTOR, F. J. 2013. Hallmarks of mechanochemistry: from nanoparticles to technology. *Chemical Society Reviews,* 42**,** 7571-7637.

BARBIERI, E. M. S., LIMA, E. P. C., CANTARINO, S. J., LELIS, M. F. F. & FREITAS, M. B. J. G. 2014a. Recycling of spent ion-lithium batteries as cobalt hydroxide, and cobalt oxide films formed under a conductive glass substrate, and their electrochemical properties. *Journal of Power Sources,* 269**,** 158-163.

BARBIERI, E. M. S., LIMA, E. P. C., LELIS, M. F. F. & FREITAS, M. B. J. G. 2014b. Recycling of cobalt from spent Li-ion batteries as β-Co(OH) 2 and the application of Co 3 O 4 as a pseudocapacitor. *Journal of Power Sources,* 270**,** 158-165.

BARIK, S. P., PRABAHARAN, G. & KUMAR, L. 2017. Leaching and separation of Co and Mn from electrode materials of spent lithium-ion batteries using hydrochloric acid: Laboratory and pilot scale study. *Journal of Cleaner Production,* 147**,** 37-43.

BAYLEY, R. W. & BIGGS, C. A. 2005. Characterisation of an attrition scrubber for the removal of high molecular weight contaminants in sand. *Chemical Engineering Journal,* 111**,** 71-79.

BEAULIEU, L., EBERMAN, K., TURNER, R., KRAUSE, L. & DAHN, J. 2001. Colossal reversible volume changes in lithium alloys. *Electrochemical and Solid-State Letters,* 4**,** A137-A140.

BERTUOL, D. A., TONIASSO, C., JIMÉNEZ, B. M., MEILI, L., DOTTO, G. L., TANABE, E. H. & AGUIAR, M. L. 2015. Application of spouted bed elutriation in the recycling of lithium ion batteries. *Journal of Power Sources,* 275**,** 627-632.

BLOMGREN, G. E. 2017. The Development and Future of Lithium Ion Batteries. *Journal of The Electrochemical Society,* 164**,** A5019-A5025.

BRAITHWAITE, J. W., GONZALES, A., NAGASUBRAMANIAN, G., LUCERO, S. J., PEEBLES, D. E., OHLHAUSEN, J. A. & CIESLAK, W. R. 1999. Corrosion of lithium‐ion battery current collectors. *Journal of the electrochemical society,* 146**,** 448-456.

BRITISH_STANDARD_INSTITUTION 1986. Determination of particle size distribution. *Part 1: Guide to powder sampling.* BSI Standard Publication.

BRITISH_STANDARD_INSTITUTION 1990. BS 812-109: 1990 Testing aggregates. *Part 109: Methods for determination of moisture content.*

BRITISH_STANDARD_INSTITUTION 1995. BS EN ISO 3696:1995 Water for analytical laboratory use. *Specification and test methods.*

BRITISH_STANDARD_INSTITUTION 2012. BS EN 933-1 : 2012 Tests for geometrical properties of aggregates. *Part 1: Determination of particle size distribution — Sieving method.*

BRITISH_STANDARD_INSTITUTION 2013. BS ISO 3310-2:2013 Test sieves-Technical requirements and testing *Part 2: Test sieves of perforated metal plate.*

BRITISH_STANDARD_INSTITUTION 2014. BS EN 62321-5:2014 Determination of certain substances in electrotechnical products. *Part 5: Cadmium, lead and chromium in polymers and electronics and cadmium and lead in metals by AAS, AFS, ICP-OES and ICP-MS.* BSI Standard Publication.

BRITISH_STANDARD_INSTITUTION 2016. BS ISO 3310-1:2016 Test sieves -Technical requirements and testing *Part 1: Test sieves of metal wire cloth.*

BRITISH_STANDARD_INSTITUTION 2017. BS EN 61960-3:2017 Secondary cells and batteries containing alkaline or other non-acid electrolytes - Secondary lithium cells and batteries for portable applications. *Part 3: Prismatic and cylindrical lithium secondary cells, and batteries made from them (IEC 61960-3:2017).* BSI Standard Publication.

BUTT, J., MEBRAHTU, H. & SHIRVANI, H. 2016. Microstructure and mechanical properties of dissimilar pure copper foil/1050 aluminium composites made with composite metal foil manufacturing. *Journal of Materials Processing Technology,* 238**,** 96-107.

CASTILLO, S., ANSART, F., LABERTY-ROBERT, C. & PORTAL, J. 2002. Advances in the recovering of spent lithium battery compounds. *Journal of Power Sources,* 112**,** 247-254.

CERRUTI, C., CURUTCHET, G. & DONATI, E. 1998. Bio-dissolution of spent nickel–cadmium batteries using Thiobacillus ferrooxidans. *Journal of Biotechnology,* 62**,** 209-219.

CHEN, J., LI, Q., SONG, J., SONG, D., ZHANG, L. & SHI, X. 2016a. Environmentally friendly recycling and effective repairing of cathode powders from spent LiFePO4 batteries. *Green Chemistry,* 18**,** 2500-2506.

CHEN, J., LIU, J., QI, Y., SUN, T. & LI, X. 2013. Unveiling the roles of binder in the mechanical integrity of electrodes

for lithium-ion batteries. *Journal of The Electrochemical Society,* 160**,** A1502-A1509.

CHEN, J., YAN, Y., SUN, T., QI, Y. & LI, X. 2014. Deformation and fracture behaviors of microporous polymer separators for lithium ion batteries. *Rsc Advances,* 4**,** 14904-14914.

CHEN, L., TANG, X., ZHANG, Y., LI, L., ZENG, Z. & ZHANG, Y. 2011. Process for the recovery of cobalt oxalate from spent lithium-ion batteries. *Hydrometallurgy,* 108**,** 80-86.

CHEN, S., HE, T., LU, Y., SU, Y., TIAN, J., LI, N., CHEN, G., BAO, L. & WU, F. 2016b. Renovation of LiCoO 2 with outstanding cycling stability by thermal treatment with Li 2 CO 3 from spent Li-ion batteries. *Journal of Energy Storage,* 8**,** 262-273.

CHEN, X., CHEN, Y., ZHOU, T., LIU, D., HU, H. & FAN, S. 2015a. Hydrometallurgical recovery of metal values from sulfuric acid leaching liquor of spent lithium-ion batteries. *Waste Manag,* 38**,** 349-56.

CHEN, X., FAN, B., XU, L., ZHOU, T. & KONG, J. 2016c. An atom-economic process for the recovery of high value-added metals from spent lithium-ion batteries. *Journal of Cleaner Production,* 112**,** 3562-3570.

CHEN, X., LUO, C., ZHANG, J., KONG, J. & ZHOU, T. 2015b. Sustainable recovery of metals from spent lithium-ion

batteries: a green process. *ACS Sustainable Chemistry & Engineering,* 3**,** 3104-3113.

CHEN, X., MA, H., LUO, C. & ZHOU, T. 2017. Recovery of valuable metals from waste cathode materials of spent lithium-ion batteries using mild phosphoric acid. *J Hazard Mater,* 326**,** 77-86.

CHEN, X., ZHOU, T., KONG, J., FANG, H. & CHEN, Y. 2015c. Separation and recovery of metal values from leach liquor of waste lithium nickel cobalt manganese oxide based cathodes. *Separation and Purification Technology,* 141**,** 76-83.

CIEZ, R. E. & WHITACRE, J. F. 2019. Examining different recycling processes for lithium-ion batteries. *Nature Sustainability,* 2**,** 148-156.

CLEANESE. 2016. *Methyl Isobutyl Carbinol* [Online]. Available: https://www.911metallurgist.com/blog/wp-content/uploads/2016/07/MIBC_Frother.pdf [Accessed 5 January 2020 2020].

CONTESTABILE, M., PANERO, S. & SCROSATI, B. 2001. A laboratory-scale lithium-ion battery recycling process. *Journal of Power Sources,* 92**,** 65-69.

CRAWFORD, A. J., HUANG, Q., KINTNER-MEYER, M. C. W., ZHANG, J.-G., REED, D. M., SPRENKLE, V. L., VISWANATHAN, V. V. & CHOI, D. 2018. Lifecycle comparison of selected Li-ion battery chemistries under

grid and electric vehicle duty cycle combinations. *Journal of Power Sources,* 380**,** 185-193.

DA COSTA, A. J., MATOS, J. F., BERNARDES, A. M. & MÜLLER, I. L. 2015. Beneficiation of cobalt, copper and aluminum from wasted lithium-ion batteries by mechanical processing. *International Journal of Mineral Processing,* 145**,** 77-82.

DAHLE, A., SUMITOMO, T. & INSTONE, S. 2003. Relationship between tensile and shear strengths of the mushy zone in solidifying aluminum alloys. *Metallurgical and Materials Transactions A,* 34**,** 105-113.

DAI, C., WANG, Z., LIU, K., ZHU, X., LIAO, X., CHEN, X. & PAN, Y. 2019. Effects of cycle times and C-rate on mechanical properties of copper foil and adhesive strength of electrodes in commercial LiCoO2 LIBs. *Engineering Failure Analysis,* 101**,** 193-205.

DIEKMANN, J., HANISCH, C., FROBÖSE, L., SCHÄLICKE, G., LOELLHOEFFEL, T., FÖLSTER, A.-S. & KWADE, A. 2017. Ecological Recycling of Lithium-Ion Batteries from Electric Vehicles with Focus on Mechanical Processes. *Journal of The Electrochemical Society,* 164**,** A6184-A6191.

DIOUF, B. & PODE, R. 2015. Potential of lithium-ion batteries in renewable energy. *Renewable Energy,* 76**,** 375-380.

DORELLA, G. & MANSUR, M. B. 2007. A study of the separation of cobalt from spent Li-ion battery residues. *Journal of Power Sources,* 170**,** 210-215.

DU, X., LIANG, C., HOU, D., SUN, Z. & ZHENG, S. 2019. Scrubbing and Inhibiting Coagulation Effect on the Purification of Natural Powder Quartz. *Minerals,* 9**,** 140.

DUNN, J. B., GAINES, L., BARNES, M., SULLIVAN, J. L. & WANG, M. 2014. Material and energy flows in the materials production, assembly, and end-of-life stages of the automotive lithium-ion battery life cycle. Argonne National Lab.(ANL), Argonne, IL (United States).

ECKER, M., SHAFIEI SABET, P. & SAUER, D. U. 2017. Influence of operational condition on lithium plating for commercial lithium-ion batteries – Electrochemical experiments and post-mortem-analysis. *Applied Energy,* 206**,** 934-946.

ELLIS, B. L., LEE, K. T. & NAZAR, L. F. 2010. Positive Electrode Materials for Li-Ion and Li-Batteries†. *Chemistry of Materials,* 22**,** 691-714.

ELLIS, T. W. & MONTENEGRO, J. A. 2016. *Magnetic separation of electrochemical cell materials*.

FANDRICH, R., BEARMAN, R., BOLAND, J. & LIM, W. 1997. Mineral liberation by particle bed breakage. *Minerals Engineering,* 10**,** 175-187.

FARROKHPAY, S. 2011. The significance of froth stability in mineral flotation — A review. *Advances in Colloid and Interface Science,* 166**,** 1-7.

FERREIRA, D. A., PRADOS, L. M. Z., MAJUSTE, D. & MANSUR, M. B. 2009. Hydrometallurgical separation of aluminium, cobalt, copper and lithium from spent Li-ion batteries. *Journal of Power Sources,* 187**,** 238-246.

FEW, S., SCHMIDT, O., OFFER, G. J., BRANDON, N., NELSON, J. & GAMBHIR, A. 2018. Prospective improvements in cost and cycle life of off-grid lithium-ion battery packs: An analysis informed by expert elicitations. *Energy Policy,* 114**,** 578-590.

FREITAS, M. B. J. G., CELANTE, V. G. & PIETRE, M. K. 2010. Electrochemical recovery of cobalt and copper from spent Li-ion batteries as multilayer deposits. *Journal of Power Sources,* 195**,** 3309-3315.

GAINES, L. 2014. The future of automotive lithium-ion battery recycling: Charting a sustainable course. *Sustainable Materials and Technologies,* 1-2**,** 2-7.

GAINES, L. 2018. Lithium-ion battery recycling processes: Research towards a sustainable course. *Sustainable Materials and Technologies,* 17**,** e00068.

GAINES, L., SULLIVAN, J., BURNHAM, A. & BELHAROUAK, I. Life-cycle analysis for lithium-ion battery production and recycling. 2011. 23-27.

GALLO, A. B., SIMÕES-MOREIRA, J. R., COSTA, H. K. M., SANTOS, M. M. & MOUTINHO DOS SANTOS, E. 2016. Energy storage in the energy transition context: A technology review. *Renewable and Sustainable Energy Reviews,* 65**,** 800-822.

GANTER, M. J., LANDI, B. J., BABBITT, C. W., ANCTIL, A. & GAUSTAD, G. 2014. Cathode refunctionalization as a lithium ion battery recycling alternative. *Journal of Power Sources,* 256**,** 274-280.

GAO, G., LUO, X., LOU, X., GUO, Y., SU, R., GUAN, J., LI, Y., YUAN, H., DAI, J. & JIAO, Z. 2019. Efficient sulfuric acid-Vitamin C leaching system: Towards enhanced extraction of cobalt from spent lithium-ion batteries. *Journal of Material Cycles and Waste Management*.

GAO, M. & FORSSBERG, E. 1995. Prediction of product size distributions for a stirred ball mill. *Powder Technology,* 84**,** 101-106.

GAO, W., ZHANG, X., ZHENG, X., LIN, X., CAO, H., ZHANG, Y. & SUN, Z. 2017. Lithium Carbonate Recovery from Cathode Scrap of Spent Lithium-Ion Battery: A Closed-Loop Process. *Environ Sci Technol,* 51**,** 1662-1669.

GARCIA, D., LIN, C. L. & MILLER, J. D. 2009. Quantitative analysis of grain boundary fracture in the breakage of single multiphase particles using X-ray microtomography procedures. *Minerals Engineering,* 22**,** 236-243.

GAUDIN, A. M. 1939. Principles of mineral dressing.

GEIGER, M., CALLAHAN, R., DIWIGGINS, C., FISHER, H., HOFFMAN, D., YU, W., ABRAHAM, K., JILLSON, M. & NGUYEN, T. The eleventh international seminar on primary and secondary battery technology and application. Fort Lauderdale, FL, Florida Educational Seminars Inc, 1994.

GOLMOHAMMADZADEH, R., RASHCHI, F. & VAHIDI, E. 2017. Recovery of lithium and cobalt from spent lithium-ion batteries using organic acids: Process optimization and kinetic aspects. *Waste Manag,* 64**,** 244-254.

GRANATA, G., MOSCARDINI, E., PAGNANELLI, F., TRABUCCO, F. & TORO, L. 2012a. Product recovery from Li-ion battery wastes coming from an industrial pre-treatment plant: Lab scale tests and process simulations. *Journal of Power Sources,* 206**,** 393-401.

GRANATA, G., PAGNANELLI, F., MOSCARDINI, E., TAKACOVA, Z., HAVLIK, T. & TORO, L. 2012b. Simultaneous recycling of nickel metal hydride, lithium ion and primary lithium batteries: Accomplishment of European Guidelines by optimizing mechanical pre-treatment and solvent extraction operations. *Journal of Power Sources,* 212**,** 205-211.

GRATZ, E., SA, Q., APELIAN, D. & WANG, Y. 2014. A closed loop process for recycling spent lithium ion batteries. *Journal of Power Sources,* 262**,** 255-262.

GRISSA, R., ABRAMOVA, A., TAMBIO, S. J., LECUYER, M., DESCHAMPS, M., FERNANDEZ, V., GRENECHE, J. M., GUYOMARD, D., LESTRIEZ, B. & MOREAU, P. 2019. Thermomechanical Polymer Binder Reactivity with Positive Active Materials for Li Metal Polymer and Li-Ion Batteries: An XPS and XPS Imaging Study. *ACS Appl Mater Interfaces,* 11**,** 18368-18376.

GROUP, Q. 2011. Technical Data Sheet for Polyvinylidene Rod & Sheet. Quadrant Group.

GU, F., GUO, J., YAO, X., SUMMERS, P. A., WIDIJATMOKO, S. D. & HALL, P. 2017. An investigation of the current status of recycling spent lithium-ion batteries from consumer electronics in China. *Journal of Cleaner Production,* 161**,** 765-780.

GUAN, J., LI, Y., GUO, Y., SU, R., GAO, G., SONG, H., YUAN, H., LIANG, B. & GUO, Z. 2016. Mechanochemical Process Enhanced Cobalt and Lithium Recycling from Wasted Lithium-Ion Batteries. *ACS Sustainable Chemistry & Engineering,* 5**,** 1026-1032.

GUO, X., CAO, X., HUANG, G., TIAN, Q. & SUN, H. 2017. Recovery of lithium from the effluent obtained in the process of spent lithium-ion batteries recycling. *J Environ Manage,* 198**,** 84-89.

GUO, Y., LI, F., ZHU, H., LI, G., HUANG, J. & HE, W. 2016. Leaching lithium from the anode electrode materials of

spent lithium-ion batteries by hydrochloric acid (HCl). *Waste Manag,* 51**,** 227-33.

HANISCH, C., LOELLHOEFFEL, T., DIEKMANN, J., MARKLEY, K. J., HASELRIEDER, W. & KWADE, A. 2015. Recycling of lithium-ion batteries: a novel method to separate coating and foil of electrodes. *Journal of Cleaner Production,* 108**,** 301-311.

HARDIE, C., LEICHTLE, G., WATSON, J., FINCH, J. & GOMEZ, C. 1999. Application of mineral processing techniques to the recycling of wastepaper. *CIM bulletin,* 92**,** 131-137.

HE, L.-P., SUN, S.-Y., MU, Y.-Y., SONG, X.-F. & YU, J.-G. 2016. Recovery of Lithium, Nickel, Cobalt, and Manganese from Spent Lithium-Ion Batteries Using l-Tartaric Acid as a Leachant. *ACS Sustainable Chemistry & Engineering,* 5**,** 714-721.

HE, L. P., SUN, S. Y., SONG, X. F. & YU, J. G. 2015. Recovery of cathode materials and Al from spent lithium-ion batteries by ultrasonic cleaning. *Waste Manag,* 46**,** 523-8.

HE, L. P., SUN, S. Y., SONG, X. F. & YU, J. G. 2017a. Leaching process for recovering valuable metals from the LiNi1/3Co1/3Mn1/3O2 cathode of lithium-ion batteries. *Waste Manag,* 64**,** 171-181.

HE, Y., ZHANG, T., WANG, F., ZHANG, G., ZHANG, W. & WANG, J. 2017b. Recovery of LiCoO2 and graphite from spent

lithium-ion batteries by Fenton reagent-assisted flotation. *Journal of Cleaner Production,* 143**,** 319-325.

HESSE, M., POPOV, O. & LIEBERWIRTH, H. 2017. Increasing efficiency by selective comminution. *Minerals Engineering,* 103-104**,** 112-126.

HINDLE, C. 2017. *Polypropylene* [Online]. United Kingdom: British Plastics Federation. Available: http://www.bpf.co.uk/plastipedia/polymers/pp.aspx [Accessed 12 March 2017].

HOREH, N. B., MOUSAVI, S. M. & SHOJAOSADATI, S. A. 2016. Bioleaching of valuable metals from spent lithium-ion mobile phone batteries using Aspergillus niger. *Journal of Power Sources,* 320**,** 257-266.

HU, J., ZHANG, J., LI, H., CHEN, Y. & WANG, C. 2017. A promising approach for the recovery of high value-added metals from spent lithium-ion batteries. *Journal of Power Sources,* 351**,** 192-199.

HUANG, B., PAN, Z., SU, X. & AN, L. 2018. Recycling of lithium-ion batteries: Recent advances and perspectives. *Journal of Power Sources,* 399**,** 274-286.

JHA, A. K., JHA, M. K., KUMARI, A., SAHU, S. K., KUMAR, V. & PANDEY, B. D. 2013a. Selective separation and recovery of cobalt from leach liquor of discarded Li–ion batteries using thiophosphinic extractant. *Separation and Purification Technology,* 104**,** 160-166.

JHA, M. K., KUMARI, A., JHA, A. K., KUMAR, V., HAIT, J. & PANDEY, B. D. 2013b. Recovery of lithium and cobalt from waste lithium ion batteries of mobile phone. *Waste Manag,* 33**,** 1890-7.

JOO, S.-H., SHIN, D., OH, C., WANG, J.-P. & SHIN, S. M. 2016a. Extraction of manganese by alkyl monocarboxylic acid in a mixed extractant from a leaching solution of spent lithium-ion battery ternary cathodic material. *Journal of Power Sources,* 305**,** 175-181.

JOO, S.-H., SHIN, D. J., OH, C., WANG, J.-P., SENANAYAKE, G. & SHIN, S. M. 2016b. Selective extraction and separation of nickel from cobalt, manganese and lithium in pre-treated leach liquors of ternary cathode material of spent lithium-ion batteries using synergism caused by Versatic 10 acid and LIX 84-I. *Hydrometallurgy,* 159**,** 65-74.

JOO, S.-H., SHIN, S. M., SHIN, D., OH, C. & WANG, J.-P. 2015. Extractive separation studies of manganese from spent lithium battery leachate using mixture of PC88A and Versatic 10 acid in kerosene. *Hydrometallurgy,* 156**,** 136-141.

JOULIÉ, M., BILLY, E., LAUCOURNET, R. & MEYER, D. 2017. Current collectors as reducing agent to dissolve active materials of positive electrodes from Li-ion battery wastes. *Hydrometallurgy,* 169**,** 426-432.

KANG, J., SENANAYAKE, G., SOHN, J. & SHIN, S. M. 2010. Recovery of cobalt sulfate from spent lithium ion batteries

by reductive leaching and solvent extraction with Cyanex 272. *Hydrometallurgy,* 100**,** 168-171.

KELLNER, R. & GOOSEY, E. 2019. Chapter 9. The Recycling of Lithium-ion Batteries: Current and Potential Approaches. *Electronic Waste Management.*

KELLY, E. & SPOTTISWOOD, D. 1989. The theory of electrostatic separations: A review Part I. Fundamentals. *Minerals Engineering,* 2**,** 33-46.

KIM, D.-S., SOHN, J.-S., LEE, C.-K., LEE, J.-H., HAN, K.-S. & LEE, Y.-I. 2004. Simultaneous separation and renovation of lithium cobalt oxide from the cathode of spent lithium ion rechargeable batteries. *Journal of Power Sources,* 132**,** 145-149.

KIM, H. S. & SHIN, E. J. 2013. Re-synthesis and Electrochemical Characteristics of LiFePO4Cathode Materials Recycled from Scrap Electrodes. *Bulletin of the Korean Chemical Society,* 34**,** 851-855.

KIM, J.-Y., JEONG, Y. W., CHO, H. Y. & CHANG, H. J. 2017. Alternative Sample Preparation Method for Large-Area Cross-Section View Observation of Lithium Ion Battery. *Applied Microscopy,* 47**,** 77-83.

KIM, S., YANG, D., RHEE, K. & SOHN, J. 2014. Recycling process of spent battery modules in used hybrid electric vehicles using physical/chemical treatments. *Research on Chemical Intermediates,* 40**,** 2447-2456.

KIM, W., KIM, B., CHOI, D., OKI, T. & KIM, S. 2010. Selective recovery of catalyst layer from supporting matrix of ceramic-honeycomb-type automobile catalyst. *J Hazard Mater,* 183**,** 29-34.

KING, R. & SCHNEIDER, C. 1998. Mineral liberation and the batch comminution equation. *Minerals engineering,* 11**,** 1143-1160.

KRÜGER, S., HANISCH, C., KWADE, A., WINTER, M. & NOWAK, S. 2014. Effect of impurities caused by a recycling process on the electrochemical performance of Li[Ni0.33Co0.33Mn0.33]O2. *Journal of Electroanalytical Chemistry,* 726**,** 91-96.

KU, H., JUNG, Y., JO, M., PARK, S., KIM, S., YANG, D., RHEE, K., AN, E. M., SOHN, J. & KWON, K. 2016. Recycling of spent lithium-ion battery cathode materials by ammoniacal leaching. *J Hazard Mater,* 313**,** 138-46.

KYNAR. 2017. *Kynar® PVDF (http://www.boedeker.com/pvdf_p.htm)* [Online]. Texas, USA: Boedeker Plastics, Inc. Available: http://www.boedeker.com/pvdf_p.htm [Accessed 12 March 2017 2017].

LAIN, M. J. 2001. Recycling of lithium ion cells and batteries. *Journal of Power Sources,* 97**,** 736-738.

LEE, C. K. & RHEE, K.-I. 2002. Preparation of LiCoO2 from spent lithium-ion batteries. *Journal of Power Sources,* 109**,** 17-21.

LEE, S., YANG, J. & LU, W. 2016. Debonding at the interface between active particles and PVDF binder in Li-ion batteries. *Extreme Mechanics Letters,* 6**,** 37-44.

LEIßNER, T., HOANG, D. H., RUDOLPH, M., HEINIG, T., BACHMANN, K., GUTZMER, J., SCHUBERT, H. & PEUKER, U. A. 2016. A mineral liberation study of grain boundary fracture based on measurements of the surface exposure after milling. *International Journal of Mineral Processing,* 156**,** 3-13.

LEIßNER, T., MÜTZE, T., ATANASOVA, P., BACHMANN, K. & PEUKER, U. A. Method for evaluation of upgrading by liberation and separation. XXVII International Mineral Processing Congress, 2014a. 8.

LEIßNER, T., MÜTZE, T. & PEUKER, U. A. 2014b. Nutzung der direkten Messung des Aufschlussgrades in Sortierkennfeldern. *Chemie Ingenieur Technik,* 86**,** 899-905.

LENG, F., WEI, Z., TAN, C. M. & YAZAMI, R. 2017. Hierarchical degradation processes in lithium-ion batteries during ageing. *Electrochimica Acta,* 256**,** 52-62.

LI, H., XING, S., LIU, Y., LI, F., GUO, H. & KUANG, G. 2017a. Recovery of lithium, iron, and phosphorus from spent

LiFePO4 batteries using stoichiometric sulfuric acid leaching system. *ACS sustainable chemistry & engineering,* 5**,** 8017-8024.

LI, J., LI, X., HU, Q., WANG, Z., ZHENG, J., WU, L. & ZHANG, L. 2009a. Study of extraction and purification of Ni, Co and Mn from spent battery material. *Hydrometallurgy,* 99**,** 7-12.

LI, J., SHI, P., WANG, Z., CHEN, Y. & CHANG, C. C. 2009b. A combined recovery process of metals in spent lithium-ion batteries. *Chemosphere,* 77**,** 1132-6.

LI, J., WANG, G. & XU, Z. 2016. Environmentally-friendly oxygen-free roasting/wet magnetic separation technology for in situ recycling cobalt, lithium carbonate and graphite from spent LiCoO2/graphite lithium batteries. *J Hazard Mater,* 302**,** 97-104.

LI, J., ZHANG, Q., XIAO, X., CHENG, Y. T., LIANG, C. & DUDNEY, N. J. 2015a. Unravelling the Impact of Reaction Paths on Mechanical Degradation of Intercalation Cathodes for Lithium-Ion Batteries. *J Am Chem Soc,* 137**,** 13732-5.

LI, L., BIAN, Y., ZHANG, X., GUAN, Y., FAN, E., WU, F. & CHEN, R. 2018a. Process for recycling mixed-cathode materials from spent lithium-ion batteries and kinetics of leaching. *Waste Manag,* 71**,** 362-371.

LI, L., BIAN, Y., ZHANG, X., XUE, Q., FAN, E., WU, F. & CHEN, R. 2018b. Economical recycling process for spent lithium-

ion batteries and macro- and micro-scale mechanistic study. *Journal of Power Sources,* 377**,** 70-79.

LI, L., CHEN, R., SUN, F., WU, F. & LIU, J. 2011. Preparation of LiCoO2 films from spent lithium-ion batteries by a combined recycling process. *Hydrometallurgy,* 108**,** 220-225.

LI, L., DUNN, J. B., ZHANG, X. X., GAINES, L., CHEN, R. J., WU, F. & AMINE, K. 2013a. Recovery of metals from spent lithium-ion batteries with organic acids as leaching reagents and environmental assessment. *Journal of Power Sources,* 233**,** 180-189.

LI, L., FAN, E., GUAN, Y., ZHANG, X., XUE, Q., WEI, L., WU, F. & CHEN, R. 2017b. Sustainable recovery of cathode materials from spent lithium-ion batteries using lactic acid leaching system. *ACS Sustainable Chemistry & Engineering,* 5**,** 5224-5233.

LI, L., GE, J., CHEN, R., WU, F., CHEN, S. & ZHANG, X. 2010a. Environmental friendly leaching reagent for cobalt and lithium recovery from spent lithium-ion batteries. *Waste Manag,* 30**,** 2615-21.

LI, L., GE, J., WU, F., CHEN, R., CHEN, S. & WU, B. 2010b. Recovery of cobalt and lithium from spent lithium ion batteries using organic citric acid as leachant. *J Hazard Mater,* 176**,** 288-93.

LI, L., QU, W., ZHANG, X., LU, J., CHEN, R., WU, F. & AMINE, K. 2015b. Succinic acid-based leaching system: A sustainable process for recovery of valuable metals from spent Li-ion batteries. *Journal of Power Sources,* 282**,** 544-551.

LI, L., ZENG, G.-S., LUO, S.-L., DENG, X.-R. & XIE, Q.-J. 2013b. Influences of solution pH and redox potential on the bioleaching of LiCoO2 from spent lithium-ion batteries. *Journal of the Korean Society for Applied Biological Chemistry,* 56**,** 187-192.

LI, M., LU, J., CHEN, Z. & AMINE, K. 2018c. 30 Years of Lithium-Ion Batteries. *Adv Mater***,** e1800561.

LITTLE, L., MAINZA, A. N., BECKER, M. & WIESE, J. G. 2016. Using mineralogical and particle shape analysis to investigate enhanced mineral liberation through phase boundary fracture. *Powder Technology,* 301**,** 794-804.

LIU, C., LIN, J., CAO, H., ZHANG, Y. & SUN, Z. 2019a. Recycling of spent lithium-ion batteries in view of lithium recovery: A critical review. *Journal of Cleaner Production*.

LIU, K. 2009. Some factors affecting sieving performance and efficiency. *Powder Technology,* 193**,** 208-213.

LIU, K. & ZHANG, F. S. 2016. Innovative leaching of cobalt and lithium from spent lithium-ion batteries and simultaneous dechlorination of polyvinyl chloride in subcritical water. *J Hazard Mater,* 316**,** 19-25.

LIU, S., ZHONG, H., ZHANG, C., YAN, X., ZHAO, X. & ZHANG, L. 2019b. Improving the processability and cycling stability of nano-LiFePO4 cathode by using PVDF/TX binary binder. *Composite Interfaces*, 1-12.

LME. 2019. *Featured LME Prices* [Online]. Available: https://www.lme.com/ [Accessed 23 August 2019].

LU, M., ZHANG, H., WANG, B., ZHENG, X. & DAI, C. 2013. The re-synthesis of LiCoO2 from spent lithium ion batteries separated by vacuum-assisted heat-treating method. *Int. J. Electrochem. Sci,* 8**,** 8201-8209.

LU, X. & FORSSBERG, E. 2001. Flotation selectivity and upgrading of Woxna fine graphite concentrate. *Minerals engineering,* 14**,** 1541-1543.

LUPI, C., PASQUALI, M. & DELL'ERA, A. 2005. Nickel and cobalt recycling from lithium-ion batteries by electrochemical processes. *Waste Management,* 25**,** 215-220.

MANTUANO, D. P., DORELLA, G., ELIAS, R. C. A. & MANSUR, M. B. 2006. Analysis of a hydrometallurgical route to recover base metals from spent rechargeable batteries by liquid–liquid extraction with Cyanex 272. *Journal of Power Sources,* 159**,** 1510-1518.

MARIANO, R. A., EVANS, C. L. & MANLAPIG, E. 2016. Definition of random and non-random breakage in mineral liberation - A review. *Minerals Engineering,* 94**,** 51-60.

MARINOS, D. & MISHRA, B. 2015. An Approach to Processing of Lithium-Ion Batteries for the Zero-Waste Recovery of Materials. *Journal of Sustainable Metallurgy,* 1**,** 263-274.

MATERIC, V., HOLT, R., HYLAND, M. & JONES, M. I. 2014. An internally circulating fluid bed for attrition testing of Ca looping sorbents. *Fuel,* 127**,** 116-123.

MATWEB. 2019. *AISI Type 304 Stainless Steel* [Online]. Available: http://asm.matweb.com/search/SpecificMaterial.asp?bassnum=mq304a [Accessed 21 December 2019].

MAY, T. W. & WIEDMEYER, R. H. 1998. A table of polyatomic interferences in ICP-MS. *ATOMIC SPECTROSCOPY-NORWALK CONNECTICUT-,* 19**,** 150-155.

MENG, Q., ZHANG, Y. & DONG, P. 2017. Use of glucose as reductant to recover Co from spent lithium ions batteries. *Waste Manag,* 64**,** 214-218.

MENG, Q., ZHANG, Y. & DONG, P. 2018. A combined process for cobalt recovering and cathode material regeneration from spent LiCoO2 batteries: Process optimization and kinetics aspects. *Waste Manag,* 71**,** 372-380.

MENG, X. & HAN, K. N. 1996. The principles and applications of ammonia leaching of metals—a review. *Mineral Processing and Extractive Metullargy Review,* 16**,** 23-61.

MESHRAM, P., PANDEY, B. D. & MANKHAND, T. R. 2014. Extraction of lithium from primary and secondary sources by pre-treatment, leaching and separation: A comprehensive review. *Hydrometallurgy,* 150**,** 192-208.

MESHRAM, P., PANDEY, B. D. & MANKHAND, T. R. 2015a. Hydrometallurgical processing of spent lithium ion batteries (LIBs) in the presence of a reducing agent with emphasis on kinetics of leaching. *Chemical Engineering Journal,* 281**,** 418-427.

MESHRAM, P., PANDEY, B. D. & MANKHAND, T. R. 2015b. Recovery of valuable metals from cathodic active material of spent lithium ion batteries: Leaching and kinetic aspects. *Waste Manag,* 45**,** 306-13.

MISHRA, D., KIM, D. J., RALPH, D. E., AHN, J. G. & RHEE, Y. H. 2008. Bioleaching of metals from spent lithium ion secondary batteries using Acidithiobacillus ferrooxidans. *Waste Manag,* 28**,** 333-8.

MORADI, B. & BOTTE, G. G. 2016. Recycling of graphite anodes for the next generation of lithium ion batteries. *Journal of Applied Electrochemistry,* 46**,** 123-148.

MYOUNG, J., JUNG, Y., LEE, J. & TAK, Y. 2002. Cobalt oxide preparation from waste LiCoO2 by electrochemical–hydrothermal method. *Journal of power sources,* 112**,** 639-642.

NAN, J., HAN, D., YANG, M., CUI, M. & HOU, X. 2006. Recovery of metal values from a mixture of spent lithium-ion batteries and nickel-metal hydride batteries. *Hydrometallurgy,* 84**,** 75-80.

NAN, J., HAN, D. & ZUO, X. 2005. Recovery of metal values from spent lithium-ion batteries with chemical deposition and solvent extraction. *Journal of Power Sources,* 152**,** 278-284.

NAYAKA, G. P., MANJANNA, J., PAI, K. V., VADAVI, R., KENY, S. J. & TRIPATHI, V. S. 2015. Recovery of valuable metal ions from the spent lithium-ion battery using aqueous mixture of mild organic acids as alternative to mineral acids. *Hydrometallurgy,* 151**,** 73-77.

NAYAKA, G. P., PAI, K. V., MANJANNA, J. & KENY, S. J. 2016a. Use of mild organic acid reagents to recover the Co and Li from spent Li-ion batteries. *Waste Manag,* 51**,** 234-238.

NAYAKA, G. P., PAI, K. V., SANTHOSH, G. & MANJANNA, J. 2016b. Dissolution of cathode active material of spent Li-ion batteries using tartaric acid and ascorbic acid mixture to recover Co. *Hydrometallurgy,* 161**,** 54-57.

NAYAKA, G. P., PAI, K. V., SANTHOSH, G. & MANJANNA, J. 2016c. Recovery of cobalt as cobalt oxalate from spent lithium ion batteries by using glycine as leaching agent. *Journal of Environmental Chemical Engineering,* 4**,** 2378-2383.

NEETHLING, S. J. & CILLIERS, J. J. 2008. Predicting and correcting grade-recovery curves: Theoretical aspects. *International Journal of Mineral Processing,* 89**,** 17-22.

NIE, H., XU, L., SONG, D., SONG, J., SHI, X., WANG, X., ZHANG, L. & YUAN, Z. 2015. LiCoO2: recycling from spent batteries and regeneration with solid state synthesis. *Green Chemistry,* 17**,** 1276-1280.

O'KELLY, B. C. & SIVAKUMAR, V. 2014. Water Content Determinations for Peat and Other Organic Soils Using the Oven-Drying Method. *Drying Technology,* 32**,** 631-643.

OBROVAC, M., CHRISTENSEN, L., LE, D. B. & DAHN, J. R. 2007. Alloy design for lithium-ion battery anodes. *Journal of The Electrochemical Society,* 154**,** A849-A855.

OJANEN, S., LUNDSTROM, M., SANTASALO-AARNIO, A. & SERNA-GUERRERO, R. 2018. Challenging the concept of electrochemical discharge using salt solutions for lithium-ion batteries recycling. *Waste Manag,* 76**,** 242-249.

OLIVETTI, E. A., CEDER, G., GAUSTAD, G. G. & FU, X. 2017. Lithium-Ion Battery Supply Chain Considerations: Analysis of Potential Bottlenecks in Critical Metals. *Joule,* 1**,** 229-243.

OU, Z., LI, J. & WANG, Z. 2015. Application of mechanochemistry to metal recovery from second-hand

resources: a technical overview. *Environmental Science: Processes & Impacts,* 17**,** 1522-1530.

PAGNANELLI, F., MOSCARDINI, E., ALTIMARI, P., ABO ATIA, T. & TORO, L. 2016. Cobalt products from real waste fractions of end of life lithium ion batteries. *Waste Manag,* 51**,** 214-221.

PAGNANELLI, F., MOSCARDINI, E., ALTIMARI, P., ABO ATIA, T. & TORO, L. 2017. Leaching of electrodic powders from lithium ion batteries: Optimization of operating conditions and effect of physical pretreatment for waste fraction retrieval. *Waste Manag,* 60**,** 706-715.

PAGNANELLI, F., MOSCARDINI, E., GRANATA, G., CERBELLI, S., AGOSTA, L., FIERAMOSCA, A. & TORO, L. 2014. Acid reducing leaching of cathodic powder from spent lithium ion batteries: Glucose oxidative pathways and particle area evolution. *Journal of Industrial and Engineering Chemistry,* 20**,** 3201-3207.

PANT, D. & DOLKER, T. 2017. Green and facile method for the recovery of spent Lithium Nickel Manganese Cobalt Oxide (NMC) based Lithium ion batteries. *Waste Manag,* 60**,** 689-695.

PAVONI, F. H., SITA, L. E., DOS SANTOS, C. S., DA SILVA, S. P., DA SILVA, P. R. C. & SCARMINIO, J. 2018. LiCoO2 particle size distribution as a function of the state of health of discarded cell phone batteries. *Powder Technology,* 326**,** 78-83.

PEGORETTI, V. C. B., DIXINI, P. V. M., SMECELLATO, P. C., BIAGGIO, S. R. & FREITAS, M. B. J. G. 2017. Thermal synthesis, characterization and electrochemical study of high-temperature (HT) LiCoO 2 obtained from Co(OH) 2 recycled of spent lithium ion batteries. *Materials Research Bulletin,* 86**,** 5-9.

PELED, E. & MENKIN, S. 2017. Review—SEI: Past, Present and Future. *Journal of The Electrochemical Society,* 164**,** A1703-A1719.

PENG, C., HAMUYUNI, J., WILSON, B. P. & LUNDSTROM, M. 2018. Selective reductive leaching of cobalt and lithium from industrially crushed waste Li-ion batteries in sulfuric acid system. *Waste Manag,* 76**,** 582-590.

PÉTAVY, F., RUBAN, V. & CONIL, P. 2009. Treatment of stormwater sediments: Efficiency of an attrition scrubber – laboratory and pilot-scale studies. *Chemical Engineering Journal,* 145**,** 475-482.

PETERSEN, L., DAHL, C. K. & ESBENSEN, K. H. 2004. Representative mass reduction in sampling—a critical survey of techniques and hardware. *Chemometrics and Intelligent Laboratory Systems,* 74**,** 95-114.

PETERSEN, L., MINKKINEN, P. & ESBENSEN, K. H. 2005. Representative sampling for reliable data analysis: Theory of Sampling. *Chemometrics and Intelligent Laboratory Systems,* 77**,** 261-277.

PILLOT, C. 2013. Li-ion battery material market review and forecast 2012-2025. *3rd Israeli Power Sources Conference 2013.* Hertzlia (Israel).

PINNA, E. G., RUIZ, M. C., OJEDA, M. W. & RODRIGUEZ, M. H. 2017. Cathodes of spent Li-ion batteries: Dissolution with phosphoric acid and recovery of lithium and cobalt from leach liquors. *Hydrometallurgy,* 167**,** 66-71.

PRANOLO, Y., ZHANG, W. & CHENG, C. Y. 2010. Recovery of metals from spent lithium-ion battery leach solutions with a mixed solvent extractant system. *Hydrometallurgy,* 102**,** 37-42.

PRIETO-SANDOVAL, V., JACA, C. & ORMAZABAL, M. 2017. Towards a consensus on the circular economy. *Journal of Cleaner Production*.

RAWLINS, C. H. 2009. Flotation of fine oil droplets in petroleum production circuits. *Recent Advances in Mineral Processing Plant Design,* 232.

REDDY, T. B. 2011. *Linden's handbook of batteries*, McGraw-hill New York.

REICHERT, M., GEROLD, C., FREDRIKSSON, A., ADOLFSSON, G. & LIEBERWIRTH, H. 2015. Research of iron ore grinding in a vertical-roller-mill. *Minerals Engineering,* 73**,** 109-115.

RICHA, K., BABBITT, C. W. & GAUSTAD, G. 2017. Eco-Efficiency Analysis of a Lithium-Ion Battery Waste Hierarchy Inspired by Circular Economy. *Journal of Industrial Ecology,* 21**,** 715-730.

RICHA, K., BABBITT, C. W., GAUSTAD, G. & WANG, X. 2014. A future perspective on lithium-ion battery waste flows from electric vehicles. *Resources, Conservation and Recycling,* 83**,** 63-76.

ROUNDY, D., KRENN, C. R., COHEN, M. L. & MORRIS, J. W. 1999. Ideal Shear Strengths of fcc Aluminum and Copper. *Physical Review Letters,* 82**,** 2713-2716.

SA, Q., GRATZ, E., HE, M., LU, W., APELIAN, D. & WANG, Y. 2015a. Synthesis of high performance LiNi 1/3 Mn 1/3 Co 1/3 O 2 from lithium ion battery recovery stream. *Journal of Power Sources,* 282**,** 140-145.

SA, Q., HEELAN, J. A., LU, Y., APELIAN, D. & WANG, Y. 2015b. Copper Impurity Effects on LiNi(1/3)Mn(1/3)Co(1/3)O2 Cathode Material. *ACS Appl Mater Interfaces,* 7**,** 20585-90.

SADLER III, L. Y., STANLEY, A. D. & BROOKS, D. R. 1975. Attrition mill operating characteristics. *Powder Technology,* 12**,** 19-28.

SAEKI, S., LEE, J., ZHANG, Q. & SAITO, F. 2004. Co-grinding LiCoO2 with PVC and water leaching of metal chlorides

formed in ground product. *International Journal of Mineral Processing,* 74**,** S373-S378.

SALOOJEE, F. & LLOYD, J. 2015. Lithium battery recycling process. *Department of Environmental Affairs Development Bank of South Africa (Project No. DB-074 (RW1/1016),* 1.

SANDGREN, E., BERGLIND, B. & MODIGH, S. 2016. *Basics in Minerals Processing* [Online]. Metso. Available: https://www.metso.com/contentassets/0efc5d1a7c5a43 57baecc5e990dc1fe7/basics-in-mineral-processing-handbook-18-lr.pdf [Accessed 16 November 2016].

SCHIPPER, F., ERICKSON, E. M., ERK, C., SHIN, J.-Y., CHESNEAU, F. F. & AURBACH, D. 2017. Review—Recent Advances and Remaining Challenges for Lithium Ion Battery Cathodes I. Nickel-Rich, LiNixCoyMnzO2. *Journal of The Electrochemical Society,* 164**,** A6220-A6228

SCHUBERT, G. & BERNOTAT, S. 2004. Comminution of non-brittle materials. *International Journal of Mineral Processing,* 74**,** S19-S30.

SCHULZ, N. F. 1970. Separation efficiency. *Trans. SME-AIME,* 247**,** 56.

SENĆANSKI, J., BAJUK-BOGDANOVIĆ, D., MAJSTOROVIĆ, D., TCHERNYCHOVA, E., PAPAN, J. & VUJKOVIĆ, M. 2017. The synthesis of Li(Co Mn Ni)O 2 cathode material from spent-Li ion batteries and the proof of its functionality in

aqueous lithium and sodium electrolytic solutions. *Journal of Power Sources,* 342**,** 690-703.

SHAW-STEWART, J., ALVAREZ-REGUERA, A., GRESZTA, A., MARCO, J., MASOOD, M., SOMMERVILLE, R. & KENDRICK, E. 2019. Aqueous solution discharge of cylindrical lithium-ion cells. *Sustainable Materials and Technologies***,** e00110.

SHIN, S. M., KIM, N. H., SOHN, J. S., YANG, D. H. & KIM, Y. H. 2005. Development of a metal recovery process from Li-ion battery wastes. *Hydrometallurgy,* 79**,** 172-181.

SILVEIRA, A. V. M., SANTANA, M. P., TANABE, E. H. & BERTUOL, D. A. 2017. Recovery of valuable materials from spent lithium ion batteries using electrostatic separation. *International Journal of Mineral Processing,* 169**,** 91-98.

SMM. 2019. *Shanghai Metals Market (SMM) Price* [Online]. Shanghai Metals Market. Available: https://price.metal.com/prices/manganese [Accessed 23 August 2019].

SONG, D., WANG, X., ZHOU, E., HOU, P., GUO, F. & ZHANG, L. 2013. Recovery and heat treatment of the Li(Ni1/3Co1/3Mn1/3)O2 cathode scrap material for lithium ion battery. *Journal of Power Sources,* 232**,** 348-352.

SONG, H.-Y. & JEONG, S.-K. 2018. Investigating continuous co-intercalation of solvated lithium ions and graphite

exfoliation in propylene carbonate-based electrolyte solutions. *Journal of Power Sources,* 373**,** 110-118.

SONG, X., HU, T., LIANG, C., LONG, H. L., ZHOU, L., SONG, W., YOU, L., WU, Z. S. & LIU, J. W. 2017. Direct regeneration of cathode materials from spent lithium iron phosphate batteries using a solid phase sintering method. *RSC Advances,* 7**,** 4783-4790.

SONOC, A., JESWIET, J. & SOO, V. K. 2015. Opportunities to improve recycling of automotive lithium ion batteries. *Procedia cIRP,* 29**,** 752-757.

SOUSA, R., SIMONS, B., BRU, K., DE SOUSA, A. B., ROLLINSON, G., ANDERSEN, J., MARTIN, M. & MACHADO LEITE, M. 2018. Use of mineral liberation quantitative data to assess separation efficiency in mineral processing – Some case studies. *Minerals Engineering,* 127**,** 134-142.

SU, B. L., SANCHEZ, C. & YANG, X.-Y. 2012. *Hierarchically structured porous materials: from nanoscience to catalysis, separation, optics, energy, and life science*, John Wiley & Sons.

SUBRAHMANYAM, T. V. & FORSSBEG, E. 1988. FROTH CHARACTERISTICS AND GRADE-RECOVERY RELATIONSHIPS IN THE FLOTATION OF LEAD-ZINC AND COPPER ORES. *Minerals Engineering,* 1**,** 41-52.

SUN, C., XU, L., CHEN, X., QIU, T. & ZHOU, T. 2018. Sustainable recovery of valuable metals from spent

lithium-ion batteries using DL-malic acid: Leaching and kinetics aspect. *Waste Manag Res,* 36**,** 113-120.

SUN, L. & QIU, K. 2011. Vacuum pyrolysis and hydrometallurgical process for the recovery of valuable metals from spent lithium-ion batteries. *J Hazard Mater,* 194**,** 378-84.

SUN, L. & QIU, K. 2012. Organic oxalate as leachant and precipitant for the recovery of valuable metals from spent lithium-ion batteries. *Waste Manag,* 32**,** 1575-82.

SUN, Z., XIAO, Y., SIETSMA, J., AGTERHUIS, H. & YANG, Y. 2015. A cleaner process for selective recovery of valuable metals from electronic waste of complex mixtures of end-of-life electronic products. *Environmental science & technology,* 49**,** 7981-7988.

SUZUKI, T., NAKAMURA, T., INOUE, Y., NIINAE, M. & SHIBATA, J. 2012. A hydrometallurgical process for the separation of aluminum, cobalt, copper and lithium in acidic sulfate media. *Separation and Purification Technology,* 98**,** 396-401.

SVOBODA, J. & FUJITA, T. 2003. Recent developments in magnetic methods of material separation. *Minerals Engineering,* 16**,** 785-792.

SWAIN, B. 2017. Recovery and recycling of lithium: A review. *Separation and Purification Technology,* 172**,** 388-403.

SWAIN, B., JEONG, J., LEE, J.-C. & LEE, G.-H. 2008. Development of process flow sheet for recovery of high pure cobalt from sulfate leach liquor of LIB industry waste: A mathematical model correlation to predict optimum operational conditions. *Separation and Purification Technology,* 63**,** 360-369.

SWAIN, B., JEONG, J., LEE, J.-C., LEE, G.-H. & SOHN, J.-S. 2007. Hydrometallurgical process for recovery of cobalt from waste cathodic active material generated during manufacturing of lithium ion batteries. *Journal of Power Sources,* 167**,** 536-544.

TAGAWA, K. & BRODD, R. J. 2009. Production processes for fabrication of lithium-ion batteries. *Lithium-ion batteries.* Springer.

TAKACOVA, Z., HAVLIK, T., KUKURUGYA, F. & ORAC, D. 2016. Cobalt and lithium recovery from active mass of spent Li-ion batteries: Theoretical and experimental approach. *Hydrometallurgy,* 163**,** 9-17.

TANONG, K., COUDERT, L., CHARTIER, M., MERCIER, G. & BLAIS, J. F. 2017. Study of the factors influencing the metals solubilisation from a mixture of waste batteries by response surface methodology. *Environ Technol,* 38**,** 3167-3179.

TARASCON, J. M. & ARMAND, M. 2001. Issues and challenges facing rechargeable lithium batteries. *Nature,* 414**,** 359-367.

TSATOUHAS, G., GRANO, S. R. & VERA, M. 2006. Case studies on the performance and characterisation of the froth phase in industrial flotation circuits. *Minerals Engineering,* 19**,** 774-783.

VARINOT, C., HILTGUN, S., PONS, M.-N. & DODDS, J. 1997. Identification of the fragmentation mechanisms in wet-phase fine grinding in a stirred bead mill. *Chemical Engineering Science,* 52**,** 3605-3612.

VEIT, H. M., DIEHL, T. R., SALAMI, A. P., RODRIGUES, J. S., BERNARDES, A. M. & TENORIO, J. A. 2005. Utilization of magnetic and electrostatic separation in the recycling of printed circuit boards scrap. *Waste Manag,* 25**,** 67-74.

VETTER, J., NOVÁK, P., WAGNER, M. R., VEIT, C., MÖLLER, K. C., BESENHARD, J. O., WINTER, M., WOHLFAHRT-MEHRENS, M., VOGLER, C. & HAMMOUCHE, A. 2005. Ageing mechanisms in lithium-ion batteries. *Journal of Power Sources,* 147**,** 269-281.

VIECELI, N., NOGUEIRA, C. A., GUIMARAES, C., PEREIRA, M. F. C., DURAO, F. O. & MARGARIDO, F. 2018. Hydrometallurgical recycling of lithium-ion batteries by reductive leaching with sodium metabisulphite. *Waste Manag,* 71**,** 350-361.

VILLARS, P. & CENZUAL, K. 2012a. graphite (C gra hex) Crystal Structure: Datasheet from "PAULING FILE Multinaries Edition – 2012" in SpringerMaterials (http://materials.springer.com/isp/crystallographic/docs

/sd_1251859). Available: http://materials.springer.com/isp/crystallographic/docs/sd_1251859.

VILLARS, P. & CENZUAL, K. 2012b. LiCoO2 Crystal Structure: Datasheet from "PAULING FILE Multinaries Edition – 2012" in SpringerMaterials (http://materials.springer.com/isp/crystallographic/docs/sd_1222814). Available: http://materials.springer.com/isp/crystallographic/docs/sd_1222814.

VILLARS, P. & CENZUAL, K. 2012c. LiFePO4 (LiFe[PO4] rt) Crystal Structure: Datasheet from "PAULING FILE Multinaries Edition – 2012" in SpringerMaterials (http://materials.springer.com/isp/crystallographic/docs/sd_1716952). Available: http://materials.springer.com/isp/crystallographic/docs/sd_1716952.

VILLARS, P. & CENZUAL, K. 2012d. LiMn2O4 Tf phase (LiMn2O4 hp tet, p = 7.5 GPa) Crystal Structure: Datasheet from "PAULING FILE Multinaries Edition – 2012" in SpringerMaterials (http://materials.springer.com/isp/crystallographic/docs/sd_1628133). Available: http://materials.springer.com/isp/crystallographic/docs/sd_1628133.

VILLARS, P. & CENZUAL, K. 2012e. "LiNiO2", "LiNi1−yAlyO2" y= 0 (LiNiO2 rhom) Crystal Structure: Datasheet from

"PAULING FILE Multinaries Edition – 2012" in SpringerMaterials (http://materials.springer.com/isp/crystallographic/docs/sd_1628376). Available: http://materials.springer.com/isp/crystallographic/docs/sd_1628376.

VIROLAINEN, S., FALLAH FINI, M., LAITINEN, A. & SAINIO, T. 2017. Solvent extraction fractionation of Li-ion battery leachate containing Li, Ni, and Co. *Separation and Purification Technology,* 179**,** 274-282.

WALDMANN, T., GORSE, S., SAMTLEBEN, T., SCHNEIDER, G., KNOBLAUCH, V. & WOHLFAHRT-MEHRENS, M. 2014. A mechanical aging mechanism in lithium-ion batteries. *Journal of The Electrochemical Society,* 161**,** A1742-A1747.

WANG, F., HE, F., ZHAO, J., SUI, N., XU, L. & LIU, H. 2012a. Extraction and separation of cobalt(II), copper(II) and manganese(II) by Cyanex272, PC-88A and their mixtures. *Separation and Purification Technology,* 93**,** 8-14.

WANG, F., SUN, R., XU, J., CHEN, Z. & KANG, M. 2016a. Recovery of cobalt from spent lithium ion batteries using sulphuric acid leaching followed by solid–liquid separation and solvent extraction. *RSC Advances,* 6**,** 85303-85311.

WANG, J., CHEN, M., CHEN, H., LUO, T. & XU, Z. 2012b. Leaching Study of Spent Li-ion Batteries. *Procedia Environmental Sciences,* 16**,** 443-450.

WANG, M. M., ZHANG, C. C. & ZHANG, F. S. 2016b. An environmental benign process for cobalt and lithium recovery from spent lithium-ion batteries by mechanochemical approach. *Waste Manag,* 51**,** 239-244.

WANG, M. M., ZHANG, C. C. & ZHANG, F. S. 2017. Recycling of spent lithium-ion battery with polyvinyl chloride by mechanochemical process. *Waste Manag,* 67**,** 232-239.

WANG, Q., PING, P., ZHAO, X., CHU, G., SUN, J. & CHEN, C. 2012c. Thermal runaway caused fire and explosion of lithium ion battery. *Journal of Power Sources,* 208**,** 210-224.

WANG, R.-C., LIN, Y.-C. & WU, S.-H. 2009. A novel recovery process of metal values from the cathode active materials of the lithium-ion secondary batteries. *Hydrometallurgy,* 99**,** 194-201.

WANG, X., GAUSTAD, G. & BABBITT, C. W. 2016c. Targeting high value metals in lithium-ion battery recycling via shredding and size-based separation. *Waste Manag,* 51**,** 204-213.

WANG, X., GAUSTAD, G., BABBITT, C. W. & RICHA, K. 2014. Economies of scale for future lithium-ion battery recycling infrastructure. *Resources, Conservation and Recycling,* 83**,** 53-62.

WENG, Y., XU, S., HUANG, G. & JIANG, C. 2013. Synthesis and performance of Li[(Ni1/3Co1/3Mn1/3)(1-x)Mgx]O2

prepared from spent lithium ion batteries. *J Hazard Mater,* 246-247**,** 163-72.

WILLS, B. A. & FINCH, J. A. 2016a. Froth Flotation. 265-380.

WILLS, B. A. & FINCH, J. A. 2016b. Gravity Concentration. 223-244.

WILLS, B. A. & FINCH, J. A. 2016c. Industrial Screening. 181-197.

WILLS, B. A. & FINCH, J. A. 2016d. Magnetic and Electrical Separation. 381-407.

WILLS, B. A. & FINCH, J. A. 2016e. *Particle Size Analysis*.

WILSON, R., VEASEY, T. & SQUIRES, D. 1994. The application of mineral processing techniques for the recovery of metal from post-consumer wastes. *Minerals engineering,* 7**,** 975-984.

WINSLOW, K. M., LAUX, S. J. & TOWNSEND, T. G. 2018. A review on the growing concern and potential management strategies of waste lithium-ion batteries. *Resources, Conservation and Recycling,* 129**,** 263-277.

XIAO, J., LI, J. & XU, Z. 2017a. Novel approach for in situ recovery of lithium carbonate from spent lithium ion batteries using vacuum metallurgy. *Environmental science & technology,* 51**,** 11960-11966.

XIAO, J., LI, J. & XU, Z. 2017b. Recycling metals from lithium ion battery by mechanical separation and vacuum metallurgy. *J Hazard Mater,* 338**,** 124-131.

XIN, B., ZHANG, D., ZHANG, X., XIA, Y., WU, F., CHEN, S. & LI, L. 2009. Bioleaching mechanism of Co and Li from spent lithium-ion battery by the mixed culture of acidophilic sulfur-oxidizing and iron-oxidizing bacteria. *Bioresour Technol,* 100**,** 6163-9.

XIN, Y., GUO, X., CHEN, S., WANG, J., WU, F. & XIN, B. 2016. Bioleaching of valuable metals Li, Co, Ni and Mn from spent electric vehicle Li-ion batteries for the purpose of recovery. *Journal of Cleaner Production,* 116**,** 249-258.

XU, J., TOMAS, H. R., FRANCIS, R. W., LUM, K. R., WANG, J. & LIANG, B. 2008. A review of processes and technologies for the recycling of lithium-ion secondary batteries. *Journal of Power Sources,* 177**,** 512-527.

XU, W., DHAWAN, N., LIN, C.-L. & MILLER, J. D. 2013. Further study of grain boundary fracture in the breakage of single multiphase particles using X-ray microtomography procedures. *Minerals Engineering,* 46-47**,** 89-94.

YANG, H., ZHUANG, G. V. & ROSS, P. N. 2006. Thermal stability of LiPF6 salt and Li-ion battery electrolytes containing LiPF6. *Journal of Power Sources,* 161**,** 573-579.

YANG, Y., XU, S. & HE, Y. 2017a. Lithium recycling and cathode material regeneration from acid leach liquor of spent

lithium-ion battery via facile co-extraction and co-precipitation processes. *Waste Manag,* 64**,** 219-227.

YANG, Y., ZHENG, X., CAO, H., ZHAO, C., LIN, X., NING, P., ZHANG, Y., JIN, W. & SUN, Z. 2017b. A Closed-Loop Process for Selective Metal Recovery from Spent Lithium Iron Phosphate Batteries through Mechanochemical Activation. *ACS Sustainable Chemistry & Engineering,* 5**,** 9972-9980.

YAO, L., FENG, Y. & XI, G. 2015. A new method for the synthesis of LiNi1/3Co1/3Mn1/3O2 from waste lithium ion batteries. *RSC Advances,* 5**,** 44107-44114.

YAO, L., YAO, H., XI, G. & FENG, Y. 2016a. Recycling and synthesis of LiNi1/3Co1/3Mn1/3O2 from waste lithium ion batteries using d,l-malic acid. *RSC Advances,* 6**,** 17947-17954.

YAO, L., YAO, H., XI, G. & FENG, Y. 2016b. Recycling and synthesis of LiNi1/3Co1/3Mn1/3O2from waste lithium ion batteries usingd,l-malic acid. *RSC Adv.,* 6**,** 17947-17954.

YEN, J. P., LEE, C. M., WU, T. L., WU, H. C., SU, C. Y., WU, N. L. & HONG, J. L. 2012. Enhanced High-Temperature Cycle-Life of Mesophase Graphite Anode with Styrene-Butadiene Rubber/Carboxymethyl Cellulose Binder. *ECS Electrochemistry Letters,* 1**,** A80-A82.

YOSHIO, M., BRODD, R. J. & KOZAWA, A. 2010. *Lithium-ion batteries: science and technologies*, Springer Science & Business Media.

YU, J., HE, Y., GE, Z., LI, H., XIE, W. & WANG, S. 2018. A promising physical method for recovery of LiCoO 2 and graphite from spent lithium-ion batteries: Grinding flotation. *Separation and Purification Technology,* 190**,** 45-52.

YU, J., HE, Y., LI, H., XIE, W. & ZHANG, T. 2017. Effect of the secondary product of semi-solid phase Fenton on the flotability of electrode material from spent lithium-ion battery. *Powder Technology,* 315**,** 139-146.

YU, W.-C. & HUX, S. E. 1999. Method of making a trilayer battery separator. Google Patents.

ZENG, X., LI, J. & SHEN, B. 2015. Novel approach to recover cobalt and lithium from spent lithium-ion battery using oxalic acid. *J Hazard Mater,* 295**,** 112-8.

ZENG, X., LI, J. & SINGH, N. 2014. Recycling of Spent Lithium-Ion Battery: A Critical Review. *Critical Reviews in Environmental Science and Technology,* 44**,** 1129-1165.

ZHAN, R., OLDENBURG, Z. & PAN, L. 2018. Recovery of active cathode materials from lithium-ion batteries using froth flotation. *Sustainable Materials and Technologies,* 17**,** e00062.

ZHANG, G., HE, Y., WANG, H., FENG, Y., XIE, W. & ZHU, X. 2019. Application of mechanical crushing combined with pyrolysis-enhanced flotation technology to recover graphite and LiCoO2 from spent lithium-ion batteries. *Journal of Cleaner Production,* 231**,** 1418-1427.

ZHANG, P., YOKOYAMA, T., ITABASHI, O., SUZUKI, T. M. & INOUE, K. 1998. Hydrometallurgical process for recovery of metal values from spent lithium-ion secondary batteries. *Hydrometallurgy,* 47**,** 259-271.

ZHANG, Q., LU, J., SAITO, F., NAGATA, C. & ITO, Y. 2000. Room temperature acid extraction of Co from LiCo0. 2Ni0. 8O2 scrap by a mechanochemical treatment. *Advanced Powder Technology,* 11**,** 353-359.

ZHANG, S. S. 2006. A review on electrolyte additives for lithium-ion batteries. *Journal of Power Sources,* 162**,** 1379-1394.

ZHANG, S. S. 2007. A review on the separators of liquid electrolyte Li-ion batteries. *Journal of Power Sources,* 164**,** 351-364.

ZHANG, T., HE, Y., GE, L., FU, R., ZHANG, X. & HUANG, Y. 2013. Characteristics of wet and dry crushing methods in the recycling process of spent lithium-ion batteries. *Journal of Power Sources,* 240**,** 766-771.

ZHANG, T., HE, Y., WANG, F., GE, L., ZHU, X. & LI, H. 2014a. Chemical and process mineralogical characterizations of

spent lithium-ion batteries: an approach by multi-analytical techniques. *Waste Manag,* 34**,** 1051-8.

ZHANG, T., HE, Y., WANG, F., LI, H., DUAN, C. & WU, C. 2014b. Surface analysis of cobalt-enriched crushed products of spent lithium-ion batteries by X-ray photoelectron spectroscopy. *Separation and Purification Technology,* 138**,** 21-27.

ZHANG, X., CAO, H., XIE, Y., NING, P., AN, H., YOU, H. & NAWAZ, F. 2015. A closed-loop process for recycling LiNi1/3Co1/3Mn1/3O2 from the cathode scraps of lithium-ion batteries: Process optimization and kinetics analysis. *Separation and Purification Technology,* 150**,** 186-195.

ZHANG, X., XIE, Y., CAO, H., NAWAZ, F. & ZHANG, Y. 2014c. A novel process for recycling and resynthesizing LiNi1/3Co1/3Mn1/3O2 from the cathode scraps intended for lithium-ion batteries. *Waste Manag,* 34**,** 1715-24.

ZHANG, X., XUE, Q., LI, L., FAN, E., WU, F. & CHEN, R. 2016. Sustainable recycling and regeneration of cathode scraps from industrial production of lithium-ion batteries. *ACS Sustainable Chemistry & Engineering,* 4**,** 7041-7049.

ZHENG, R., WANG, W., DAI, Y., MA, Q., LIU, Y., MU, D., LI, R., REN, J. & DAI, C. 2017a. A closed-loop process for recycling LiNi x Co y Mn (1−x−y) O 2 from mixed cathode materials of lithium-ion batteries. *Green Energy & Environment,* 2**,** 42-50.

ZHENG, R., ZHAO, L., WANG, W., LIU, Y., MA, Q., MU, D., LI, R. & DAI, C. 2016. Optimized Li and Fe recovery from spent lithium-ion batteries via a solution-precipitation method. *RSC Advances,* 6**,** 43613-43625.

ZHENG, X., GAO, W., ZHANG, X., HE, M., LIN, X., CAO, H., ZHANG, Y. & SUN, Z. 2017b. Spent lithium-ion battery recycling - Reductive ammonia leaching of metals from cathode scrap by sodium sulphite. *Waste Manag,* 60**,** 680-688.

ZHOU, A., WANG, W., LIU, Q., WANG, Y., YAO, X., QING, F., LI, E., YANG, T., ZHANG, L. & LI, J. 2017. Stable, fast and high-energy-density LiCoO 2 cathode at high operation voltage enabled by glassy B 2 O 3 modification. *Journal of Power Sources,* 362**,** 131-139.

ZHU, S.-G., HE, W.-Z., LI, G.-M., ZHOU, X., ZHANG, X.-J. & HUANG, J.-W. 2012. Recovery of Co and Li from spent lithium-ion batteries by combination method of acid leaching and chemical precipitation. *Transactions of Nonferrous Metals Society of China,* 22**,** 2274-2281.

ZHU, S., HE, W., LI, G., ZHOU, X., HUANG, J. & ZHANG, X. Recovering copper from spent lithium ion battery by a mechanical separation process. 2011 International Conference on Materials for Renewable Energy & Environment, 2011. IEEE, 1008-1012.

ZIEMANN, S., MÜLLER, D. B., SCHEBEK, L. & WEIL, M. 2018. Modeling the potential impact of lithium recycling from

EV batteries on lithium demand: A dynamic MFA approach. *Resources, Conservation and Recycling,* 133**,** 76-85.

ZOU, H., GRATZ, E., APELIAN, D. & WANG, Y. 2013. A novel method to recycle mixed cathode materials for lithium ion batteries. *Green Chemistry,* 15**,** 1183.

Appendix I – List of Publications

The following publications are attached in this appendix:

GU, F., GUO, J., YAO, X., SUMMERS, P. A., WIDIJATMOKO, S. D. & HALL, P. 2017. An investigation of the current status of recycling spent lithium-ion batteries from consumer electronics in China. Journal of Cleaner Production, 161, 765-780. https://doi.org/10.1016/j.jclepro.2017.05.181

WIDIJATMOKO, S. D., GU, F., WANG, Z. & HALL, P. 2020. Selective liberation in dry milled spent lithium-ion batteries. Sustainable Materials and Technologies, 23, e00134. https://doi.org/10.1016/j.susmat.2019.e00134

WIDIJATMOKO, S. D., FU, G., WANG, Z. & HALL, P. 2020. Recovering lithium cobalt oxide, aluminium, and copper from spent lithium-ion battery via attrition scrubbing. Journal of Cleaner Production, 260, 120869. https://doi.org/10.1016/j.jclepro.2020.120869

An investigation of the current status of recycling spent lithium-ion batteries from consumer electronics in China

CrossMark

Fu Gu [a], Jianfeng Guo [b,*], Xing Yao [b], Peter A. Summers [a], Samuel D. Widijatmoko [a], Philip Hall [a]

[a] Department of Chemical and Environmental Engineering, Nottingham University, Ningbo, 315100, China
[b] Center of Energy and Environmental Policy Research, Institute of Policy and Management, Chinese Academy of Sciences, Beijing, 100190, China

ABSTRACT

Ever-increasing demand and production of lithium-ion batteries result in disposal problems. There is little known information about recycling lithium-ion batteries from consumer electronics in China, despite China is the largest lithium-ion battery manufacturer and consumer. To address this gap, this paper aims at investigating the current status of recycling spent lithium-ion batteries from consumer electronics in China, and to provide recommendations for improving spent lithium-ion battery recycling rate. Generation, collection and recycling of spent lithium-ion batteries were investigated using a combined methodology consists of online surveys, field investigations and estimations. The survey shows that although respondents have expressed their willingness towards recycling, most of them did not know where to send their spent lithium-ion batteries. Field investigations were carried out to trace the material flow of spent lithium-ion batteries in current waste electric and electronic equipment collection systems. It was found that the spent lithium-ion batteries are not included in current collection systems, as only few recycling practitioners are collecting spent lithium-ion batteries. Inadequate supply was found to have a significant impact on current recycling industry. Combining official statistics, survey results and actual throughput of the recycling plants, it was roughly estimated that less than 10% of lithium-ion batteries used in consumer electronics are currently recycled, while others always end up in idle or landfill. This study provides essential information on status quo of recycling lithium-ion batteries from consumer electronics in China including consumers' behaviours, recycling practices and estimated recycling rate. Further, policy implications were proposed with the purpose of promoting recycling rates of spent LIBs from CEs.

© 2017 Elsevier Ltd. All rights reserved.

1. Introduction

Owing to a higher energy density and cell voltage, less memory effect, low self-discharge and environmental impact, the applications of lithium-ion batteries (lithium-ion secondary batteries or li-ion batteries, LIBs) are vast and extensive. LIBs are intensively used in two major areas: (1) consumer electronics (CE), especially portable devices including laptops, tablet computers mobile phones and digital cameras; (2) electric vehicles (EV) (Zeng et al., 2012). Currently, CE is the largest consumer for LIBs in China (Zeng et al., 2012). Taking mobile phone for example, there were more than 1.3 billion mobile phone subscriptions in China at the end of 2015 (MIIT, 2016). Obsolete mobile phones in China have already become one of the major components in the waste electric and electronic equipment (WEEE) stream. Li et al. (2015) estimated that there were about 740 M mobile phones retired in 2012 alone, which is more than 15 times compared to the amount in 2002. Wang et al. (2011) claimed there are over 70 M mobile phones retired annually. The average life span of a LIB in a mobile phone is between 300 and 500 charging-discharging cycles (BU, 2010), that is, approximately two years in use (Zeng et al., 2012). The actual service life of LIB is shorter than the actual service life of a mobile phone (Yin et al., 2014). Hence, spent LIBs from CEs constitute a great waste stream, and their amount is expected to grow in the forthcoming years.

Generally, LIBs are composed of a cathode, anode, electrolyte and separator, and contain conducting carbons, polymers and lithium transition metal oxides, such as $LiCoO_2$, $LiMn_2O_4$, $LiNiO_2$,

and LiCo$_x$Mn$_y$Ni$_z$O$_2$ (Zhang et al., 2013). Spent LIBs can be classified as hazardous materials due to the existence of heavy metals, including lead, cobalt, copper, nickel, thallium, and silver (Kang et al., 2013). The leakage of organic electrolytes as well as heavy metals will lead to serious soil contamination if the spent LIBs are directly dumped into landfill (Li et al., 2012). Aside from human toxicity and eco-toxicity, valuable materials in spent LIBs, such as lithium (Zeng and Li, 2013) and cobalt (Zeng and Li, 2015), are worthy to be recycled due to limited natural reserves and ever-increasing demands (Sun et al., 2015). Thus, recycling spent LIBs recycling from CEs is beneficial in improving environmental and social-economic sustainability (Zhang et al., 2013; Zhang and Xu, 2016).

It was estimated that the waste electric and electronic equipments (WEEE) in China grow at a more rapid rate (13–15%) (He et al., 2008) than the world average growth (3–5%) (Rahimifard et al., 2009). In face of ever-increasing amount of WEEE and to create a circular "manufacturing-consumption-recycling" mode (Gu et al., 2016a), multiple legislations and regulations on WEEE management have been proposed by the Chinese government since 2000 (Zhou and Xu, 2012). In October 2003, the Ministry of Environmental Protection (MEP), the National Development and Reform Commission (NDRC), the Ministry of Housing and Urban-Rural Development, the Ministry of Science and Technology, the Ministry of Commerce of China issued *Technical Policy on Pollution Prevention and Control of Spent Batteries* based on *Law of the People's Republic of China on the Prevention and Control of Environmental Pollution by Solid Waste* (MEP, 2006). This technical policy emphasizes on controlling the pollution caused by spent mercury, nickel-cadmium and lead-acid batteries, and the collection of spent LIBs is also included (MEP, 2006). In December 2003, the NDRC launched a national pilot program for WEEE recycling, which included battery recycling plants (Zhou and Xu, 2012). Although there have been several published articles on related subjects, including predicting the generation of spent LIBs (Zeng et al., 2012) and consumer behaviour towards spent battery collection (Sun et al., 2015) and WEEE management (Cao et al., 2016a), there is no published information on the current status of recycling spent LIBs from CEs in China.

This study focuses on investigating the current status of recycling spent LIBs from CEs in China. A combined methodology was employed in this study, which consisted of online surveys, field investigations and estimations. Through this combined study, the status quo of recycling spent LIBs from CEs was rendered, as public perceptions and behaviours were surveyed, collection and disposing practices were investigated, and actual recycling rates were estimated. This paper is organised as follows: the combined methodology is illustrated in Section 2, the results and related discussions are presented in Section 3, and policy implications for improving spent LIB recycling are provided in Section 4, conclusions are given in Section 5.

2. Methodology

2.1. Data sources

The data used in this study were collected from the following data sources: (1) official statistic yearbooks and published reports; (2) online surveys; (3). field investigations. The data was collected from official statistic yearbooks published by the National Bureau of Statistics of China (NBS) and annual reports which were provided by the China Industrial Association of Power Sources (CIAPS), the China branch of *GfK SE Group Co., Ltd* and *Yoboinfo Co., Ltd*, includes the production and sale (trade of second-hand products was not included) statistics of LIBs and related CEs (See Table S1 to Table S3

in Supporting Information, SI). Four major types of LIB are included in this study: laptops and tablet computers, mobile phones, digital cameras and mobile power sources, since their annual production in China were all over 20 M during the past three years. New types of CEs, such as smart bracelets, smart watches and smart glasses were not included due to lack of data.

China is a major destination of illegal global transportation of WEEE (Zeng et al., 2016a), and the actual amount of illegal imported WEEE is impossible to acquire since those activities operate underground. Zeng et al. (2016a) estimated that there was roughly 600,000 t of WEEE imported in 2014 which mainly consisted of CEs, and a decreasing trend of illegal WEEE importation was also forecasted. No valid information was found on illegal importation of spent LIBs, and the importation of spent LIBs has thereby been excluded from this study.

2.2. Questionnaire design

In order to investigate the current status of spent LIBs from CEs, behaviours and attitudes of consumers are essential, thus a questionnaire survey was conducted. Prior to the formal questionnaire survey, a pilot interview-based survey was conducted to facilitate the design of the formal questionnaire (see Table S4 in the SI). The survey was based on a face-to-face interview on a random sample of 200 people. According to the pilot survey, digital cameras are regarded as fixed assets, and they have an almost infinite service life since they are resold rather than discarded. The service life of mobile power sources is equal to generic service life of LIBs. Therefore, the service life of LIBs in digital cameras and mobile power sources is assumed to be 2 y, as Zeng et al. (2012) reported. Replacements of LIBs for related CEs are not considered, since these activities are not properly monitored. In the formal questionnaire, attention was paid to assessing public attitudes on spent LIBs disposal, collection and recycling rather than surveying public awareness of potential environmental impact. To investigate an array of different aspects of the consumers' attitudes and behaviours on LIBs and related CEs for providing credible information for further statistical estimation, the questionnaire consisted of following parts (see Table S5 in SI):

(1). The socio-economic (demographic) information of the respondents;
(2). The ownerships, replacement rates and reasons of the related CEs use LIBs, which mainly refer to laptops, tablet computers, mobile phones, digital cameras and mobile power sources in this study;
(3). The perception, attitude and behaviours towards spent LIBs and related CEs disposal, collection and recycling.

Since this study is set on a national scale, an online method was employed, and it was conducted during July 2016 to Dec 2016. The online method was adopted due to coverage, speed, convenience and efficiency, and it posed no requirement on the availability of interviewers (Duffy et al., 2005). Compared with telephone surveys and face-to-face surveys, online surveys exhibit less social desirability response bias (Duffy et al., 2005). However, the representativeness of an online surveying method has been questioned due to the existence of non-response bias (Evans and Mathur, 2005). Several measures were taken to enhance the representativeness and accuracy of the survey results:

(1). Dissemination of the questionnaire was based on WeChat, a cross-platform instant messaging and social networking integrated service with more than 700 M active users, in which

247

90% are in China (BI, 2016). Mail surveying has been avoided as it can be perceived as junk mail (Evans and Mathur, 2005).

(2). Owing to a higher response rate, a shorter response time and less missing data (Healey, 2007), radio buttons were used in scrolling design of the questionnaire.

(3). Small incentives were used for improving initiative from respondents, thereby reducing selective samples and the related non-response bias (Evans and Mathur, 2005).

(4). Internet protocols (IPs) of the respondents were recorded, and later analysed according with the corresponding regional statistics, and repeated responses from same IP address were excluded.

(5). Post-stratification adjustment was used for correcting possible respondent bias, the weight for each respondent (typically, the inverse of the case's responsing probability) in a weighting cell (or post-stratum) is multiplied by an adjustment factor using the following equation (Holt and Smith, 1979):

$$w_i = \frac{\frac{N_i}{N_{total}}}{\frac{S_i}{S_{total}}} w_i^p \tag{1}$$

where w_i is the post-stratified or adjusted weight, w_i^p is the unadjusted weight, N_i is the population for cell i in total population N_{total}, and S_i is the sample size for cell i in total sample S_{total}. Due to the availability of the data source, demographic information of detailed cells (intersection of the four selected multitudes) is unobtainable. Thus, the product of individual post-stratification adjustment factors was used:

$$w = \prod^i w_i \tag{2}$$

where w_i is the post-stratified weight according to single attribution, and w is the product of all related post-stratified weights. Since individual human behaviour is related to the level of the region's economic development, GDP was used as one of the basis for the post-stratification adjustments for national scale survey (Yin et al., 2014). The locations of the respondents were divided into four categories based on GDP per capita per month (NBS, 2016), as summarised in Table 1.

2.3. Field investigations

According to the definitions given by Cao et al. (2016a), collectors collect WEEE directly from consumers, dismantlers dismantle WEEE into different parts and sell parts to different purchasers, and disposers recycle WEEE. Gu et al. (2016b) divided the WEEE collectors into four categories: peddlers, collection stations, distributors, and middleman. The first three categories are belong to the first-tier of collectors who are directly connected to the consumer, while the middleman belongs to second-tier collectors who gathers the WEEE from first-tier collectors and sells them to disposers (Gu et al., 2016b). With the support of government, large WEEE recycling facilities have been set up in recent years, however, most of which focus only on dismantling (Zhou and Xu, 2012).

Although some battery recycling companies have been identified in previous research (Zhou and Xu, 2012), the materials flow and recycling practices of spent LIBs in China remains unknown. The aims of the field investigation were to fulfill this knowledge gap, and to provide critical information for the related parties, including policy makers, business stakeholders and academic researchers.

From Jan 2015 to Dec 2016, the field investigation consisted of two parts: (1). tracking materials flow of spent LIBs (reverse logistics) and (2). identifying current disposal treatments (material extraction). The first part was carried out in ten major cities in China: Beijing, Shanghai, Guangzhou, Shenzhen, Chongqing, Suzhou, Wuhan, Chengdu, Hangzhou and Ningbo, nine of which are among the top ten cities of annual GDP in China in 2015 (NBS, 2016). The research targets of the first part included peddlers or private traders, second-hand stores, repair stores, collection stations, middlemen and internet-based collection entities. Face-to-face interview was the primary method in the first part of the field investigation, as a short list of questions were used to avoid time pressure upon the respondents (Alreck and Settle, 2004). An observational study was also included in the first part. The second part of the field investigation included interviews of the production managers of two formal spent battery recycling plants in Hubei Province (*GEM High-tech Co., Ltd*) and Hunan Province (*Brunp Co., Ltd*), and an on-site observational study was carried out. Some informal WEEE recycling workshops in two major WEEE recycling areas - Guiyu in Guangdong Province and Taizhou in Zhejiang Province were visited. The "Capital of Battery Industry in China" - Xinxiang in Henan Province was also visited. The study on informal disposers was conducted discreetly and information was extracted tactfully. Examples of questions are listed in Table 2. Despite extensive efforts, only a few interviewed WEEE recycling stakeholders responded to our investigation. Most of the stakeholders in this trade are unwilling to reveal any information, as they do not want to be regulated (Orlins and Guan, 2016). The number of respondents are also presented in Table 2.

2.4. Estimation approach

Generation of WEEE is attributed to products' manufacturing, exportation, and importation, which can be defined by the following equation (Zeng et al., 2016a):

$$T = D + I = P - E + I' + I \tag{3}$$

where T is total WEEE, D is net domestic generation of WEEE, I is imported WEEE, P is domestic product, E is exported product, and I' is imported product. Due to availability of data sources described in Section 2.1 and the applications of LIBs cannot be accurately allocated, statistics of sale S was used and it was assumed that $S = D$. In this study, WEEE referred to spent LIBs and market supply method was employed to predict domestic spent LIBs generation:

$$T_t^D = \sum_{t=2007}^{2020} S_t \cdot n \tag{4}$$

where T_t^D denotes the generation of spent LIBs in year t, n is the

Table 1
Region division of the respondents.

Region	GDP per capita per month (RMB)	Provinces and Municipalities
A	Above 6000	Tianjing, Beijing, Shanghai, Jiangsu, Zhejiang, Inner Mongolia
B	4000–6000	Fujian, Guangdong, Shandong, Liaoning, Chongqing, Jilin, Hubei, Shaanxi
C	3000–4000	Ningxia, Qinghai, Xinjiang, Hainan, Hebei, Hunan, Henan, Heilongjiang, Sichuan, Jiangxi, Anhui, Guangxi, Xizang
D	2000–3000	Shanxi, Guizhou, Yunan, Gansu

Table 2
The methodology of the field investigation.

Segments	Stages	Questions	Respondents
Part I: Reverse logistics investigation	1. Involvement	Are you collecting related CEs? Are you collecting spent LIBs? If yes, what is the throughput?	236 peddlers, 82 CEs second-hand stores, 127 repair stores, 74 collection stations, and 21 middlemen in the ten selected cities.
	2. Treatment	Are you dismantling the CEs? How do you deal with the LIBs from CEs?	
	3. Business	Who is the customers of spent LIBs if any?	
Part II: Material extraction investigation	1. Involvement	Are you dealing with related CEs? Are you dealing with spent LIBs? If yes, what is the throughput?	2 formal spent LIBs recycling plants in Jingmen and Foshan, and an unidentified number of informal WEEE recycling workshops in Guiyu, Taizhou and Xinxiang
	2. Treatment	How do you treat the CEs and LIBs? Can you describe your procedure? What are the major products? What are the pollution control measurements?	
	3. Business	Who is customers of the products?	

average service life of related CEs and S_{t-n} stands for the sales volume of related CEs in year $(t - n)$. The service life n of the related CEs was acquired from the online survey mentioned in Section 2.2. As the average lifespan of LIB was around 2 y (Zeng et al., 2012), therefore the period for this estimation was 2007–2020, as shown in Eq. (4).

Instead of using a linear fitting, a grey model (GM) method was utilised to predict the generation of LIBs and related CEs. GM is a mathematical prediction technique based on limited observed data (Deng, 1989). The generation of spent LIBs can be considered as a grey system, since it has partially known and partially unknown information, which is similar to fast fashion (Choi et al., 2014) and energy consumption (Pao et al., 2012). Grey Verhulst model (GVM) of its original form (Deng, 1989) was used in this study to predict future trends of domestic sale statistics. Typically, GVM is used to predict data of an S-curve pattern with a saturation region (Wang et al., 2009). The statistics over the past four years were used for GVM predictions, which meet the minimum data set required by GM (Deng, 1989). The calculation procedure of GVM was presented in SI.

3. Results and discussion

3.1. Survey results and analysis

The total number of validly returned questionnaires was 810. Excluding all foreign IP addresses, the number of effective questionnaires was 786, thereby the availability rate was 97.0% with an average completion time of 172.2 s. There are three possible reasons behind the high effective rate: (1) a series of small incentives were used to stimulate the participation of WeChat users; (2) the questions were kept short and concise, which would improve the participation and completion of online surveys; and (3) a completion reminder function was employed, as the submit button would not be activated before finishing the questionnaire. According to Leedy and Ormrod (2010), sample size over 400 is acceptable for a large population even for a national scale survey.

3.1.1. Demographic information

The demographic composition of the sample and their post-stratified weights are presented in Table 3, with post-stratification adjustment factors are also presented. Among the 786 effective questionnaires, there was a bias in the sample toward 18–24 y old (39.6%), students (40.1%), low income (0–2000 RMB per month) (41.9%) and rich regions (57.8%) respondents. The demographic composition implies young people had more time and more motivation in completing the questionnaires. 79.4% and 87.1% of respondents of 18–24 y were either students or low-income

earners. In addition, the correlations within demographic composition were checked by Pearson correlation coefficient (PCC) which is a statistical metric measures the strength and direction of a linear relationship between two random variables (Rodgers and Nicewander, 1988). According to PCC analysis, three pairs of demographic variables - age & occupation, age & income and occupation & income showed some moderate correlations with their PCC values of 0.581, 0.475 and 0.452, and no firm link was observed elsewhere. That means no strong bias existed in the questionnaire samples. Due to availability of official data, w_i of each demographic dimension was calculated according to the general population of China in 2014 (NBS, 2016).

3.1.2. Ownerships and replacements

Through the online questionnaire survey, the distributions of ownerships (units per capita) and replacements (service life, measured in y) of the related CEs are presented in Fig. 1 and Fig. 2. Compared to the previous research on Zhejiang Province which belongs to Region A (Cao et al., 2016a), the national-scale average ownerships of laptops & tablet computers, mobile phones and digital cameras obtained in this online questionnaire survey are noticeably less. A slight decrease in ownership statistics after the post-stratification adjustment is found, which indicates the samples lean toward the richer regions. The results confirmed that the effect of regional economic performance on its residents' consumption habits.

The average service life is shorter than previous research (Yin et al., 2014; Cao et al., 2016a), and cause attribute to two possible reasons: (1) value n is selected for calculation of all "n units and above" options; (2) the online questionnaire survey leans towards young people who tend to replace their CEs more frequently. As shown in Fig. 3, malfunction is the primary reason for CE replacements (50.8% unadjusted, 61.1% adjusted), which is comparable with the previous research on mobile phones (Yin et al., 2014). Pursuing new functions and appearances is the second important reason, and its proportion remains unchanged before (23.5%) and after (23.5%) the post-stratification adjustment. The third important reason is that battery degradation shrinks dramatically after the post-stratification adjustment, from 16.0% to 9.2%. This probably resulted from the sample leaning towards youngsters who might spend more time with their CEs. In general, the findings of ownerships and replacements are compatible with previous research (Yin et al., 2014; Cao et al., 2016a), and figures for further estimation were obtained.

3.1.3. Behaviours and attitudes

According to the survey, most the respondents (70.2%) expressed their willingness to sell their spent CEs (Fig. 4 (a)).

Table 3
Demographic composition of the survey sample.

	Number (N_i)	Percentage (%)	W_i
Age			
<18	11	1.4	15.90
20–24	311	39.6	0.20
25–34	248	31.6	0.51
35–50	174	22.1	1.14
>50	42	5.3	4.01
Occupation			
Students[a]	315	40.1	0.38
Enterprise Employees[b]	206	26.2	1.83
Public Servants and Public Institution Employees[c]	135	17.2	0.16
Self Employed[d]	65	8.3	0.70
Other	65	8.3	3.41
Income Per Month (RMB)[e]			
<2000	329	41.9	N/A
2000–4000	134	17.0	N/A
4000–6000	118	15.0	N/A
6000–10000	106	13.5	N/A
>10000	99	12.6	N/A
Region[f]			
A	454	57.8	0.28
B	108	13.7	2.35
C	112	14.2	2.87
D	112	14.2	0.74

[a] Includes elementary schools, middle schools, high schools, universities and career colleges, Ph.D candidates and master students are also included.
[b] Employees exclude government employees and business owners.
[c] Government employees.
[d] Various business owners.
[e] Monthly income distribution data unavailable.
[f] Statistics of permanent population was used, and cases of travel or evection were not considered in this study.
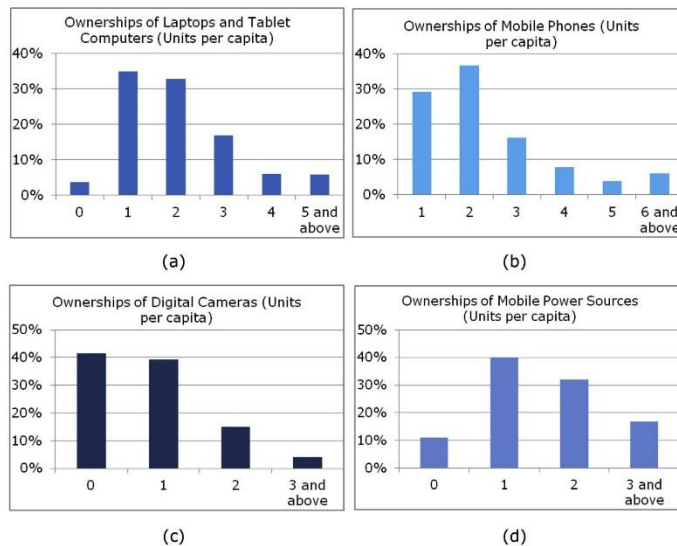
Fig. 1. The ownerships of related CEs: (a) laptops & tablet computers, (b) mobile phones, (c) digital cameras, and (d) mobile power sources.

250
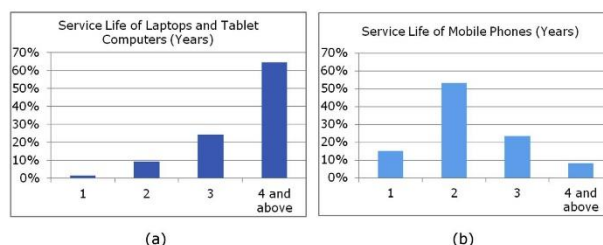
Fig. 2. The service life (replacing rate) of (a) laptops & tablet computers and (b) mobile phones.

However, 83.0% of respondents did not know how to recycle their CEs (Fig. 4 (a)), regardless as their willingness towards recycling. For spent LIBs recycling, the situation is even worse, with 93.8% of respondents not knowing where to dispose of their degraded batteries (Fig. 4 (b)). Despite spent LIBs being listed in the "should-be-collected batteries" by *Technical Policy of Spent Batteries Pollution Prevention and Control* (MEP, 2006), the actual situation indicates an absence of spent LIBs collection system, which will be further confirmed in the following field investigation section.

Through the online questionnaire survey (Fig. 5), 59.6% of respondents stored their spent LIBs at home (in idle), only 29.5% of respondents recycle spent LIBs with the whole CE units or the batteries alone, while 15.9% of respondents directly dump their spent LIBs into trash bins. The idle rate of spent LIBs was found to be higher than other types of batteries (Sun et al., 2015), and this survey confirms this fact. Cao et al. (2016a) found that among various household electric and electronic appliances, CEs had a noticeably higher idle rate, especially of mobile phones. The high idle rate of spent LIBs indicates that most the respondents do care about environmental issues, as suggested by Sun et al. (2015).

To investigate public opinion towards why spent LIBs are not recycled, a multiple choice question was included in the online questionnaire. From the questionnaire survey results, the most common reason is consumers do not know where to send the spent LIBs (65.5%), followed by concern of unexpected privacy disclosure (31.9%) and troublesome procedure (24.6%). In addition, 20.0% of respondents expressed their concern of lack of public awareness on spent LIBs recycling. Sun et al. (2015) speculated that people value the prices of LIBs since they are used in high-tech electronic appliances, and might believe that these spent batteries have a higher

economic value. Therefore, the expected sale price for spent LIBs was also surveyed and the results have been plotted in Fig. 6.

For estimating the current recycling rate of spent LIBs from CEs, the average survey results are summarised in Table 2. In Table 4, there is no significant difference observed between the statistics before and after the post-stratification adjustment, which means no strong bias is found in the surveyed sample. Therefore, the results are valid for the estimation section.

3.2. Current recycling practices

3.2.1. Reverse logistics study

(1). Peddlers or Private Traders

Peddlers or private traders have been identified as one of the most important WEEE recycling entities in China (Orlins and Guan, 2016; Steuer et al., 2017), and also play a vital role in recycling spent batteries (Sun et al., 2015). They are located in populated urban residential areas and running their business without a license (Cao et al., 2016a). They have no aware of the potential risks linked with informal recycling, and they also know little about legislation or policy and are unwilling to be regulated (Orlins and Guan, 2016). Most of the interview peddlers are migrant workers (96.2%), the constitution is as similar as reported by Orlins and Guan (2016). All interviewed peddlers purchase and collect spent laptops, tablet computers and mobile phones, which are compatible with previous research (Cao et al., 2016a). They know that the printed circuit boards (PCBs) of spent laptops, tablet computers and mobile phones contain precious gold and valuable copper, and can be sold
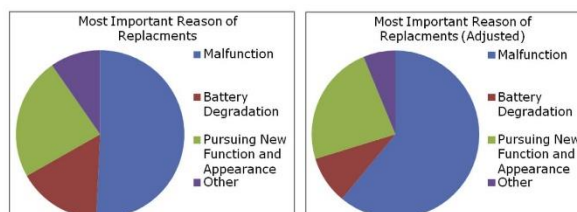

Fig. 3. The most important reason behinds CE replacements: (a) Before post-stratification adjustment and (b) after post-stratification adjustment.
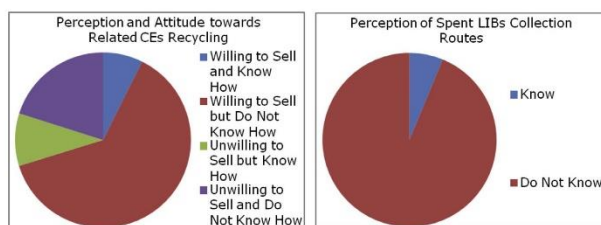
251

Fig. 4. (a) Perception and attitude toward related CEs recycling, and (b) perception of collection routes that aims at LIBs recycling.
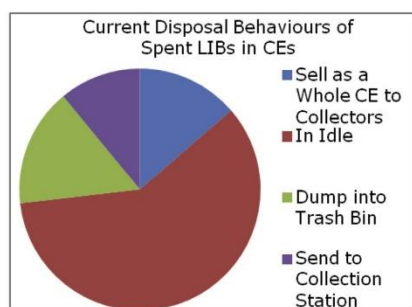

Fig. 5. Current disposal behaviours of spent LIBs in CEs.

to various buyers including second-hand stores, collection stations, middlemen, and formal or informal disposers. Few people are willing to purchase or collect digital cameras and mobile power sources, since the suitable prices and the potential buyer for these CEs are unknown to these peddlers. In addition, 36.9% of the interviewees have experience in dealing with digital cameras. Although all of the interviewed peddlers have handled over spent LIBs during their career, no one is willing to pay the prices for spent

Fig. 6. Expected sale price for spent LIBs.

LIBs, unless there exists a certain buyer who asks them to collect these batteries and pays a decent fee. Around 80% of the interviewed peddlers have dismantled the collected CEs to get PCBs, but usually they prefer selling the CEs directly rather than dismantling. Batteries, including LIBs, are stored after dismantling. However, if no suitable buyer is located, the peddlers would dump the batteries.

(2). Second-hand Stores

Traditional second-hand stores are located in second-hand markets (Cao et al., 2016a). There are some traditional second-hand stores which focus on CEs only, where all the four LIBs related CEs can be found. Typically, the second-hand CEs are collected from local residents, peddlers, middlemen, repair stores, retailers and even manufacturers. The received goods are firstly checked, followed by basic repair, and then are resold. Check and change of batteries is included in the basic repair process, and spent LIBs are either discarded right away or temporally stored till someone buys them. For malfunctioned CEs, there is an attempt to claim useable components, such as LIBs, lens, mice, hard drives and memory-chips, and sell the rest to peddlers, middlemen or directly to disposers. All the visited second-hand stores do not collect LIBs on purpose, only some of them would store some useable LIBs from malfunction CEs of popular models for potential repair works. There are two major reasons of not collecting spent LIBs: (1) difficult for these small business owners to evaluate the remaining capacity, thus suitable price is impossible to determine; (2) certain LIBs only have limited applications, different CEs have different LIBs.

Another type of second-hand store is online trading platform, typical examples including Xianyu (2.taobao.com), Ganji (www.ganji.com), and 58 (www.58.com). They all adopt a customer to customer mode, as anyone has an authenticated account can sell or purchase second-hand EEEs online, and no CEs or LIBs are collected by the websites themselves. All the CEs can be found in these websites. The sellers have to guarantee the quality of second-hand CEs, as credit systems are incorporated in these online trading platforms.

(3). Repair Stores

Repair stores for CEs are usually located at clustered electronic markets in populated urban residential areas, such as Zhongguan-cun in Beijing, Qiujiang Rd in Shanghai, Huaqiang North in Shenzhen, Town God's Temple in Chengdu, Eutaw Street in Guangzhou. All the visited repair stores sell new and second-hand products at the same time when repair them. The typical business objects are laptops, tablet computers and mobile phones. Among
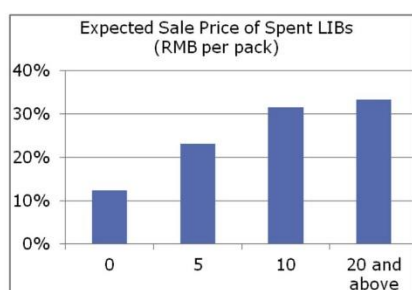
Table 4
Average survey results (Ownerships, replacements and expected sale price for spent LIB) before and after post-stratification adjustment.

		Before post-stratification	After post-stratification
Ownerships (Units)[a]	Laptops and Tablet Computers	2.04	1.89
	Mobile Phones	2.38	2.33
	Digital Cameras	0.82	0.77
	Mobile Power Sources	1.55	1.40
Replacements (Years)[b]	Laptops and Tablet Computers	3.52	3.44
	Mobile Phones	2.25	2.28
Expected collection price for spent LIBs (RMB per pack)[c]		14.27	13.92

[a] For the option of "*n* units and above", the value *n* was used in calculation.
[b] For the option of "*n* y and above", the value *n* was used in calculation.
[c] For the option of "*n* y and above", the value *n* was used in calculation.

these CEs, mobile phones are the most frequently repaired items, and the typical repair activities including changing broken display units and dried batteries. According to the interviews with owners of repair stores, digital cameras are too expensive and delicate, and all famous brands have after sales service stations in major cities. For mobile power sources, the major cause of failure is battery degradation, and the repair stores usually can do nothing about it. Over 70% of the 127 visited repair stores have dismantled malfunctioned CEs for reclaiming the valuable components, such as PCBs. Normally, they collect neither CEs nor LIBs on their own initiative. Spent LIBs are treated same as other low value or damaged components, either discarded or temporally stored.

(4). Collection Stations

There are two types of WEEE collection stations in China: ones established by local governments and ones established by the private sector which including companies, organisations and foundations. In this field investigation, 71 out of 74 visited collection stations are private. All of the visited collection stations deal with the related CEs, and their shipments are highly unstable ranging from 0 to 50 packs of CEs per d per station. Classification takes place in these collection stations, and there exists a fixed channel for almost every piece of WEEE. According to the interviews with the managers, these WEEE collection stations lean towards collecting WEEE with subsidies and valuable copper-rich components (e.g. PCBs), since these items represent higher economic value and it is easy to attract buyers. The "*Administrative Measure on Tax Levy and Use for WEEE Recycling*" set the amounts of subsidy for the following WEEEs: television (85 RMB per unit), refrigerator (80 RMB per unit), washing machine (35 RMB per unit), air conditioner (35 RMB per unit), and microcomputer (personal computer, PC, 85 RMB per unit) (CPG, 2012). The collected WEEE are usually sold to secondhand stores, middlemen, and formal or informal disposers. Although collecting LIBs is emphasized in *Technical Policy of Spent Batteries Pollution Prevention and Control* (MEP, 2006), no collection station intentionally collects spent LIBs. Most of the visited collection stations just dump these batteries or send them to landfill, while few of them manage to sell the spent LIBs to some disposers. "LIBs are worthless items, we do not waste time and money to collect these things", said by some managers of WEEE collection stations.

(5). Middlemen

All interviewed middlemen were self-employed and operating without licenses. WEEE is just a part of their business, for they would purchase anything with economic value from peddlers or collection stations, such as copper wires, cardboard boxes and soda cans, and resell them to various disposers. Concerning WEEE, only valuable products and components are purchased by these interest driven merchants, which including PCBs, PCs, televisions and refrigerators. The collecting targets of middlemen are similar to the targets of the WEEE collection stations. All of the interviewed middlemen collect laptops, tablet computers and mobile phones, since the value of these CEs are already known to them. Other CEs, including digital cameras and mobile power sources, do not appeared in their purchase list, as well as spent LIBs. There are two prerequisites for selecting merchandise: 1) economic value and 2) quantity available. According to the interviewed middlemen, spent LIBs meet none of these prerequisites, since no one is willing pay a price and very few people collect them.

(6). Internet-based Collection Entities

Aiming at enormous market potential of WEEE in China, several internet-based collection entities have been founded during recent years. The typical example is - *Aihuishou* (Chinese phonics, means "love recycling"), the largest internet-based WEEE collection company in China. The company was founded in 2010 as an online exchange platform, and turned to collect WEEE in 2011. *Aihuishou* got series A round investment of 2 M USD from Chenxing Capital in 2012, have received series B round investment of 8 M USD from International Finance Corporation and *Chenxing Capital* in 2014, and received series C round investment of 60 M USD from *Tiantu Capital, Jingdong Group Co., Ltd, Jinglin Capital* and *GEM High-tech Co., Ltd.* in 2015. From 2013, *Aihuishou* opened a series of outlets for purchasing and reselling WEEE, and a basic repair service is also provided, including change of batteries. There are three routes for consumers sending their unwanted EEEs to *Aihuishou*: 1). By mail; 2). Door-to-door collection; 3). Outlets. Over 50% of deals done in the *Aihuishou* outlets, "only 40% of consumers are willing to mail their EEEs, only 60–70% mailed goods are consistent with their description, and many invisible costs are generated by mail, including communication and loss of reputation" said by Xuefeng Chen, the CEO of *Aihuishou* (Chinese Entrepreneurs, 2016). On the website (www.aihuishou.com/), the maximum take-back prices for each EEE product mode have been listed. The purchase list includes CEs, such as laptops, tablet computers, mobile phones and digital cameras, and household electric appliances, such as televisions, refrigerators, washing machines and air conditioners. According to the manager of an *Aihuishou* outlet near Wukesong Stadium in Beijing, Aihuishou lean towards certain CEs, especially mobile phones, which is also confirmed by its CEO's interview (Chinese Entrepreneurs, 2016). Ordinary intake of an outlet is around 10–20 units of CEs per d, and this figure is affected by the launch of new products from famous brands. On the 18th September 2016, the day the iPhone 7 launched on the market, *Aihuishou* received over 25,000 sale requests (Chinese Entrepreneurs, 2016), and the outlet received over one hundred mobile phones. *Aihuishou* sell the collected items to various parties via a price bidding system, around 30% mobile phones go to disposers while the others are sold as

second-hand goods (Chinese Entrepreneurs, 2016). There is no explicit policy or practice on treating spent LIBs from mobile phones and other CEs, according to the manager of the outlet. The spent LIBs are temporally stored until someone come to collect them.

Huishouge (Chinese phonics, means "recycling guy") is another internet-based WEEE collection company, founded by *GEM High-tech Co., Ltd*. Rather than second-hand trading, *Huishouge* focuses on collecting WEEE for fulfilling the production capacity of its parent company - *GEM High-tech Co., Ltd* (Chinese Brands, 2015). After placing recycling requests on the mobile phone application, its offline team will come and collect the waste. Many peddlers and other WEEE collectors have joined the offline team of this O2O platform due to the higher service fee paid by *Huishouge*, as their monthly income can be increased to 6000 RMB (Chinese Brands, 2015) which is much higher than their current income level - 1200 RMB per month (Steuer et al., 2017). "By removing intermediate links of WEEE reverse logistics, a high service fee is sustainable and the total operating cost is lower", said by Yuping Zhang, the general manager of *Huishouge* (Chinese Brands, 2015). *Huishouge* initiated its operation in four cities in 2015: Wuhan, Shenzhen, Jingmen, and Tianjin (Chinese Brands, 2015). Spent LIBs from CEs are included in the targets of *Huishouge*, but their collecting prices are next to nothing as only reward points are gained, which is far below the expected price in the online survey (Table 4).

Other internet-based WEEE collection entities, such as *Gecko Recycling*, *Taofeibao* (Chinese phonics, means "search for goods in wastes"), *Huishoubao* (Chinese phonics, means "recycling goods"), *Huanqianhuishou* (Chinese phonics, means "recycling for money"), and *Sound Recycling Union*, are also investigated during this study. Their targets are similar to *Aihuishou*, and spent LIBs from CEs are not included in any of these internet-based collection entities.

To sum up, although WEEE reverse logistics systems are well-established in China (Cao et al., 2016a; Steuer et al., 2017), spent LIBs from CEs are not generally included within this system. The current WEEE reverse logistics systems are purely driven by economic interests, the stakeholders focus on collecting valuable items, such as televisions, refrigerators, washing machines, air conditioners, computers, mobile phones and PCBs. Spent LIBs from CEs are generally considered to be low-value or no-value items, for they not only present a low economic value but also their potential buyers are difficult to be identified, thus, these LIBs always end up in trash bins or landfill. *Huishouge*, an O2O WEEE collection company launched by a formal battery disposer - *GEM High-tech Co., Ltd*, is the only entity found to be collecting spent LIBs. Absence of spent LIBs collection system was confirmed, and it is actually an absence of public service, especially in case of WEEE collection stations. The Extended Producer Responsibility (EPR) principle is used in the EU for spent battery management, and it has been proposed in China (Sun et al., 2015). However, a long period and low efficiency on subsidies audits of EPR in China (Cao et al., 2016b) would severely hinder its application in spent LIBs management.

3.2.2. Recycling practices

(1). Formal Disposers

Among hundreds of formal WEEE recycling plants in China, there are only a few dealing with spent batteries, as Zhou and Xu (2012) reported. Currently, most of the formal battery recycling plants focus on recovering lead from lead-acid batteries. According to China Environment News (CEN, 2016), there are already 28 licensed disposers of lead-acid battery recycling in Zhejiang Province alone. Hence, according to the registration information provided by NDRC, there is no formal LIB recycling plant exists in Zhejiang Province. *GEM High-tech Co., Ltd* and *Brunp Co., Ltd* are the only existing formal LIB disposers in China, information obtained from the field investigation is summarised in Table 5.
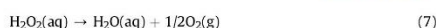
According to the interviews with production managers of both the plants (*GEM* and *Brunp*), similar procedures are employed for recycling lithium batteries (including LIBs), as indicated in Table 5. Their pretreatment processes are conventional, and a sulfuric acid leaching based hydrometallurgy process is used as the core process for material extraction. Sulfuric acid and hydrogen peroxide solution are used as the main lixiviant, which are efficient in recovering cobalt and nickel in LIBs (Gratz et al., 2014). The leaching reaction of $LiCoO_2$ in sulfuric acid and hydrogen peroxide solution is described as follows (Ferreira et al., 2009; Zhu et al., 2012):

$$2LiCoO_2(s) + 3H_2SO_4(aq) + H_2O_2(aq) \rightarrow 2CoSO_4(aq) + Li_2SO_4(aq) + 4H_2O(g) + O_2(g) \tag{5}$$
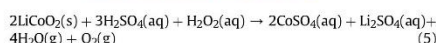
Higher concentrations of hydrogen peroxide has a positive impact on the leaching of both cobalt and lithium (Zhu et al., 2012), as indicated by the following equation:

$$LiCoO_2(s) + 3H^+(aq) + H_2O_2(aq) \rightarrow Co^{2+}(aq) + Li^+(aq) + 3/2H_2O(aq) + 1/4O_2(g) \tag{6}$$
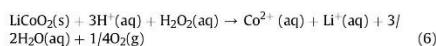
However, hydrogen peroxide will decompose (Zhu et al., 2012).

$$H_2O_2(aq) \rightarrow H_2O(aq) + 1/2O_2(g) \tag{7}$$

In both plants, the solution after leaching process is then neutralised and evaporated, and the desirable salts are precipitated. High evaporation rate of water leads to high crystallisation rate of metals, especially cobalt (Ferreira et al., 2009). In general, their procedures are similar to Gratz et al. (2014) and Zheng et al. (2017), as the sulfuric acid and hydrogen peroxide solution is used, and ternary cathode materials are re-synthesised and sold as major products for battery manufacturers. The major products and recycling procedures indicate that these plants lean toward recovery cobalt and nickel from spent batteries since the metals represent a higher economic value. However, this economic incentive of recycling spent LIBs is diminishing, as the battery developers and manufacturers are turning to replace cobalt with less expensive, lower human toxicity, and more environmentally friendly materials, such as iron and manganese (Wang et al., 2014). The process is not the suitable method to recycle these types of LIBs due to the recycling efficiencies for both iron and manganese based LIBs are lower than cobalt based LIBs (Wang et al., 2014). From the view point of material sustainability, recycling of lithium should be emphasized.

Pollution control facilities are installed in both plants. In 2015, *GEM High-tech Co., Ltd* has invested 22.56 M RMB to upgrade the pollution control facilities of its WEEE recycling plants in Jingmen, including the battery recycling plant. Through improving the wastewater treatment procedure, the throughput of cobalt and nickel has increased by 250 t per y. Ventilation systems are installed and personal protection equipments are used, as pollutants will be released during the mechanical pretreatment (Li et al., 2016b). However, the acid leaching process contributes a most significant part in the total environmental impacts of a hydrometallurgical WEEE recycling plant (Iannicelli-Zubiani et al., 2017). Therefore, reducing the amount of acid used can improve the environmental performance of the recycling plants.

The production managers of both the plants have expressed the same concern: insufficient sources of spent LIBs, which is similar to formal lead-acid battery recycling (CEN, 2016). Lack of collection schemes and policy support are the main reasons behind the spent

254

Table 5
General information of investigated formal spent LIBs recycling plants.

		GEM High-tech Co., Ltd	Brunp Co., Ltd
General Information	Plant Location	Jingmen, Hubei Province	Changsha, Hunan Province
	Year of Battery Recycling Plant Establishment	2004	2008
Production Information	Designed Capacity of Battery Recycling	300,000 t per y	20,000 t per y
	Actual Throughput of Battery Recycling	100,000 t per y	20,000 t per y
	Actual Throughput of Lithium Battery Recycling	25,000–30,000 t per y	10,000 t
	Actual Throughput of LIB Recycling	N/A	6000 t
	Sources of LIB	Mainly from its collection system which acquiring spent LIBs from consumers	Majority is rejected products from LIB manufacturers and a few from WEEE collectors
	Major Products	3000 t of cobalt - nickel powder per y, cobaltosic oxide, cobalt and nickle sulfate, cobalt carbonate, cobalt chloride, cobalt oxalate and spherical cobalt hydroxide	$Ni_xCo_yMn_z$ and their hydroxides, total production of 4500 t per y
Processing Information	Pretreatment	Dismantling, shredding and separation	Dismantling, shredding and separation
	Core Process	Hydrometallurgy	Hydrometallurgy
	Major Chemicals Involved	Sulfuric acid and hydrogen peroxide	Sulfuric acid and hydrogen peroxide

battery collection problem, as discussed previously (Sun et al., 2015). The battery recycling plant of *GEM High-tech Co., Ltd* deals with different types of spent batteries, and relies heavily on its WEEE collection system. *GEM High-tech Co., Ltd* have set up an extensive WEEE collection network by cooperation with local governments, communities, schools, universities, collection stations, electronic markets and waste recycling markets. In 2015, *GEM High-tech Co., Ltd* founded *Huishouge*, and has invested in *Aihuishou*. Despite all the effort in setting up spent battery collection system, full designed capacity of the *GEM* plant still has not been reached, and the plant is continuously operating at the breakeven point. Realising the current situation, the *Brunp* plant focuses on rejected products and other related industrial wastes from LIB manufacturers, while spent batteries from traditional WEEE collection systems are regarded as supplements. "The industrial wastes are far more stable than spent batteries collected via WEEE collection system, in both quantity and quality", said Mr. Yannan Ou, the production manager of the *Brunp* plant. Thus, the *Brunp* plant is running at its full capacity and above the breakeven point. In addition, the lack of sorting has been identified as the second most important issue regarding spent LIBs recycling, and recycling would be greatly enhanced if the batteries are properly labelled and sorted after collection (Wang et al., 2014).

(2). Informal Disposers

During recent years, due to improved legislation, stricter enforcement and increased labour cost, and decreasing WEEE importation which results in diminishing source of supply (Zeng et al., 2016a), countless informal WEEE recycling plants or workshops have been shutdown in Guiyu and Taizhou, or have moved to hinterland provinces where battery manufacturers are located. For most of the visited informal WEEE recycling plants or workshops, copper-rich WEEE, especially PCBs are still their primary targets. Precious metals (gold, silver and copper) and a simplified toxic recycling procedure can sustain the profit and the higher collection fee paid to consumers. Only a very limited number of informal battery disposers could be found. Lead-acid batteries from electric vehicles or bicycles are more preferable, since the recycling procedure (smelting) is much more simple, requires less investment, and the supply chain of spent lead-acid batteries is more stable, as sources and buyers are easy to locate. Similar to formal disposers, there are only handful informal disposers recycling spent lithium batteries.

An informal disposer in Xinxiang presents a typical example of informal spent lithium battery recycling. The plant deals only with cylindrical lithium batteries and Ni-MH batteries at a quantity of 200–300 t per month. The choice of objects is based on sources of supply and values of metals contained. The cost and the net profit of disposing one t of mixed spent batteries are 1500 RMB and 2000 RMB, respectively. The material recovery procedure consists of dismantling and smelting processes. Due to the limitations of the procedure employed, the plant cannot treat any LIBs which have aluminum foils or shells, thus most of the spent LIBs from CEs are either rejected or discarded. Prices of spent batteries are related to the metal contents, ranging from 1000 RMB per t to 8000 RMB per t, thereby the calculated actual collection price for one spent lithium battery is less than 1 RMB, which is also far below the expected collection price (Table 4). Compared to the collection price in *Huishouge*, the informal disposer can afford a higher collection price, which compatible with previous literature (Li et al., 2016a).

3.3. Estimation results

Before conducting GVM based forecasting, a fitting trial was carried out for verifying the availability of GVM. The results indicated a good correlation, as small variations are observed in Table S6 in SI. Therefore, GVM can be validly applied in forecasting future sale volumes of related CEs, and the results are presented in Table S7. For estimating the weight of spent LIBs from CEs, around 500 LIB samples (see Fig. S1 in SI) which used in related CEs were collected from peddlers, second-hand stores, repair stores and middlemen. Then the samples were weighted using a digital balance, and the average values are presented in Table S9. Major brands were included in this study, such as *Apple, Samsung, OPPO, Huawei, Xiaomi, Nokia, Sony* and *Canon*. Based on the historical sale volumes (Table S3), the forecasted sale volumes (Table S7), the surveyed service life (Table S4) and the average weight (Table S8), the accumulative amounts of spent LIBs from CEs are estimated using Eq. (4). The accumulative sums and the accumulative weights of spent LIBs from CEs are presented in Table S9 and Table S10, respectively, and the results are plotted in Fig. 7. Fig. 7 shows that mobile phones contribute most spent LIB units, while mobile power sources contribute the largest proportion of total weight of spent LIBs from CEs.

According to Table 5, the total throughput of lithium battery recycling in the two formal recycling plants was around 35,000 to 40,000 t per y, and less than 50% of the lithium batteries for recycling are LIBs from CEs. Thus, similar to the situation in the US (Wang et al., 2014), the current collection and recycling rate of spent LIBs from CEs in China is less than 10%, or even less than 5%. Due to increasing demands from the LIBs used in EV sector, the
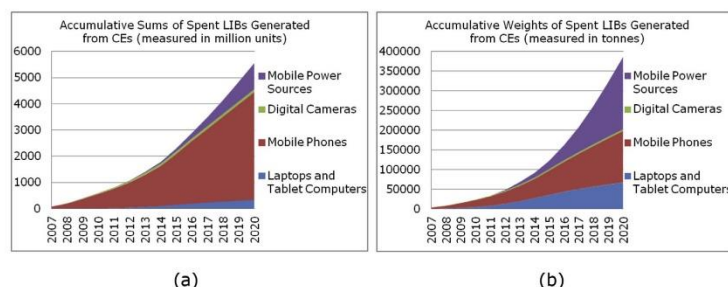
Fig. 7. Estimated accumulative amounts of spent LIBs generated from related CEs: (a). Accumulative sums and (b). Accumulative weights.

recycling rate should be 90% in 2020 (Zeng and Li, 2013, 2015).

3.4. Shortcomings

The results of the three essential parts in the combined methodology are presented and discussed in Section 3.1, Section 3.2 and Section 3.3, respectively. The major existing shortcomings of current recycling system are identified as follows:

(1). An intention-behaviour gap is found in the results of the online survey, as most of respondents are willing to recycle their spent LIBs but do not know how to dispose them, which results in a high idle rate.
(2). Spent LIBs from CEs are not generally included in the present WEEE collection system due to low profitability which resulted from low value metal contents and few identified buyers, while lack of supply is the major concern of disposers.
(3). Current formal recycling processes for disposing spent LIBs focus on valuable metals such as cobalt and nickel primarily and are not suitable for processing new environmentally friendly LIBs which based on iron and manganese, and separation of aluminum is impossible for informal disposers.

As a result, the current recycling rate of LIBs is very low, which is far from the expected target for achieving resource sustainability (Zeng and Li, 2013, 2015). Through this investigation, absence of corresponding collection system is the bottleneck in recycling spent LIBs from CEs, as the general public do not know where to send their spent LIBs, current WEEE collection systems lack of motivation to collect spent LIBs, and battery disposal plants do not get sufficient sources of supply. The processes employed by LIBs' disposers also show limitations in recovering certain metals including lithium. To establish an effective collection and recycling system, improvements in legislation, infrastructure, technologies and education are desirable, and detailed recommendations are presented in the following section.

4. Policy implications

Recycling spent LIBs from CEs is essential for achieving material sustainability and creating a circular economy. To promote recycling rate of spent LIBs from CEs, the following recommendations are proposed based on the analysis of shortcomings.

4.1. Improving legislation

Legislation plays an important role in WEEE management (Zhou and Xu, 2012). In 2003, the first edition of *Technical Policy of Spent Batteries Pollution Prevention and Control* was issued (Sun et al., 2015). A series of laws were subsequently released, includes the second edition of *Technical Policy of Spent Batteries Pollution Prevention and Control* which included collection of spent LIBs (MEP, 2006). Currently, the battery recycling laws and policies mostly focus on controlling batteries which contain cadmium, lead, mercury and zinc, as emissions from production are strictly regulated, informal disposers are banned and pilot recycling plants have been established (Tian et al., 2014). Little attention has been paid on recycling LIBs from CEs, as no explicit legal provision can be found and the only existing pilot LIBs recycling plant is focusing on recycling spent LIBs from EVs (ChinaNEV, 2016). Though collection of spent LIBs is encouraged by *Technical Policy of Spent Batteries Pollution Prevention and Control*, legislation improvement is highly required and it is a first step for promoting the recycling rate of spent LIBs from CEs. Based on analysis of current practices, laws and policies should be improved in the following aspects.

(1). Mandatory Labelling

Besides capacity and safety notes, LIBs should be properly labelled according to their material contents, to facilitate recycling. The label is particularly useful for sorting and disposing after collection, as suitable procedures can be selected and higher material recovery rate can be achieved. Also, spent LIBs should be legally classified as hazardous wastes, since they contain heavy metals, such as cobalt, copper and nickel (Kang et al., 2013), and toxic organic electrolytes (Li et al., 2012).

(2). Setting Targets

Targets should be set on collection and recycling of spent LIBs from CEs for enhancing resource efficiency and sustainability, especially when facing a rapid growth of lithium and cobalt demand brought by growing EV production (Zeng and Li, 2013, 2015). These targets can be used as a key performance indicators for monitoring and evaluating the performance of stakeholders, especially licensed ones, and policies and investments can be accurately allocated.

(3). Lifecycle Regulation

256

Proper safeguards should be enforced legally during the whole lifecycle of LIBs, from cradle to grave, as LIBs contain both resources and hazards. Treatments of spent LIBs should be strictly regulated as other types of hazardous WEEEs, since landfill will result in leakage of heavy metals and organic electrolytes (Li et al., 2012; Kang et al., 2013), dismantling, direct shredding or smelting will cause fire (Lisbona and Snee, 2011) and toxic gases will therefore be released (Lisbona and Snee, 2011). Recycling practices of formal disposing (the *GEM* plant and the *Brunp* plant) are compatible with current laws and regulations, as pollution control measurements and PPE are used for operators. However, the amount of formally recycled spent LIBs only consist a very limited proportion of the waste generated, while most spent LIBs from CEs end up in landfill. Therefore, regulation on the whole lifecycle of LIBs is highly essential, and should be included in legal systems.

(4). Facilitating Collection

Fiscal policy should be allocated to establish more non-profit WEEE collection stations for collecting spent LIBs from CEs, and these stations should be made accessible to local residents, peddlers, second-hand stores and repair stores. According to the field investigation, the whole WEEE collection system is purely driven by economic interests. Since spent LIBs from CEs are regarded as low-value or no-value items, a very few WEEE recycling practitioners are willing to collect them. Therefore, establishment of non-profit WEEE collection stations would fill the vacancy, and the responsibility of spent LIBs collection could be clarified. Besides, current subsidies on WEEE recycling are difficult to apply (Zeng et al., 2016b) and to audit (Cao et al., 2016b).

(5). Mandatory Education

Education on proper spent LIBs disposal should be legally mandatory to both the general public and the recycling stakeholders, with the purpose of making the public understand the potential hazards and proper disposal routes of spent LIBs used in CEs. Education to the general public is emphasized by Sun et al. (2015), since consumers play a crucial role in WEEE collection. Instructions or illustrations on battery disposal should be mandatorily included in the user manuals of the CEs. Notices, slogans and posters should be posted in residential areas, for guiding stakeholders to practice spent LIBs recycling properly.

4.2. Upgrading infrastructures

According to the field investigation described above, collection of spent LIBs from CEs is not included in the current profit-oriented WEEE collection system. As a result, 93.8% of surveyed respondents did not know where to dispose their spent LIBs. Availability and proximity (geographic distance) to waste collection sites are among the key factors in consumers' disposal behaviours (Wagner et al., 2013).

Establishment of non-profit state-owned WEEE collection stations is a potential solution. To avoid potential fluid leakage, flammability, and other hazards, Sun et al. (2015) suggested that a retail take-back scheme which might be more effective and environmental-friendly compared to curbside collection containers. However, the consumers are not the only group of people who have spent LIBs to be disposed, as spent LIBs accumulated during the daily activities of peddlers, second-hand stores and repair stores, have to be disposed properly. Thus, centralised non-profit WEEE collection stations are highly needed. For the convenience of both the consumers and the practitioners, clustered electronic markets in populated urban residential areas are the

perfect locations for these collection stations. Explicit instructions and signs should be made available and noticeable to all the stakeholders within a certain radius. To store a large amount of spent LIBs from CEs, facilities should be constructed to a high safety standard, safety measurements should be implemented and safety education should be mandatory to any stakeholder. In addition, curbside collection containers are still required in other populated areas, such as central business districts, schools and universities.

The collected batteries should be shipped to related formal disposers without charging. If a bidding system is used, the non-profit collection stations will turn to a profit-oriented operating model, which only focus on collecting high value WEEE. It can also be considered as a fiscal policy to foster formal disposers, as the government takes part in solving the problem of insufficient sources and covers the collection cost. Compared to the current "tax-subsidy" fiscal policy in WEEE management (Cao et al., 2016b; Zeng et al., 2016b), spent LIB collection carried out by governments can greatly improve the overall efficiency, as long and low efficient subsidies apply and the audit procedure can be avoided, and cheating for subsidies also can be diminished.

4.3. Fostering technologies

Technologies play an important role in spent LIBs recycling. The technologies involved can be divided into two segments: (1). Material recovery technologies to promote environmental and economic sustainability; (2). Information technologies to monitor, evaluate and improve the whole spent LIBs recycling system.

4.3.1. Material recovering technologies

According to the field investigation, cobalt and nickel are favourable to the LIBs both formal and informal disposers due to their economic values. However, a 90% lithium recovering rate is desirable in the future due to demand triggered by increasing production of EVs (Zeng and Li, 2013). During manufacturing of LIBs, production of lithium and its compounds contribute the largest proportion of total carbon footprints (Wang et al., 2016a). An extended range of recovered materials would increase the economic profit, which could fundamentally change the status of spent battery collection and recycling (Sun et al., 2015). Currently, hydrometallurgy processes are employed by formal battery disposers as the core process of material extraction, and sulfuric acid is used as the major lixiviant for both the interviewed formal disposers. Although sulfuric acid is more environmental-friendly compared to hydrochloric acid and nitric acid (Jian et al., 2012), further improvements are still needed due to the huge environmental impacts associated with the use of acid (Iannicelli-Zubiani et al., 2017). Further development of LIBs also proposes a challenge to material extraction process, as iron and manganese are more frequently used in LIBs (Wang et al., 2014). Based on the analysis of current disposal practices, there are three aspects require further attention to achieve sustainable recycling: (1) efficient separation to reduce acid usage; (2) selective leaching to achieve effective separation; (3) extending coverage of materials.

During recent years, lots of academics paid attention to developing novel approaches for recovering materials from spent LIBs. Based on the previous discussion, a brief review of existing literature has been conducted, and some promising technologies are selected according the three identified aspects, as summarised in Table 6. Although certain improvements in the desirable aspects have been reported, these methods still need for further attention before industrialisation, as their limitations are also identified and listed in Table 6. Therefore, further research should be encouraged, funds should be invested, and cooperation between academic and industry should be intensified.

Table 6
Promising technologies for improving material recovery technologies.

Reference	Description	Findings	Limitations
Hanisch et al. (2015)	Thermal decomposition of the binder followed by air-jet-separation	97.1% of the electrode coating can be regained with 0.1% of aluminum impurities from foils	Calcination of the binder requires extra treatment
Wang et al. (2016b)	Co-grinding lithium cobalt oxide with additives for separation of lithium and cobalt	Ethylene diamine tetraacetic acid (EDTA) is found to be the suitable additive, and empty orbit of lithium and cobalt is filled by atoms of EDTA	Ball milling and long milling period (4 h) are barriers for industrialisation
Wang et al. (2016c)	Enriching metallic content by shredding and size-based separation	Cobalt is concentrated in ultrafine and fine fractions, while copper and nickel are enriched in large pieces	Released air pollutants need treatment
Zeng et al. (2015)	Recovering cobalt and lithium from spent LIBs using oxalic acid	Without using hydrogen peroxide, and leaching and precipitation are carried out synchronously	Purification needed due to coexistence of products
Chen et al. (2016)	Using citric acid and d-glucose to achieve selective metal recovery	96%, 97% and 93% of nickel, cobalt and lithium are recovered, and citric acid can be reused up to 5 times	Low pulp density and high reductant dosage
Chen et al. (2017)	Phosphoric acid and hydrogen peroxide are used for leaching	Over 99% cobalt and lithium are leached and separated in a single leaching step	Precipitation needed for lithium ions in the solution
Ku et al. (2016)	Reductive ammonia leaching using ammonia, ammonium sulfite and ammonium carbonate	Cobalt, nickel and copper are fully leached out selectively, while manganese and aluminium are hardly leached	Lithium is neglected in the procedure
Zheng et al. (2017)	Reductive ammonia leaching of metals from spent LIBs	Nickel, cobalt and lithium are selectively leached, their selectivity in the final solution is over 98%	Low pulp density and long leaching period
Horeh et al. (2016)	Fungal bioleaching of spent LIBs using *Aspergillus niger* produce citric acid	Fungal bioleaching extend the list of target metals and their leaching rates compared to other bioleaching	Extra long leaching period compared to acid leaching

4.3.2. Information management technologies

Management Information Systems (MIS) are one of the prerequisites for WEEE disposers to gain the subsidy from the Chinese government (Cao et al., 2016b), and it provides a solution to subsidies audit problem (Cao et al., 2016b). However, the current WEEE collection systems, which mainly consist of informal collectors, traders and disposers is remained unmonitored, and these informal practitioners are unwilling to be regulated (Orlins and Guan, 2016).

Implementation and construction of an integrated MIS with the assistance of barcode technology to cover the life cycle of LIBs could be a potential solution to the spent LIBs management problem. During production of LIBs, every piece of the battery should be properly labelled with a unique code to illustrate its specifications, such as metal contents and potential hazards. Radio Frequency IDentification (RFID) is not preferable in case of LIB, since its cost (3–5 RMB) and could be higher than the direct manufacturing cost of battery itself. In this case, quick response (QR) codes which a type of matrix barcode and an optically machine-readable label (Wang and Wang, 2014), can be implemented to improve LIB tracking in a distributed consuming and recycling environment. The QR tags are particularly suitable for CEs (Wang and Wang, 2014). Thus, the reserve logistics system of spent LIBs from CEs can be clarified, since every piece of LIB is effectively monitored from cradle to grave with a traceable tag. MIS should be implemented in every WEEE collection and disposing sites including landfill sites, as well as those clustered electronic markets in populated urban residential areas. The use of surveillance cameras on disposing sites is suggested by Cao et al. (2016b). The integration of distributed MIS can be achieved by cloud-based technology, as a Cloud WEEE Recovery system is formed where data is collected, stored and shared in the cloud (Wang and Wang, 2014). Consumers and stakeholders are enabled to interact with the big data in the cloud, and the following tasks can be achieved:

(1). Legislation can be well supported and fully discussed, as data are available to legislators, advisors, government officials, policy researchers and the general public;

(2). Fiscal administration can be improved, as taxes can be effectively collected based on full-scale monitoring on the activities of recycling stakeholders;

(3). Eco-design of LIBs and related CEs can be improved, as the disposal information is made available to product designers through the cloud-based data sharing platform;

(4). Values of academic research can be promoted, as the researchers can locate problems and barriers in current practices, therefore the values and quality of research can be improved;

(5). Profitability of recycling practitioners can be increased, as comprehensive decision support tools (Li et al., 2016a) can be effectively applied on business planning, investment and management based on availability of data;

(6). Participation of general public in spent LIBs recycling can be enhanced, as recycling routes and practices are known to general public as well as the potential hazards of improper disposal of spent LIBs in CEs.

Therefore, implementation and integration of MIS should be encouraged or even mandated, and related fiscal policy should be allocated. Despite the cost-effective analysis is still required for construction of an integrated system, information management technologies offer a potential solution to the problems existing in current "tax-subsidy" system, such as imbalance between levies and subsidies (Zeng et al., 2016b) and audition (Cao et al., 2016b).

4.4. Extending education

In spent battery collection and recycling, public education is crucial, as it not only changes personal attitudes and behaviours, but also creates a social atmosphere (Rioux, 2011). The effectiveness of information campaigns (Blumberga et al., 2015) and slogans (Hansmann et al., 2009) concerning collecting spent batteries have been confirmed. Governments, schools, manufacturers are the three important roles in public education, and consumers are targeted as education receivers (Sun et al., 2015). However, according to the survey results, despite people are generally willing to recycle their spent LIBs, 93.8% of respondents do not know where to dispose the spent batteries, which is much higher than previous findings on generic WEEE recycling (Cao et al., 2016a). Therefore, the providers and receivers of public education systems should be extended. Researchers and battery recycling stakeholders should be included as the providers of education. Collection sites and routes should be known to the general public. Academic research should also be available to law makers, general public and recycling practitioners, which including contents: the values and hazards of spent LIBs, management strategies, policy recommendations, assessments on recycling practices, and novel recycling processes.

258

Battery recycling stakeholders should receive education on spent LIBs and instruction of proper disposal, especially for peddlers who are aware of neither potential dangers of WEEE exposure nor proper treatment procedure (Orlins and Guan, 2016). With changes in laws and policies, construction of infrastructure, and implementation of advanced information technologies, a public education system with a high degree of participation and interaction can be realised, which significantly improve recycling rate of spent LIBs from CEs.

5. Conclusions

Recycling spent LIBs is of vital importance for social-economic and environmental sustainability, especially for China, the largest LIB manufacturer and consumer in the world. Currently, most LIBs are used in CEs, despite a rapid growth of LIBs consumption led by increasing production of EVs. With the purpose of improving the sustainability, it is essential to understand current status of recycling spent LIBs from CEs in China. However, little information about their disposal is available. Therefore, a combined methodology was adopted in this study, which consists of online surveys, field investigations and statistical estimations. The generation, collection and recycling of spent LIBs were investigated to expound status quo of recycling spent LIBs from CEs in China, and to provide policy recommendations for stakeholders.

The survey was conducted online, and a post-stratification adjustment was used for correcting possible respondent bias. The ownerships and replacements of related CEs were surveyed for statistical estimation. 59.6% of respondents store their spent LIBs at home, and 93.8% of respondents do not know where to dispose the spent batteries. This situation has been mainly attributed to the absence of collection systems, and this fact has been confirmed by interview-based field investigations on current WEEE collection systems. Generally, all stakeholders in current WEEE reverse logistics systems, including peddlers, second-hand stores, repair stores, collection stations, and middlemen, not intentionally collect spent LIBs, as this type of WEEE is regarded as low-value items or trashes. As a consequence, formal battery disposers are either running under the breakeven point or turning to production rejects. Informal battery disposers not deal with spent LIBs in CEs due to technical limitations of the methods they used. Based on official statistics, survey results, and processing capacities of disposers, the actual recycling rate of spent LIBs from CEs in China is estimated to be less than 10%. Moreover, the acid leaching process employed by the formal disposers also has certain limitations, including processing capacity and physical hazards.

Based on analysis of the findings, policy implications are given to tackle with the existing problems. Legislation improvement is firstly proposed, as laws and policies impact significantly on WEEE recycling. Labels and regulations should be enforced for LIBs, and spent LIBs should be classified into hazardous wastes. Fiscal policy should more focus on establishing a spent LIBs collection system, and collection and recycling targets should be clarified. State-owned non-profit collection stations are recommended as a necessary supplementary to current pure profit-driven WEEE collection system. Development of novel recycling approaches and implementation of information management technologies can also make significant contributions in improving spent LIBs recycling from material extraction and administration perspectives, and thus these technologies need to be fostered for industrialisation. In addition, the scope of public education should be expanded.

Acknowledgements

Appendix A. Supplementary data

Supplementary data related to this article can be found at http://dx.doi.org/10.1016/j.jclepro.2017.05.181.

Nomenclature

Abbreviations

CE	Consumer electronic
CEN	China Environment News
CEO	Chief executive officer
CIAPS	China Industrial Association of Power Sources
CPG	Central People's Government
EDTA	Ethytlene diamine tetraacetic acid
EEE	Electrical and electronic equipment
EPR	Extended producer responsibility
EU	European Union
EV	Electric vehicle
GDP	Gross domestic product
GM	Grey model
GVM	Grey Verhulst model
IP	Internet protocol
LIB	Lithium-ion battery
LPB	Lithium primary battery
MEP	Ministry of Environmental Protection
MIS	Management information system
NBS	National Bureau of Statistics
NDRC	National Development and Reform Commission
O2O	Online To Offline
PC	Personal computer
PCB	Printed circuit boards
PCC	Pearson correlation coefficient
QR	Quick response
RFID	Radio frequency identification
SI	Supporting information
WEEE	Waste electrical and electronic equipment

Symbols

D	Domestic generation
e	Natural base
E	Exportation
I	Importation of spent LIBs (WEEE)
I'	Importation
k	kth count
n	Sum
N	Population
P	Domestic production
S	Sale

T	Total generation
w	Weight

Superscripts

D	Domestic generation

Subscripts

n	Average service years
t	tth count

References

Alreck, P., Settle, R., 2004. Survey Research Handbook, third ed. McGraw Hill, New York.

Business Insider (BI). 2016. Available form: www.businessinsider.com/wechat-breaks-700-million-monthly-active-users-2016-4 [retrieved on 10th Nov 2016].

Blumberga, Andra, Timma, Lelde, Romagnoli, Francesco, Blumberga, Dagnija, 2015. Dynamic modelling of a collection scheme of waste portable batteries for ecological and economic sustainability. J. Clean. Prod. 88, 224–233.

Battery University (BU), 2010. BU-808: how to prolong lithium-based batteries. Available from: www.batteryuniversity.com/learn/article/how_to_prolong_lithium_based_batteries [retrieved on 15th, Oct 2016].

Cao, Jian, Chen, Yangyang, Shi, Bin, Lu, Bo, Zhang, Xuemei, Ye, Xuhong, Zhai, Guangshu, Zhu, Chenbo, Zhou, Gengui, 2016. WEEE recycling in Zhejiang Province, China: generation, treatment, and public awareness. J. Clean. Prod. 127, 311–324.

Cao, J., Lu, B., Chen, Y., Zhang, X., Zhai, G., Zhou, G., Zhou, G., Jiang, B., Schnoor, J.L., 2016b. Extended producer responsibility system in China improves e-waste recycling: government policies, enterprise, and public awareness. Renew. Sust. Energy Rev. 62, 882–894.

Chen, Xiangping, Fan, Bailin, Xu, Liping, Zhou, Tao, Kong, Jiangrong, 2016. An atom-economic process for the recovery of high value-added metals from spent lithium-ion batteries. J. Clean. Prod. 112, 3562–3570.

Chen, X., Ma, H., Luo, C., Zhou, T., 2017. Recovery of valuable metals from waste cathode materials of spent lithium-ion batteries using mild phosphoric acid. J. Hazard. Mater. 326, 77–86.

China Environment News, 2016. Lead-acid Battery Recycling Should Be Licensed and Regulated (In Chinese). Available from: news.smm.cn/news/3805525 [retrieved on 10th Nov 2016].

ChinaNEV, 2016. The First Domestic Lithium-ion Battery Recycling Line Has Been Established (In Chinese). Available from. www.diandong.com/news/2016092740376.shtml [retrieved on 10th Nov 2016].

Chinese Brands, 2015. O2O Platform "Huishouge" Founded by GEM Who about to Enter Waste Collection Trade (In Chinese). Available from. pinpai.china.com.cn/2015-12/24/content_8473356.htm [retrieved on 10th Nov 2016].

Chinese Entrepreneurs, 2016. Interview with Xuefeng Chen - CEO of Aihuishou: How to Make Mobile Phone Recycling into a Big Business (In Chinese). Available from. tech.sina.com.cn/t/2016-10-08/doc-ifxwrhpn9358803.shtml [retrieved on 10th Nov 2016].

Choi, Tsan-Ming, Hui, Chi-Leung, Liu, Na, Ng, Sau-Fun, Yu, Yong, 2014. Fast fashion sales forecasting with limited data and time. Decis. Support Syst. 59, 84–92.

Central People's Government (CPG), 2012. Administrative Measure on Tax Levy and Use for WEEE Recycling. Available form. www.gov.cn/gzdt/2012-05/30/content_2149195.html [retrieved on 10th Nov 2016].

Deng, J., 1989. Introduction to grey system theory. J. Grey Syst. 1 (1), 1–24.

Duffy, B., Smith, K., Terhanian, G., Bremer, J., 2005. Comparing data from online and face-to-face surveys. Int. J. Mark. Res. 47 (6), 615–639.

Evans, J.R., Mathur, A., 2005. The value of online surveys. Internet Res. 15 (2), 195–219.

Ferreira, Daniel Alvarenga, Prados, Luisa Martins Zimmer, Majuste, Daniel, Mansur, Marcelo Borges, 2009. Hydrometallurgical separation of aluminium, cobalt, copper and lithium from spent Li-ion batteries. J. Power Sources 187 (1), 238–246.

Gratz, Eric, Sa, Qina, Apelian, Diran, Wang, Yan, 2014. A closed loop process for recycling spent lithium ion batteries. J. Power Sources 262, 255–262.

Gu, Yifan, Wu, Yufeng, Xu, Ming, Mu, Xianzhong, Zuo, Tieyong, 2016. Waste electrical and electronic equipment (WEEE) recycling for a sustainable resource supply in the electronics industry in China. J. Clean. Prod. 127, 331–338.

Gu, Yifan, Wu, Yufeng, Xu, Ming, Wang, Huaidong, Zuo, Tieyong, 2016. The stability and profitability of the informal WEEE collector in developing countries: a case study of China. Resour. Conserv. Recycl. 107, 18–26.

Hanisch, C., Loellhoeffel, T., Diekmann, J., Markley, K.J., Haselrieder, W., Kwade, A., 2015. Recycling of lithium-ion batteries: a novel method to separate coating and foil of electrodes. J. Clean. Prod. 108, 301–311.

Hansmann, Ralf, Loukopoulos, Peter, Scholz, Roland W., 2009. Characteristics of effective battery recycling slogans: a Swiss field study. Resour. Conserv. Recycl. 53 (4), 218–234.

He, K., Li, L., Ding, W., 2008. Research on recovery logistics network of waste electronic and electrical equipment in China. 3rd IEEE Conf. Ind. Electron. Appl. 1797–1802.

Healey, B., 2007. Drop downs and scroll mice: the effect of response option format and input mechanism employed on data quality in web surveys. Soc. Sci. Comput. Rev. 25 (1), 111–128.

Holt, D., Smith, T., 1979. Post stratification. J. R. Stat. Soc. 142 (1), 33–46.

Horeh, N. Bahaloo, Mousavi, S.M., Shojaosadati, S.A., 2016. Bioleaching of valuable metals from spent lithium-ion mobile phone batteries using Aspergillus Niger. J. Power Sources 320, 257–266.

Iannicelli-Zubiani, Elena Maria, Giani, Martina Irene, Recanati, Francesca, Dotelli, Giovanni, Puricelli, Stefano, Cristiani, Cinzia, 2017. Environmental impacts of a hydrometallurgical process for electronic waste treatment: a life cycle assessment case study. J. Clean. Prod. 140, 1204–1216.

Jian, G., Guo, J., Wang, X., Sun, C., Zhou, Z., Yu, L., Kong, F., Qiu, J., 2012. Study on separation of cobalt and lithium salts from waste mobile-phone batteries. Proc. Environ. Sci. 495–499.

Kang, Daniel Hsing Po, Chen, Mengjun, Ogunseitan, Oladele A., 2013. Potential environmental and human health impacts of rechargeable lithium batteries in electronic waste. Environ. Sci. Technol. 47 (10), 5495–5503.

Ku, H., Jung, Y., Jo, M., Park, S., Kim, S., Yang, D., Rhee, K., An, E., Sohn, J., Kwon, K., 2016. Recycling of spent lithium-ion battery cathode materials by ammoniacal leaching. J. Hazard. Mater. 313, 138–146.

Leedy, P.D., Ormrod, J.E., 2010. Practical Research: Planning and Design, ninth ed. Pearson Education, Inc., United States.

Li, Li, Lu, Jun, Ren, Yang, Zhang, Xiao Xiao, Chen, Ren Jie, Wu, Feng, Amine, Khalil, 2012. Ascorbic-acid-assisted recovery of cobalt and lithium from spent Li-ion batteries. J. Power Sources 218, 21–27.

Li, B., Yang, J., Lu, B., Song, X., 2015. Estimation of retired mobile phones generation in China: a comparative study on methodology. Waste Manag. 35 (1), 247–254.

Li, J., He, X., Zeng, X., 2016a. Designing and examining e-waste recycling process: methodology and case studies. Environ. Technol. 1–9.

Li, Jia, Wang, Guangxu, Xu, Zhenming, 2016. Generation and detection of metal ions and volatile organic compounds (VOCs) emissions from the pretreatment processes for recycling spent lithium-ion batteries. Waste Manag. 52, 221–227.

Lisbona, Diego, Snee, Timothy, 2011. A review of hazards associated with primary lithium and lithium-ion batteries. Process Saf. Environ. Prot. 89 (6), 434–442.

Ministry of Environmental Protection (MEP), 2006. Technical Policy of Spent Batteries Pollution Prevention and Control (In Chinese). Available from. kjs.mep.gov.cn/hjbhbz/bzwb/wrfzjszc/200611/t20061120_96225.htm [retrieved on 15th, Oct 2016].

Ministry of Industry and Information Technology (MIIT), 2016. The Telecommunication Industry Operation Condition in January 2016. Beijing, China.

National Bureau of Statistics (NBS), 2016. Annual Data of 2015. Available from. www.stats.gov.cn/english/Statisticaldata/AnnualData/ [retrieved on 15th, Oct 2016].

Orlins, Sabrina, Guan, Dabo, 2016. China's toxic informal e-waste recycling: local approaches to a global environmental problem. J. Clean. Prod. 114, 71–80.

Pao, H., Fu, H., Tseng, C.L., 2012. Forecasting of CO_2 emissions, energy consumption and economic growth in China using an improved grey model. Energy 40 (1), 400–409.

Rahimifard, S., Abu Bakar, M.S., Williams, D.J., 2009. Recycling process planning for the End-of-Life management of waste from electrical and electronic equipment. CIRP Ann. - Manuf. Technol. 58 (1), 5–8.

Rioux, Liliane, 2011. Promoting pro-environmental behaviour: collection of used batteries by secondary school pupils. Environ. Educ. Res. 17 (3), 353–373.

Rodgers, J.L., Nicewander, W.A., 1988. Thirteen ways to look at the correlation coefficient. Am. Stat. 42 (1988), 59–66.

Steuer, Benjamin, Ramusch, Roland, Part, Florian, Salhofer, Stefan, 2017. Analysis of the value chain and network structure of informal waste recycling in Beijing, China. Resour. Conserv. Recycl. 117, 137–150.

Sun, Mingxing, Yang, Xuechun, Huisingh, Donald, Wang, Renqing, Wang, Yutao, 2015. Consumer behavior and perspectives concerning spent household battery collection and recycling in China: a case study. J. Clean. Prod. 107, 775–785.

Tian, Xi, Gong, Yu, Wu, Yufeng, Agyeiwaa, Amma, Zuo, Tieyong, 2014. Management of used lead acid battery in China: secondary lead industry progress, policies and problems. Resour. Conserv. Recycl. 93, 75–84.

Wagner, T.P., Toews, P., Bouvier, R., 2013. Increasing diversion of household hazardous wastes and materials through mandatory retail take-back. J. Environ. Manag. 123, 88–97.

Wang, Xi Vincent, Wang, Lihui, 2014. From Cloud manufacturing to Cloud remanufacturing: a Cloud-based approach for WEEE recovery. Manuf. Lett. 2 (4), 91–95.

Wang, Zheng-xin, Dang, Yao-guo, Liu, Si-feng, 2009. Unbiased grey Verhulst model and its application. Syst. Eng. - Theory & Pract. 29 (10), 138–144.

Wang, Zhaohua, Zhang, Bin, Yin, Jianhua, Zhang, Xiang, 2011. Willingness and behavior towards e-waste recycling for residents in Beijing city, China. J. Clean. Prod. 19 (9–10), 977–984.

Wang, Xue, Gaustad, Gabrielle, Babbitt, Callie W., Richa, Kirti, 2014. Economies of scale for future lithium-ion battery recycling infrastructure. Resour. Conserv. Recycl. 83, 53–62.

Wang, Cong, Chen, Bo, Yu, Yajuan, Wang, Yixuan, Zhang, Wanying, 2016a. Carbon footprint analysis of lithium ion secondary battery industry: two case studies from China. J. Clean. Prod.

Wang, M., Zhang, C., Zhang, F., 2016b. An environmental benign process for cobalt and lithium recovery from spent lithium-ion batteries by mechanochemical approach. Waste Manage. 51, 239–244.

Wang, X., Gaustad, G., Babbitt, C.W., 2016c. Targeting high value metals in lithium-ion battery recycling via shredding and size-based separation. Waste Manage.

51, 204–213.

Yin, Jianfeng, Gao, Yingnan, Xu, He, 2014. Survey and analysis of consumers' behaviour of waste mobile phone recycling in China. J. Clean. Prod. 65, 517–525.

Zeng, X., Li, J., Y Ren, 2012. Prediction of various discarded lithium batteries in China. In: Proceedings of 2012 IEEE International Symposium on Sustainable Systems and Technology, 16–18 May 2012, Boston, MA, USA, 1-4.

Zeng, Xianlai, Li, Jinhui, 2013. Implications for the carrying capacity of lithium reserve in China. Resour. Conserv. Recycl. 80, 58–63.

Zeng, X., Li, J., 2015. On the sustainability of cobalt utilization in China. Resour. Conserv. Recy. 104 (A), 12–18.

Zeng, X., Li, J., Shen, B., 2015. Novel approach to recover cobalt and lithium from spent lithium-ion battery using oxalic acid. J. Hazard. Mater. 295, 112–118.

Zeng, X., Gong, R., Chen, W.Q., Li, J., 2016a. Uncovering the recycling potential of "new" WEEE in China. Environ. Sci. Technol. 50 (3), 1347–1358.

Zeng, X., Duan, H., Wang, F., Li, J., 2016b. Examining environmental management of e-waste: China's experience and lessons. Renew. Sust. Energy Rev. 72, 1076–1082.

Zhang, Lingen, Xu, Zhenming, 2016. A review of current progress of recycling technologies for metals from waste electrical and electronic equipment. J. Clean. Prod. 127, 19–36.

Zhang, Xihua, Xie, Yongbing, Lin, Xiao, Li, Haitao, Cao, Hongbin, 2013. An overview on the processes and technologies for recycling cathodic active materials from spent lithium-ion batteries. J. Mater. Cycles Waste Manag. 15 (4), 420–430.

Zheng, Xiaohong, Gao, Wenfang, Zhang, Xihua, He, Mingming, Lin, Xiao, Cao, Hongbin, Zhang, Yi, Sun, Zhi, 2017. Spent lithium-ion battery recycling — reductive ammonia leaching of metals from cathode scrap by sodium sulphite. Waste Manag. 60, 680–688.

Zhou, Lei, Xu, Zhenming, 2012. Response to waste electrical and electronic equipments in China: legislation, recycling system, and advanced integrated process. Environ. Sci. Technol. 46 (9), 4713–4724.

Zhu, S., He, W., Li, G., Zhou, X., Zhang, X., Huang, J., 2012. Recovery of Co and Li from spent lithium-ion batteries by combination method of acid leaching and chemical precipitation. T. Nonferr. Metal. Soc. 22 (9), 2274–2281.

Selective liberation in dry milled spent lithium-ion batteries

Samuel D. Widijatmoko [a], Fu Gu [b,c], Zheng Wang [a], Philip Hall [a,*]

[a] Department of Chemical and Environmental Engineering, University of Nottingham Ningbo, China
[b] Department of Industrial Engineering, Zhejiang University, Hangzhou 310027, China
[c] National Institute of Innovation Management, Zhejiang University, Hangzhou 310027, China

ARTICLE INFO

ABSTRACT

Lithium-ion batteries (LIBs) have an established role in the consumer electronics markets with minimum risk of replacement from any other contender in the near future. The recent momentum towards electric vehicles and the renewable energy storage market is creating an increased demand for LIBs. The large amount of hazardous waste generated from the disposal of LIBs is driving research into a sustainable approach for LIB treatment and recovery. The positive electrode active materials being the main targeted component as it is the greatest cost contributor to LIBs production. During the production of the positive electrode, a powder of active material typically Lithium Cobalt Oxide is applied to aluminium foil and held together using a polyvinylidene fluoride (PVDF) binder.

The recovery of positive electrode active material involves physical and chemical treatment. Where effective and efficient physical treatment would reduce the cost incurred for the subsequent chemical treatment. Mechanical treatment is an integral part of liberating and concentrating positive electrode active material. The positive electrode active materials have been reported are being concentrated in the finer size region. However, the cut point at which the positive electrode active material being concentrated is substantially greater than the size of the positive electrode active material particle size as found in spent LIBs.

This paper studies the characteristics of milled spent LIBs concerning particle size. The results suggest that a cut point of 850 μm gives the best composition of the positive electrode active materials recovery that minimises the involvement of copper and aluminium. However, most of the active materials are still held together by the PVDF binder that creates a substantially higher cut point proposed that the actual size of the positive electrode active material contained within spent LIBs. The interaction of copper and aluminium current collector based on size also further discussed in this paper. A comparison between selective liberation in the new and spent LIBs has been made to assess the difference in mechanical properties that contribute to its overall liberation efficiency.

© 2019 Elsevier B.V. All rights reserved.

1. Introduction

Electrical energy is the basis of our modern lifestyle. Batteries are currently being developed to power an increasingly diverse range of applications, from electric vehicles to smartwatches. Owing to its higher energy density, lightweight, and its relatively low cost, lithium-ion batteries (LIBs) are the predominant energy storage choice for many consumer electronics and electric grids [1]. Despite the advancement of battery technology, presently LIBs meet most of the requirements dictated by the large volume of applications linked to renewable energy and electric transportation field [2].

A battery pack may consist of one or several cells that can be connected in series or parallel. In its conventional form, the main component of a LIB cell comprises of graphite negative electrode (e.g.

mesocarbon microbeads, MCMB) with copper foil as current collector, a positive electrode formed by lithium-transition metal-oxides (Li-M-O$_2$, e.g. LiCoO$_2$) with an aluminium foil current collector, a liquid electrolyte consisting of lithium salts (e.g. LiPF$_6$) in a mixed organic solvent (e.g. ethylene carbonate-dimethyl carbonate, EC-DMC), all imbedded in a separator layer (e.g. polypropylene/polyethylene, PP/PE). The active materials for the positive and negative electrodes are in powder form, cast onto the current collector and held by a binder, commonly polyvinyldene fluoride (PVDF) [3,4].

As technology continues to develop, the demand for LIBs is expected to increase, which leads to a large amount of potential waste being generated. Spent LIBs are considered hazardous waste and should not be released into the environment [2]. The recent impetus of electric vehicle has become a driving force in LIBs recycling. Currently, LIBs recycling

262

is hindered by the low collection rate [5]. In the past decade, LIBs that were contained within consumer electronics were relatively small in size and were generally stored by the consumer or disposed of improperly through the municipal waste stream at the end-of-life. However, the low collection rate may not be a problem in the future because of the sheer size of the electric vehicle battery [6]. There is the need to tackle this waste problem and promote a circular economy approach which can mitigate resource scarcity [7,8]. This has led to extensive research into processes for the recovery of valuable metals found in spent LIBs. From components used in the manufacturing of LIBs, positive electrode active materials being the main targeted component as it is where the most valuable resources are found [9].

The recovery of positive electrode active material involves physical and chemical processes [10]. Spent LIBs still contain some residual energy, which may cause a runaway reaction during recycling and therefore discharging is always a necessary step before further treatment [11,12]. Physical processes separate material according to different properties such as size, density, conductivity, magnetic properties, etc. [13]. The chemical processes may be classified into pyrometallurgical and hydrometallurgical processes. Hydrometallurgical treatment involves leaching, extraction, and chemical or electrochemical precipitation [14]. In contrast, pyrometallurgy feeds the spent LIBs into a furnace in which copper recovered as a mixed alloy product and the lithium and aluminium to the slag. Pyrometallurgy products also often recovered through hydrometallurgy [15].

Physical processes have always been a pre-treatment process in the field of LIBs recycling. Effective and efficient physical processes are required to minimise the energy consumption for the subsequent chemical processes. Mechanical liberation of spent LIBs has been reported to exhibit selective comminution, in which the positive electrode active materials are being concentrated in the finer size region with minimum contamination from other battery components [16–18]. Components such as iron are easily recovered through a magnetic separation after liberation [13,19]. Therefore, the components from mechanical liberation only concern the electrode active materials, polymeric material, copper and aluminium.

Selective liberation has been proposed and used to concentrate positive electrode active materials before further separation. The cut point proposed varies from 0.25 mm to 2 mm [19–22]. However, this cut point size range is substantially greater when compared to the positive electrode active materials powder found in LIBs (ca. 1.50 μm – 7.80 μm) [23]. Smaller cut point such as 0.25 mm has been reported to give high purity of positive electrode active material, but it only recovers 56.38% positive electrode active material [22]. Diekmann et al., [20] reveal that it is possible to re-grind the bigger size fraction to liberate the positive electrode active material further, resulting in 75 wt% recovery in size range of <0.50 mm. However, it comes with the expense of a closer particle size distribution that makes the size-based separation more challenging, and therefore, a third stage re-milling may not be a viable option.

In summary, shredding has been proposed and used to concentrate on the positive electrode active materials. Shredding of spent LIBs aims at exploiting selective liberation of positive electrode active materials as well as size range adjustment for subsequent separation processes [19–22]. The different cut point proposed previously may be attributed by a different type of milling machine and the parameters employed by different researchers. However, the understanding related to the characteristics of LIBs particles after shredding has not yet been thoroughly discussed. Much of the attention has been given to concentrate on positive electrode active materials with very little attention to the current collectors.

Therefore, this research aims at understanding the characteristics of milled spent LIBs. The components of milled LIBs are divided into two constituents of leachable and non-leachable components. Assuming that leaching is the primary process after liberation and hence, the discussion will mainly be concerned with the key leachable components.

The key leachable components include positive electrode active material and the copper and aluminium current collector. This research not only explores the selective liberation of positive electrodes active materials towards the current collectors, but also the selective liberations between the copper and aluminium current collectors. Moreover, as the LIB cell undergoes ageing, the current collectors and the binder experience degradation in terms of mechanical strength and the adhesiveness [24–26]. Therefore, the comparison of selective liberation of new and spent battery are made in this research. This comparison then allows the understanding of the effect of ageing towards the selective liberation and would be discussed further in this manuscript.

2. Materials and method

2.1. Materials

The spent LIBs used in this study were collected from local electronic repair shops within Ningbo China. All the spent batteries used were previously used in smartphones and came from a range of manufacturers to represent typical waste. Only prismatic LIBs with predominantly cobalt as positive electrode active materials were used. The type of active materials within a LIB can be identified by the marking available that follows *BS EN 61960-3:2017* [27]. This is identified by the "ICP" marking; the letter "I" designates the carbon negative electrode basis; the letter "C" designates the cobalt positive electrode basis; the letter "P" designates the prismatic shape of the cell. Other designations for other types of positive and negative electrode basis as well as the shape of the cell can be found in *BS EN 61960-3:2017*. The types of positive electrode active material were identified by using an XRD (XRD - CuKα, Bruker AXS D8 Advance), and it was found to be $LiCoO_2$. For elemental analysis, analytical grade HNO_3, HCl, H_2O_2 (Jingrui, UP-S Grade), and water (Mili-Q) were used for the entire digestion and dilution.

At present, PVDF or SBR-CMC can be used as the binder for the negative electrode, while the positive electrode uses PVDF [28]. The type of the active material binder can be deduced by identifying the presence of fluorine atoms. and sodium atoms (that suggest SBR-CMC binder) by using a Scanning Electron Microscopy-Energy Dispersive X-Ray (SEM-EDX, Zeiss – Oxford/ Sigma VP) [29,30]. It was found that only Fluorine was detected which shows PVDF was used as the negative electrode binder material.

2.2. Method

Spent LIBs were first discharged by using 56-ohm resistor until the voltage is near zero (0.2 V – 0.5 V). Spent LIBs were then shredded in a Restch SM 2000 cutting mill with an 8 mm grid. The shredded LIBs were then dried in an oven at 80 °C to constant weight to remove volatile organic electrolytes. Three representative samples of 69.8 g on average were prepared by using a riffle splitter. The sample then screened for iron using a rare earth magnet roll enclosed in polyvinyl chloride (PVC) pipe.

The three samples taken from the riffling exercise were analysed for particle size distribution using certified test sieve (Endecotts) and a fix amplitude shaker (Capco Inclino Sieve Shaker 3). The sieves used were with a nominal aperture diameter of 13,200 μm, 9500 μm, 6700 μm, 4750 μm, and then 2360 μm, 850 μm, 212 μm, and 38 μm. Sieving with nominal aperture size >4750 μm was performed separately, and the sieves were brushed after every use to collect fine particles that are trapped between the joint of adjacent holes. All the sieves for size fraction <4750 μm were put together to assess the particle size distribution. Each different size fraction then analysed for elemental content.

As a baseline comparison, new LIBs of the same type of the spent LIBs were purchased. These were subjected to the same treatment as the spent LIBs. 94.8 g of dried milled new LIBs were used in this study.

Samples were transferred to porcelain lidded crucibles and calcined in a muffle furnace to remove difficult to mill materials (e.g. polymer

materials). The calcination was performed in multiple stages to prevent a sudden release of gas. The temperature was increased at a rate of 10 °C min⁻¹ up to 350 °C with 2 h holding time. Followed an increase in temperature at the same rate to 500 °C with 3 h holding time. The sample was then allowed to cool to room temperature. The samples were then milled using a centrifugal mill (Retsch ZM 200) with a 0.25 mm grid. Samples from inside and outside the grid were collected and sieved using 212 μm nominal aperture size, and the size fraction >212 μm was re-milled until the recovery rate <212 μm was >95 wt%. The samples that initially had particle sizes of <212 μm were excluded from the above steps.

The digestions were adapted from *BS EN 62321–5:2014* [31]. Approximately 0.2 g of sample was weighed to four decimal places using an analytical balance. Microwave digester (CEM MARS 5) equipped with temperature control was used to digest the samples and dissolve the materials present to enable analysis. The digestion is carried out in multiple stages, and the details are summarised in Table 1.

The digested sample then analysed using Inductively Coupled Plasma – Mass Spectrometry (ICP-MS, Nexion 300×). Multi-elements standard calibration curves were made by diluting and mixing different single element standard reference stock solutions (Sigma-Aldrich).

A morphology study of the milled LIB particles was carried out using an SEM-EDX. The EDX helps in identifying the material being studied. The samples were mounted onto aluminium stage by using conductive carbon tape. The surface of the sample then made conductive by applying a 4 nm gold layer by using a gold sputtering machine (LEICA EM SCD 500).

2.3. Data processing and analysis

Selective crushing has been exploited in the minerals industry where the typical case presents the different distribution of valuable and waste minerals concentrated by particle size. In this study, the milled LIBs were sieved into eight different size fractions of 13,200 μm – 9500 μm, 9500 μm – 6700 μm, 6700 μm – 4750 μm, 4750 μm – 2360 μm, 2360 μm – 850 μm, 850 μm – 212 μm, 212 μm – 38 μm, and <38 μm. The weight percentage at given a size range is then calculated.

The results of sieving should always be plotted graphically to assess their full significance, the most common being that plotting either cumulative undersize or oversize against particle size [32]. The plot of cumulative undersize is a mirror image of cumulative oversize, and therefore, it is not necessary to plot both curves. The plot is carried out using a semi-logarithmic coordinate to avoid finer aperture sizes become congested. In this study, the cumulative undersize is used as a means to interpret the particle size distribution. Samples at a given size range then analysed for aluminium, cobalt and copper content, and the recovery rate of a certain element at a given size range can then be found.

In minerals engineering, selective liberation has been observed by researchers, an example of which is iron ore and lead-zinc ore [33,34]. Analysis of selective liberation may be carried out using a Fuerstenau and ore separation degree (η_{ore}) diagrams. The Fuerstenau diagram gives meaningful information, whether the valuable material that is being recovered is concentrated in the finer or coarser size region. Fig. 1 shows a method for evaluating the effect of selective comminution. This is a Fuerstenau upgrading diagram showing recovery plots

of the classified comminution product [35,36]. The recovery of valuable minerals (R_V) and the waste material (R_W) can be plotted in the diagram for various separation cut points t_d, for either fine or coarse fraction. Fig. 1 shows the result for the fine fraction. A linear diagonal line indicates that there is no selectivity in the investigated material (Line 2 in Fig. 1). Enrichment of the valuable component in the finer fraction is documented by a recovery curve positioned above the diagonal line (Line 1 in Fig. 1). A recovery curve below the diagonal line shows enrichment of valuable component occurs in coarser fraction (Line 3 in Fig. 1).

Other than Fuerstenau upgrading diagram, the η_{ore} diagram gives meaningful information related to the cut point t_d that maximise the recovery of valuable material while minimising the recovery of waste material. The η_{ore} is described as the difference in the recovery of valuable and waste material and summarised in Eq. (1).

$$\eta_{ore} = R_V - R_W \qquad (1)$$

When the concentration of valuable minerals depends on the particle size of the product, then η_{ore} changes and is dependent on the separation cut t_d. Thus, the optimum cut point corresponds to the highest ore separation degree ($\eta_{ore,max}$). Moreover, the η_{ore} may be regarded as the efficiency of selective liberation. When R_V is equal to 100% and R_W is 0% implies η_{ore} of 100%, in other words, all the valuable materials have been recovered below the cut point t_d with no contamination from the waste or unwanted material.

The Fuerstenau upgrading diagram and η_{ore} are used to assess the selective liberation that occurs when milling spent LIBs. Such that, the liberation of the LiCoO₂ laminate (identified by the detection of cobalt), copper and aluminium at different cut point size can then be identified. The compensation effect between LiCoO₂l laminate and the copper and aluminium current collectors by increasing cut point will be identified. Moreover, the selective liberation of aluminium towards copper can also be identified.

3. Results and discussion

3.1. Size-based hierarchy of milled LIBs

From Table 2, milling spent LIBs in a cutting mill with an 8 mm grid, resulted in a wide range particle size distribution and the average particle size (d_{50}) of new and spent LIBs were revealed to be 1600 μm and 1552 μm respectively. The average particle size of new LIBs is only slightly bigger and does not significantly different to that of spent LIBs. However, it is realized that there is more <38 μm particles in spent LIBs (7.7 wt%) than in new LIBs (4.4 wt%).

Comparing the cobalt grade between different size fractions in Table 2 (Spent LIBs), it was found that the size fraction <38 μm has the highest grade of 36.5 wt% cobalt. The size fraction <38 μm also has the lowest contamination of aluminium and copper, which are 1.6 wt% and 0.8 wt% respectively. Nonetheless, this size fraction only contributes 7.7 wt% from the entire feed and equates to LiCoO₂ recovery rate of 11.4 wt%. Compared to that of the new LIBs (Table 2), the <38 μm size fraction contains lower grade of 24.9 wt% cobalt with lower aluminium and copper contamination of 0.5 wt% and 0.6 wt% respectively. In the case of new LIBs, the size fraction of 212 μm – 38 μm contains the

Table 1
Microwave digestion parameters.

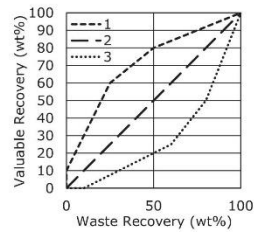| Stage	Number of vessels	Power level (W)	Ramp time (min)	Temperature (°C)	Hold time (Min)	Description
1	8	800	8	80	2	~0.2 g of solid with 1 ml H₂O + 4 ml UP-S Grade 68 wt% HNO₃ + 1 ml H₂O₂.
2	8	800	4	120	5	
3	8	800	8	80	2	The solution then allowed to cool down below 30 °C then 4 ml of UP-S Grade 30 wt% HCl was added.
4	8	800	4	120	5	

Fig. 1. An example of recovery plot as Fuerstenau upgrading curve with percentage finer; re-drawn from Hesse, Popov [33].

highest grade of 31.2 wt% cobalt with minimum contamination from aluminium (0.4 wt%) and copper (0.5 wt%). Therefore, to make an objective judgement related to whether milling LIBs does induce selective liberation of LiCoO$_2$ laminate, Fuerstenau upgrading diagram, and η_{lore} was plotted. By this way, the interactions between LiCoO$_2$ laminate (cobalt), copper and aluminium can then be studied. Moreover, the comparison between the new and spent LIBs can also be made in order to understand the phenomenon described above.

Fig. 2 shows that milling spent LIBs does induce selective liberation of LiCoO$_2$ particles. The recovery of cobalt is greater than the recovery of copper and aluminium in the finer size region. The Fuerstenau upgrading diagram can be broken down into two distinct regions, which are the recovering region and the re-mixing region. In the recovering region, the cobalt recovery increases by increasing the cut point size also accompanied by a minimum increase in copper and aluminium recovery. Further increase in cut point yield higher wt% recovery of cobalt but the increase is outweighed by the increase in copper as well as aluminium recovery and called the re-mixing region. When there is a point of inflection, the recovering line changes into re-mixing line; it marks the optimum cut point that balances the compensation between valuable material recovery and waste material recovery. For both Co-Al and Co-Cu, the transition can be seen at point 850 μm. Comparing the η_{lore} curves in Fig. 2, the cut point 850 μm gives the highest efficiency to recover cobalt while minimising the contamination of aluminium and copper (Co-Al $\eta_{lore,max}$ = 37.8% and Co-Cu $\eta_{lore,max}$ = 33.4%). Moreover, a dramatic decrease in Co-Cu η_{lore} is observed when compared to Co-Al η_{lore} above cut point 850 μm. This indicates that above the cut point 850 μm, the copper contamination is more dominant than the aluminium contamination.

Inside the cutting chamber, size reduction occurs through shearing and cutting stress [37]. Cutting actions applies a localised force that induces failure of the material right next to the knife edge as a result of shear and tensile stresses. With the assumption that there is no

Table 2
The cumulative undersize semi-logarithmic plot of shredded spent and new lithium-ion battery and the concentration of key material for a given size range.
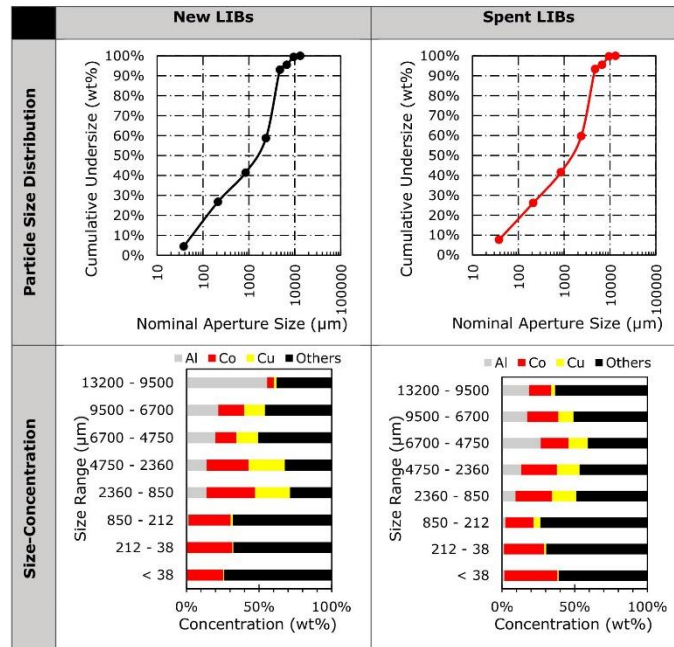
interaction between the active materials assembly and the electrode. The tensile strength of copper (220 MPa) has been reported to be higher than the tensile strength of aluminium (105 MPa – 145 MPa) [38]. Moreover, copper (2.65 GPa) also has a higher ideal shear strength as compared to aluminium (1.85 GPa) shear strength [39]. In light of these facts, inconsistency was found. By considering the shear and tensile strength of copper and aluminium, it is expected that the aluminium would be more readily liberated in the finer size region. However, the revealed finding seems to contradict this fact. By comparing the interactions of Co-Al and Co-Cu in the Fuerstenau upgrading curve, there is a trend switch in the recovery and re-mixing region. Where, in the recovery region, increasing the cut point size leads to a higher increase in aluminium recovery rather than copper recovery. Additionally, in the re-mixing region, this trend does not hold true and switch towards more copper being recovered as the cut point become bigger.

To make a better graphical representation, the interaction between aluminium and copper (Al-Cu) then plotted for Fuerstenau upgrading curve and η_{ore}, in which the aluminium is taken as the valuable component. As it can be seen from Fig. 2, the Fuerstenau upgrading curve of Al-Cu also shows a switch in trend. Initially, the Fuerstenau upgrading diagram shows recovery of aluminium above the diagonal line prior to approaching cut point 212 μm. However, as the cut point size increased, the re-mixing line lies below the diagonal line. Similarly, for the η_{ore} curve, the efficiency is only positive in the region of <212 μm and the η_{ore} become a negative value onwards. The η_{ore} negative value implies that the recovery rate of waste material (copper) is higher than that of the valuable material (aluminium) as the cut point become bigger. With the highest η_{ore} for Al-Cu is 1.6% with cut point 212 μm. Moreover, the cut point 2360 μm gives the highest η_{ore} of copper towards aluminium.

From the findings described above, indicates that the interaction between the active materials assembly towards the current collector cannot be negated. This also demonstrate that $LiCoO_2$-PVDF-Al is more resilient than that of C_6-PVDF-Cu. The mechanical strength of current collectors and the adhesive strength of the binder are dependent upon the number of discharging and charging cycles the battery undergone. The repetitive cycle of charging and discharging the active materials undergoes causes repeated expansion and shrinkage due to the periodic intercalation and de-intercalation of lithium ions [40–42]. The repetitive deformation then induces mechanical ageing to the current collectors [43]. Furthermore, degradation of PVDF adhesiveness on to the current collector has also been reported to weaken, causing contact loss of active material [24,25]. Therefore, a comparison to the new milled LIBs was made to observe the difference in selective liberation in new and spent LIBs. The comparison of selective liberation of new and spent LIBs are summarised in Table 3.

From Table 3, it can be deduced that the milling of new LIBs does induce selective liberation of positive electrode active materials in the finer size region. Additionally, the trend for the Fuerstenau upgrading curve as well as the η_{ore} indicates a similar trend in selective liberation of positive electrode active materials. The cut point of 850 μm applies as the optimum cut point to concentrate positive electrode active material while minimising the contamination from copper and aluminium.

Comparing the new and spent LIBs, in Table 3, the Co-Al and Co-Cu curves indicate better separation efficiency for the new LIBs. From Table 3 (η_{ore}), after Co-Al and Co-Cu curves approach $\eta_{ore,max}$, the efficiency quickly decreases as the cut point became bigger for both LIBs. Furthermore, the decrease in efficiency is more apparent for the Co-Cu η_{ore} curve, compared to the Co-Al η_{ore} curve for spent LIBs. This is thought to occur due to the difference in adhesive strength of PVDF binder with the copper and aluminium current collector. The active materials on the copper current collector (graphite) and on the aluminium current collector ($LiCoO_2$) are held together by the PVDF binder to form a composite. The cushioning of copper and aluminium current collector by its respective active materials may help in preventing breakage during mechanical liberation. It has been reported that the adhesive strength of PVDF to copper is 285.6 kPa in a new LIB battery is lower than that of aluminium which is 841.2 kPa [26]. Therefore, in the case of new LIBs, the lower PVDF adhesive strength towards copper current collector as compared to the aluminium current collector counterpart, may help explain the higher rate of decrease in efficiency as the η_{ore} curve approaching $\eta_{ore,max}$ in the Co-Cu η_{ore} curve as compared to the Co-Al η_{ore} curve.

As the LIBs are used in multiple cycles, the adhesive strength of PVDF onto copper and aluminium current collectors decreases to 55.5 kPa and 132.8 kPa respectively, after 200 cycles [26]. Moreover, the elastic modulus of copper further decreases as the battery is cycled a reduction of 78%-80% has been reported [26]. For spent LIBs, the degradation of PVDF adhesive strength and the elastic modulus of the copper current collector causes more copper to be liberated in the finer size region. The aluminium current collector counterpart also undergoes localised corrosion and produces perforation [44]. This corrosion induced perforation potentially weakened the mechanical properties of the aluminium foil in spent LIBs. Thus, in the case of spent LIBs, the copper and aluminium current collectors are more contaminating in the finer size fraction (< 850 μm) and therefore translated as a lower overall $\eta_{ore,max}$ value.

From Table 3, the Fuerstenau upgrading diagram shows an Al-Cu curve of spent LIBs below the diagonal line in the size range of >212 μm. Whereas, the new LIBs shows a recovery curve below the diagonal line in the size range of >2360 μm. Moreover, the η_{ore} curves reveal that the cut point required to exploit this selectivity increases from 2360 μm
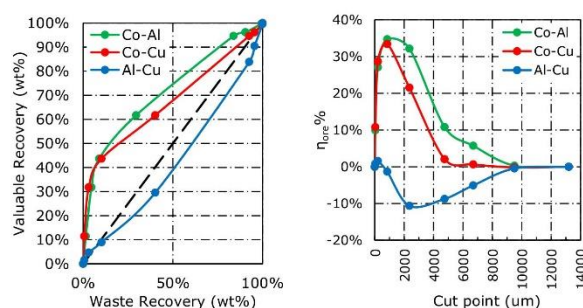
Fig. 2. Fuerstenau upgrading curve (left) and ore separation degree (η_{ore}) (right) of the milled spent LIBs.

266

Table 3
Comparison of Fuerstenau upgrading curve and ore separation degree (η_{ore}) of Co-Al, Co-Cu and Al-Cu for new and spent lithium-ion battery.
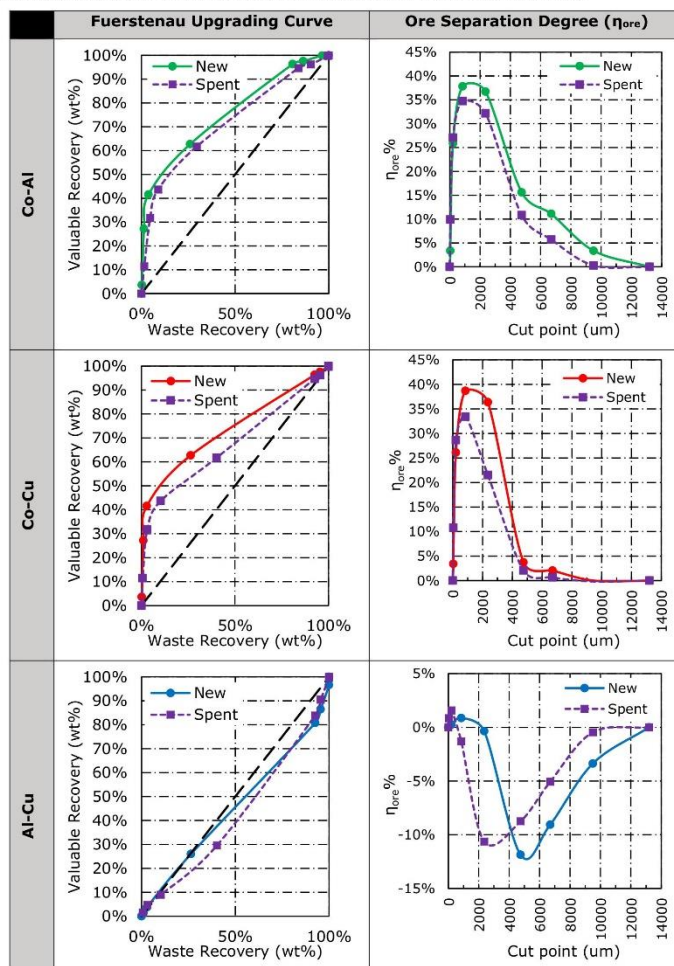
($\eta_{ore,max} = 10.6\%$) to 4750 µm ($\eta_{ore,max} = 11.9\%$). It is also important to point out that the Al-Cu η_{ore} curve predominant size is different for spent and new LIBs. The new LIBs has an Al-Cu η_{ore} curve that is more dominant towards the larger size region. Whereas, the η_{ore} curve of spent LIBs has shifted towards the finer size region. The change in predominant size towards the finer size region, in milling spent LIBs, indicates the copper and aluminium favour further breakage into the smaller size region. Therefore, the better mechanical properties of positive and negative electrode in new LIBs synergistically translates to a bigger cut point as compared to spent LIBs. While the increase in $\eta_{ore,max}$ is caused by the lower recovery of copper towards aluminium in size range of <2360 µm.

Thus, to investigate this phenomenon, a morphology study of classified milled product is done by using SEM-EDX.

267

3.2. Particles morphology of milled LIBs

Fig. 3 presents the classified product from milled spent LIBs. The polymeric materials from the separator and the battery chassis are mainly found in the bigger size fraction (>850 μm). Through visual inspection, separator in the size region of <850 μm was found to be minimum. Observation by using SEM for different size fraction then made. This morphological analysis aims to understand the characteristics of active materials for different size fraction. Samples were mounted to aluminium stage with adhesive carbon tape. The size fraction of >4750 μm was not analysed and based on visual inspection; it is assumed to be the same as the size fraction 4750 μm – 2360 μm. This is thought not to bias the results for the size fraction of >4750 μm only holds <7 wt%. The positive electrodes, negative electrodes, and separators were manually collected by using a tweezer for size fraction 4750 μm – 2360 μm and 2360 μm – 850 μm. Whereas, Size fraction 850 μm – 212 μm, 212 μm – 38 μm and < 38 μm were directly mounted onto the adhesive carbon tape. The same preparation also carried out for the milled classified new LIBs. Gold sputtering then carried out at 4 nm thickness to make the sample surface conductive.

From Fig. 4, it was discovered that both positive and negative electrode active materials are contaminating the surface of the current collector. Fig. 4 also demonstrates that there are no difference in terms of morphology for the new and spent LIBs. From Fig. 4.1 and 4.4, there is a partial detachment of $LiCoO_2$ laminate from the aluminium current collector. The $LiCoO_2$ that are still attached to the current collector is still firmly held by the binder. Moreover, the preliminary liberation induces the detachment of positive electrode active materials from its current collector in the form of a big package, indicated by the crack and the clear transition between the side that has $LiCoO_2$ lamination partially removed and intact (Fig. 4.1 and 4.4). Moreover, the side that has already lost many of its active materials is still contaminated with a thin layer of $LiCoO_2$ lamination.

Similar observation also made with the negative electrode that still have graphite lamination partially intact (Fig. 4.2 and 4.5). However, there is a transition region between the side that has graphite lamination that are partially removed and intact. This indicates that graphite-PVDF-graphite interaction is relatively weaker compared to $LiCoO_2$-PVDF-$LiCoO_2$ interaction.

The separators collected from the size fraction 4750 μm – 2360 μm are contaminated with both $LiCoO_2$ and Graphite laminates. This may have been due to the compression action in the cutting mill. However, the attachment of the active materials is weak. By manually folding the separator using a tweezer, the powders attached to the separator were transferred onto the carbon tape (Figs. 4, 3). This indicates that the attachment of positive and negative electrode active materials onto the separator is relatively weak, but sieving alone does not help in detaching the active materials cast on the separator. The new LIBs also shows the same characteristics (Figs. 4–6).

For the size fraction >2360 μm, the particles in this region contain positive and negative electrodes that have undergone size reduction and accompanied by the partial liberation of active materials. The active materials laminate are still firmly attached and contaminating the surface of the electrodes. The analysis also shows that the graphite laminate is more liberated compared to the $LiCoO_2$ laminate. Some active materials laminate are also found to be attached on to the separator, and as a result, it may reduce the recovery of $LiCoO_2$ during size-based separation.

Fig. 5, which is the 2360 μm – 850 μm reveals that the $LiCoO_2$ and graphite lamination are still contaminating the surface of the current collectors as well as the separator. Fig. 5 also indicates no morphological difference between the new and spent LIBs. From Fig. 5.1 and 5.4, $LiCoO_2$ particles in the size fraction of 2360 μm – 850 μm are firmly held by the binder and laminating the aluminium current collector. This phenomenon indicates that the preliminary liberation also induces size reduction with the minimum liberation of $LiCoO_2$ lamination from its aluminium

current collector (i.e. the aluminium and $LiCoO_2$ lamination breaks in unity). From Fig. 5.2 and 5.5, the copper current collector still has graphite lamination. However, it is cleaner when compared to the positive electrode. This also indicates that the graphite lamination is more readily liberated as compared to $LiCoO_2$ lamination that remain fixed. From Fig. 5.3 and 5.6, the separator is contaminated with $LiCoO_2$ and graphite laminates. The attachment of $LiCoO_2$ and graphite laminates to the separator is relatively weak, as discussed in the size range 4750 μm – 2360 μm.

From the size fraction 2360 μm – 850 μm, it is shown that this region contains a positive electrode that has undergone a reduction in size with the minimum liberation of $LiCoO_2$ laminate. However, the negative electrode is relatively clean from graphite laminate. Similarly, with the finding from size range 4750 μm – 2360 μm, the graphite laminate is more readily liberated than the $LiCoO_2$ laminate from its current collector. Active materials laminate also found to be contaminating the separator that also hinders size-based separation.

Fig. 6 presents the morphology of new and spent LIBs in size range of <850 μm, and it can be concluded that there is no significant difference between the two. From Fig. 6.1 and 6.5, the size fraction 850 μm – 212 μm contains initially graphite and $LiCoO_2$ laminate that have been detached from its current collector and only held together by the binder. Moreover, there are substantial $LiCoO_2$ fine particles aggregates (Fig. 6.2 and 6.6) that are covered by the binder. Similar observation also made for the size range of 212 μm – 38 μm (Fig. 6.3 and 6.7) as well as size range of <38 μm (Fig. 6.4 and 6.8). With the only difference being the size of the aggregates, where the size fraction <38 μm shows the least aggregation between particles. Thus, the size fraction of <850 μm may be classified as the size fraction that concentrates detached $LiCoO_2$ and graphite laminate but is still held together by the PVDF binder.

The surface morphology study allows the identification of the breakage mechanism of LIBs during mechanical liberation. The combination of size-based hierarchy and morphology study can be used to understand the impact of PVDF adhesiveness towards the current collector breakage in mechanical liberation by comparing the new and spent LIBs and further discussed.

3.3. The concurrence of size-based hierarchy and its particle morphology

From the observation above, the new and spent LIBs does not exhibit a significant difference in terms of morphological characteristics. From the morphological analysis, a distinct property is observed above the cut point 850 μm. The copper foils are cleaner compared to the aluminium foils due to graphite laminate are more readily liberated as compared to $LiCoO_2$ laminate. The positive and negative electrode active materials show similar morphology below the cut point of 850 μm. Moreover, the separator is also contaminated by positive and negative electrode active materials.

From the morphological study that has been carried out using SEM, the liberated LIBs can be classified into four major categories based on the attachment of active materials onto the current collector and the size of the active materials detached. The bigger size fractions with active materials laminate on to it are categorised as Category 1 and Category 2. While the detached active materials that are still aggregated and held together by the binder are categorised as Category 3 and Category 4. The characteristics of different particles in different size fraction are summarised in Table 4.

In the case of spent LIBs, the stronger attachment of $LiCoO_2$ laminate on to the aluminium foil compared to graphite laminate on to the copper foil may help in explaining the change of trend in the re-mixing line of Fuerstenau upgrading diagram discussed in the previous section. The positive electrode found in the size region of 2360 μm – 850 μm were aluminium foils covered with $LiCoO_2$ laminate. The negative electrode counterpart has a minimum graphite lamination. Therefore, the $LiCoO_2$ lamination prevents the aluminium from breaking even further.
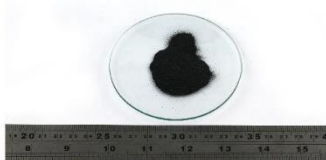
268

3.1

3.5

3.2

3.6

3.3

3.7

3.4

3.8

Fig. 3. Classified milled spent LIBs; 3.1)13200 μm–9500 μm, 3.2)9500 μm–6700 μm, 3.3) 6700 μm–4750 μm, 3.4)4750 μm–2360 μm, 3.5)2360 μm–850 μm, 3.6)850 μm–212 μm, 3.7)212 μm–38 μm, 3.8) <38 μm.

While the the weaker graphite lamination on to the copper collector have minimised this benefit and therefore concentrated at smaller size fraction. This can be seen from the size-based recovery rate in Table 4. The size-based recovery rate explains the recovery rate of a certain recoverable given it is isolated in a given size range and the sum of recovery rate of a certain recoverable for the entire size range is unity.

From Table 4, in the case of spent LIBs, when the size fraction above 2360 μm is isolated, the recovery rate of aluminium is higher than that of copper. Moreover, the recovery rate of copper is higher than aluminium in size range of 2360 μm to 212 μm and became aluminium dominant in the size fraction <212 μm. Although copper has better ideal mechanical properties and the perforation that occurs on the aluminium current collector, the stronger attachment of $LiCoO_2$ laminate on
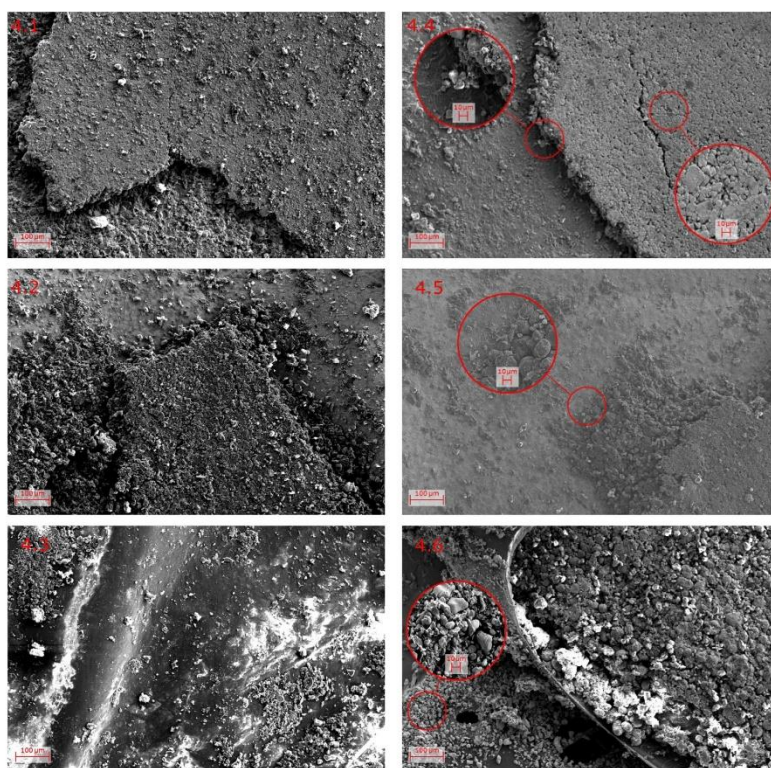
Fig. 4. SEM image of size fraction 4750 μm – 2360 μm; New LIBs: 4.1 Positive electrode, 4.2 Negative electrode, 4.3 Separator; Spent LIBs: 4.4 Positive electrode, 4.5 Negative electrode, 4.6 Separator.

to aluminium current collector seems to improve its overall mechanical properties and preventing it from breaking during milling. Instead, the shear and tensile stresses induced by the cutting mill dislodged the $LiCoO_2$ laminate in the form of big package forming Category 1 particles and the dislodged $LiCoO_2$ package concentrated in the size region of <850 μm (Category 3 and 4). However, when the stress-strain induced by the cutting mill does not dislodge the materials on its surface. Instead, it reduces the particle size while maintaining the active materials intact, covering the whole surface area resulting in Category 2 particles. On the other hand, there may not be a tangible benefit towards the mechanical properties for copper current collector due to weak bonding between graphite laminate on to the copper current collector and combined with the reduction in elastic modulus of copper current collector as the battery is cycled, causing the copper to be selectively liberated in the finer region when compared to aluminium.

As a baseline, comparison to the milled new LIBs was carried out. From Table 4, it can be seen that the new LIBs have minimum contamination from copper and aluminium in the size region of <850 μm. The better mechanical properties of the current collector and attachment of PVDF binder translates to lower contamination of copper and aluminium in the finer size region. A large difference is observed when comparing the copper recovery in the size region of >2360 μm (Category 1) for the new and spent LIBs. The milled new LIBs showed a recovery rate of 73.6 wt% copper, whereas the spent LIBs showed a recovery rate of only 59.8 wt% copper. The milled new LIBs produces more Category 1 copper particles. This indicates the significance of the graphite lamination strength in preventing the breakage of the copper current collector. Moreover, the better mechanical properties of the copper current collector in the new LIBs inhibits the breakage of copper particles with minimum active materials attachment (2360 μm – 850 μm) into fine particles that contaminates the finer size region (< 850 μm).

Similar interpretation also made with the aluminium particles, in which in the case of new LIBs is less contaminating in the finer size region. Instead, an increase in the recovery of aluminium in the Category 1 and Category 2 particles are observed. The better mechanical properties of the $LiCoO_2$ lamination also prevent the breakage of Category 3 particles into Category 4 particles during mechanical liberation.

270
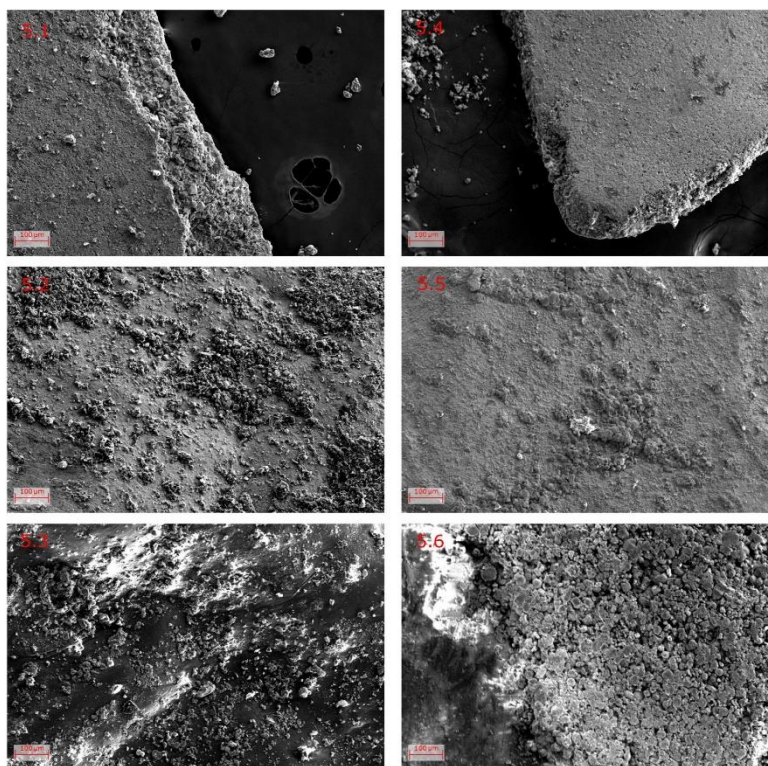
Fig. 5. SEM image of size fraction 2360 μm – 850 μm; New LIBs: 5.1 Positive electrode, 5.2 Negative electrode, 5.3 Separator; Spent LIBs: 5.4 Positive electrode, 5.5 Negative electrode, 5.6 Separator.

4. Conclusion

This article presents a systematic experimental study aimed at understanding the selective liberation of positive electrode active material during milling. From the analysis that has been carried out, the liberation is indeed a selective phenomenon with the optimum cut point of 850 μm. In the size fraction <850 μm, the recovery for spent LIBs is 43.7 wt% of $LiCoO_2$ with a minimum recovery of aluminium and copper (8.8 wt% and 10.3 wt%) from the feed. However, >50 wt% of $LiCoO_2$ is found in the size region of >850 μm, and it contains a substantial amount of aluminium and copper (91.2 wt% and 89.7 wt%) from the feed and are not suitable to be treated with leaching.

Milling spent LIBs induces selective liberation of $LiCoO_2$ laminate. From the morphological analysis, $LiCoO_2$ laminate have a stronger attachment to its current collector than the graphite laminate counterparts. From the morphological analysis done, a significant difference between the positive and negative current collector's surface can be seen in the size fraction of 2360 μm – 850 μm where the negative electrodes are cleaner compared to the positive electrode. The contradiction between copper and aluminium recovery rate towards $LiCoO_2$ recovery rate in the re-mixing line of Fuerstenau upgrading curve may be explained by the stronger $LiCoO_2$ lamination to the aluminium foil as compared to graphite lamination to copper. Other than the positive and negative electrode, some of the $LiCoO_2$ laminate was adhering on to the separator after liberation due to the compression action of the cutting mill. This also reduces the recovery rate of liberated $LiCoO_2$ in smaller size fraction.

The comparison between new and spent LIBs was made. A distinct difference was observed for the interaction of copper towards cobalt and aluminium. Better separation efficiency of $LiCoO_2$ particles is observed in the selective liberation of new LIBs. The better mechanical properties of current collectors and the adhesiveness of the binder in the new LIBs have made the finer size region to be less contaminated by the copper and aluminium. The effect of PVDF binder in preventing the breakage of copper current collector can be observed by the higher occurrence of copper in Category 1 particles in new LIBs than in spent

271
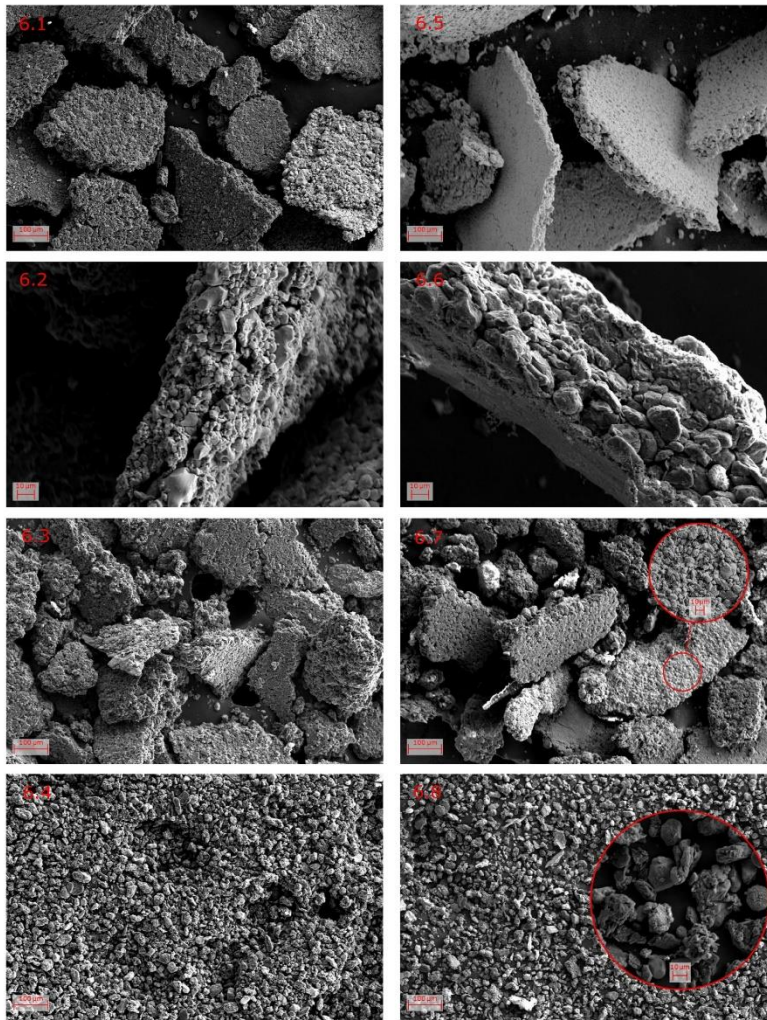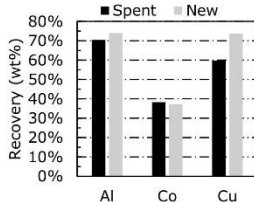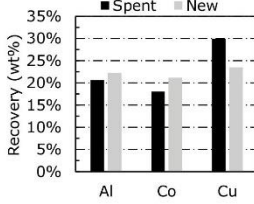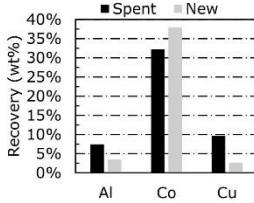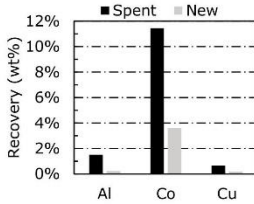
Fig. 6. SEM image of size fraction <850 μm; New LIBs: 6.1 Powder from size fraction 850 μm – 212 μm, 6.2 Zoomed LiCoO$_2$-PVDF aggregate from size fraction 850 μm – 212 μm identified by EDX, 6.3 Powder from size fraction 212 μm – 38 μm, 6.4 Powder from size fraction <38 μm; Spent LIBs: 6.5 Powder from size fraction 850 μm – 212 μm, 6.6 Zoomed LiCoO$_2$-PVDF aggregate from size fraction 850 μm – 212 μm identified by EDX, 6.7 Powder from size fraction 212 μm – 38 μm, 6.8 Powder from size fraction <38 μm.

LIBs. The better mechanical properties of new LIBs prevents the breakage of current collectors that contaminates the fine size region (<850 μm).

The mechanism of the selective liberation of LiCoO$_2$ laminate has been proposed. During milling, two possible outcomes may arise. Either LiCoO$_2$ laminate are dislodged and released in the

272

Table 4
Characterisation of classified LIBs powder.

Characteristics	Schematic Diagram	Size-Based Recovery Rate
Category 1: Include the majority of particles that have experience reduction in size, accompanied by some detachment of its active materials such as particles in the range of >2360 μm.		
Category 2: Include particles that have a reduction in size with active materials lamination, such as in the range of 2360 μm – 850 μm. (only true for positive electrode)		
Category 3: Active materials laminate that have been detached from its current collector and still held together by the binder. This type of particles comes as aggregates for the particle size of 850 μm – 38 μm.		
Category 4: Active materials laminate that have been detached from current collector and accompanied with minimum aggregation for the particle size of < 38 μm.		

form of $LiCoO_2$-PVDF aggregates that are concentrated in the size fraction of <850 μm or size reduction occurs while maintaining its attachment to the current collector. However, the size of the $LiCoO_2$-PVDF aggregates that are dislodged is still far from the actual size of $LiCoO_2$ particles as found in spent LIBs. Therefore, the cut point proposed (850 μm) is much greater than the actual size of $LiCoO_2$ particles found in spent LIBs (ca. 1.50 μm – 7.80 μm [23]).

Declaration of Competing Interest

The authors declare that there is no conflict of interest.

273

References

[1] G.E. Blomgren, The development and future of Lithium ion batteries, J. Electrochem. Soc. 164 (1) (2017) A5019–A5025.
[2] K.M. Winslow, S.J. Laux, T.G. Townsend, A review on the growing concern and potential management strategies of waste lithium-ion batteries, Resour. Conserv. Recycl. 129 (2018) 263–277.
[3] B. Moradi, G.G. Botte, Recycling of graphite anodes for the next generation of lithium ion batteries, J. Appl. Electrochem. 46 (2) (2016) 123–148.
[4] X. Zeng, J. Li, N. Singh, Recycling of spent Lithium-ion battery: a critical review, Crit. Rev. Environ. Sci. Technol. 44 (10) (2014) 1129–1165.
[5] F. Gu, et al., An investigation of the current status of recycling spent Lithium-ion batteries from consumer electronics in China, J. Clean. Prod. 161 (2017) 765–780.
[6] J. Gardiner, The Rise of Electric Cars Could Leave us with a big Battery Waste Problem, [cited 2017 10 November]; Available from https://www.theguardian.com/sustainable-business/2017/aug/10/electric-cars-big-battery-waste-problem-lithium-recycling 2017.
[7] V. Prieto-Sandoval, C. Jaca, M. Ormazabal, Towards a consensus on the circular economy, J. Clean. Prod. 179 (1 April 2018) 605–615.
[8] B. Swain, Recovery and recycling of lithium: a review, Sep. Purif. Technol. 172 (2017) 388–403.
[9] C. Pillot, Li-ion battery material market review and forecast 2012–2025, 3rd Israeli Power Sources Conference, 2013 , (Hertzlia (Israel)).
[10] B. Huang, et al., Recycling of lithium-ion batteries: recent advances and perspectives, J. Power Sources 399 (2018) 274–286.
[11] Y. Chen, et al., Thermal treatment and ammoniacal leaching for the recovery of valuable metals from spent lithium-ion batteries, Waste Manag. 75 (2018) 469–476.
[12] S. Ojanen, et al., Challenging the concept of electrochemical discharge using salt solutions for lithium-ion batteries recycling, Waste Manag. 76 (2018) 242–249.
[13] J. Xu, et al., A review of processes and technologies for the recycling of lithium-ion secondary batteries, J. Power Sources 177 (2008) 512–527.
[14] J. Ordoñez, E. Gago, A. Girard, Processes and technologies for the recycling and recovery of spent lithium-ion batteries, Renew. Sust. Energ. Rev. 60 (2016) 195–205.
[15] L. Gaines, Lithium-ion battery recycling processes: research towards a sustainable course, Sustain. Mater. Technol. 17 (2018), e00068.
[16] A.V.M. Silveira, et al., Recovery of valuable materials from spent lithium ion batteries using electrostatic separation, Int. J. Miner. Process. 169 (2017) 91–98.
[17] J. Yu, et al., A promising physical method for recovery of LiCoO 2 and graphite from spent lithium-ion batteries: grinding flotation, Sep. Purif. Technol. 190 (2018) 45–52.
[18] T. Zhang, et al., Characteristics of wet and dry crushing methods in the recycling process of spent lithium-ion batteries, J. Power Sources 240 (2013) 766–771.
[19] S.M. Shin, et al., Development of a metal recovery process from Li-ion battery wastes, Hydrometallurgy 79 (3–4) (2005) 172–181.
[20] J. Diekmann, et al., Ecological recycling of Lithium-ion batteries from electric vehicles with focus on mechanical processes, J. Electrochem. Soc. 164 (1) (2017) A6184–A6191.
[21] J. Li, et al., A combined recovery process of metals in spent lithium-ion batteries, Chemosphere 77 (8) (2009) 1132–1136.
[22] Y. He, et al., Recovery of LiCoO2 and graphite from spent lithium-ion batteries by Fenton reagent-assisted flotation, J. Clean. Prod. 143 (2017) 319–325.
[23] F.H. Pavoni, et al., LiCoO2 particle size distribution as a function of the state of health of discarded cell phone batteries, Powder Technol. 326 (2018) 78–83.
[24] S. Lee, J. Yang, W. Lu, Debonding at the interface between active particles and PVDF binder in Li-ion batteries, Extreme Mech. Lett. 6 (2016) 37–44.
[25] J. Vetter, et al., Ageing mechanisms in lithium-ion batteries, J. Power Sources 147 (1–2) (2005) 269–281.
[26] C. Dai, et al., Effects of cycle times and C-rate on mechanical properties of copper foil and adhesive strength of electrodes in commercial LiCoO2 LIBs, Eng. Fail. Anal. 101 (2019) 193–205.
[27] B. Standard, Secondary cells and batteries containing alkaline or other non-acid electrolytes – Secondary lithium cells and batteries for portable applications, Part 3: Prismatic and Cylindrical Lithium Secondary Cells, and Batteries Made from Them (IEC 61960–3:2017), BSI Standard Publication, 2017.
[28] M. Yoshio, R.J. Brodd, A. Kozawa, Lithium-ion Batteries: Science and Technologies, Springer Science & Business Media, 2010.
[29] F. Jeschull, M.J. Lacey, D. Brandell, Functional binders as graphite exfoliation suppressants in aggressive electrolytes for lithium-ion batteries, Electrochim. Acta 175 (2015) 141–150.
[30] M. Müller, et al., Investigation of binder distribution in graphite anodes for lithium-ion batteries, J. Power Sources 340 (2017) 1–5.
[31] B. Standard, Determination of ceratin substances in electrochemical products, Part 5: Cadmium, Lead and Chromium in Polymers and Electronics Cadmium and lead in Metals by AAS, AFS, ICP-OES and ICP-MS, BSI Standard Publication, 2014.
[32] Wills, B.A. and J.A. Finch, Particle Size Analysis. 2016: p. 91–107.
[33] M. Hesse, O. Popov, H. Lieberwirth, Increasing efficiency by selective comminution, Miner. Eng. 103–104 (2017) 112–126.
[34] M.A. Bérubé, J.C. Marchand, Evolution of the minerla liberation characteristics of an iron ore undergoing grinding, Int. J. Miner. Process. 13 (3) (1984) 223–237.
[35] M. Reichert, et al., Research of iron ore grinding in a vertical-roller-mill, Miner. Eng. 73 (2015) 109–115.
[36] T. Leißner, T. Mütze, U.A. Peuker, Nutzung der direkten Messung des Aufschlussgrades in Sortierkennfeldern, Chemie Ing. Tech. 86 (6) (2014) 899–905.
[37] G. Schubert, S. Bernotat, Comminution of non-brittle materials, Int. J. Miner. Process. 74 (2004) S19–S30.
[38] J. Butt, H. Mebrahtu, H. Shirvani, Microstructure and mechanical properties of dissimilar pure copper foil/1050 aluminium composites made with composite metal foil manufacturing, J. Mater. Process. Technol. 238 (2016) 96–107.
[39] D. Roundy, et al., Ideal shear strengths of fcc Aluminum and copper, Phys. Rev. Lett. 82 (13) (1999) 2713–2716.
[40] L. Beaulieu, et al., Colossal reversible volume changes in lithium alloys, Electrochem. Solid-State Lett. 4 (9) (2001) A137–A140.
[41] M.N. Obrovac, et al., Alloy design for lithium-ion battery anodes, J. Electrochem. Soc. 154 (9) (2007) A849–A855.
[42] J. Li, et al., Unravelling the impact of reaction paths on mechanical degradation of intercalation cathodes for Lithium-ion batteries, J. Am. Chem. Soc. 137 (43) (2015) 13732–13735.
[43] T. Waldmann, et al., A mechanical aging mechanism in lithium-ion batteries, J. Electrochem. Soc. 161 (10) (2014) A1742–A1747.
[44] J.W. Braithwaite, et al., Corrosion of lithium-ion battery current collectors, J. Electrochem. Soc. 146 (2) (1999) 448–456.
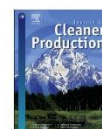
274

Recovering lithium cobalt oxide, aluminium, and copper from spent lithium-ion battery via attrition scrubbing

Samuel D. Widijatmoko [a], Gu Fu [b, c], Zheng Wang [a], Philip Hall [a, d, *]

[a] Department of Chemical and Environmental Engineering, University of Nottingham Ningbo China, 199 Taikang East Road Ningbo 315100, China
[b] Department of Industrial Engineering, Zhejiang University, Hangzhou, 310027, China
[c] National Institute of Innovation Management, Zhejiang University, Hangzhou, 310027, China
[d] Ningbo New Materials Institute, The University of Nottingham, Ningbo, 315042, China

ARTICLE INFO

ABSTRACT

In this manuscript, the results show that the single-stage liberation by using a cutting mill is sub-optimum. From the analysis, that the size fraction of <850 μm only recovers 43.7 wt% LiCoO2. With the recovery of 9.0 wt% aluminium and 10.6 wt% copper the remainder of the copper being in the >850 μm size fraction. The low recovery of LiCoO2 is caused by the particles that are still adhering on to the surface of the aluminium current collector. This lack of liberation prompted the use of attrition scrubbing as a secondary stage of mechanical treatment. 2.5 min Attrition scrubbing improves the selective liberation of cobalt towards aluminium and copper by 36.6% and 42.6% respectively. Attrition induces abrasion and it is shown to liberate the LiCoO2 particles. Results show a minimum of 80 wt% LiCoO2 particles can be recovered in the size fraction of <38 μm with 7.0 wt% aluminium and 6.1 wt% copper recovery, making attrition scrubbing a suitable second stage mechanical treatment for the recovery of LiCoO2.

© 2020 Elsevier Ltd. All rights reserved.

1. Introduction

Lithium-ion battery (LIB) technology has become the dominant energy storage for many consumer electronics and electric grids (Blomgren, 2017; Dunn et al., 2011). Despite the advancement of battery technology, present LIBs meet most of the requirements dictated by the large volume of the application linked to renewable energy and electric transportation field (Winslow et al., 2018). The spent LIBs from electric vehicles will emerge as the future waste problem with at least 25 billion units and 500 thousand tonnes of spent LIBs would be generated by 2020 (Richa et al., 2014; Zeng et al., 2014). When considering the natural scarcity and the demand projected for materials used in LIB production, cobalt is the most critical material as the demand for the future types of LIB is likely to contain embedded cobalt (Zubi et al., 2018).

In recent years, much research has been focused on developing efficient recovery methods for the materials found in spent LIBs.

With the positive electrode active materials as the main targeted component as it is where the incentive of LIBs recycling come from (Gaines, 2018). Current research to recover positive electrode active materials are focused on leaching processes (Li et al., 2018).

The components that makeup LIBs can be generalised into two major components, leachable and non-leachable. This is based on whether it can be dissolved or deconstructed to its elemental form during leaching. The positive electrode active materials, iron, and current collectors are of the leachable components. Whereas, other components such as graphite and polymeric materials are non-leachable components. The current practice is to obtain the positive electrode active materials via manual dismantling (Chen et al., 2019; Roshanfar et al., 2019; Yu et al., 2019), which is not practical on an industrial scale. In the mechanical treatment of spent LIBs leachable contamination by iron, copper, and aluminium are expected. The challenge in LIB recycling is to produce a positive electrode active material concentrate (LiCoO$_2$) that is suitable for the hydrometallurgical process without involving manual dismantling of LIB cell. Impurities such as iron aluminium and copper in the leach liquor can be effectively precipitated by adjusting the pH value between 4.5 (Joo et al., 2016) to 5.5 (Chen et al., 2011) using NaOH. Sa et al. (2015) argue that the removal of

Cu^{2+} is more difficult than the removal of Al^{3+} and Fe^{3+} due to the higher solubility constant of Cu^{2+} and led to the study of how the presence of copper may affect the performance of LiNi$_{1/3}$Mn$_{1/3}$Co$_{1/3}$O$_2$ (NMC) positive electrode active materials. The results suggest that 5 wt% copper impurity is acceptable for NMC battery (Sa et al., 2015).

The mechanical treatment of LIBs has been reported to be a selective phenomenon (Widijatmoko et al., 2020). The positive and negative electrode active materials can be concentrated in the finer size region without over crushing of other battery components in both wet and dry grinding (Zhang et al., 2013). The occurrence of selective liberation can then allow size-based separation to be carried out. The sieve size of the acts as the cut point to concentrate the positive electrode active materials. The positive and negative electrode active materials are concentrated below the cut point. Whereas, the copper, aluminium, and iron are predominantly found above the cut point. To concentrate positive electrode active materials, the cut point reported varies from 250 μm (He et al., 2017) to 2000 μm (Li et al., 2009). The smaller cut point of 250 μm has been reported to give high purity of positive electrode active material, but it only recovers 56.38% LiCoO$_2$ (He et al., 2017). Moreover, the cut point size of 250 μm is substantially greater when compared to the positive electrode active materials powder size found in LIBs (1.50 μm–7.80 μm) (Pavoni et al., 2018). This is due to the active materials are still aggregated or attached to the current collectors (Widijatmoko et al., 2020).

The occurrence of selective liberation also depends on the comminution technique being used (Hesse et al., 2017). Different techniques may result in different size distributions due to the predominant force acting during comminution as well as the milling conditions being employed (Gao and Forssberg, 1995). Selective liberation occurs when the breakage of a component is dependent on physical and mechanical properties (Mariano et al., 2016). Hesse et al. (2017) demonstrate that different predominant load being applied to a mineral would result in different liberation selectivity.

Considering the LIBs assembly, the active materials cast on the surface of current collectors can be scoured and liberated from the current collectors. Therefore, the use of liberation technique based on impact and abrasion is hypothesized to be a suitable method to promote selective libation of positive electrode active material. The use of attrition scrubbing is proposed to liberate the positive electrode active materials while minimising the breakage of copper and aluminium components.

Attrition scrubber has been designed to induce impact and shearing action between particles that promote surface abrasion and produces fine particles (Bayley and Biggs, 2005). Attrition scrubbing is conventionally used to upgrade minerals by removing surface impurities such as sand for glass making (METSO, 2018) and shown to be applicable for environmental remediation purposes such as the decontamination of storm water sediment (Petavy et al., 2009).

The original contribution of this work is related to the application of attrition scrubbing in the liberation of LiCoO$_2$ particles. The novel use of inert silica sand media as the abrasive allows the liberation LiCoO$_2$ which then allows for the concentration of LiCoO$_2$ in the finer size region. The LiCoO$_2$ product contains low copper contamination that is below the reported maximum tolerable contamination when undergoing hydrometallurgical processes. This paper will firstly describe the cause of poor liberation of LiCoO$_2$ when using a single-stage size-reduction. The proof of concept of using attrition scrubbing as a secondary liberation technique is then discussed and the mechanism is conveyed. Additionally, the breakage kinetics of LiCoO$_2$, copper, and aluminium are studied to understand the relative breakage of different components. Finally, a

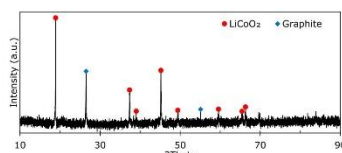Fig. 1. XRD spectra from spent LIBs. (The size fraction of <38 μm that is later collected after sieving is tested by using an XRD and comparison is then made with LiCoO$_2$ and graphite standard powder).

demonstration for the use of electrostatic separator to recover the copper and aluminium current collector is presented.

2. Experimental

2.1. Spent LIBs sample

The spent prismatic LIBs used in this study were collected from local electronic repair shops in Ningbo, China. Only LIBs containing LiCoO$_2$ as positive electrode active materials were used. The type of positive electrode active materials was later confirmed as LiCoO$_2$ using an X-ray Diffraction (XRD, Bruker-AXS D8 Advance) and the result is presented in Fig. 1.

All spent LIBs were firstly discharged by connecting to a 56-Ω resistor until the voltage is below 0.3 V to render them safe.

The spent LIBs were crushed using a cutting mill (Retsch SM2000) with 8 mm grid. The samples then dried in an oven at 80 °C until a constant weight was achieved to remove the volatile organic electrolytes. The bulk dried sample was then split into aliquots by using a static rifle with chute size of 31 mm × 160 mm with 16 alternating chutes.

The representative samples were then screened for ferromagnetic materials by using a cylindrical rare earth magnet enclosed in polyvinyl chloride (PVC) pipe. The ferromagnetic materials were found to be less than 2 wt%.

2.2. Attrition scrubbing experiment

Attrition scrubbing experiments were carried out using a WEMCO 1L lab-scale attrition scrubber with a constant impeller speed of 1000 rpm. Clean low iron silica sand in size range of 2360 μm–850 μm was used. In this study, the pulp density of 70 wt% with 10 wt% ratio of spent LIBs to silica sand media is used. The attrition time then varied from 2.5 min to 20 min.

Following attrition scrubbing, the product was wet sieved using 5 L water. Since the LiCoO$_2$ particles found in LIBs are in size range of 1.5 μm–7.8 μm (Pavoni et al., 2018), a 38 μm sieve was used as the cut point. Moreover, to prevent damage to the 38 μm sieve, the attrition product was firstly sieved by using a 212 μm sieve.

Following wet sieving, the products were dried in an oven at 80 °C until a constant weight was achieved.

The size fraction of >212 μm was further dry sieved into different size fractions. In this study, the attrition products were sieved into the size fraction of >4750 μm, 4750 μm–2360 μm and 2360 μm–850 μm and weighted to the nearest 0.1 g. The 212 μm–38 μm and <38 μm product from dry sieving are combined with the dried sample from wet sieving and weighted the same way. The classified products are then analysed for elemental content.

2.3. Elemental analysis

The elemental analysis is adapted from *BS EN 62321-5:2014* (Standard, 2014). It is important that the sample tested is a representative of the entire aliquots and particle size of <250 μm is suggested in the standard. To fulfil this requirement, calcination was firstly carried for particles with a size greater than 212 μm to remove polymers that are difficult to mill. The calcination was carried out in multiple stages to prevent a sudden release of gas with the final stage at 500 °C for 3 h. The samples are allowed to cool down to room temperature and milled using a centrifugal mill (Retsch ZM200) with 0.25 mm grid. All product was sieved with a nominal aperture size of 212 μm. The size fraction of >212 μm was re-milled until the mass recovery rate of <212 μm is greater than 95 wt%. Approximately 0.2000 g ± 0.010 g of sample were weighed to four decimal places using an analytical balance.

The digestion is carried out in multiple stages of acid addition. The first stage includes 0.2 g of solid digested wit 4 ml USP grade 68 wt% HNO_3, 1 ml H_2O and 1 ml 30 wt% H_2O_2. The digestion vessels the sealed and was digested with a microwave digester (CEM MARS 5) equipped with temperature control. The microwave was set to 80 °C with a ramp time of 8 min and holding time of 2 min, followed by a further increase in temperature to 120 °C with a ramp time of 4 min and holding time of 5 min. The solution was let to cool down to a temperature below 30 °C and 4 ml of USP grade 37 wt% HCl then added and digested with the same setting previously stated. Multi-elements standard calibration curves were made by diluting and mixing different single element standard reference stock solutions (Sigma-Aldrich). The sample then analysed using an Inductively Coupled Plasma – Mass Spectrometry (ICP-MS, Nexion 300x).

2.4. Morphology observation

Scanning Electron Microscopy – Energy Dispersive X-Ray (SEM-EDX, Zeiss-Sigma-VP). The backscattered detector allows a different compound to be identified based on the average molecular weight. The heavier average molecular weight being brighter than the lighter average molecular weight. The backscattered detector was used to observe the morphological characteristics with the EDX identifies the different element present. Prior to morphological analysis, the surface is mace conductive by applying 4 nm gold layer by using gold sputtering machine (LEICA EM SCD 500).

There are currently two types of binder that are widely used; which are PVDF and SBR-CMC. The morphology analysis with EDX shows the presence of fluorine atoms and the absence of sodium atoms. This observation suggest that the binder used in positive and negative electrode is PVDF.

2.5. Electrostatic separation experiment

The electrostatic separator allows the separation of materials based on the difference in surface conductivity or by the preferential charging and attraction materials to an electric field of opposing charge potential (Kelly and Spottiswood, 1989). The electrodynamic mode involves the use of ionizing electrode and static electrode, whereby all particles receive a positive or negative charge. The separation then occurs by leakage of this assumed charge by the conductive materials compared to the retention of charge by the non-conductors. Thus, the electro-dynamic mode is able to produce fractions that concentrate non-conductive, middling, and conductive components (Kelly and Spottiswood, 1989).

Silveira et al. (2017) demonstrate that the combination of size-based separation and electrostatic separations in electro-dynamic mode allows the separation of milled LIBs components into four different product class of active materials powder, polymers, mixture (polymers and metal), and the metallic fractions. The reported optimum parameters were initially used as a starting point and adjusted accordingly based on the visual inspection of the separated products.

In this manuscript, a roll-type electrostatic separator (Carpco, HT (15,25,36)) was used to separate the attrition products > 38 μm. The size of the static electrode is 71.5 cm × 12.5 cm X 5 cm (length x width x height), ionization electrode is a 0.010 mm wire of 10 cm in length, and roll radius of 12.7 cm. The experiment was performed at air relative humidity of 40%–50% and temperature of 20 °C. The feeder vibration was maintained constant at 30% of its maximum power.

3. Results and discussion

3.1. Characteristics of spent LIBs sample

Three representative samples that were crushed using a cutting mill only were classified. The average particle diameter (d_{50}) was found to be 1.5 mm. Each different size fraction then subjects to elemental analysis for the desired element content. The size-based recovery rate of the key elements is presented in Fig. 1.

Fig. 2 shows that the recovery of copper and aluminium decrease as the particle size decreases. Whilst, the recovery of cobalt is dispersed throughout the various size fractions. The recovery of cobalt is higher than that of copper and aluminium below cut point 850 μm. The use of 850 μm as the cut point concentrates 43.7 wt% cobalt from the feed with the recovery of copper and aluminium of 10.3 wt% and 9.0 wt% respectively. Therefore, the size reduction of spent LIBs by using a cutting mill does induce a selective liberation of $LiCoO_2$ particles in the finer size region of <850 μm. The occurrence of selective liberation by a cutting mill also confirms previously published results (Wang et al., 2016). Where the smaller size fraction seems to concentrate positive electrode active materials. However, instead of $LiCoO_2$ particles being liberated by the cutting mill, the occurrence of selective liberation of $LiCoO_2$ particles is attributed by the minimum breakage of the copper and aluminium counterparts. This then results in the size fraction above the cut point 850 μm concentrates 89.7 wt% copper and 91.0 wt% aluminium with as much as 56.3 wt% of cobalt is also found in this size fraction. The reason why the single-stage liberation by using only a cutting mill is of sub-optimum is as it does not inherently liberate $LiCoO_2$ particles.

To understand the sub-optimum liberation of $LiCoO_2$ particles, the morphological observation by using SEM-EDX with a back-scattered detector was carried out for the size fraction above and below 850 μm. The back scattered detector identifies different LIB components by the different contrast. The compound with heavier average molecular weight would be perceived brighter than the lighter average molecular weight. The EDX identifies the different elements present in the compound. Furthermore, the EDX can detect the presence of fluorine atoms with no sodium atom detected for the both $LiCoO_2$ and graphite laminates. Based on this observation, the binder used in the spent LIBs is deduced to be PVDF rather than SBR-CMC that contains sodium atoms.

Fig. 3 shows the morphology of milled spent LIB particles above and below the 850 μm size fraction. From Fig. 3a and b, it is shown the aluminium and copper current collectors are still contaminated by the $LiCoO_2$ and graphite particles. Moreover, from Fig. 3c, it can be observed that the cutting mill induces liberation of $LiCoO_2$ and graphite particles in the form of aggregates that are still held together by the PVDF binder. The $LiCoO_2$ particles are not liberated and the morphological observation suggests that the initial
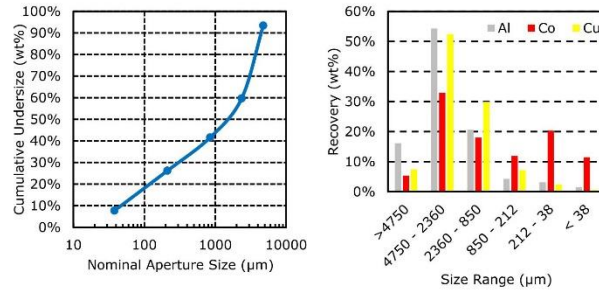
Fig. 2. The cumulative undersize semi-logarithmic pot of shredded spent LIBs and the size-recovery rate for respective size range.

liberation of spent LIBs by using a cutting mill only leads to a sub-optimum result.

3.2. Attrition liberation proof of concept

The suitability of an attrition scrubber as a second liberation stage to selectively liberate LiCoO₂ particles is initially measured by assessing the attrition from a short duration of 2.5 min attrition time with 70 wt% pulp density and 10 wt% of LIBs to silica sand ratio. The product was then sieved to produce different size fractions and digested for elemental analysis as previously described in the experimental method. The aluminium, cobalt, and copper elements were detected, and the size-based recovery rate is presented in Fig. 4.
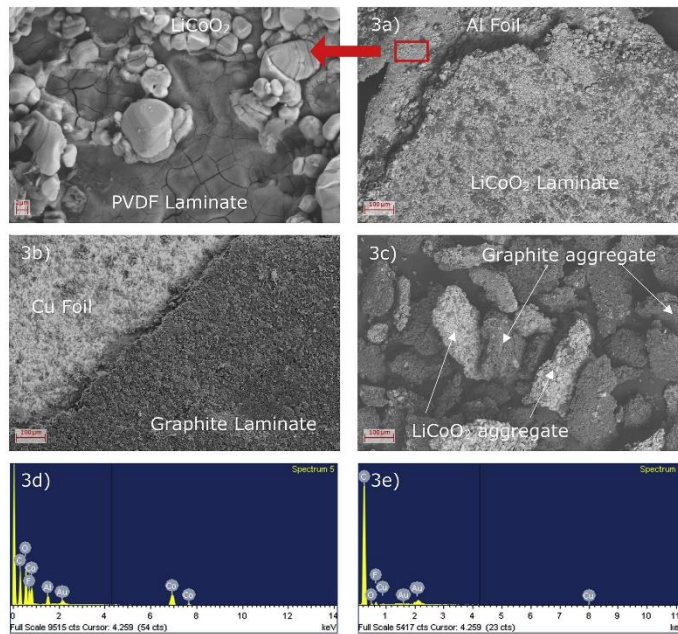
Fig. 3. SEM image by using back scatted detector of 3a) Positive electrode >850 μm 3b) Negative electrode >850 μm 3c) Powder <850 μm 3d) EDX spectra from positive electrode 3e) EDX spectra from negative electrode.

278

Fig. 4 shows the size-based recovery rate of aluminium, cobalt, and copper after attrition. Comparing the result of size-based recovery distribution for the sample before (Fig. 2) and after (Fig. 4) attrition, the copper and aluminium components are still dispersed in the size fraction of >38 μm. However, cobalt has a much higher recovery rate increase in the size fraction of <38 μm from 11.4 wt% to 80.0 wt%. From Fig. 4, the size fraction of <38 μm recovers 7.0 wt % aluminium and 6.1 wt% copper. The majority of the copper and aluminium can be found in the size fraction of >38 μm. The results indicate that attrition scrubbing allows the selective liberation of LiCoO$_2$ particles.

In order to quantify the degree of improvement of selective liberation, the Fuerstenau upgrading curve in a recovery plot for the classified comminution product in percentage finer is used (Hesse et al., 2017). To plot the Fuerstenau recovery plot, the desired (valuable) component and undesired (waste) is firstly defined. In this case, the valuable component is cobalt with the waste components of copper and aluminium. The cumulative recovery of valuable and waste with increasing cut point size is plotted in the same graph. By this way, the selective liberation of cobalt, copper, and aluminium can be determined. Moreover, by taking the aluminium as valuable and copper as waste, the selective liberation occurrence between the two can also be assessed.

Fig. 5 presents the comparison of selective liberation in the form of Fuerstenau recovery curves for the cobalt-aluminium (Co–Al), cobalt-copper (Co–Cu), and aluminium-copper (Al–Cu). In a Fuerstenau recovery plot, the selective comminution product is always separated into two fractions of the fine and coarse fraction. When the plot of the cumulative valuable and waste is of a diagonal line, it indicates that there is no selective liberation. A recovery curve above the diagonal line indicates that the valuable component is selectively liberated in the finer size region. Otherwise, the recovery curve below the diagonal line indicates the enrichment of valuable component in the bigger size fraction.

From Fig. 5, the first stage of liberation using a cutting mill does induce selective liberation of cobalt in the finer size region. The result suggests that selective liberation of LiCoO$_2$ in the finer size region is improved using an attrition scrubber. This is indicated by the recovery line of Co–Al and Co–Cu that are further from the diagonal following attrition. Furthermore, the Fuerstenau plot which takes account of the interaction between aluminium and copper (Al–Cu) is also shown in Fig. 5 indicates that the aluminium is concentrated in the larger size fraction relative to copper.

From the Al–Cu plot shown in Fig. 5, the result suggests that there is a minimum improvement in the enrichment of the two components based on size. Therefore, the use of size-based separation to separate copper and aluminium is a challenging task.

The selective liberation improvement employing attrition scrubber as the second stage can quantified by measuring the area bound by the recovery line and the diagonal line. It is important to point out that the area of 0.50 arbitrary unit (a.u.) between the recovering line and diagonal line is the highest area achievable if perfect separation has occurred. In this discussion, the integration is carried using the trapezium method. The results are presented as selective liberation efficiency %; that is the area bound by the recovery line and the diagonal line divided by 0.50 a.u. and summarised in Table 1.

From the results presented in Table 1, the initial liberation using only a cutting mill does induce a degree of selective liberation of cobalt towards aluminium and copper by 42.7% and 34.4 % respectively. Attrition scrubbing as the second stage of liberation improves the selective liberation of cobalt towards aluminium and copper by 36.6% and 42.6% respectively. There is only a slight increase in the selective liberation efficiency between aluminium and copper by 2.2%. Thus, the separation of aluminium and copper based on size for attrition scrubbing product is still unlikely.

From the proof of concept laid out, the initially sub-optimum liberation of LiCoO$_2$ particles using cutting mill only can be further improved by the use of attrition scrubbing as a second stage for liberation. The attrition products concentrate the majority of LiCoO$_2$ particles in the fine size region of less than 38 μm in 2.5 min attrition time. Furthermore, it is also expected that the graphite is also concentrated together with the LiCoO$_2$ particles due to the weaker attachment of graphite laminate onto the copper current collector as compared to the LiCoO$_2$ laminate counterparts (Dai et al., 2019). This weaker attachment of the negative electrode active materials may also help to explain the Fuerstenau Al–Cu curve that is below the diagonal line. The LiCoO$_2$ laminate may help in maintaining the aluminium current collector shape and preventing further breakage. Whereas, the copper current collector may not have this benefit.

Morphology observation of attrition product is presented in Fig. 6. The weaker attachment of graphite towards copper current collector as compared to the aluminium counterparts can be clearly seen by comparing Fig. 6a–b. The copper current collector is relatively cleaner than that of the aluminium counterpart. Fig. 6c shows clean copper and aluminium in the size fraction of 850 μm–212 μm. This results from the breakage of copper and aluminium from the size fraction >850 μm after 2.5 min attrition time. Furthermore, the initially aggregated LiCoO$_2$ particles are no longer can be found in this size fraction. Instead, the particles have been disaggregated into the size fraction of <38 μm as observed in Fig. 6d. Moreover, the copper and aluminium components were not observed in Fig. 6d and suspected to break into fine particles and contaminate
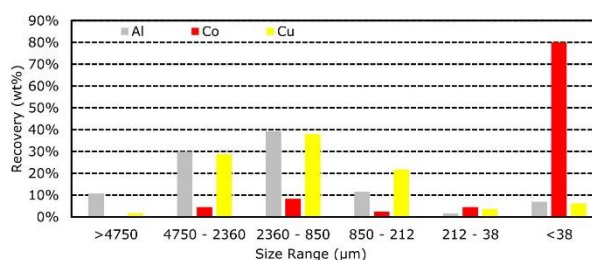

Fig. 4. The size-based recovery distribution of aluminium, cobalt and copper for different size fraction after size reduction and attrition.
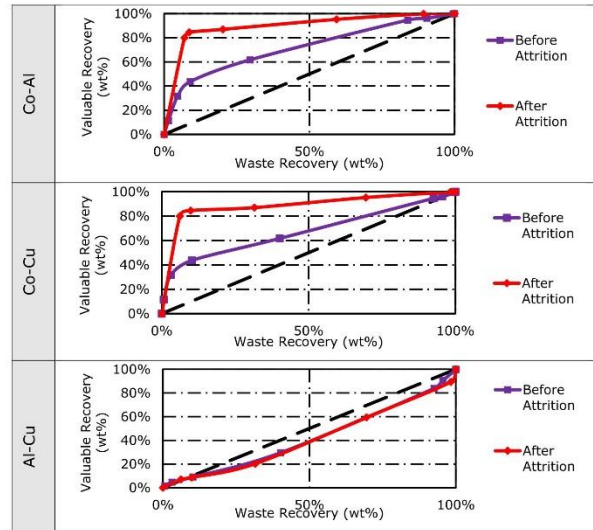
279

Fig. 5. Fuerstenau recovery curves comparison before and after attrition.

Table 1
Comparison of selective liberation efficiency before and after attrition.

| Recovery Line | Selective Liberation Efficiency | | | | | |
| | 1st Stage | | 2nd Stage | | Change | |
	a.u.	%	a.u.	%	a.u.	%
Co–Al	0.21	42.7	0.40	79.3	0.18	36.6
Co–Cu	0.17	34.4	0.38	77.0	0.21	42.6
Al–Cu	0.07	14.3	0.08	16.5	0.01	2.2

the surface of the larger particles.

To confirm that the copper and aluminium contaminating the surface of the larger particles, elemental mapping by using EDX was carried out for the attrition product of <38 μm. The EDX-elemental mapping was set to detect the cobalt, silicon, copper and aluminium elements and the results of the elemental mapping is presented in Fig. 7. From the observation, it was found that some of the graphite, LiCoO$_2$ and SiO$_2$ particles are contaminated by copper and aluminium fine particles. From the elemental mapping results, it is understood that further mechanical separation of copper and aluminium from this powder may be challenging.

Comparing the particle morphology of before and after attrition, the impact and shearing load appears to liberate the active materials that laminate the positive and negative electrodes. The impact load causes the disaggregation of LiCoO$_2$ and graphite and is concentrated in the size fraction <38 μm and scours the particles from the aluminium and copper current collectors. The size fraction of 850 μm–212 μm does not initially have clean copper and aluminium. However, after attrition, clean copper and aluminium can be found in this region. Thus, the liberation of LiCoO$_2$ and graphite particles also followed by the breakage of copper and

aluminium. The breakage of copper and aluminium current collector is deduced to be slower than that of the active materials. To confirm this, the study related to the breakage kinetics of LiCoO$_2$ laminate as compared to the copper and aluminium current collector was carried out.

3.3. The breakage kinetics and its implication

The pulp density and the LIBs to silica sand ratio were kept constant at 70 wt% and 10 wt% respectively. Samples from the size fractions 4750 μm–2360 μm, 2360 μm–850 μm, 850 μm–212 μm, 212 μm–38 μm, and <38 μm with different attrition time is analysed for aluminium, cobalt, and copper. The comparison of breakage kinetics can then be made for different components of spent LIBs. Breakage kinetics of wet and dry grinding has been reported to be a first-order (Sadler et al., 1975). The rate of disappearance, by breakage, from a given narrow size, is given by Equation (1).

$$\frac{dw}{dt} = -kw \qquad\qquad 1$$

Where w is the weight of material in the given size fraction, t is time, and k is milling rate constant for the given size fraction. k is, in general, different for each size fraction present and is dependent on operating parameters, mill design, the material being milled, and the environment inside the mill.

Equation (1) may be integrated to give Equation (2).

$$w = w_0 e^{-kt} \qquad\qquad 2$$

Where w$_0$ is the initial amount of material present in the specific
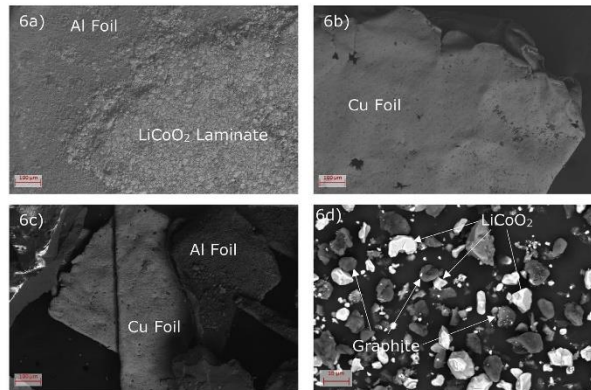
Fig. 6. SEM image after 2.5 min attrition time by using back scatted detector of 6a) Positive electrode >850 μm 6b) Negative electrode >850 μm 6c) Powder 850 μm−212 μm 6d) Powder <38 μm.

size range. Equation (2) suggests that a plot of ln w versus t should be a straight line with ordinate intercept ln w_0 and slope equal to −k.

Two cut points of 2360 μm and 38 μm are assessed to compare the breakage kinetics.

From Fig. 8, in the initial phase, the breakage kinetics of aluminium, copper, and cobalt does not initially follow the first-order breakage kinetics for both the 2360 μm and 38 μm cut point. This is ignored when calculating the breakage kinetics. The breakage rate comparison of aluminium, copper and cobalt is calculated using the linear region. Therefore, in this study, the breakage kinetics were calculated using the points after initial breakage.

From Fig. 8a, by comparing the aluminium and copper breakage gradient, it can be seen that the aluminium component experiences a slower breakage rate than that of the copper component. This can be explained via the copper foil mechanical degradation after the battery is being cycled that makes copper mechanically weaker than aluminium. The weaker attachment of graphite laminate on to copper than that of LiCoO$_2$ laminate on to aluminium may also help to explain this phenomenon. The copper became more susceptible to breakage by the attrition media as compared to the aluminium foil that is more protected by the LiCoO$_2$ laminate.

Fig. 8b shows the breakage kinetics of the LiCoO$_2$ particles via the detection of cobalt through the cut point 2360 μm. Comparing the gradient of LiCoO$_2$ laminate breakage kinetic to that of aluminium and copper, it can be seen that the LiCoO$_2$ laminate breaks at a faster rate than that of copper and aluminium. This also implies that the liberation of LiCoO$_2$ particles is required prior to the breaking of the aluminium. Hence, this also confirms that the LiCoO$_2$ laminate prevents the breakage of the aluminium component.

The breakage kinetics of aluminium and copper passing through the cut point of 38 μm is presented in Fig. 8c. Similarly, to the phenomenon described for Fig. 8a, the aluminium breaks slower than that of copper.

From Fig. 8d, it can be seen that the LiCoO$_2$ laminate breakage rate towards the cut point of 38 μm is faster than that of copper and

aluminium. The gradient of the cobalt breakage kinetics is much higher than that of copper and cobalt. The substantially faster breakage of LiCoO$_2$ laminates towards the cut point of less than 38 μm is expected. The LiCoO$_2$ particle size range found in spent LIBs is between 1.50 μm−7.80 μm (Pavoni et al., 2018). This indicates that the liberation of LiCoO$_2$ particles that are still held together by the binder is much faster than the fines produced by the breakage of aluminium and copper.

The comparison of the breakage kinetics of aluminium, copper and LiCoO$_2$ laminate shows that the LiCoO$_2$ laminate breaks faster than that of copper and aluminium. The faster rate of LiCoO$_2$ laminate shows that it is selectively liberated during attrition. Moreover, the copper component breaks faster than the aluminium component. These may be caused by the following factors:

- The copper and aluminium foils in the bigger size fraction are still coated by the active materials and thus resulting in the liberation of active material laminates prior to the breakage of the copper and aluminium component during attrition.
- The weaker attachment of graphite lamination on to copper current collector than that of LiCoO$_2$ lamination on to aluminium. Moreover, as the battery is cycled, the mechanical properties of copper degrade more severely than the aluminium counterparts. These helps explain the faster breakage rate of copper when compared to aluminium.
- The LiCoO$_2$ laminate is held together by PVDF binder that has weaker mechanical properties than that of copper and aluminium. The copper and aluminium foil has higher tensile strength than PVDF (Butt et al., 2016; Group, 2011). As a result, the LiCoO$_2$ particles are being disaggregated and thus resulting in faster liberation rate as compared to the copper and aluminium counterparts. This effect is more apparent for the breakage rate of cobalt in comparison with copper and aluminium into the size fraction of less than 38 μm.

Fig. 9 presents the recovery rate of aluminium, cobalt and copper concentrated in the size fraction of less than 38 μm. From Fig. 9, LiCoO2 has the highest recovery rate compared to copper and

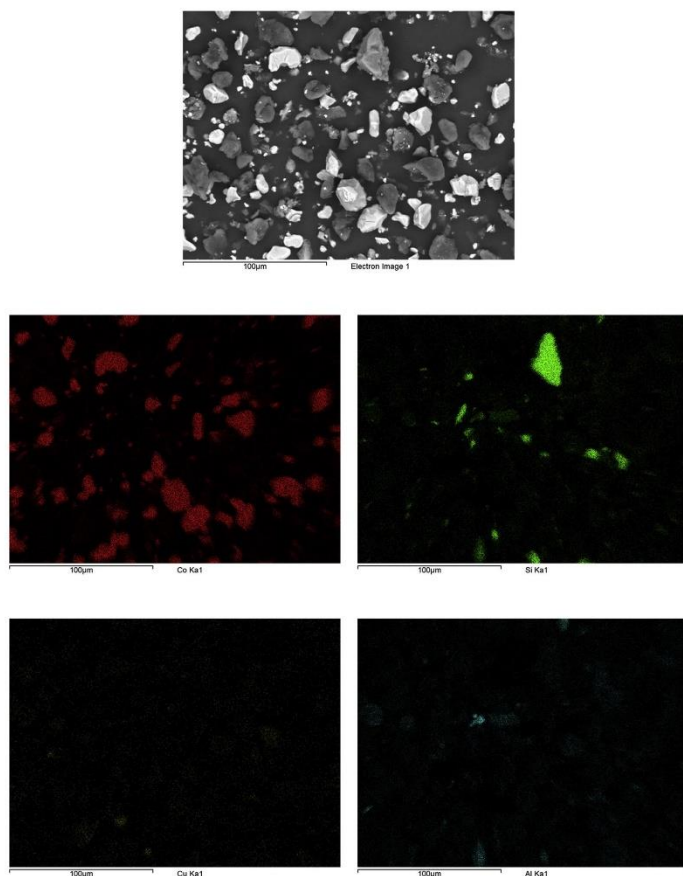**Fig. 7.** EDX-Elemental mapping of 2.5 min < 38 μm attrition product.

aluminium. The increase recovery of $LiCoO_2$ particles also followed by the decrease in $LiCoO_2$ grade. With the assumption that the graphite is liberated with the same degree than that of $LiCoO_2$ particle and the ratio of $LiCoO_2$ to graphite is constant. The concentration of the graphite particles in the size fraction <38 μm is calculated based on the ratio of cobalt to graphite in $LiCoO_2$ batteries from the published data by (Wang et al., 2016). By this way, the concentration of the silica sand in the <38 μm attrition product can also be estimated and summarised in Table 2.

From Table 2, despite the increase in recovery of $LiCoO_2$ particles as attrition time increases, the $LiCoO_2$ grade decreases as the attrition time increases. This is attributed to the contamination caused by the silica sand media as attrition time increases. This is caused following the breakage of silica particles. The contamination from the attrition media is expected, and low iron silica sand has been chosen for it is chemically resistance to the lixiviant which has been proposed by researchers to leach the $LiCoO_2$ particles. Therefore, the main leachable contamination of attrition products is copper and aluminium. From previously reported literature, a proportion of 5 wt% copper relative to $LiCoO_2$ is a tolerable contamination for leaching and resynthesizing (Sa et al., 2015). Aluminium can initially be removed via dissolution by using NaOH. From Table 2, the 20 min attrition time results in only 3 wt% copper relative to $LiCoO_2$. Therefore, the attrition product can be concluded

282
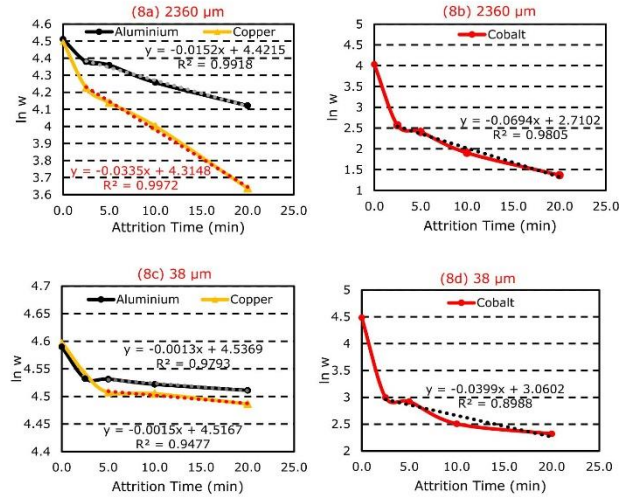
Fig. 8. The breakage kinetics of aluminium, copper, and LiCoO₂ laminate (cobalt) for less than 2360 μm and 38 μm.

Fig. 9. Recovery rate of aluminium, LiCoO₂ (cobalt) and copper in the size fraction of less than 38 μm with varying attrition time.

Table 2
Composition of attrition products following attrition against time.

Attrition Time (min)	Concentration (wt%)				
	Al	LiCoO₂	Cu	Graphite	Sand
0.0	1.6	60.7	0.8	36.9	0.0
2.5	0.8	48.7	1.0	39.1	1s0.4
5.0	0.8	45.6	1.3	36.7	15.6
10.0	0.9	44.6	1.3	35.9	17.4
20.0	0.9	40.9	1.3	32.9	23.9

to be suitable for subsequent hydrometallurgical processes. Remaining graphite can be separated from silica sand by using froth flotation due to the hydrophilicity difference (i.e. graphite is hydrophobic and silica sand is hydrophilic) (Lu and Forssberg, 2001).

Diekmann et al. (2017) have proposed a second stage liberation by using a cutting mill, the active material fine particles concentrate were recovered by using air classifier, this method resulted in 75% recovery. Comparing the method proposed, higher recovery rate of active materials from second stage wet liberation by using an attrition scrubbing can be found (80.0 wt% - 89.8 wt%). Moreover, the use of air classifier to recover spent LIBs active materials may impose serious hazard related to respiratory health.

3.4. The separation of attrition scrubber >38 μm product

The majority of the LiCoO₂ particles are concentrated in the size fraction of less than 38 μm. The size fraction >38 then concentrates the copper and aluminium current collectors. The >38 μm sample obtained then subject to the electrostatic separation to separate polymer, silica sand and the current collector. A roll-type electro-static separator (Carpco, HT (15,25,36)) was used in this study.

The electrostatic separator comprises of two main components which are the beam and static electrode. The ionizing electrode pinned nonconductive materials on to the roll and collected at the end of the roll by a static brush. For the particles that are heavier than the pinning action are collected as middlings. The static electrode attracts conductive materials while leaving the non-conductive to fall through the roll and collected. Considering the composition of the sample, both electrodes were used to separate the sample into three different fractions, such that the polymeric separator and fine silica sand would be pinned on to the roll and collected on the left hand side of the receptacle, the voltage is adjusted so that the silica sand >850 μm would not be pinned as strongly as the polymeric separator and collected as middling, and the conductive materials are thrown into the right side of the receptacle.

The optimum conditions reported by Silveira et al. (2017) were initially used and need to be adjusted for a workable parameter. The

283

Table 3
Parameters set for the electrostatic separator.

Parameters	Silveira et al. (2017)	Adjusted Value
Roll Speed (RPM)	20	50
Electrode Voltage (kV)	25	20
d1-Ionization Electrode Distance (cm)	6	5
d2-Static Electrode Distance (cm)	6	8
θ_1 (°)	25	35
θ_2 (°)	75	65
Deflector I Angle (°)	N/A	50
Deflector II Angle (°)	N/A	35

particles were flowing unevenly and arching between the electrodes towards copper and aluminium foils was observed. Moreover, that the silica sand with particle size of >850 μm was strongly pinned onto the roll and can be found in the non-conductor fraction. To overcome these issues, adjustment trial and error based on visual inspection was carried out to adjust the parameters and minimise these issue. The key parameters of the electrostatic separator are shown in Table 3.

The deflector angle I and II were kept constant at 50° and 35° respectively. The roll speed was initially 20 rpm and adjusted to 50 rpm to make the particle flows evenly. After adjusting the roll speed, the arching from the ionization electrodes to the copper and aluminium foils are still observed, the electrode voltage is then reduced from 25 kV to 20 kV. The decrease in electrode voltage also causes the larger silica sand >850 μm to be less strongly pinned on to the roll and less lifting action for the copper and aluminium foils. This then result in LIB separator found as middling and copper and aluminium foils were observed to falls together with the silica sand.

The ionization electrode is then moved closer to the roll from 6 cm to 5 cm and cause more separator pinned onto the roll. However, visual inspection reveals that the copper and aluminium foil is visually flowing together with the silica sand. The distance between the ionization electrode and the feeder (θ_1) was adjusted from 25° to 35°. This is done to extend the charging time for the particles to acquire charge. However, keeping the distance between the two electrodes constant seems to do not allow enough residence time for the copper and aluminium foils to undergoes charge reversal that is sufficient to lift the particles. The distance between the two electrodes was made narrower and adjusted from 50° to 40° (from $\theta_2 = 75°$ to $\theta_2 = 65°$). After adjusting the ionizing and static electrode angle, the copper and aluminium is lifted and hitting the static electrode. Therefore, the static electrode (lifting electrode) is moved further from the roll to minimise the electrode getting hit by the copper and aluminium foils.

In a one-pass electrostatic separation, only copper and aluminium foils are registered as a conductive fraction. However, it was observed that the middling still contains a substantial amount of conductor materials and therefore the middling was re-introduced into the feeder. The middling was re-introduced to the feeder for five times. To assess the grade of the resulting separation, manual picking was done. The schematic diagram of the electrostatic separator, as well as the resulting separated products, are shown in Fig. 10. The conductive fractions obtained (Fig. 10a) were of 97.65 wt% metal, the impurities came from the short-circuiting of the silica sand from the middling. The middling obtained (Fig. 10b) contain 99.01 wt% silica sand with small impurities from the copper and aluminium current collector. The nonconductive (Fig. 10c) obtained contains 95 v% (14.87 wt%) battery
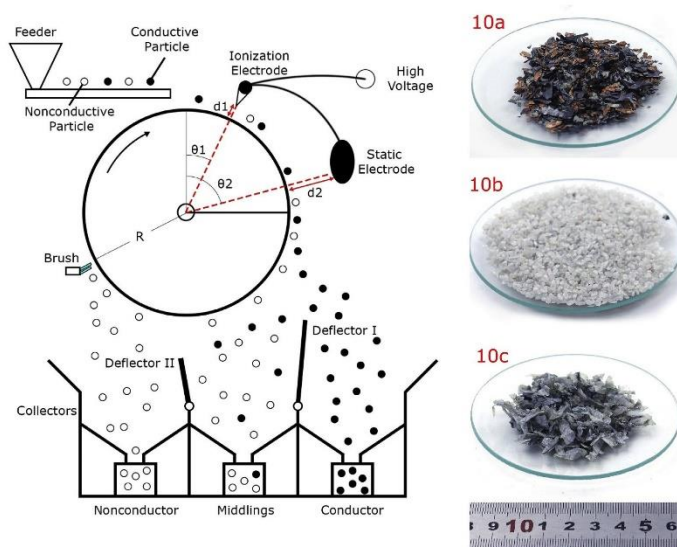
Fig. 10. Schematic diagram of an electrostatic separator and the resulting products; 10.a – Conductor, 10b - Middlings, 10c – Non-conductor.

separator, with the main contamination from the fine (<850 μm) silica sand.

The results from this exploratory study suggest that electrostatic separator is a useful technique in separating the current collectors and polymeric materials from the attrition media. It is also observed that the attrition media that has undergone size reduction <850 μm are registered as nonconductive and collected together with the polymeric materials. The recovered attrition media are visually clean from the separator and with minimum contamination from copper and aluminium, and therefore can be re-used for the subsequent attrition media.

4. Conclusion

Mineral processing technique is an important part in LIBs recycling to liberate and concentrate valuable metals due to its high throughput (Al-Thyabat et al., 2013). The recovery technique proposed in this research allows the majority of LiCoO2 particles to be recovered in the size fraction of <38 μm with minimum contamination from copper and aluminium components and therefore reducing the need for leachate purification during hydrometallurgical process. This is achieved by using attrition scrubbing as the second stage of liberation.

From the morphological analysis of particles before attrition, above and below cut point of 850 μm shows a distinct difference. Above the cut point 850 μm, the LiCoO2 particles are still laminating the aluminium current collector. Whereas, below the cut point 850 μm, the LiCoO2 particles are in the form of aggregate. Based on this observation, two cut points of 2360 μm and 38 μm were selected. The cut points selected in order to study the different breakage rate for delamination (2360 μm) and deaggregation (38 μm) of LiCoO2 particles. The breakage kinetics of LiCoO2 particles for cut point 2360 μm is faster than that of cut point 38 μm. This indicates the delamination is faster than the deaggregation of LiCoO2 particles. Moreover, the results show that the breakage rate follows the order of LiCoO2>Cu > Al for both cut points. This result indicates that the LiCoO2 delamination and disaggregation is faster than the breakage of the copper and aluminium foil. This then results in 89.8 wt% LiCoO2 recovery with minimum 9.0 wt% aluminium and 11.2 wt% copper recovery within 20 min attrition time.

The use of attrition scrubbing as a second stage liberation technique has been proposed to concentrate LiCoO2. Moreover, the copper and aluminium can be recovered by using electrostatic separator. However, the technique proposed is still carried out in a lab scale and have not yet been tested in a pilot scale and is the main drawback of the proposed study. Future work should include the scaling up of attrition scrubbing.

Declaration of competing interest

The authors declare that there is no conflict of interest.

CRediT authorship contribution statement

Samuel D. Widijatmoko: Conceptualization, Visualization, Methodology, Investigation, Writing - original draft. **Gu Fu:** Resources. **Zheng Wang:** Resources. **Philip Hall:** Supervision, Funding acquisition, Project administration, Writing - review & editing.

Acknowledgement

References

Al-Thyabat, S., Nakamura, T., Shibata, E., Iizuka, A., 2013. Adaptation of minerals processing operations for lithium-ion (LiBs) and nickel metal hydride (NiMH) batteries recycling: critical review. Miner. Eng. 45, 4–17. https://doi.org/10.1016/j.mineng.2012.12.005.

Bayley, R.W., Biggs, C.A., 2005. Characterisation of an attrition scrubber for the removal of high molecular weight contaminants in sand. Chem. Eng. J. 111 (1), 71–79. https://doi.org/10.1016/j.cej.2005.05.009.

Blomgren, G.E., 2017. The development and future of lithium ion batteries. J. Electrochem. Soc. 164 (1), A5019–A5025. https://doi.org/10.1149/2.0251701jes.

Butt, J., Mebrahtu, H., Shirvani, H., 2016. Microstructure and mechanical properties of dissimilar pure copper foil/1050 aluminium composites made with composite metal foil manufacturing. J. Mater. Process. Technol. 238, 96–107. https://doi.org/10.1016/j.jmatprotec.2016.07.014.

Chen, L., Tang, X., Zhang, Y., Li, L., Zeng, Z., Zhang, Y., 2011. Process for the recovery of cobalt oxalate from spent lithium-ion batteries. Hydrometallurgy 108 (1–2), 80–86. https://doi.org/10.1016/j.hydromet.2011.02.010.

Chen, X., Kang, D., Cao, L., Li, J., Zhou, T., Ma, H., 2019. Separation and recovery of valuable metals from spent lithium ion batteries: simultaneous recovery of Li and Co in a single step. Separ. Purif. Technol. 210, 690–697. https://doi.org/10.1016/j.seppur.2018.08.072.

Dai, C., Wang, Z., Liu, K., Zhu, X., Liao, X., Chen, X., Pan, Y., 2019. Effects of cycle times and C-rate on mechanical properties of copper foil and adhesive strength of electrodes in commercial LiCoO2 LIBs. Eng. Fail. Anal. 101, 193–205. https://doi.org/10.1016/j.engfailanal.2019.03.015.

Diekmann, J., Hanisch, C., Froböse, L., Schälicke, G., Loellhoeffel, T., Fölster, A.-S., Kwade, A., 2017. Ecological recycling of lithium-ion batteries from electric vehicles with focus on mechanical processes. J. Electrochem. Soc. 164 (1), A6184–A6191. https://doi.org/10.1149/2.0271701jes.

Dunn, B., Kamath, H., Tarascon, J.-M., 2011. Electrical energy storage for the grid: a battery of choices. Science 334 (6058), 928–935.

Gaines, L., 2018. Lithium-ion battery recycling processes: research towards a sustainable course. Sustain. Mater. Technol. 17, e00068 https://doi.org/10.1016/j.susmat.2018.e00068.

Gao, M., Forssberg, E., 1995. Prediction of product size distributions for a stirred ball mill. Powder Technol. 84 (2), 101–106.

Group, Q., 2011. Technical Data Sheet for Polyvinylidene Rod & Sheet. Quadrant Group.

He, Y., Zhang, T., Wang, F., Zhang, G., Zhang, W., Wang, J., 2017. Recovery of LiCoO2 and graphite from spent lithium-ion batteries by Fenton reagent-assisted flotation. J. Clean. Prod. 143, 319–325. https://doi.org/10.1016/j.jclepro.2016.12.106.

Hesse, M., Popov, O., Lieberwirth, H., 2017. Increasing efficiency by selective comminution. Miner. Eng. 103–104, 112–126. https://doi.org/10.1016/j.mineng.2016.09.003.

Joo, S.-H., Shin, D., Oh, C., Wang, J.-P., Shin, S.M., 2016. Extraction of manganese by alkyl monocarboxylic acid in a mixed extractant from a leaching solution of spent lithium-ion battery ternary cathodic material. J. Power Sources 305, 175–181. https://doi.org/10.1016/j.jpowsour.2015.11.039.

Kelly, E., Spottiswood, D., 1989. The theory of electrostatic separations: a review Part I. Fundamentals. Miner. Eng. 2 (1), 33–46.

Li, J., Shi, P., Wang, Z., Chen, Y., Chang, C.C., 2009. A combined recovery process of metals in spent lithium-ion batteries. Chemosphere 77 (8), 1132–1136. https://doi.org/10.1016/j.chemosphere.2009.08.040.

Li, L., Zhang, X., Li, M., Chen, R., Wu, F., Amine, K., Lu, J., 2018. The recycling of spent lithium-ion batteries: a review of current processes and technologies. Electrochem. Energy Rev. 1 (4), 461–482. https://doi.org/10.1007/s41918-018-0012-1.

Lu, X., Forssberg, E., 2001. Flotation selectivity and upgrading of Woxna fine graphite concentrate. Miner. Eng. 14 (11), 1541–1543.

Mariano, R.A., Evans, C.L., Manlapig, E., 2016. Definition of random and non-random breakage in mineral liberation - a review. Miner. Eng. 94, 51–60. https://doi.org/10.1016/j.mineng.2016.05.005.

Metso, 2018. Basics in Minerals Processing, 11 ed.

Pavoni, F.H., Sita, L.E., dos Santos, C.S., da Silva, S.P., da Silva, P.R.C., Scarminio, J., 2018. LiCoO2 particle size distribution as a function of the state of health of discarded cell phone batteries. Powder Technol. 326, 78–83. https://doi.org/10.1016/j.powtec.2017.12.059.

Petavy, F., Ruban, V., Conil, P., Viau, J.Y., 2009. Attrition efficiency in the decontamination of stormwater sediments. Appl. Geochem. 24 (1), 153–161. https://

doi.org/10.1016/j.apgeochem.2008.09.014.

Richa, K., Babbitt, C.W., Gaustad, G., Wang, X., 2014. A future perspective on lithium-ion battery waste flows from electric vehicles. Resour. Conserv. Recycl. 83, 63–76. https://doi.org/10.1016/j.resconrec.2013.11.008.

Roshanfar, M., Golmohammadzadeh, R., Rashchi, F., 2019. An environmentally friendly method for recovery of lithium and cobalt from spent lithium-ion batteries using gluconic and lactic acids. J. Environ. Chem. Eng. 7 (1), 102794 https://doi.org/10.1016/j.jece.2018.11.039.

Sa, Q., Heelan, J.A., Lu, Y., Apelian, D., Wang, Y., 2015. Copper impurity effects on LiNi(1/3)Mn(1/3)Co(1/3)O2 cathode material. ACS Appl. Mater. Interfaces 7 (37), 20585–20590. https://doi.org/10.1021/acsami.5b04426.

Sadler III, L.Y., Stanley, A.D., Brooks, D.R., 1975. Attrition mill operating character-istics. Powder Technol. 12 (1), 19–28. https://doi.org/10.1016/0032-5910(75)85004-2.

Silveira, A.V.M., Santana, M.P., Tanabe, E.H., Bertuol, D.A., 2017. Recovery of valuable materials from spent lithium ion batteries using electrostatic separation. Int. J. Miner. Process. 169, 91–98. https://doi.org/10.1016/j.minpro.2017.11.003.

Standard, B., 2014. Determination of certain substances in electrochemical products, Part 5: cadmium, lead and chromium in polymers and electronics cadmium and lead in metals by AAS. AFS, ICP-OES and ICP-MS. BSI Standard Publication. BS EN 62321-5:2014.

Wang, X., Gaustad, G., Babbitt, C.W., 2016. Targeting high value metals in lithium-ion battery recycling via shredding and size-based separation. Waste Manag. 51, 204–213. https://doi.org/10.1016/j.wasman.2015.10.026.

Widijatmoko, S.D., Gu, F., Wang, Z., Hall, P., 2020. Selective liberation in dry milled spent lithium-ion batteries. Sustain. Mater. Technol. 23, e00134.

Winslow, K.M., Laux, S.J., Townsend, T.G., 2018. A review on the growing concern and potential management strategies of waste lithium-ion batteries. Resour. Conserv. Recycl. 129, 263–277. https://doi.org/10.1016/j.resconrec.2017.11.001.

Yu, M., Zhang, Z., Xue, F., Yang, B., Guo, G., Qiu, J., 2019. A more simple and efficient process for recovery of cobalt and lithium from spent lithium-ion batteries with citric acid. Separ. Purif. Technol. 215, 398–402. https://doi.org/10.1016/j.seppur.2019.01.027.

Zeng, X., Li, J., Singh, N., 2014. Recycling of spent lithium-ion battery: a critical re-view. Crit. Rev. Environ. Sci. Technol. 44 (10), 1129–1165. https://doi.org/10.1080/10643389.2013.763578.

Zhang, T., He, Y., Ge, L., Fu, R., Zhang, X., Huang, Y., 2013. Characteristics of wet and dry crushing methods in the recycling process of spent lithium-ion batteries. J. Power Sources 240, 766–771. https://doi.org/10.1016/j.jpowsour.2013.05.009.

Zubi, G., Dufo-López, R., Carvalho, M., Pasaoglu, G., 2018. The lithium-ion battery: state of the art and future perspectives. Renew. Sustain. Energy Rev. 89, 292–308. https://doi.org/10.1016/j.rser.2018.03.002.

Appendix II – Reference Materials Certificate

The certificate for the reference materials for ICP-MS of the following metals are attached in this appendix:

- Aluminium
- Cobalt
- Copper

The details can be found in the next page.

TraceCERT®
Traceable Certified Reference Materials

SIGMA-ALDRICH®

Certificate

This certificate is designed in accordance with ISO Guide 31 [1].

Object of certification:	**Aluminum Standard for ICP**
Product no.:	**61935**
Lot no.	**BCCB2789**
Composition:	Aluminum nitrate x 9 H_2O (high-purity material) in 2% HNO_3 (prepared with HNO_3 suitable for trace analysis and high purity water, 18.2 MΩcm, 0.22 μm filtered)
Intended use:	Calibration of ICP, AAS, spectrophotometry or any other analytical technique.
Storing and handling:	This reference material shall be stored in the original closed bag between 5°C and 30°C. Before every use of the material the bottle must be shaken well and its temperature has to be 20°C. If storage of a partially used bottle is necessary, the cap should be tightly sealed and the bottle should be stored at reduced temperature (e.g. refrigerator) to minimize transpiration rate. We highly recommend using this reference material no longer than 15 months after the aluminum bag was opened.
Expiry date:	**FEB 2023** (unopened bottle in aluminized bag)
Certificate issue date:	21 MAY 2019
Certificate version:	01
Bottle opening date:	_ _

The certified values and uncertainties are according to ISO Guide 35 [2] and Eurachem/CITAC Guide [3]

Constituent	Certified value at 20°C and expanded uncertainty [$U = ku_c$; $k = 2$]	
Aluminum	**983 mg kg^{-1} ± 5 mg kg^{-1}**	**998 mg L^{-1} ± 5 mg L^{-1}**
Traceability [4]	NIST SRM 3101a, Aluminum Standard Solution	

Measurand	Certified value and expanded uncertainty [$U = ku_c$; $k = 2$]
Density at 20°C	**1.0152 g mL^{-1} ± 0.0005 g mL^{-1}**

CRM operations:	*S. Matt*
	S.Matt
Approving Officer:	
	P. Zell, Ph.D.

ISO 17034
SRMS 0001

ISO/IEC 17025
STS 0490

ISO 9001
005356 QM08

Certificate page 1 of 3   Sigma-Aldrich Production GmbH, Industriestrasse 25, 9471 Buchs/Switzerland, Tel +41-81-755-2511, Fax +41-81-756-5449   SIGMA-ALDRICH®

288

1. CERTIFICATION

Production and certification of this CRM are performed under double-accreditation in accordance with ISO/IEC 17025 [5] and also ISO 17034 [6]. Storage stability, leaching and homogeneity tests are considered for certification (see storing behavior, chapter 3).

1.1 HP-ICP-OES MEASUREMENT

The certified value of the content (mg/kg) is determined using high-performance inductively coupled plasma optical emission spectrometry (HP-ICP-OES). To obtain performance comparable to isotope dilution and classical methods (titration and gravimetric analysis) the HP-ICP-OES measurement is performed using an internal standard and a drift correction procedure [7].
The mean value is based on 20 measurements (two samples and 10 measurements per sample). All measurements are traced gravimetrically to an internationally accepted reference material e.g. from NIST (USA) or BAM (Germany).

1.2 DENSITY MEASUREMENT

The density measurement is carried out according to ISO 15212-1 [8] and using the digital density meter DMA 4500M from Anton Paar with an oscillating U-tube installed. The measurement uncertainty is calculated according to Eurachem/CITAC Guide and reported as combined expanded uncertainty at the 95% confidence level.

1.3 UNCERTAINTY EVALUATION

All uncertainties are calculated according to Eurachem/CITAC Guide [3] and reported as combined expanded uncertainties at the 95% confidence level. The main uncertainty contributions are illustrated by the following cause-effect diagram.

Typical relative contributions are:

$u(w_{CRM})$ 0.1 - 0.3 %
$u(Store)$ < 0.1 %
$u(\rho)$ < 0.05 %
$u(Hom)$ < 0.03 %

The combined uncertainty u_c is calculated by combination of the squared contribution values.

2. TRACE IMPURITIES IN BOTTLED SOLUTION

Up to 75 trace impurities were determined with ICP-OES, ICP-MS and AAS. Some of the impurities are determined in the starting material and calculated for the solution (e.g. for rare earth elements contamination during the preparation is rendered impossible). Other elements are determined both in the starting material as well as in the bottled solution.

All values listed below are given in mg kg^{-1} (ppm), <X = below detection limit, m = matrix, n.a. = not analyzed:

Li	Be											B	C	N	O	F	Ne
<0.010	<0.005											<0.050	n.a.	n.a.	n.a.	n.a.	n.a.
Na	Mg											Al	Si	P	S	Cl	Ar
<0.050	<0.005											m	<0.004	<0.073	<0.073	n.a.	n.a.
K	Ca	Sc	Ti	V	Cr	Mn	Fe	Co	Ni	Cu	Zn	Ga	Ge	As	Se	Br	Kr
<0.050	<0.010	<0.002	<0.001	<0.001	<0.025	<0.005	0.080	<0.001	<0.001	<0.001	<0.001	0.080	<0.001	<0.001	<0.002	n.a.	n.a.
Rb	Sr	Y	Zr	Nb	Mo	Tc	Ru	Rh	Pd	Ag	Cd	In	Sn	Sb	Te	I	Xe
<0.001	<0.001	<0.001	<0.001	<0.001	<0.001	n.a.	<0.001	<0.001	<0.001	<0.001	<0.001	<0.001	<0.001	<0.001	<0.001	n.a.	n.a.
Cs	Ba	La	Hf	Ta	W	Re	Os	Ir	Pt	Au	Hg	Tl	Pb	Bi	Po	At	Rn
<0.001	0.007	<0.001	<0.001	<0.001	<0.001	<0.001	<0.001	<0.001	<0.001	<0.001	<0.001	<0.001	<0.001	<0.001	n.a.	n.a.	n.a.
Fr	Ra	Ac															
n.a.	n.a.	n.a.															

Ce	Pr	Nd	Pm	Sm	Eu	Gd	Tb	Dy	Ho	Er	Tm	Yb	Lu
<0.001	<0.001	<0.001	n.a.	<0.001	<0.001	<0.001	<0.001	<0.001	<0.001	<0.001	<0.001	<0.001	<0.001
Th	Pa	U											
<0.001	n.a.	<0.001											

Sigma-Aldrich Production GmbH, Industriestrasse 25, 9471 Buchs/Switzerland, Tel +41-81-755-2511, Fax +41-81-756-5449

SIGMA-ALDRICH®

3. STORING BEHAVIOR

The storage behavior of standard solutions is of greatest importance with regard to the certified value. Therefore the two most important effects were investigated by in-depth studies in a cooperation with EMPA, St. Gallen:

1. The leach out of trace impurities from HDPE (high-density polyethylene) bottles was determined with HR-ICP-MS after leaching the bottles with 2% nitric acid. Maximum contamination levels were found in the ng L^{-1} level for 12 elements.

2. To avoid significant loss of mass through transpiration the bottle is delivered in aluminum coated bags. After the bottle has been removed from the bag, transpiration will occur at an accelerated rate (see figure). We highly recommend not to open the bag until the solution is needed. Once the bottle is opened the solution should be stored at reduced temperature (4°C) to reduce transpiration.

Transpiration through 100 mL HD-PE bottles

References
[1]   ISO Guide 31:2015, "Reference materials - Contents of certificates, labels and accompanying documentation"
[2]   ISO Guide 35:2017, "Reference materials – Guidance for characterization and assessment of homogeneity and stability"
[3]   Eurachem/CITAC Guide, 3rd Ed. (2012), "Quantifying uncertainty in analytical measurement"
[4]   Eurachem/CITAC Guide, 1st Ed. (2003) "Traceability in chemical measurement"
[5]   ISO/IEC 17025:2017, "General requirements for the competence of testing and calibration laboratories"
[6]   ISO 17034:2016, "General requirements for the competence of reference material producers"
[7]   Marc L. Salit et al., Anal. Chem. 2001, 73, 4821-4829, "Single-Element Solution Comparisons with a High-Performance Inductively Coupled Plasma Optical Emission Spectrometric Method"
[8]   DIN EN ISO 15212-1:1998, Oscillation-type density meters - Part 1: Laboratory instruments

TraceCERT®
Traceable Certified Reference Materials

SIGMA-ALDRICH®

Certificate

Produced in double accredited laboratory fulfilling ISO/IEC 17025 and ISO 17034

This certificate is designed in accordance with ISO Guide 31 [1].

Object of certification:	**Cobalt Standard for ICP**
Product No.:	**30329**
Lot:	**BCBX3534**
Composition:	Cobalt metal (high-purity quality) in 2% HNO_3 (prepared with HNO_3 suitable for trace analysis and high-purity water, 18.2 MΩcm, 0.22 µm filtered).
Density at 20°C:	$\rho = 1011.4$ kg m^{-3} $u_c(\rho) = 0.5$ kg m^{-3}
Intended use:	Calibration of ICP, AAS, spectrophotometry or any other analytical technique.
Storing and handling:	This reference material shall be stored in the original closed bag between 5°C and 30°C. Before every use of the material the bottle must be shaken well and its temperature has to be 20°C. If storage of a partially used bottle is necessary, the cap should be tightly sealed and the bottle should be stored at reduced temperature (e.g. refrigerator) to minimize transpiration rate. We highly recommend using this reference material no longer than 15 months after the aluminum bag was opened.
Expiry date:	**MAY 2022** (unopened bottle in aluminized bag)
Certificate issue date:	11 JUL 2018
Certificate version:	01
Bottle opening date:	_ _

Certified value traceable to SI unit kg and uncertainty according to ISO Guide 35 [2] and Eurachem/CITAC Guide [3]		
Constituent	Certified value at 20°C and expanded uncertainty [$U = k u_c$; $k = 2$]	
Cobalt	**989 mg kg^{-1} ± 2 mg kg^{-1}**	**1'000 mg L^{-1} ± 2 mg L^{-1}**

1. CONCEPT OF CERTIFICATION AND TRACEABILITY STATEMENT

To guarantee top reliability of the values for this *Trace*CERT® certified reference material three independent procedures were followed. The values have to agree in the range of their uncertainties, but the impurity corrected value from the gravimetric preparation has been chosen as certified value [4]:

1. Gravimetric preparation using pure materials is a practical realization of concentration units, through conversion of masses and mole fraction to mass fraction [4]. If the purity of the materials is demonstrated and if contamination and loss of material is strictly prevented this approach allows highest accuracy and small uncertainties. The certified value of *Trace*CERT® reference materials is based on this approach and directly traceable to the SI unit kilogram.

    Therefore comprehensively characterized materials of highest purity are used (see paragraph 2). All balances are certified by DKD and calibrated with OIML Class E2 (up to 12 kg) and F2 (up to 64 kg) weights. The bulk solution was homogenized by overhead tumbling in a PVDF container for at least 6 hours. A peristaltic pump with perfluorinated polymer tubings was used for bottling. Detailed information about the long-term stability of the bottled solution is given in paragraph 5 of this certificate.

2. The starting material is measured against a certified reference material (e.g. NIST or BAM) followed by gravimetric preparation using balances calibrated with SI-traceable weights. Consequently the value calculated by this unbroken chain of comparisons is traceable to the reference to which the starting material is compared.

3. Whenever applicable the bottled *Trace*CERT® calibration solution is compared to a second reference which is independent from the first reference.

2. PURITY OF STARTING MATERIALS

For high purity materials (P >99.9%) the most appropriate way of purity determination is to quantify the impurities (w_i) and to subtract the sum from 100%. Impurities below the detection limit are considered with a contribution of half of the detection limit (DL_j).

$$P = 100\% - \sum_i w_i - \sum_j \left(\frac{DL_j}{2} \right)$$

Water containing materials were dried to absolute dryness by individual drying conditions (up to 600°C). When drying is impossible due to decomposition water was determined by high-precision KF-titration.
High-purity water (18.2 MΩcm; 0.22 µm filtered, all metallic traces at ng kg^{-1}-level) and high-purity acid for trace analysis were used for preparation.

3. TRACE IMPURITIES IN BOTTLED SOLUTION

Up to 75 trace impurities were determined with ICP-OES, ICP-MS and AAS. Some of the impurities are determined in the starting material and calculated for the solution (e.g. for rare earth elements contamination during the preparation is rendered impossible). Other elements are determined both in the starting material as well as in the bottled solution.

All values listed below are given in mg kg^{-1} (ppm), <X = below detection limit, m = matrix, n.a. = not analyzed:

Li	Be											B	C	N	O	F	Ne
<0.010	<0.005											<0.025	n.a.	n.a.	n.a.	n.a.	n.a.
Na	Mg											Al	Si	P	S	Cl	Ar
<0.050	<0.005											0.050	<0.020	<0.050	<0.050	n.a.	n.a.
K	Ca	Sc	Ti	V	Cr	Mn	Fe	Co	Ni	Cu	Zn	Ga	Ge	As	Se	Br	Kr
<0.10	<0.010	<0.001	0.002	<0.001	<0.001	<0.001	<0.020	m	0.18	0.009	<0.001	<0.001	<0.001	<0.005	<0.005	n.a.	n.a.
Rb	Sr	Y	Zr	Nb	Mo	Tc	Ru	Rh	Pd	Ag	Cd	In	Sn	Sb	Te	I	Xe
<0.001	<0.005	<0.001	<0.001	<0.001	<0.001	n.a.	<0.001	<0.001	<0.001	<0.001	<0.001	<0.001	<0.001	<0.001	<0.001	n.a.	n.a.
Cs	Ba	La	Hf	Ta	W	Re	Os	Ir	Pt	Au	Hg	Tl	Pb	Bi	Po	At	Rn
<0.001	<0.005	<0.001	<0.001	<0.001	<0.001	<0.001	<0.001	<0.001	<0.001	<0.001	<0.001	<0.001	<0.001	<0.001	n.a.	n.a.	n.a.
Fr	Ra	Ac															
n.a.	n.a.	n.a.															

Ce	Pr	Nd	Pm	Sm	Eu	Gd	Tb	Dy	Ho	Er	Tm	Yb	Lu
<0.001	<0.001	<0.001	n.a.	<0.001	<0.001	<0.001	<0.001	<0.001	<0.001	<0.001	<0.001	<0.001	<0.001
Th	Pa	U											
<0.001	n.a.	<0.001											

4. TRACEABILITY MEASUREMENTS

Only internationally accepted reference materials e.g. from NIST (USA) or BAM (Germany) have been carefully selected to provide the basis for traceability to the SI unit mole. When no such reference is available, an elemental metal or an adequate salt of highest available purity is used to confirm traceability to this pure material (and therefore to the SI unit kg).

To underpin the certified gravimetric value all traceability measurements are performed with the most accurate and precise analytical technique available. Therefore titrimetry measurement series are applied whenever possible (corrected for trace impurities). When no titrimetric technique is available, the traceability measurements are performed with another analytical technique, e.g. ICP-OES or AAS.

Reference and applied technique used for traceability measurements of the

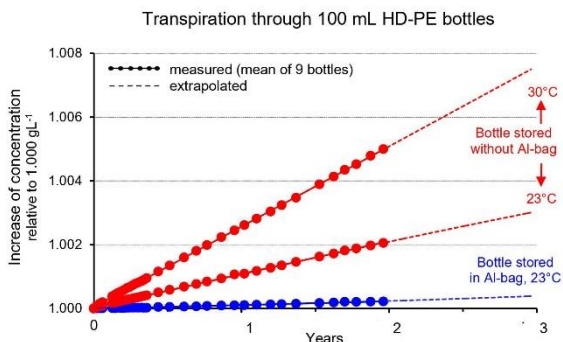starting material: NIST SRM 728 / complexometric titration

bottled solution: BAM 365 / complexometric titration

SIGMA-ALDRICH

292

5. STORING BEHAVIOR

The storage behavior of standard solutions is of greatest importance with regard to the certified value. Therefore the two most important effects were investigated by in-depth studies in a cooperation with EMPA, St. Gallen:
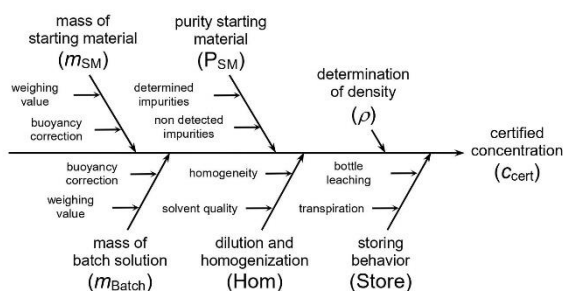
1. The leach out of trace impurities from HDPE (high-density polyethylene) bottles was determined with HR-ICP-MS after leaching the bottles with 2% nitric acid. Maximum contamination levels were found in the ng L^{-1} level for 12 elements.

2. To avoid significant loss of mass through transpiration the bottle is delivered in aluminum coated bags. After the bottle has been removed from the bag, transpiration will occur at an accelerated rate (see figure). We highly recommend not to open the bag until the solution is needed. Once the bottle is opened the solution should be stored at reduced temperature (4°C) to reduce transpiration.

Transpiration through 100 mL HD-PE bottles

6. UNCERTAINTY EVALUATION

All uncertainties are calculated according to Eurachem/CITAC Guide [3] and reported as combined expanded uncertainties at the 95% confidence level. For gravimetric preparation the uncertainty contributions are illustrated by the following cause-effect diagram [5]:

Typical contributions:

$u(m_{SM})$	< 0.01%
$u(m_{Batch})$	< 0.01%
$u(P_{SM})$	< 0.05%
$u(Hom)$	< 0.03%
$u(Store)$	< 0.09%
$u(\rho)$	< 0.05%

Combined uncertainty [6]:

$u_c(c_{cert})$ < 0.1%

Expanded uncertainty:

$U(c_{cert})$ < 0.2%

CRM operations: _S. Matt_

S.Matt

Approving Officer:

P. Zell, Ph.D.

ISO 17034
SRMS 0001

ISO/IEC 17025
STS 0490

ISO 9001
005356 QM08

[1]   ISO Guide 31:2015, "Reference materials - Contents of certificates, labels and accompanying documentation"
[2]   ISO Guide 35:2017, "Reference materials – Guidance for characterization and assessment of homogeneity and stability"
[3]   Eurachem/CITAC Guide, 3rd Ed. (2012), "Quantifying uncertainty in analytical measurement"
[4]   Eurachem/CITAC Guide, 1st Ed. (2003) "Traceability in chemical measurement"
[5]   Reichmuth, A., Wunderli, S., Weber, M., Meyer, V. R. (2004), "The uncertainty of weighing data obtained with electronic analytical balances", Microchimica Acta 148: 133-141.
[6]   Calculated by combination of the squared contribution values

SIGMA-ALDRICH

TraceCERT®
Traceable Certified Reference Materials

SIGMA-ALDRICH®

Certificate

Produced in double accredited laboratory fulfilling ISO/IEC 17025 and ISO 17034

This certificate is designed in accordance with ISO Guide 31 [1].

Object of certification:	**Copper Standard for ICP**
Product No.:	**68921**
Lot:	**BCBW9300**
Composition:	Copper metal (high-purity quality) in 2% HNO_3 (prepared with HNO_3 suitable for trace analysis and high-purity water, 18.2 MΩ·cm, 0.22 µm filtered).
Density at 20°C:	$\rho = 1011.1$ kg m^{-3} $u_c(\rho) = 0.5$ kg m^{-3}
Intended use:	Calibration of ICP, AAS, spectrophotometry or any other analytical technique.
Storing and handling:	This reference material shall be stored in the original closed bag between 5°C and 30°C. Before every use of the material the bottle must be shaken well and its temperature has to be 20°C. If storage of a partially used bottle is necessary, the cap should be tightly sealed and the bottle should be stored at reduced temperature (e.g. refrigerator) to minimize transpiration rate. We highly recommend using this reference material no longer than 15 months after the aluminum bag was opened.
Expiry date:	**APR 2022** (unopened bottle in aluminized bag)
Certificate issue date:	16 MAY 2018
Certificate version:	01
Bottle opening date:	_ _

Certified value traceable to SI unit kg and uncertainty according to ISO Guide 35 [2] and Eurachem/CITAC Guide [3]		
Constituent	Certified value at 20°C and expanded uncertainty [$U = k u_c$; $k = 2$]	
Copper	**989 mg kg^{-1} ± 2 mg kg^{-1}**	**1'000 mg L^{-1} ± 2 mg L^{-1}**

1. CONCEPT OF CERTIFICATION AND TRACEABILITY STATEMENT

To guarantee top reliability of the values for this *Trace*CERT® certified reference material three independent procedures were followed. The values have to agree in the range of their uncertainties, but the impurity corrected value from the gravimetric preparation has been chosen as certified value [4]:

1. Gravimetric preparation using pure materials is a practical realization of concentration units, through conversion of masses and mole fraction to mass fraction [4]. If the purity of the materials is demonstrated and if contamination and loss of material is strictly prevented this approach allows highest accuracy and small uncertainties. The certified value of *Trace*CERT® reference materials is based on this approach and directly traceable to the SI unit kilogram.

   Therefore comprehensively characterized materials of highest purity are used (see paragraph 2). All balances are certified by DKD and calibrated with OIML Class E2 (up to 12 kg) and F2 (up to 64 kg) weights. The bulk solution was homogenized by overhead tumbling in a PVDF container for at least 6 hours. A peristaltic pump with perfluorinated polymer tubings was used for bottling. Detailed information about the long-term stability of the bottled solution is given in paragraph 5 of this certificate.

2. The starting material is measured against a certified reference material (e.g. NIST or BAM) followed by gravimetric preparation using balances calibrated with SI-traceable weights. Consequently the value calculated by this unbroken chain of comparisons is traceable to the reference to which the starting material is compared.

3. Whenever applicable the bottled *Trace*CERT® calibration solution is compared to a second reference which is independent from the first reference.

Sigma-Aldrich Production GmbH, Industriestrasse 25, 9471 Buchs/Switzerland, Tel +41-81-755-2511, Fax +41-81-756-5449

SIGMA-ALDRICH®

2. PURITY OF STARTING MATERIALS

For high purity materials (P >99.9 %) the most appropriate way of purity determination is to quantify the impurities (w_i) and to subtract the sum from 100 %. Impurities below the detection limit are considered with a contribution of half of the detection limit (DL_j).

$$P = 100\% - \sum_i w_i - \sum_j \left(\frac{DL_j}{2} \right)$$

Water containing materials were dried to absolute dryness by individual drying conditions (up to 600°C). When drying is impossible due to decomposition water was determined by high-precision KF-titration.
High-purity water (18.2 MΩcm; 0.22 μm filtered, all metallic traces at ng kg^{-1}-level) and high-purity acid for trace analysis were used for preparation.

3. TRACE IMPURITIES IN BOTTLED SOLUTION

Up to 75 trace impurities were determined with ICP-OES, ICP-MS and AAS. Some of the impurities are determined in the starting material and calculated for the solution (e.g. for rare earth elements contamination during the preparation is rendered impossible). Other elements are determined both in the starting material as well as in the bottled solution.

All values listed below are given in mg kg^{-1} (ppm), <X = below detection limit, m = matrix, n.a. = not analyzed:

Li	Be											B	C	N	O	F	Ne
<0.010	<0.005											<0.025	n.a.	n.a.	n.a.	n.a.	n.a.
Na	Mg											Al	Si	P	S	Cl	Ar
<0.050	<0.005											<0.050	<0.005	<0.010	<0.020	n.a.	n.a.
K	Ca	Sc	Ti	V	Cr	Mn	Fe	Co	Ni	Cu	Zn	Ga	Ge	As	Se	Br	Kr
<0.050	<0.010	<0.002	<0.001	<0.001	<0.001	<0.005	<0.005	<0.001	<0.010	m	<0.010	<0.001	<0.001	<0.001	<0.004	n.a.	n.a.
Rb	Sr	Y	Zr	Nb	Mo	Tc	Ru	Rh	Pd	Ag	Cd	In	Sn	Sb	Te	I	Xe
<0.001	<0.005	<0.001	<0.001	<0.001	<0.001	n.a.	<0.001	<0.001	<0.001	0.015	<0.001	<0.001	<0.001	<0.001	<0.001	n.a.	n.a.
Cs	Ba	La	Hf	Ta	W	Re	Os	Ir	Pt	Au	Hg	Tl	Pb	Bi	Po	At	Rn
<0.001	<0.001	<0.001	<0.001	<0.001	<0.001	<0.001	<0.001	<0.001	<0.001	<0.001	<0.001	<0.001	<0.001	<0.001	n.a.	n.a.	n.a.
Fr	Ra	Ac															
n.a.	n.a.	n.a.															

Ce	Pr	Nd	Pm	Sm	Eu	Gd	Tb	Dy	Ho	Er	Tm	Yb	Lu
<0.001	<0.001	<0.001	n.a.	<0.001	<0.001	<0.001	<0.001	<0.001	<0.001	<0.001	<0.001	<0.001	<0.001
Th	Pa	U											
<0.001	n.a.	<0.001											

4. TRACEABILITY MEASUREMENTS

Only internationally accepted reference materials e.g. from NIST (USA) or BAM (Germany) have been carefully selected to provide the basis for traceability to the SI unit mole. When no such reference is available, an elemental metal or an adequate salt of highest available purity is used to confirm traceability to this pure material (and therefore to the SI unit kg).

To underpin the certified gravimetric value all traceability measurements are performed with the most accurate and precise analytical technique available. Therefore titrimetry measurement series are applied whenever possible (corrected for trace impurities). When no titrimetric technique is available, the traceability measurements are performed with another analytical technique, e.g. ICP-OES or AAS.

Reference and applied technique used for traceability measurements of the

starting material: NIST SRM 728 / complexometric titration

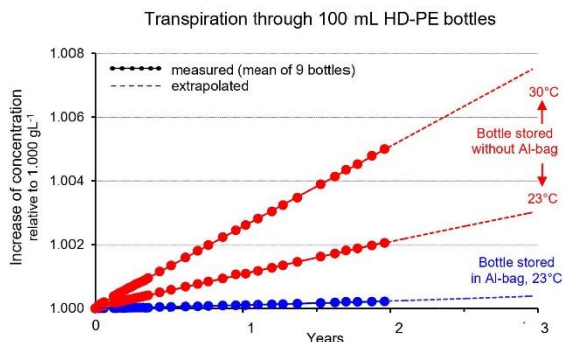bottled solution: BAM 365 / complexometric titration

SIGMA-ALDRICH®

5. STORING BEHAVIOR

The storage behavior of standard solutions is of greatest importance with regard to the certified value. Therefore the two most important effects were investigated by in-depth studies in a cooperation with EMPA, St. Gallen:
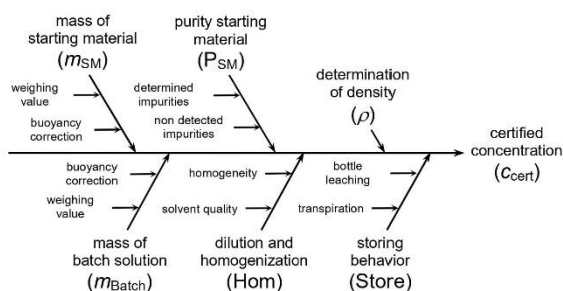
1. The leach out of trace impurities from HDPE (high-density polyethylene) bottles was determined with HR-ICP-MS after leaching the bottles with 2% nitric acid. Maximum contamination levels were found in the ng L^{-1} level for 12 elements.

2. To avoid significant loss of mass through transpiration the bottle is delivered in aluminium coated bags. After the bottle has been removed from the bag, transpiration will occur at an accelerated rate (see figure). We highly recommend not to open the bag until the solution is needed. Once the bottle is opened the solution should be stored at reduced temperature (4°C) to reduce transpiration.

Transpiration through 100 mL HD-PE bottles

6. UNCERTAINTY EVALUATION

All uncertainties are calculated according to Eurachem/CITAC Guide [3] and reported as combined expanded uncertainties at the 95% confidence level. For gravimetric preparation the uncertainty contributions are illustrated by the following cause-effect diagram [5]:

Typical contributions:

$u(m_{SM})$ < 0.01%
$u(m_{Batch})$ < 0.01%
$u(P_{SM})$ < 0.05%
$u(Hom)$ < 0.03%
$u(Store)$ < 0.09%
$u(\rho)$ < 0.05%

Combined uncertainty [6]:

$u_c(c_{cert})$ < 0.1%

Expanded uncertainty:

$U(c_{cert})$ < 0.2%

CRM operations:	S. Matt			
	S.Matt			
Approving Officer:				
	P. Zell, Ph.D.	ISO 17034 SRMS 0001	ISO/IEC 17025 STS 0490	ISO 9001 005356 QM08

[1]   ISO Guide 31:2015, "Reference materials - Contents of certificates, labels and accompanying documentation"
[2]   ISO Guide 35:2017, "Reference materials – Guidance for characterization and assessment of homogeneity and stability"
[3]   Eurachem/CITAC Guide, 3rd Ed. (2012), "Quantifying uncertainty in analytical measurement"
[4]   Eurachem/CITAC Guide, 1st Ed. (2003) "Traceability in chemical measurement"
[5]   Reichmuth, A., Wunderli, S., Weber, M., Meyer, V. R. (2004), "The uncertainty of weighing data obtained with electronic analytical balances", Microchimica Acta 148: 133-141.
[6]   Calculated by combination of the squared contribution values

Sigma-Aldrich Production GmbH, Industriestrasse 25, 9471 Buchs/Switzerland, Tel +41-81-755-2511, Fax +41-81-756-5449

SIGMA-ALDRICH

Appendix III – Spent LIBs Representative Samples

The supporting data for the representative samples produced and used are presented in this appendix. Two batches of sample splitting were carried out for the entire experiment reported in this thesis.

Batch 1:

- Sample No.1 to No.3 were used for characterisation of dry milled spent LIBs in Chapter 4. The sample is also used for attrition liberation proof of concept and breakage kinetics (0.0 min).
- Sample No.4 to No.6 were used for attrition scrubbing liberation proof of concept and breakage kinetics (2.5 min) in Chapter 5.
- Sample No.7 to No.9 were used for attrition scrubbing breakage kinetics (5.0 min) in Chapter 5.
- Sample No.10 to No. 12 were used for attrition scrubbing breakage kinetics (10.0 min) in Chapter 5.
- Sample No.13 to No.15 were used for attrition scrubbing breakage kinetics (20.0 min) in Chapter 5.

The sample details for Batch 1 can be found in the next page and summarised in Table A.III-1.

Batch 1

The 1110.5 g dried spent LIBs sample was reduced into 16 representative samples and presented in Table A.III-1.

Table A.III-1 Representative samples produced and used in Chapter 4 and Chapter 5.

No	Representative Sample Mass (g)	Ferromagnetic Screened (g)	Clean Sample Mass (g)
1	69.4	0.7	68.7
2	70.9	1.0	69.9
3	68.4	0.6	67.8
4	67.1	0.4	66.7
5	69.4	0.9	68.5
6	69.0	0.8	68.2
7	68.3	0.9	67.4
8	66.1	0.3	65.8
9	70.4	0.7	69.7
10	66.3	0.8	65.5
11	67.4	0.2	67.2
12	68.3	0.6	67.7
13	66.3	0.8	65.5
14	65.7	0.6	65.1
15	69.7	0.6	69.1
16	67.8	0.6	67.2

The sample total sample mass recovered from the splitting procedure is 1090.5 g. The sample splitting procedure results in 1.8 wt% mass loss.

Batch 2:

- Sample No.1 to No.5 were used for representative sample assay in Chapter 5 (Table 5-5).
- Sample No.10 to No.13 were used to study the parameters affecting attrition liberation for various pulp density in Chapter 5.
    - No.11 for 50 wt%
    - No.10 for 60 wt%
    - No.12 for 70 wt%
    - No.13 for 80 wt%
- Sample No.10 and No.14 to No.16 were used to study the parameters affecting attrition liberation for various LIBs to attrition media ratio in Chapter 5.
    - No.14 for 10 wt%
    - No.10 for 20wt%
    - No.15 for 30wt%
    - No.16 for 40 wt%
- Sample No.6 to No.10 were used to study the parameters affecting attrition liberation for attrition time in Chapter 5.
    - No.6 for 0.0 min.
    - No.7 for 2.5 min.
    - No.8 for 5 min.
    - No.9 for 10 min.
    - No.10 for 20 min.

The sample details for Batch 2 can be found in the next page and summarised in Table A.III-2.

Batch 2

The 1510.0 g dried spent LIBs sample was reduced into 16 representative samples and presented in Table A.III-2.

Table A.III-2 Representative samples produced and used in Chapter 5.

No	Representative Sample Mass (g)	Ferromagnetic Screened (g)	Clean Sample Mass (g)
1	103.1	0.6	102.5
2	84.5	0.5	84.0
3	93.6	0.8	92.8
4	89.0	0.9	88.1
5	98.7	1.1	97.6
6	85.9	0.9	85.0
7	101.6	0.7	100.9
8	91.2	0.9	90.3
9	98.5	0.7	97.8
10	90.9	1.6	89.3
11	90.1	1.4	88.7
12	87.5	0.7	86.8
13	88.0	0.7	87.3
14	88.5	0.1	88.4
15	92.4	0.9	91.5
16	90.4	1.3	89.1

The sample total sample mass recovered from the splitting procedure is 1473.9 g. The sample splitting procedure results in 2.4 wt% mass loss.

The samples presented in Table A.III-2 were used in Chapter 5. Sample No. 1 to No. 5 were assessed for elemental content, while sample No. 6 to No. 16 were used for attrition with varying parameters.